Year : 2013

CHARACTERIZATION OF ROOT APOPLASTIC BARRIERS IN ARABIDOPSIS THALIANA

RIAZ Sadaf Kashif

UNIL | Université de Lausanne
Faculté de biologie et de médecine

Département de Biologie Moléculaire Végétale (DBMV)

CHARACTERIZATION OF ROOT APOPLASTIC BARRIERS IN ARABIDOPSIS THALIANA

Thèse de doctorat ès sciences de la vie (PhD)

présentée à la

Faculté de biologie et de médecine
de l'Université de Lausanne

par

Sadaf Kashif RIAZ

Master de l'Université de Paul Sabatier Toulouse III, France

Jury

Prof. Dr. Alexandre Reymond, Président
Prof. Dr. Niko Geldner, Directeur de thèse
Prof. Dr. Malcolm J. Bennet, Expert
Prof. Dr. Yves Poirier, Expert

Lausanne 2013

UNIL | Université de Lausanne
Faculté de biologie
et de médecine

Ecole Doctorale

Doctorat ès sciences de la vie

Imprimatur

Vu le rapport présenté par le jury d'examen, composé de

Président	Monsieur	Prof. Alexandre **Reymond**
Directeur de thèse	Monsieur	Prof. Niko **Geldner**
Experts	Monsieur	Prof. Yves **Poirier**
	Monsieur	Prof. Malcolm **Bennett**

le Conseil de Faculté autorise l'impression de la thèse de

Madame Sadaf Kashif Riaz

Master of Science de l'Université Paul Sabatier, Toulouse, France

intitulée

CHARACTERIZATION OF ROOT APOPLASTIC BARRIERS IN ARABIDOPSIS THALIANA

Lausanne, le 17 décembre 2013

pour Le Doyen
de la Faculté de Biologie et de Médecine

Prof. Alexandre Reymond

“Science may set limits to knowledge,

but should not set limits to imagination”

Bertrand Russell (1872 - 1970)

“The man of science has learned to

believe in justification, not by faith,

but by verification”

Thomas Henry Huxley….

Table of Contents

Frequently used Abbreviations

BirA	Biotin ligase
BLRP	Biotin ligase recognition peptide
CASP	Casparian Strip Domain Protein
CDEF1	Cuticular Destructing Factor 1
CS	Casparian Strip
CSD	Casparian Strip Membrane Domain
COL	Columbia
FY	Fluorol yellow
GPAT5	Glycerol-3-phosphate acyltransferase5
INTACT	Isolation of nuclei tagged in specific cell type
IRT3	Iron Regulated Transporter 3
LR	Lateral root
MS	Murashige and Skoog
NLS	Nuclear localized signal
NTF	Nuclear Targeting Fusion protein
PHO1	Phosphate 1
PI	Propidium Iodide
PM	Plasma membrane
RPL18	60S Ribosomal protein
SKOR	Stelar K+ Outward Rectifying channel
WT	Wild Type
YSL2	Yellow Strip Like Protein 2

List of Figures

Summary

In vascular plants, the best-known feature of a differentiated endodermal cell is the “Casparian Strip” (CS). This structure refers to a highly localized cell wall impregnation in the transversal and anticlinal walls of the cell, which surrounds the cell like a belt/ring and is tightly coordinated with respect to neighboring cells. Analogous to tight junctions in animal epithelia, CS in plants act as a diffusion barrier that controls the movement of water and ions from soil into the stele. Since its first description by Robert Caspary in 1865 there have been many attempts to identify the chemical nature of the cell wall deposition in CS. Suberin, lignin, or both have been claimed to be the important components of CS in a series of different species. However, the exact chemical composition of CS has remained enigmatic. This controversy was due to the confusion and lack of knowledge regarding the precise measurement of three developmental stages of the endodermis. The CS represent only the primary stage of endodermal differentiation, which is followed by the deposition of suberin lamellae all around the cellular surface of endodermal cells (secondary developmental stage). Therefore, chemical analysis of whole roots, or even of isolated endodermal tissues, will always find both of the polymers present.

It was crucial to clarify this point because this will guide our efforts to understand which cell wall biosynthetic component becomes localized in order to form the CS. The main aim of my work was to find out the major components of (early) CS, as well as their spatial and temporal development, physiological roles and relationship to barrier formation. Employing the knowledge and tools that have been accumulated over the last few years in the model plant Arabidopsis thaliana, various histological and chemical assays were used in this study.

A particular feature of my work was to completely degrade, or inhibit formation of lignin and suberin biopolymers by biochemical, classical genetic and molecular approaches and to investigate its effect on CS formation and the establishment of a functional diffusion barrier. Strikingly, interference with monolignol biosynthesis abrogates CS formation and delays the formation of function diffusion barrier. In contrast, transgenic plants devoid of any detectable suberin still develop a functional CS. The combination of all these assays clearly demonstrates that the early CS polymer is made from monolignol

(lignin monomers) and is composed of lignin. By contrast, suberin is formed much later as a secondary wall during development of endodermis. These early CS are functionally sufficient to block extracellular diffusion and suberin does not play important role in the establishment of early endodermal diffusion barrier. Moreover, suberin biosynthetic machinery is not present at the time of CS formation. Our study finally concludes the long-standing debate about the chemical nature of CS and opens the door to a new approach in lignin research, specifically for the identification of the components of the CS biosynthetic pathway that mediates the localized deposition of cell walls.

I also made some efforts to understand the patterning and differentiation of endodermal passage cells in young roots. In the literature, passage cells are defined as a non-suberized xylem pole associated endodermal cells. Since these cells only contain the CS but not the suberin lamellae, it has been assumed that these cells may offer a continued low-resistance pathway for water and minerals into the stele. Thus far, no genes have been found to be expressed specifically in passage cells.

In order to understand the patterning, differentiation, and physiological role of passage it would be crucial to identify some genes that are exclusively expressed in these cells. In order to identify such genes, I first generated fluorescent marker lines of stele-expressed transporters that have been reported to be expressed in the passage cells. My aim was to first highlight the passage cells in a non-specific way. In order to find passage cell specific genes I then adapted a two-component system based on previously published methods for gene expression profiling of individual cell types. This approach will allow us to target only the passage cells and then to study gene expression specifically in this cell type. Taken together, this preparatory work will provide an entry point to understand the formation and role of endodermal passage cells.

Résumé

Chez les plantes vasculaires, la caractéristique la plus commune des cellules différentiées de l'endoderme est la présence de cadres de Caspary. Cette structure correspond à une imprégnation localisée des parties transversales et anticlinales de la paroi cellulaire. Cela donne naissance, autour de la cellule, à un anneau/cadre qui est coordonné par rapport aux cellules voisines. De manière analogue aux jonctions serrées des épithéliums chez les animaux, les cadres de Caspary agissent chez les plantes comme barrière de diffusion, contrôlant le mouvement de l'eau et des ions à travers la racine entre le sol et la stèle. Depuis leur première description par Robert Caspary en 1865, beaucoup de tentatives ont eu pour but de définir la nature chimique de ces cadres de Caspary. Après l'étude de différentes espèces végétales, à la fois la subérine, la lignine ou les deux ont été revendiquées comme étant des composants importants de ces cadres. Malgré tout, leur nature chimique exacte est restée longtemps énigmatique. Cette controverse provient de la confusion et du manque de connaissance concernant la détermination précise des trois stades de développement de l'endoderme. Les cadres de Caspary représentent uniquement le stade primaire de différentiation de l'endoderme. Celui-ci est suivi par le second stade de différentiation, la déposition de lamelles de subérine tout autour de la cellule endodermal. De ce fait, l'analyse chimique de racines entières ou de cellules d'endoderme isolées ne permet pas de séparer les stades de différentiation primaire et secondaire et aboutit donc à la présence des deux polymères.

Il est également crucial de clarifier ce point dans le but de connaître quelle machinerie cellulaire localisée à la paroi cellulaire permet l'élaboration des cadres de Caspary. En utilisant les connaissances et les outils accumulés récemment grâce à la plante modèle *Arabidopsis thaliana,* divers techniques histologiques et chimiques ont été utilisées dans cette étude. Un point particulier de mon travail a été de dégrader ou d'inhiber complètement la formation de lignine ou de subérine en utilisant des approches de génétique classique ou moléculaire. Le but étant d'observer l'effet de l'absence d'un de ces deux polymères sur la formation des cadres de Caspary et l'établissement d'une barrière de diffusion fonctionnelle. De manière frappante, le fait d'interférer avec la voie de biosynthèse de monolignol (monomères de lignine) abolit la formation des cadres de Caspary et retarde l'élaboration d'une barrière de diffusion fonctionnelle. Par contre, des

plantes transgéniques dépourvues d’une quantité détectable de subérine sont quant à elles toujours capables de développer des cadres de Caspary fonctionnels. Mises en commun, ces expériences démontrent que le polymère formant les cadres de Caspary dans la partie jeune de la racine est fait de monolignol, et que de ce fait il s’agit de lignine. La subérine, quant à elle, est formée bien plus tard durant le développement de l’endoderme, de plus il s’agit d’une modification de la paroi secondaire.

Ces cadres de Caspary précoces faits de lignine suffisent donc à bloquer la diffusion extracellulaire, contrairement à la subérine. De plus, la machinerie de biosynthèse de la subérine n'est pas encore présente au moment de la formation des cadres de Caspary. Notre étude permet donc de mettre un terme au long débat concernant la nature chimique des cadres de Caspary. De plus, elle ouvre la porte à de nouvelles approches dans la recherche sur la lignine, plus particulièrement pour identifier des composants permettant la déposition localisée de ce polymère dans la paroi cellulaire.

J'ai aussi fais des efforts pour mettre en évidence la formation ainsi que le rôle des cellules de passage dans les jeunes racines. Dans la littérature, les cellules de passage sont définies comme de la cellule endodermal faisant face aux pôles xylèmes et dont la paroi n'est pas subérisée. Du fait que ces cellules contiennent uniquement des cadres de Caspary et pas de lamelle de subérine, il a été supposé qu'elles ne devraient offrir que peu de résistance au passage de l'eau et des nutriments entre le sol et la stèle.

Le rôle de ces cellules de passage est toujours loin d'être clair, de plus aucun gène s'exprimant spécifiquement dans ces cellules n'a été découvert à ce jour. De manière à identifier de tels gènes, j'ai tout d'abord généré des marqueurs fluorescents pour des transporteurs exprimés dans la stèle mais dont l'expression avait également été signalée dans l'endoderme, uniquement dans les cellules de passage. J'ai ensuite développé un système à deux composants basé sur des méthodes déjà publiées, visant principalement à étudier le profil d'expression génique dans un type cellulaire donné. En recoupant les gènes exprimés spécifiquement dans l'endoderme à ceux exprimés dans la stèle et les cellules de passage, il nous sera possible d'identifier le transriptome spécifique de ces cellules. Pris dans leur ensemble, ces résultats devraient donner un bon point d'entrée dans la définition et la compréhension des cellules de passage.

Thesis objectives and outline

Over the last 150 years, many studies have been done in order to investigate the chemical nature of Casparian Strips (CS). Nevertheless, all the former work led to a somehow contradicting picture, indicating that either suberin or lignin, or eventually both, as the major components of CS. This has been mainly due to the lack of specific experimental manipulations of suberin and lignin contents of the CS. The **Chapter II** of this thesis is a publication in which we have addressed this issue. Throughout this study, I introduced precise experimental manipulations of lignin and suberin production, combined with various histochemical and functional assays in order to resolve the longstanding debate regarding chemical nature of CS. This study involves the use of various pharmacological and novel genetic manipulations assays for lignin and suberin production together with reporter gene expression analysis. For manipulation of suberin, transgenic lines expressing a plant cutinase were generated. Interference with lignin production was done by blocking the biosynthesis of monolignol using a genetic approach.

During whole-mount suberin staining of young roots, I observed a very particular pattern of suberin deposition in the endodermis. It first started in a patchy pattern and eventually turned into a continuous signal of endodermal cell files. Interestingly some endodermal cells at that point still did not show any staining. According to the literature, these non-suberized cells are termed “passage cells”, i.e. cells that do not develop the suberin lamellae, but have formed a CS. So far, nothing is known about the function of these non-suberized cells. Yet, the absence of a suberin lamella strongly suggests some communication/exchange function for these cells. The work in **Chapter III** describes my efforts to develop tools to define the passage cells in molecular terms and possibly distinguishing them from primary-stage endodermal cells in younger root parts.

The **Chapter IV** of this thesis is an elaboration of the findings shown in the Chapter II. Transgenic plants expressing the plant Cutinase show a strong degradation of suberin in the endodermis. However, suberin monomer analysis on 5-week-old seedlings, where most of the suberin deposition occurs in the outer periderm, shows a strong reduction in overall suberin monomer accumulation. We were puzzled with how an endodermis-specific plant cutinase would be able to degrade the suberin deposited in the periderm.

This chapter describes the different experimental approaches that I used in order to solve this problem.

Chapter V of this manuscript includes co-author publications. The **Chapter V.A** is a publication about the dirigent-domain containing protein termed as ENHANCED SUBERIN1 (ESB1). The *esb1-1* mutant was originally isolated based on its altered mineral nutrient and trace element content proposed to be caused by increased level of suberin in root endodermis. Work in this study suggests that the ESB1 is part of the lignin polymerization molecular machinery and is essential for the correct formation of the CS. I participated in this work in collaboration with Professor Dr. David Salt from University of Aberdeen, Scotland.

Chapter V.B represents a study in which, the combination of molecular and histochemical techniques allowed the identification of a membrane domain where free diffusion from one side to the other of the plasma membrane (PM) was prevented. This PM domain is formed underneath the CS and is referred to as the "Casparian Strip membrane domain (CSD)". In addition, this chapter highlights the presence of transporters exclusively localized to distinct domains facing either the stele or the cortex.

The **Chapter V.C** introduces a general mechanism in which *Arabidopsis* Retinoblastoma homolog (RBR1) regulates both cell cycle and cell differentiation genes. In *Arabidopsis*, some core cell cycle regulators (cyclin-dependent kinases, CDKs and their cyclin cofactors) were found to be expressed in a specific fashion in the cortex and endodermis initial daughter cells. RBR1 activity is predominantly regulated by CDKAs, hence allows the developmentally programmed activation of the cell cycle machinery to promote formative cell divisions. I participated in this study in order to observe how the generation of additional initial daughter cells and the delayed formation of separate endodermis and cortex files affect the subsequent formation of endodermal differentiation. **Chapter VI** of this manuscript includes a general conclusion and some hopeful valuable perspectives.

As a matter of readability, references for the chapter I and chapter VI are grouped at the end of the manuscript (see chapter VIII), except for the literature referring to chapters III and IV, which are compiled at the end of each of these chapters.

1 Chapter I: General Introduction

1.1 The root: feeding organ of terrestrial plants

Vascular plants evolved a large variety of cell types and organs; each specialized for a defined function. In order to obtain their resources, vascular plants have evolved an underground root system. The root is an organ that anchors the plant and absorbs minerals and water from the soil. In addition to providing structural support to the aerial portion of the plant, roots therefore have the fundamental role of being the interface involved in water and nutrient uptake. Yet, they must at the same time provide an efficient boundary against external biotic and abiotic stresses, such as pathogenic microorganisms or excessive ion concentrations, respectively.

1.1.1 Root growth and development

Root development is a continuous process in which different cell types arise from single cells known as the initials. The initials are responsible for maintaining the cellular organization of the root. This fact was well characterized in the root meristem of *Arabidopsis thaliana*, which has a simple root anatomy and largely reproducible cell lineage relationships. In *Arabidopsis*, initial cells, often termed as “stem cells”, give rise to all cell types of the root. The stem cells surround four mitotically less-active cells referred to as the quiescent center (QC). The region close to the initials in the root meristem are mitotically active early in root development, however, most of the cell divisions occur a short distance above the meristem in a region called zone of cell division or meristematic zone. In addition, hormones are also synthesized in the meristematic region of the root and transported upward to the aerial parts of the plant in order to stimulate plant growth and development. Upwards from the meristematic zone is the zone of elongation, where cells lose their ability to divide and increase their length by several times, driving the expansion of most of the root length and allowing this organ to grow deeper into the soil. The elongation zone is followed by the differentiation zone, in which most of the cells of the primary tissues mature. Root hairs are initiated in this zone (Fig. 1A) (Scheres et al.1995; Dolan et al.1993).

1.1.2 Primary growth and tissue differentiation

Primary growth occurs at the root apical meristem (RAM) which enables the root to extend through the soil and allows shoots to increase their exposure to light and carbon

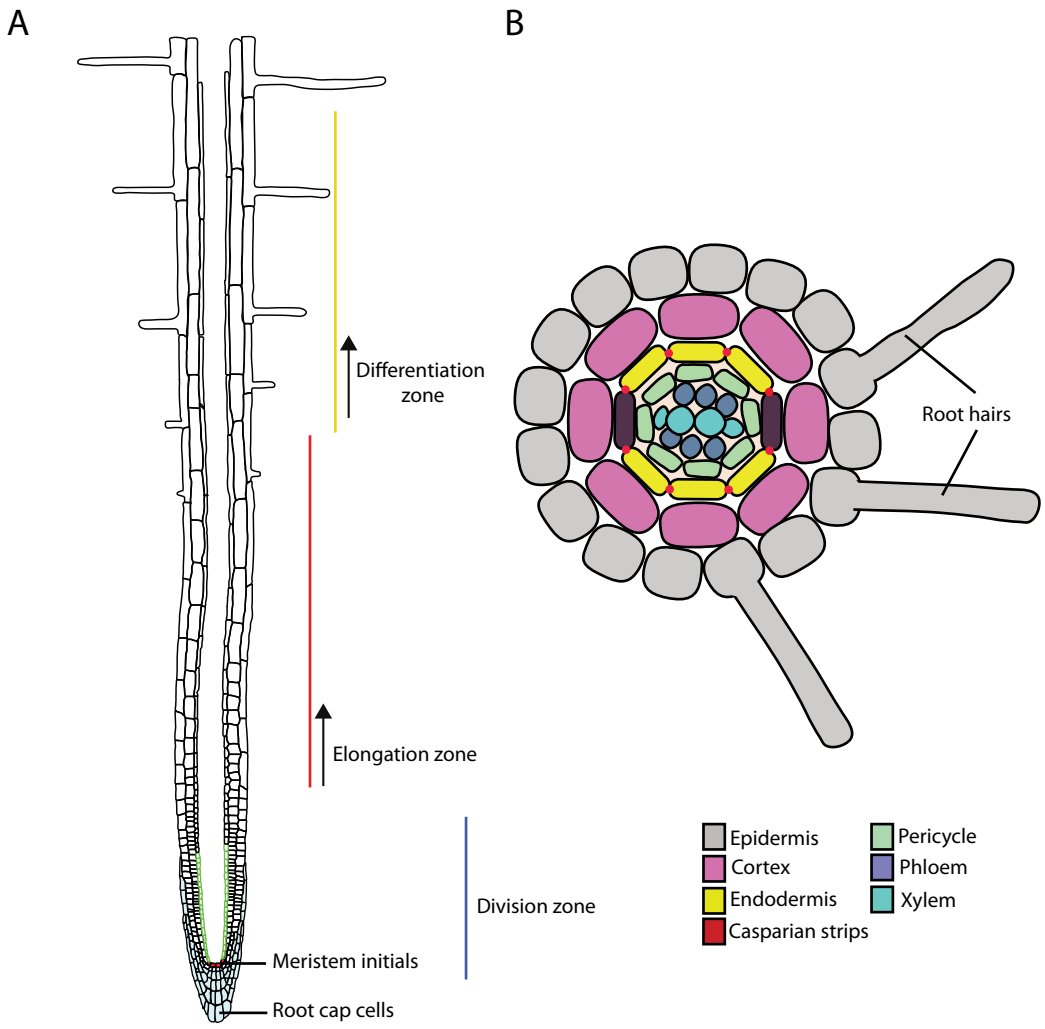

Figure 1: Schematic representation of primary root growth and tissue differentiation.

(A) Root developmental gradient, originating from initial cells with three distinct zones of growth activities; the zone of active cell division, where new cells being produced, the elongation zone, where cells undergo rapid elongation; and the differentiation zone, where cells stops rapid elongation. Differentiated structures such as root hairs appear in this zone.

(B) Schematic overview of the different root tissues. From outer to inner layers: epidermis, cortex endodermis and vascular stele tissues.

(Modified from Alassimone et al (2011), The endodermis: development and differentiation of the plant's inner skin and Geldner (2013), The Endodermis).

dioxide. The root tip is covered by the root cap, which protects the meristem as the root pushes through the soil. During primary growth, RAM give rise to the protoderm, ground meristem and procambium, which differentiate into epidermis, cortex, endodermis, and vascular system, composed of pericycle, primary xylem and primary phloem. These tissues can be simple or complex, consisting of a single cell type or several, depending on the plant species. Exceptionally, *Arabidopsis thaliana* roots has a very simple and well-defined root system consisting of single concentric layers of epidermis, cortex, endodermis and pericycle, encircling the vasculature (Fig. 1B) (Dolan et al.1993). This minimal root system is one of the most remarkable characteristics of *Arabidopsis thaliana*, which make it an excellent system to study cellular differentiation and organ development during plant growth

The epidermis (literally: the outer skin) is an outermost layer of closely packed, thin-walled cells. Root hairs, which arise from this tissue, enormously increase the absorbing surface area of the root and facilitate the absorption of water and minerals. This allows plants to take in more substances of vital importance for their physiology (Gilroy and Jones 2000).

The cortex is a tissue present on the inner side of the epidermis. It is a layer of morphologically rather unspecialized cells that can function as a storage tissue for carbohydrates and oils. It allows the diffusion of water, minerals and oxygen from the root hairs inwards.

The endodermis (literally: the inner skin) is present in all vascular plants and is of central importance for root function. It is characterized by the presence of the Casparian Strip in its walls perpendicular to the surface of the root, as a belt-like structure. In addition, it also contains the suberin lamellae that eventually cover the entire endodermal cells. The endodermis separates the outer cortex from the central core and is a key regulator of water movements into or out of the central stele (Enstone et al. 2002).

The root vascular system mainly consists of pericycle, xylem, and phloem. Both xylem and phloem are positioned in the interior of the pericycle cell layer. The center of vasculature is occupied by xylem, whereas phloem alternates between the arms of the xylem. The pericycle is differentiated into two cell types, the xylem and phloem pole pericycle cells. The former are located at the poles of the xylem axis and are the only

cells competent to become lateral root primordia, whereas the latter occupy the position between the xylem poles (Himanen et al. 2002; Jing Zhou et al. 2013).The vascular system carries out two essential functions. One is to distribute water and essential mineral nutrients to the various plant organs, and the other is to provide mechanical support.

1.1.3 Secondary growth and its effect on primary body of the root

During secondary growth, the vascular cambium arises partly from procambium and partly from pericycle cells located opposite of the primary xylem poles, resulting in the disruption of the primary body of the root (Carlsbecker et al. 2005). In most woody roots, the cork cambium is originated from the pericycle. Consequently, formation of multilayered periderm results in the isolation of the epidermis, cortex, and endodermis from the rest of the root and these cell layers eventually die and are sloughed off. The periderm, or cork, then replaces the epidermis, cortex, and endodermis and acts as the protective covering on this portion of the root. More detailed information concerning the secondary growth and periderm formation is described in Chapter IV.

1.2 The endodermis: the root's border guard

In order to be distributed through the whole plant, water and dissolved nutrients are loaded from the soil into the vasculature via two distinct pathways: the symplastic and the apoplastic pathway. The symplastic pathway represents transport of water and solutes from one cell to the other via plasmodesmata. Plasmodesmata provide intercellular connections that create a cytoplasmic continuum in between cells and allow the transport of nutrients toward the vessels. In contrast, the term “apoplastic pathway” describes the diffusion of compounds within cell wall and extracellular spaces (Fig. 2A). Water flowing through the apoplast contains many minerals that the plant needs, but it may also contain toxins and substances that the plant may not want. As the water is flowing through the apoplast, there is no way to prevent the passive transport of harmful substances. Simultaneously, the root must be able to exclude potentially harmful substances and it must prevent infection by pathogens. This necessary selectivity in root function is provided by the presence of endodermis. The endodermis establishes an apoplastic diffusion barrier surrounding the vasculature by the formation of “Casparian Strip” (CS). CS are the highly localized cell wall impregnation which seals the

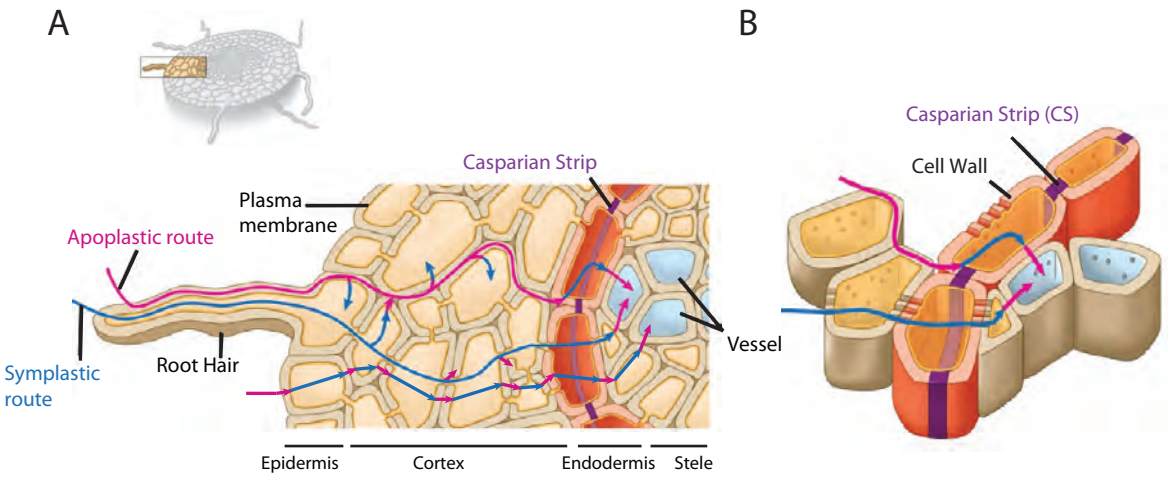

Figure 2: The endodermis presents an apoplastic barrier forcing the nutrients to be selected by plasma membranes.

(A) Cartoon depicting the different nutrient routes toward the vasculature. External compounds can move into the root through the apoplastic route (pink), through the symplastic route (blue) or via combination of both.

(B) Cartoon depicting CS apoplastic barrier.

(Modified from Biology, Campbell and Reece (2002), 6th edition, Pearson education, publishing as Benjamin Cummings).

extracellular space. Therefore, to enter the stele, water and ions absorbed by the plants must enter the symplast of the endodermal cells. From here, it can pass through plasmodesmata into the stele (Fig. 2B) (Enstone et al. 2003; Maule et al. 2008).

The endodermis has been implicated in physical processes, such as maintenance of root pressure and inhibition of ion backflow from stele to the soil, or in abiotic stress responses such as preventing heavy metal or salt entry (Enstone et al. 2002). Thus, this very specific tissue is necessary to control the kind and amount of substances entering into the vasculature.

1.2.1 Endodermis specification

Endodermis specification has been intensively studied over the last decades. Most of our knowledge regarding this process comes from research carried out in the model plant *Arabidopsis thaliana*. Specification of endodermal cells from initials is very well understood and reported to be dependent on the interaction of two transcription factors; SHORT-ROOT (SHR) and SCARECROW (SCR). SHR has been identified as an evolutionarily conserved short-range signal that moves out from the inner tissues of the stele (where it expressed) into the endodermis. Here it interacts with SCR to trigger the periclinal division of cortex-endodermal initials (Di Laurenzio et al. 1996; Helariutta et al. 2000; Nakajima et al. 2001). Interaction with SCR leads to the transcription of target genes and eventually determination of endodermal cell fate. SHR up-regulates the expression of several other transcription factors (Benfey et al. 1993; Helariutta et al. 2000; Scheres et al. 1995; Levesque et al. 2006; Sozzani et al. 2010). Some of these transcription factors, such as JACKDAW, act together with SCR to maintain the SCR/SHR complex. Thus, in the *Arabidopsis* root, the stem cell behavior is controlled through the combined activity of different transcription factors.

Proliferation of endodermal cells in the proximal meristematic zone is gibberellin regulated. Moreover, perturbation of the gibberellin regulation in endodermal cells is sufficient to physically restrict elongation of neighboring tissues, resulting in the restriction of the whole root elongation (Ubeda-Tomas et al. 2008). Recently, it has been reported that gibberellic acid (GA) is specifically accumulated in the endodermis of the root elongation zone, suggesting a specific role of the endodermis in GA regulation

(Shani et al. 2013). This indicates that in addition to its protective role, the endodermis is also fundamental for hormonal control of root development.

1.2.2 Three developmental states of the endodermis

Endodermal cell differentiation in vascular plants has been described in terms of wall-modifications resulting in the development of three different states described hereafter as primary developmental stage or state I, Secondary developmental stage or state II, Tertiary developmental stage or state III. However, the existence of all three states is varying between different plant species.

1.2.2.1 State I; Primary developmental state of endodermis; Casparian Strip (CS)

Robert Caspary described the differentiation feature of the endodermis for the first time in 1865 in terms of a highly localized cell wall deposition in the middle of anticlinal/transversal walls. This localized cell wall impregnation encircles the endodermal cells in a way that it forms a belt or ring-like structure. The perfect alignment and cohesion of these rings, gives rise to a "fishnet" structure termed as "Casparian Strip network", which surrounds the xylem vessels. This structure is highly resistant to an enzymatic treatment with cell wall-degrading enzymes (cellulase and pectinase), which leaves only the resistant walls of xylem vessels and CS intact (Fig. 3A and 3B) (Schreiber et al.1999; Van fleet 1961). It has been known for a long time that this cell wall modification is associated with special features of the underlying plasma membrane, which was shown to be very electron dense and tightly attached to the cell wall upon plasmolysis. When cells with CS are plasmolysed, the protoplast will not be detached from that region of the radial walls where the CS are developed (Bonnett 1968; Karahara and Shibaoka 1992). In *Zea mays*, width of CS has been measured and it covers almost one third of anticlinal walls. This width was also seen to increase in response to certain environmental stimuli, such as salt stresses (Karahara et al. 2004) suggesting that the development and shape of the CS can be regulated by environmental factors.

As suggested by ultrastructural studies, this cell wall thickening is driven by protein scaffolds sitting at the plasma membrane (PM) exactly underneath the position of the CS. In 2010, the zone of protein exclusion named as a "Casparian Strip membrane domain" (CSD) has been introduced by Alassimone et al. in 2010. This plasma membrane domain

A

B

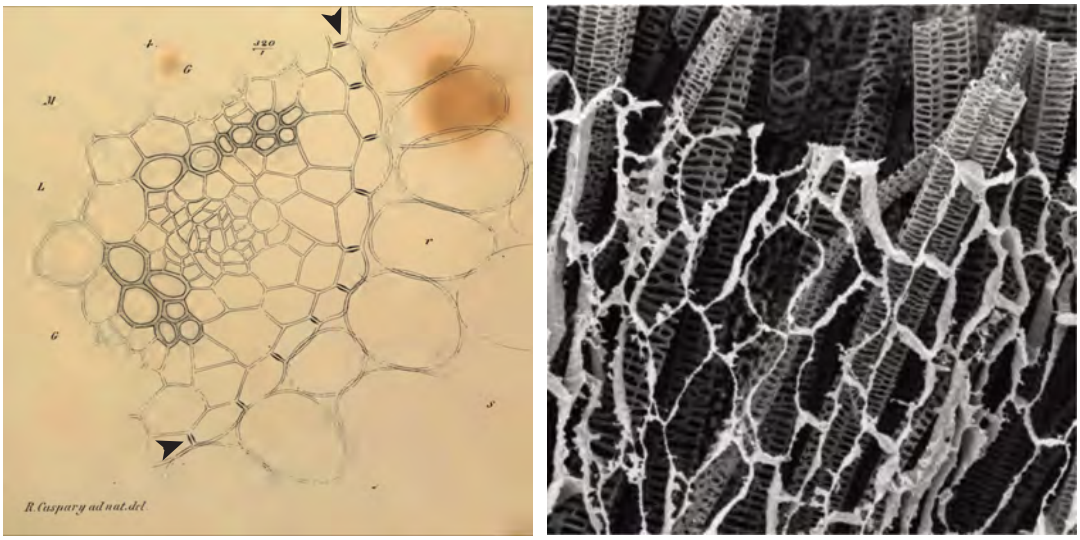

Figure 3: Description of the primary cell wall impregnation (Casparian Strip).
(A) Drawing by Robert Caspary showing the endodermal cell layer with CS in its radial walls shown by black arrows.
(B) Scanning electron microscopic pictures of enzymatically isolated endodermal cell walls, showing the 'fishnet' like structure of the CS after complete digestion with cell wall degrading enzymes. Non digested xylem vessels are shown in the background.
(Adopted from Geldner (2013), The Endodermis).

is formed underneath the CS. After plasmolysis, the CSD remained attached to the cell wall (Chapter V.B; Alassimone et al. 2010). These findings are consistent with the previous hypothesis that a protein-like structure may attach the CSD to the CS (Bonnett 1968; Karahara and Shibaoka 1992). Recently, a family of five transmembrane proteins named as CASPs (Casparian Strip membrane domain Protein) has been identified. These proteins were reported to be localizing precisely to this exclusion zone (CSD). Initially, CASPs were localizing to the plasma membrane, but prior to the development of the CS localize to the depletion zone. Their localization to the exclusion zone before the establishment of CSD suggests an early role for the CASP proteins in CSD formation. Moreover, in a *casp1casp3* double mutant, CS appeared to be more fluorescent and disorganized when compared to the CS of wild type plant. This suggests the roles of CASPs in the correct formation of CS. CASPs are the first proteins identified to localize to the CS. Therefore, they represent an excellent point of entry to explore CS function and formation (Roppolo et al. 2011).

1.2.2.1.1 Chemical nature of Casparian Strip (CS)

In order to understand the function of CS mainly as an apoplastic barrier, the chemical nature of CS must be considered. The chemical composition of CS has been studied for many decades in various species. Since the first description of the CS by Caspary, who described the CS as a biopolymer having characteristics of both *Holzstoff* (lignin) and *Korkstoff* (suberin) there have been many attempts to identify the chemical nature of CS (Geldner 2013). The basic approach in earlier studies was to use light microscopy in connection with histochemistry, giving indirect evidence of the chemical nature of the CS (Wilson and Peterson 1983). Krőmer (1903), using histochemical analysis, described the CS as a polymer of typical lignin. A few years later, Wisselingh (1926), defined the nature of the CS as mainly of lignin, but he also mentioned the presence of suberin-like compounds. Elisei (1941) based on fluorescent microscopic analysis claimed that the CS is only made out of lignin with out any suberin. Later on, Van Fleet (1961) pointed out the presence of phenolic material in the CS and cited several publications that reported the presence of lignin-like compounds based on fluorescence and staining behavior of the CS. In the 1990s, Schreiber's group, based on direct chemical analysis of CS isolated from different monocotyledonous and dicotyledonous plant species characterized the chemical composition of endodermal and hypodermal cell walls. For example, gas

chromatography study on *Clivia miniata* roots showed that lignin was one of the major biopolymers in the CS (Schreiber et al. 1994). Nevertheless, later on, many other groups continued to use the term suberized CS and relates its functional properties mainly with the presence of suberin. Even some major botany textbooks mention the CS as suberized structures. These examples show that in the past few years there was an enormous advancement in solving the puzzling of chemical nature of CS. However, if we consider the example of model plant *Arabidopsis,* there is not much known regarding nature of primary cell wall depositions and their role in the establishment of functional diffusion barrier formation. Mainly because of technical reason, as *Arabidopsis* roots are fragile and do not represent ideal material for chemical analysis, and histochemical studies, which were often used to investigate nature and role of CS.

When I started my PhD thesis, all of the above mention former work represented a somewhat contradicting picture regarding chemical nature of CS. Mainly indicating that the cell wall depositions in CS are characterized by suberin and/or by lignin. From the 90's research has been focused on suberin, and in textbooks and reviews it is often considered the major component of CS. However, the exact chemical nature of CS was still under question. In addition, the relative contributions of suberin and lignin to barrier formation were still unclear mainly due the lack of precise spatial and temporal studies on the different developmental stages of endodermis. The chapter II of this thesis includes the publication that addresses this issue. In this chapter, I introduced specific experimental manipulations of suberin and lignin production in combination with different histochemical and functional assays in order to solve this long-standing question of suberin and lignin presence in the CS.

Lignin versus suberin

Lignin, a polymer of aromatic subunits, constitutes the most abundant organic compound on the earth after cellulose. It is found specifically in vascular plants, and occurs in the secondary cell walls of xylem vessels and tracheids (Ros Barceló A.1997). Lignin is generated by radical coupling of hydroxycinnamyl subunits called monolignols (mainly coniferyl (CA), sinapyl (SA), and p-coumaryl alcohols (p-CA)). synthesized through the common phenylpropanoid pathway and monolignol specific pathway (Fig. 4; Fig. 5) (Humphreys et al. 2002). These are mainly involve the hydroxylation of the

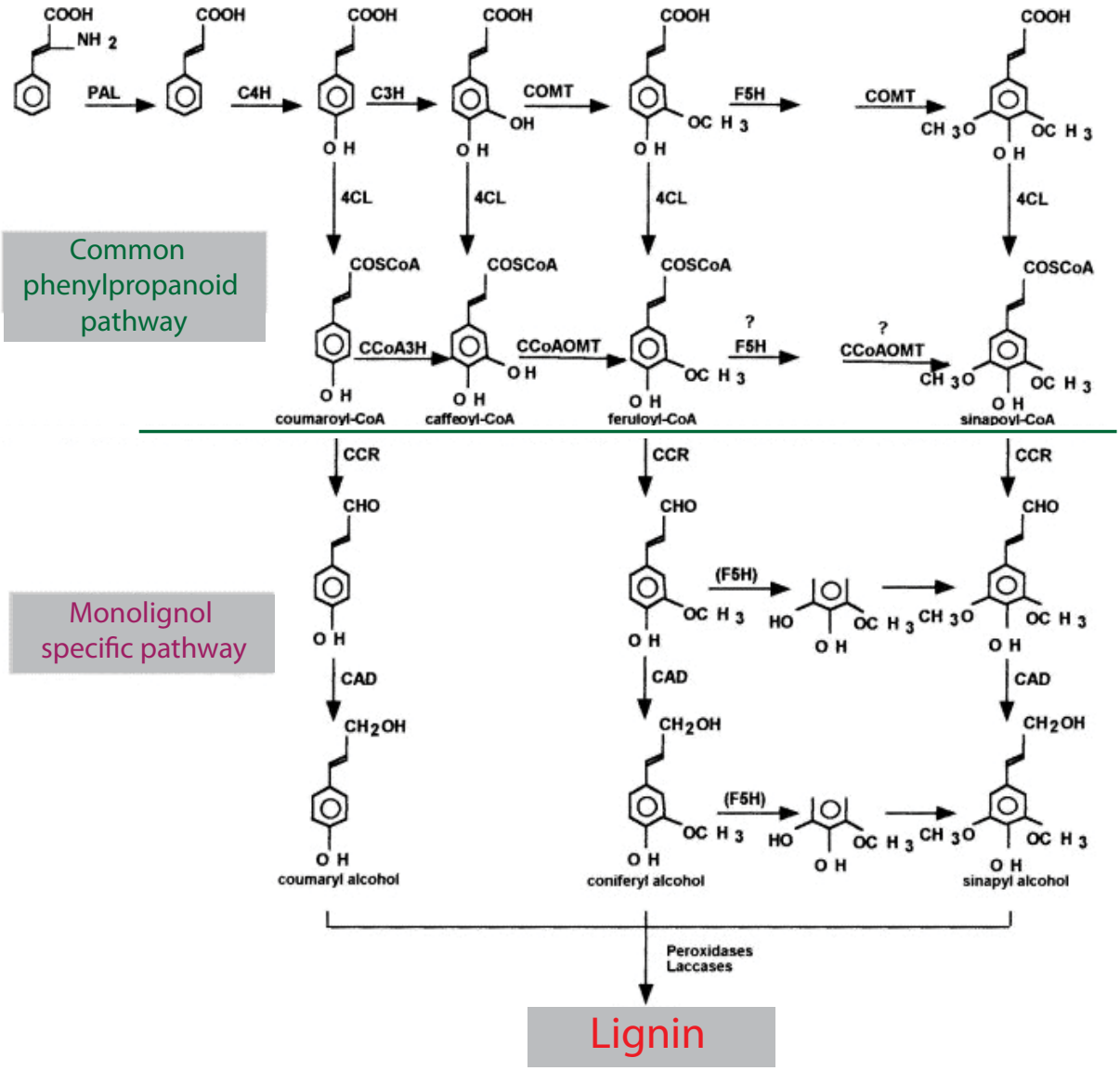

Figure 4: The Lignin biosynthetic pathway.

(Adopted from Alain.M Boudet, 2000. Lignins and lignification: Selected issues. Plant physiology and Biochemistry, 38: 81-96).

PAL	Phenylalanine ammonia-lyase
C4H	Cinnamate-4-hydroxylase
C3H	4-Coumarate-3-hydroxylase
COMT	Caffeic acid 3-O- methyltransferase
CCoAOMT	Caffeoyl-CoA 3-O-methyltransferase
F5H	Ferulate-5-hydroxylase
4CL	Hydroxycinnamate-CoA-ligase
CAD	Cinnamyl alcohol dehydrogenase

aromatic ring, phenolic O-methylation and reduction of a carboxyl group to an alcohol group (Wout Boerjan et al. 2003). After synthesis, monolignols must be transported from the cytosol to the cell wall. In the past few years, different possible mechanisms were proposed for monolignol transport through the plasma membrane, either as free monolignols or as glucosides (Kaisa Marjamaa et al. 2009). After transport of monolignols to the cell wall, lignin is formed through polymerization of these monolignols, process in which is required the oxidation of monolignols. The different classes of protein such as peroxidases and laccases are thought to be responsible for the oxidation of the monolignols (Ŏnnerud et al. 2002). Whether monolignol oxidation occurs through redox shuttle-mediated oxidation was badly understood in the past. However, recently, parallel to my work, the *Arabidopsis* ABCG29 gene, (a member of the ATP-binding cassette transporter subfamily), was characterized as a major transporter of p-coumaryl alcohol (Alejandro et al. 2012). This work suggested that other monolignols may also transported by other ABCG transporters and that this might be the major pathway by which monolignols reach the apoplast. Based on my work in chapter II, Yuree Lee in our group, recently reported that NADPH oxidases, together with peroxidases are involved in the polymerization of lignin monomers. During this process, reactive oxygen species (ROS) from the NADPH oxidases (Respiratory burst oxidase homologs) are channeled towards the cell wall peroxidases which then use the ROS for the polymerization of lignin monomers (Lee et al. 2013). These findings are break troughs in the field of lignin biosynthesis pathway and advance our knowledge of lignin polymerization and transport to the cell wall (See chapter VI for more details).

Suberin is a hydrophobic heteropolymer, consisting of aliphatic polyesters with minor amounts of hydroxycinnamic acids (mainly Ferulic acid) and glycerol (Fig. 6). Major sites of suberin deposition include outer skin of potato tubers, outer bark cells (periderm) and cotton fibers. Internal sites of suberin deposition include seed coat (Espelie et al. 1980), root endodermis (Enstone et al. 2003), bundle sheath of monocots (Espelie and Kolattukudy 1979), and conifer needles (Wu et al. 2003). Suberin deposition also occurs in response to wounding and other abiotic stresses.

Based on the compositional knowledge, the suberin biosynthetic pathway has been well described. It involves different enzymatic activities such as ω-carbon oxidation, fatty acid elongation of long-chain acyl precursors, activation of fatty acids to fatty acyl-CoA

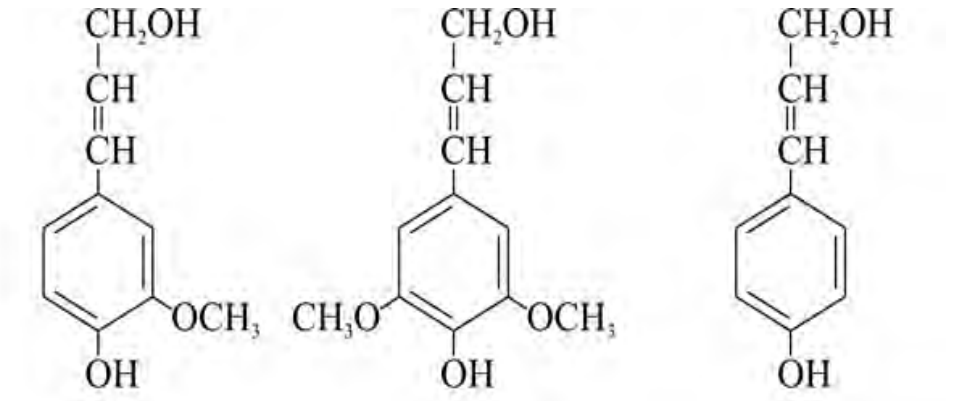

Coniferyl alcohol Sinapyl alcohol P-Coumaryl alcohol

Figure 5: Structure of the three lignin monomers (monolignols).
(Adopted from J. Ralph, et al. 2001).

ω-Hydroxyacids

α,ω-Dicarboxylic acids

Glycerol

Ferulic acid

Figure 6: Schematic representations of the major monomers of suberin.
(Adopted from Rochus Franke. 2007).

thioesters, reduction of acyl chains to primary alcohols, and various acylations, including those involving glycerol, to generate a polyester matrix. The enzymes involved in its synthesis are well described and mainly belong to the CYP86 subfamily of P450 monooxygenases and acyl-transferases of the GPAT family and thought to be mainly localized to the endoplasmic reticulum (ER) (Hofer et al. 2008; Li Y et al. 2007). However, the site of polymerization reactions and transport processes after the polyester synthesis that finally give rise to the highly organized lamellar structure of suberin depositions is still a great mystery.

1.2.2.1.2 Casparian Strips (CS) as an apoplastic diffusion barrier

Analogous to animal epithelia, in which the tight junction of the cell membrane blocks intercellular diffusion, the CS in plants acts as a diffusion barrier that controls the movement of water and ions from soil into the stele (Fig. 2B). The classic work of Rufz de Lavison in 1910 for the first time pointed out the function of the CS as an effective apoplastic barrier to ion movement. Since then it has been reported in many studies that the diffusion of some fluorescent dyes, ions, and heavy metals is blocked at the level of endodermis due to the presence of CS (Peterson 1987; Robards et al. 1974; Singh and Jacobson 1977). The work of White and Broadley (2003) shows that Calcium (Ca^{2+}) is loaded into the stele at the distal root tips and lateral root initiation sites, where the CS is absent or temporarily interrupted. However, Ca^{2+} movement across the endodermis is still unclear (Clarkson 1984; White and Broadley 2003). In accordance with endodermal cells representing the physical border between tissues facing the soil and tissues facing the stele, influx and efflux carriers have been localized to the peripheral (soil-facing) and central (stele-facing) sides of the endodermal plasma membrane depending on their function in uptake or loading of nutrients (See Chapter V.A for detail; Alassimone et al. 2010). These findings suggest that the barrier properties and polar localization of endodermal transporters can be crucial for controlling transport of nutrients from soil to vasculature.

Beyond the selective nutrient uptake, the CS also prevents the extensive ion backflow from the stele to the cortex and maintains root pressure. During transpiration, ions are swept out of the stele and their concentrations in the apoplast are kept low, however under conditions with low or no transpiration, ions may accumulate in the apoplast of the

stele faster than they are removed by the transpiration stream. In this case the concentration gradient in the apoplast favors diffusion back into the cortex and, ultimately to the soil. Thus, the CS may be necessary to prevent this backflow by and increase the plant's ability to transport water upward by creating high concentrations gradient of dissolved ions inside the root. Water with lower concentration of ions outside the root then could diffuse into the stele, creating a higher water pressure at the bottom of the plant resulting in the movement of water up into the plant. (Peterson et al. 1993).

Currently, the role of the endodermis in defense against biotic stresses remains unclear. However, it has been reported that juvenile knot nematodes, after their penetration into the root epidermis, move through the cortical apoplast towards the root tip and finally penetrate the vascular bundle at the meristematic or elongation zone, where the CS is not yet established (Williamson and Gleason 2003). Studies regarding the route of penetration of *Ralstonia solanacearum* colonization in different plant species reports that it also preferentially enters at lateral roots and root tips.

Taken together, all these observations strongly indicate that apoplastic transport in plant roots is blocked when they form CS. However, due to the lack of knowledge regarding the exact chemical nature of CS, its exact role as an apoplastic barrier has remained unclear.

1.2.2.1.3 Casparian Strip in other plant tissues

In addition to the endodermis, the CS are also formed in other plant tissues. Formation of CS in different tissues also defines its functional properties. For example, the exodermis is often compared to the endodermis because of the presence of similar differentiation events that occur in the endodermis (Enstone et al. 2002). The CS of the exodermis is also reported to be impermeable to ions and provides a substantial peripheral resistance to the entry of water and solutes into the apoplast (Peterson 1987; Hose et al. 2001).

The presence of CS-like structures has also been reported in the needles of *Pinus bungeana*. However, these CS are reported to be less solute impermeable than those of the root endodermis (Wu X et al. 2005). The vasculature of the aerials parts of the plants is also reported to be surrounded be a protective tissue called the bundle sheath. This tissue has often been compared to the endodermis as it can provide an apoplastic barrier,

forcing the trans-cellular passage of any substance that needs to reach the central tissues (Esau 1977). There are a few morphological studies describing the presence of CS-like structures in the bundle sheath, but they are rather unclear and controversial. Other reports on the induction of the CS during etiolating processes are also very unclear and might deserve more in-depth investigation (Lersten 1997). In some plant species, formation of the CS was also observed in response to salinity (Karahara et al. 2004). Recently, the CS was also detected in the mature phellem cells in both root and stem of *Pelargonium hortorum* (Meyer and Peterson 2011). However, besides all these examples, the root endodermis clearly represents the only cell layer where a CS is formed in all plant species.

1.2.2.2 State II; Secondary developmental stage of endodermis; Suberin lamellae

The secondary developmental stage of the endodermis is characterized by the formation of suberin lamellae onto the inner surface of primary cell wall. Suberin deposition eventually covers the entire endodermal cell except in the regions occupied by plasmodesmata. Thus, these cells cannot facilitate any plasma membrane exchanges, but are still connected to the surrounding cells, allowing passage of ions (Clarkson et al. 1987; Enstone et al. 2003). According to transmission electron microscopy studies (TEM), suberin exhibits the typical electron-dense and translucent lamellar ultrastructure comprises of alternating light and dark bands (Bernards 2002; Martinka et al. 2012). Suberin can be found in the root endodermis of all angiosperm species and in the exodermis or hypodermal cell walls of primary roots in different monocots (Ma and Peterson 2003). In some species (*Typha* and *Phragmites*) precursors of the suberin lamellae were found prior to CS development (Seago et al.1999). However, unlike Casparian Strips, suberin lamellae are not formed in the root of all the plant species.

1.2.2.2.1 Chemical nature of Suberin

In 1980, Kolattukudy described suberin as a biopolymer composed of two domains, a polyaliphatic (cutin-like polymer) and a polyaromatic domain (lignin-like polymer), based on the isolation of depolymerized compounds from mature tissues. However, monomer composition of these two domains varies among different species and cell types (Zeier et al.1999). In general, aliphatic suberin is primarily composed of oxygenated fatty acid derivatives. However, the polyaromatic domain is characterized as

a polyphenolic domain as it contains some unique kind of phenolics (hydroxycinnamic acids, predominantly ferulate) that are different from lignin (Bernard et al. 2001). These two domains are supposed to be cross-linked. Later on, work by Lulai and Freeman (2001) reported that there is no covalent connectivity between the polyaromatic and polyaliphatic domains.

The aliphatic domain of suberin is well described in different plant species and for the function of suberin as an apoplastic barrier; this domain will be of primary importance. However, the structure and function of the polyphenolic polymer is not yet fully understood. Recently, an *Arabidopsis* gene named Aliphatic Suberin Feruloyl Transferase (ASFT) that encodes feruloyl transferase has been identified and reported to be required for the deposition of ferulate in suberin. However, the loss of this monomer has no affect on the formation of suberin lamellae (Li Y et al. 2007).

Glycerol has been also reported as one of the major components of suberin in some plant species, which act as a bridge between the two distinct domains of suberin. Alcohols and un-substituted fatty acids are minor components also reported to be present in suberin (Frank et al. 2007).

Since the work of Kolattakudy and others, considerable progress has been made in describing the detailed and exact chemical nature of suberin lamellae. Many research groups also applied different technique specific for lignin analysis in order to study the suberized tissue. For example alkaline nitrobenzene oxidation and thioacidolysis (methods used for lignin degradation, detection and characterization). However, results obtained by applying these methods on suberized tissue reveal rather more complicating picture then solving this issue.

However, even after significant progress in recent years, chemical nature of suberin itself still is a matter of controversy, especially in *Arabidopsis* in which endodermal suberin has never been measured specifically in young roots. In addition, the development of other suberized layers such as the periderm is not well described. In addition, there are currently no strong mutants of suberin biosynthesis available.

Summing up the former work, its seems that terminology use to define suberin (a polymer containing polyaromatic/lignin-like and polyaliphatic domain) is more

confusing then useful when it come to solving the problem of the chemical nature of CS. For us it was important to define two polymers as having their own identity. If we consider the example of Cutin (polymer found in the cuticule of aerial plant organ), amounts of *p*-Coumaric acid and ferulic acid have been identified as minor constituents (Robert and Kolattukudy 1975). Yet, in the literature, cutin is always described narrowly as a polymer of hydroxy fatty acid rather than using the conflicting terms to demonstrate the presence of aromatic compounds. Since the endodermis contains both a lignin-like polymer and a poly-aliphatic polymer, it is important to use the terms lignin and suberin narrowly, instead of introducing a domain nomenclature in which the term "suberin" encompasses two polymers of a chemically very different nature. In Chapter II of this thesis, we precisely describe the distinction between lignin and suberin appearance in young *Arabidopsis* roots.

1.2.2.2.2 Suberin lamella as an apoplastic barrier

The chemical composition and site of suberin deposition determine its physiological roles. Plants synthesize suberin in order to create a hydrophobic barrier to control the water and solute transport and to provide a barrier against environmental stresses. Suberin deposition in external tissues for example in the periderm of root and outer skin of potato tuber act as an efficient apoplastic barrier that strongly reduces the movement of water, dissolved nutrients and ions (Schönherr and Ziegler 1980). Clarkson and Robards (1975) reported that in barley, deposition of suberin in endodermal cells decreased the movement of water and calcium into the stele. Suberin lamellae have also been described as a boundary against ion entrance into the stele, for example chloride (precipitated with silver salts) is clearly blocked by the suberin lamella (Lauchli 1976).

The role of suberin lamella as an apoplastic barrier against water and ion transport was largely studied in different plant species. Previously, it has been reported that the amount of suberin in corn roots is negatively correlated with the water uptake (Zimmerman et al. 2000). Recently, it has been shown in the model plant *Arabidopsis* that reduced amounts of suberin resulted in increased water permeability (Höfer R et al. 2008). However, in contrast enhanced suberin mutant (*esb1)* with enhanced levels of suberin, failed to reduce the water permeability, but exhibits increased tolerance to salt and drought stress condition (Baxter et al. 2009).

Besides all these studies, direct correlation between altered amounts and compositions of suberin and its role as apoplastic barrier against water and nutrient transport is still lacking. The major reason behind this is the controversy regarding the site of suberin deposition and its chemical nature. The apoplastic barrier function of suberin deposition was classically related to its polyaliphatic domain. Why? As the polyaliphatic domain of suberin is very similar to cutin, which is mainly deposited in the epidermal cuticle and provides a resistance barrier against water and pathogen attack. As suberin shares, roughly, the chemical composition with cutin, it was believed that they had to have similar functions. Since the suberin lamella is located between the primary cell wall and plasma membrane and not in the wall itself, it may rather prevent the movement of ions into the individual cells it surrounds. Diffusion in between cells could rather be blocked by an impregnation of the primary cell wall with a lignin-like polymer.

Suberin also plays an important role to act as an antimicrobial barrier against pathogens (Lulai and Corsini 1998). The suberin lamellae serve as one of the last lines of defense before pathogens invade the vascular cylinder and spread throughout the plant (Kolattukudy and Espelie 1989).

Suberization can also occur in response to wounding, pathogen attacks and in response to abiotic stresses (drought and salt stress) (Agrios 1997)**.** In past, several studies also report the deposition of additional suberin in response to the fungal or viral attacks around the site of penetration mainly to limit the spread of infection (Tripplett 1984; Kolattukudy and Espelie 1989). Role of suberin and suberization in plant defense against pathogen can be considered as a useful tool to increase resistance in specific plant-pathogen interactions.

Between states I and II; Passage cells: Primary stage cells in secondary stage

During the endodermis development, an intermediate zone is formed where endodermal cells in the primary state are surrounded by endodermal cells in the secondary state. The surrounded primary cells are termed as “passage cells”. Passage cells are characterized by the absence of suberin lamellae formation but do contain CS. It has been reported that the process of suberin lamellae development does not start simultaneously in all endodermal cells. The first development occurs opposite the phloem pole endodermal cells and then spreads to the part of endodermal cells opposite the xylem poles.

Therefore, the endodermal cells opposite the xylem poles do not develop suberin lamellae, what can be seen as a delay of cell wall development (Fig. 7) (Clarkson and Robards 1975; Peterson and Enstone 1996).

The assumption underlying the term “passage cells” was clearly stated by Esau (1965) as, “The name passage cells are based on the assumption that the cells allow a limited transfer of material between the cortex and the vascular cylinder”.

Clarkson et al. (1971) reported that radiolabelled phosphate ions uptake into the stele in barley roots correlates with the presence of passage cells. Later on, Robards et al. (1973) reported that the transport of radiolabelled strontium (calcium tracer) across the endodermis was remarkably decreased at the zone where suberin lamellae are formed. Peterson and Enstone (1996) explain these results by assuming that calcium moves in a radial fashion into the root through the epidermis and cortex by the apoplastic pathway. Then, it enters to the symplast of the endodermis. Suberin lamellae formation blocks the transport of calcium into suberized cells. However, ATP-dependent plasma membrane calcium pumps could then allow the transport of calcium from the cytoplasm of the passage cells into the stele. Baxter et al. in 2009 reported that an increased level of suberin in *esb1* mutant (enhanced suberin) is associated with the decreased level of calcium, magnesium, and zinc in the shoot. Recently, in collaboration with Prof. Dr. David Salt (University of Aberdeen, UK) we re-characterized the *esb1 mutant* and showed that it not only displays an early appearance of suberin, as described before, but also lacks the non-suberised passage cells (Hosmani et al. 2013). Clearly, it could be this lack of non-suberised cells that affects the ion transfer across the endodermis. (See Chapter III for details).

1.2.2.3 State III; Tertiary developmental stage of endodermis

In some plant species, especially in monocots and a few dicots, the secondary developmental stage of endodermis is followed by the heavy deposition of cellulose on the inner periclinal and radial walls, but not on the outer periclinal wall. This give cells a U-shaped appearance in the transversal view. There is no data available that describes the presence and biological role of this tertiary developmental stage especially in *Arabidopsis.* However, this U-shaped cell wall deposition has been assumed to aid in mechanical support of the root (Enstone et al. 2002; Geldner 2013). The work of Lukas

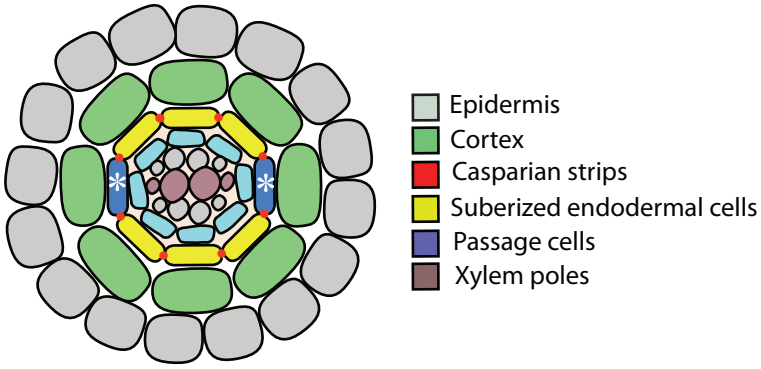

Figure 7: Schematic representation of endodermal passage cells across the xylem poles (blue) surrounded by suberized endodermal cells (yellow).

Cartoon depicting the position of passage cells across the xylem poles (mark with asterisk) with dot -like appearance of Casparian Strip (primary cell wall modification) and the absence of suberin lamellae formation (secondary cell wall modification).

Schreiber (1999) regarding the chemical composition of endodermal differentiation stages in different plant species shows presence of a high content of cellulose and xylan in the tertiary cell wall deposits. It has been reported that lignified secondary cell walls involved in mechanical support are known to have high xylan contents, supporting the view that the tertiary endodermal cell wall deposits contribute to mechanical stabilization (Seago et al. 2000).

2 Chapter II: Casparian Strip diffusion barrier in *Arabidopsis* is made of a lignin polymer without suberin

Sadaf Naseer, Yuree Lee, Catherine Lapierre, Rochus Franke, Christiane Nawrath, Niko Geldner. 2012. Casparian strip diffusion barrier in *Arabidopsis* is made of a lignin polymer without suberin. Proc. Natl. Acad. Sci. USA 109:10101–6.

2.1 Collaborators and Contributions

The main aim of this study was to solve the long-standing controversy regarding the chemical composition of Casparian Strip (CS). In this study, we show that lignin is the major component of early CS and is sufficient to establish a functional apoplastic diffusion barrier in *Arabidopsis*. By contrast, suberin is neither present nor required in early CS and for the establishment of an apoplastic barrier at least in young roots.

I contributed to the design of the study and did most of the experiments. Multiple insertion mutants of lignin biosynthetic pathway were generated and analyzed by Dr. Yuree Lee (Figure 4J and Supplementary Figure S6). Promoter::GUS fusion lines shown in Figure 2A-H were generated by Dr. Yuree Lee, but analysed by myself. Lignin monomer analysis was performed by Catherine Lapierre (Institut National de la Recherche Agronomique, Versailles, France). I prepared all figures and actively participated in the writing of the manuscript.

2.2 Original article

For details, the article is attached herewith.

Casparian strip diffusion barrier in *Arabidopsis* is made of a lignin polymer without suberin

Sadaf Naseer[a], Yuree Lee[a], Catherine Lapierre[b], Rochus Franke[c], Christiane Nawrath[a], and Niko Geldner[a,1]

[a]Department of Plant Molecular Biology, Biophore, Campus UNIL-Sorge, University of Lausanne, CH-1015 Lausanne, Switzerland; [b]Institut Jean-Pierre Bourgin, Institut National de la Recherche Agronomique-AgroParisTech, Unité Mixte de Recherche 1318, F-78026 Versailles, France; and [c]Ecophysiology of Plants, Institute of Cellular and Molecular Botany, University of Bonn, D-53115 Bonn, Germany

Edited by Philip N. Benfey, Duke University, Durham, NC, and approved May 7, 2012 (received for review April 12, 2012)

Casparian strips are ring-like cell-wall modifications in the root endodermis of vascular plants. Their presence generates a paracellular barrier, analogous to animal tight junctions, that is thought to be crucial for selective nutrient uptake, exclusion of pathogens, and many other processes. Despite their importance, the chemical nature of Casparian strips has remained a matter of debate, confounding further molecular analysis. Suberin, lignin, lignin-like polymers, or both, have been claimed to make up Casparian strips. Here we show that, in *Arabidopsis*, suberin is produced much too late to take part in Casparian strip formation. In addition, we have generated plants devoid of any detectable suberin, which still establish functional Casparian strips. In contrast, manipulating lignin biosynthesis abrogates Casparian strip formation. Finally, monolignol feeding and lignin-specific chemical analysis indicates the presence of archetypal lignin in Casparian strips. Our findings establish the chemical nature of the primary root-diffusion barrier in *Arabidopsis* and enable a mechanistic dissection of the formation of Casparian strips, which are an independent way of generating tight junctions in eukaryotes.

root development | plant nutrition | polarized epithelium

In plants, establishment of a paracellular diffusion barrier is more complex than in animals because it cannot be achieved through direct protein-mediated cell-cell contacts. Instead, establishment of the barrier relies on the coordinated, localized impregnation of the plant cell wall, guided by protein platforms in the plasma membrane of neighboring cells. This very different way of generating a tight junction remains badly understood in molecular terms. The Casparian strips of the endodermis are such localized impregnations of the primary cell wall. The strips render these walls more hydrophobic and resistant to chemical and enzymatic degradation and represent the primary diffusion barrier in young roots. Recently, a family of transmembrane proteins has been identified that is important for the localized deposition of Casparian strips. These Casparian strip membrane domain proteins (CASPs) represent the first proteins to localize to the Casparian strips and, it has been speculated that their function consists in providing a membrane platform for the localized recruitment of polymerizing enzymes (1). For a further mechanistic dissection of Casparian strip formation, it is very important to understand from what kind of polymer early Casparian strips are actually made. Unfortunately, the chemical nature of the Casparian strip polymer has remained a contentious issue for more than a century. Its discoverer, Robert Caspary, pointed out that its resistance to chemical treatments did not allow distinguishing whether it is made of "Holzstoff" (lignin) or "Korkstoff" (suberin) (2). In the following, it was concluded that Casparian strips are made of suberin, an aliphatic polyester that is the main component of cork (3). However, other works found evidence that Casparian strips largely consist of a lignin-like polymer (4). Major current textbooks now describe the Casparian strip as an essentially suberin-based structure (5–8). It is indeed intuitive to assume that Casparian strips are made of suberin because their function as an extracellular (apoplastic) diffusion barrier could be perfectly fulfilled by this hydrophobic polymer. A number of problems have long prevented drawing conclusions about the chemical nature of Casparian strips. First, the ring-like Casparian strips represent only the first stage of endodermal differentiation, which is followed by the deposition of suberin lamellae all around the cellular surface of endodermal cells (secondary stage) (9). Therefore, chemical analysis of whole roots, or even of isolated endodermal tissues, will always find both of the polymers present. Additionally, lignified xylem vessels and suberised/lignified dermal tissues form in close proximity to the endodermis and need to be separated from the Casparian strips for chemical analysis. The few studies that attempted such dissections actually found lignin in Casparian strips, but suberin was also invariably detected (9–11). Natural variation between species could partially explain some of the conflicting results (9, 12). Most importantly, however, there has been a lack of experimental manipulations of suberin and lignin content of the Casparian strips. Only these manipulations could determine which of the polymers is relevant for their functionality as a diffusion barrier. *Arabidopsis*, which allows for precise experimental manipulations, has been absent from most of the older studies, not being a traditional object of botanists. In addition, its very small root system renders chemical analysis and classic histochemical stainings challenging.

Here, we present a precise developmental staging of the appearance of various histochemical stains for suberin and lignin in *Arabidopsis*, using whole-mount staining procedures. This process is combined with functional assays, reporter gene expression analysis, in addition to various pharmacological and novel genetic manipulations of lignin and suberin production. Taken together, our data indicate that, in *Arabidopsis*, suberin is neither present nor required in early Casparian strips, and that the initial endodermal diffusion barrier is made of a lignin polymer.

Results

We had shown previously that the fluorescent dye propidium iodide (PI), widely used to highlight cell walls of *Arabidopsis* roots, can also be used as a convenient apoplastic tracer, the diffusion of which into the inner cell layers of the stele is blocked upon appearance of Casparian strips. PI therefore represents a powerful tool to visualize the presence of a functional endodermal diffusion barrier. Using PI, we compared the cellular distance from the meristem at which the diffusion barrier appears to that of green autofluorescence, indicative of phenolic, lignin-like, compounds and to Fluorol yellow staining, a fluorescent suberin dye (13) (Fig. 1). To our surprise, we observed a radical difference in the onset of the two signals. Although appearance of the green

Author contributions: C.N. and N.G. designed research; S.N., Y.L., C.L., and R.F. performed research; C.N. contributed new reagents/analytic tools; S.N., Y.L., C.L., R.F., and N.G. analyzed data; and S.N. and N.G. wrote the paper.

The authors declare no conflict of interest.

This article is a PNAS Direct Submission.

[1]To whom correspondence should be addressed. E-mail: Niko.Geldner@unil.ch.

This article contains supporting information online at www.pnas.org/lookup/suppl/doi:10.1073/pnas.1205726109/-/DCSupplemental.

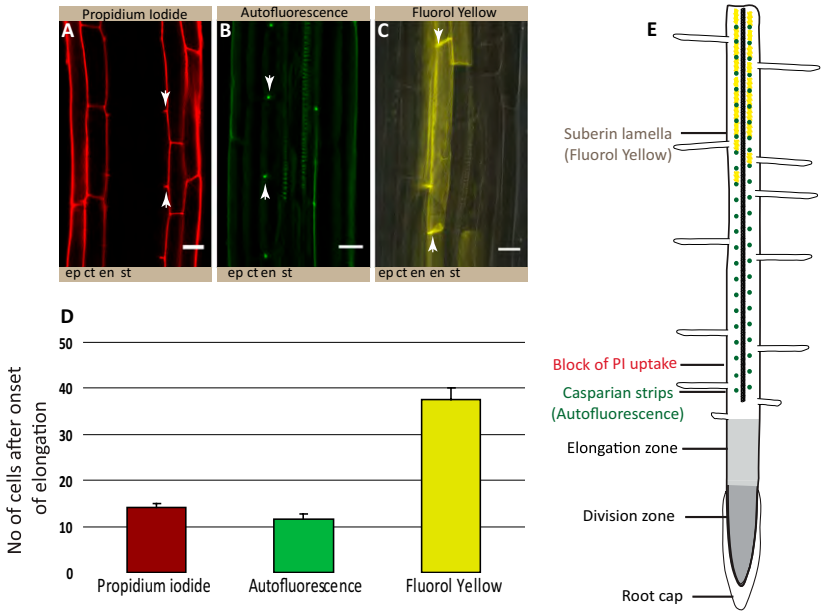

Fig. 1. Lignin, but not suberin stains, correlate with the appearance of the endodermal diffusion barrier. (*A*) Penetration of PI into the stele is blocked at 14.2 ± 0.6 endodermal cells after onset of elongation. (*B*) Dot-like appearance of Casparian strip formation at 11.7 ± 0.9 endodermal cells as visualized by green autofluorescence after clearing. (*C*) Fluorol yellow staining reveals the presence of lamellar suberin on the cellular surface of endodermal cells at 37.5 ± 2.6 endodermal cells. (Scale bars, 20 μm.) (*D*) Quantification of *A*–*C* shows that appearance of green autofluorescence correlates well with block of PI uptake; Fluorol yellow signal appears much later. (*E*) Root schematic showing the different root zones and stages of endodermal differentiation as inferred from *A*–*D*. Stele (st), endodermis (en), cortex (ct), epidermis (ep). *A*–*D*: $n \geq 20$ roots counted per condition. "Onset of elongation" was defined as the zone where an endodermal cell was clearly more than twice its width.

autofluorescence coincided precisely with the block of PI diffusion, Fluorol yellow staining appeared only much later (Fig. 1 *D* and *E*). Moreover, only green autofluorescence appeared as restricted dots in the transversal endodermal cell walls of median, longitudinal optical sections, as would be expected for a Casparian strip signal (Fig. 1*B*). In contrast, Fluorol yellow stain appeared on all cellular surfaces together, and it was impossible to observe a restricted, dot-like staining of the Casparian strip, even in initial stages (Fig. 1*C*). Interestingly, Fluorol yellow appeared in a particular fashion in which individual endodermal cells started to stain very strongly, but neighboring ones did not show any staining. This process led to an initially "patchy" appearance of the suberin stain, which only gradually turned into a continuous signal of endodermal cell files (Fig. 1*C*). We then tested a number of additional histochemical stains for lignin. All of the tested lignin stains showed an early dot-like appearance, coinciding with the block of PI uptake (Fig. S1). Taken together, the data in this analysis pointed to a lignin-like polymer as the initial constituent of Casparian strips and did not support an involvement of suberin. However, it is possible that a stain like Fluorol yellow only detects suberin lamellae, but would not pick up suberin that is associated with lignin in the Casparian strip. To address this possibility, we decided to detect the promoter activities of a number of different suberin biosynthetic genes covering most of the known biosynthetic steps. Essentially all promoter::GUS fusion showed specific activity in the endodermis and all except one displayed a very late and patchy onset of activity (Fig. 2 *A* and *I*), closely matching the appearance of the Fluorol yellow stain (Fig. 2 *J* and *K*). This finding

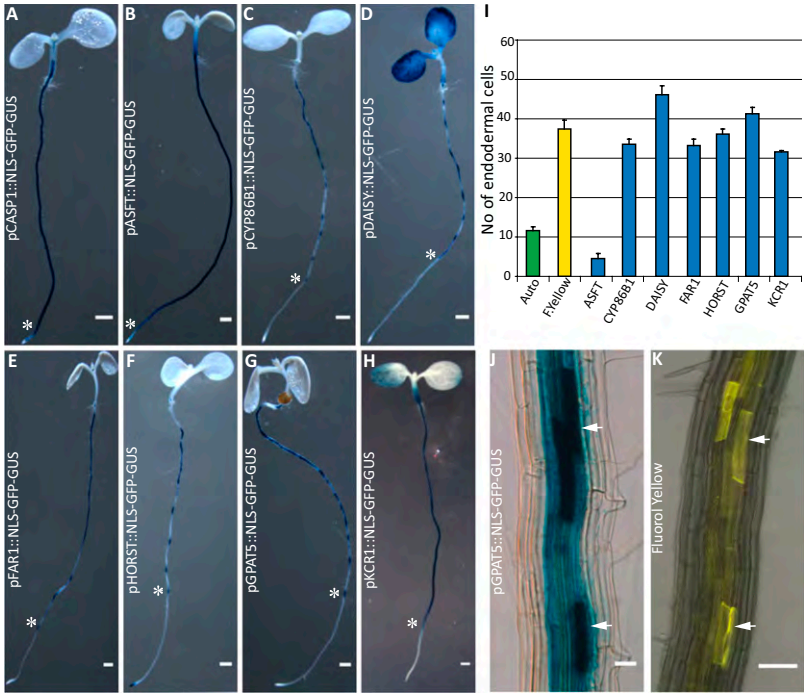

Fig. 2. Suberin biosynthetic genes are turned on after Casparian strip formation. Endodermis-specific Promoter::GUS fusion activity of (*A*) pCASP1::NLS-GFP-GUS, (*B*) pASFT::NLS-GFP-GUS, (*C*) pCYP86B1::NLS-GFP-GUS, (*D*) pDAISY::NLS-GFP-GUS, (*E*) pFAR1::NLS-GFP-GUS, (*F*) pHORST::NLS-GFP-GUS, (*G*) pGPAT5::NLS-GFP-GUS, (*H*) pKCR1::NLS-GFP-GUS; asterisks mark the start of GUS expression. n = 16 roots counted. (*I*) Quantifiation of the cellular distance from the meristem at which onset of GUS expression is observed. Appearance of all but one suberin biosynthetic reporter gene coincided well with appearance of Fluorol yellow signals but not with appearance of green autofluorescence. (*J* and *K*) Arrowheads point to patchy GUS-expression pattern (*J*), which matches closely the patterns observed with Fluorol yellow stains (*K*) (Scale bars, 50 μm.)

strongly suggests that Fluorol yellow adequately reports the presence of suberin and that the biosynthetic machinery for suberin is simply not present at the moment of Casparian strip formation. A notable exception among the suberin biosynthetic genes is *ASFT*, which is turned on as early as the *CASP1* promoter and thus slightly precedes formation of Casparian strips (Fig. 2 *A* and *B*, and Fig. S2). ALIPHATIC SUBERIN FERULOYL TRANSFERASE (ASFT) catalyses transfer of ferulic acid onto aliphatic chains (14, 15). On its own, ASFT cannot possibly mediate formation of a suberin polymer, but its early activity could allow the integration of some aliphatic ferulic acid esters into Casparian strips. Finally, we tested whether genetic interference with suberin formation or accumulation had any effect on the presence or functionality of the Casparian strips. Because of redundancy, there are currently no strong, single gene knock-outs of suberin biosynthesis. Nevertheless, we were able to observe a significant delay in the appearance of Fluorol yellow stains in insertion mutants of *HORST*, as well as for other suberin biosynthetic mutants (16) (Fig. 3*A* and Fig. S3). Despite this delay, however, no difference could be observed in the appearance of Casparian strip autofluorescence or block in PI uptake (Fig. 3 *B* and *C*, and Fig. S3).

To obtain a stronger interference with suberin accumulation, we decided to express CUTICLE DESTRUCTION FACTOR 1 (CDEF1), a plant-encoded cutinase (17), under an endodermis-specific promoter. Cutin and suberin show extensive structural similarity, which made it plausible that a cutinase would also effectively degrade suberin. Strikingly, we observed a complete lack of suberin staining in otherwise normal seedling roots in these transgenic lines (Fig. 3*D*). To our knowledge, such a strong, specific interference with suberin accumulation has never been reported and this line will be extremely useful to assess the many supposed physiological roles of suberin in roots. Despite this strong interference with suberin, the appearance of autofluorescent Casparian strips and the PI diffusion barrier remained unaltered (Fig. 3 *E*–*G*). We also observed similar effects by inducible expression of a fungal cutinase (18) (Fig. S4). Thus, our genetic manipulations strongly support the notion that suberin is neither present nor required for the establishment of the Casparian strip diffusion barrier. We then undertook reverse experiments, aimed at specifically blocking lignin biosynthesis. To do so, we used piperonylic acid (PA), targeting an early step in the biosynthesis of monolignols (19). Twenty-four hours of PA treatment does not interfere with continued root growth but clearly affects lignin levels in roots (Fig. S5). However, the treatment led to a dramatic, apparent upward-shift of Casparian strip appearance with respect to the root tip (Fig. 4 *A*–*C* and *E*). This shift results from a block of Casparian strip formation in all newly forming cells. Accordingly, PI penetration was also shifted upwards by a comparable numbers of cells (Fig. 4 *F*, *G*, and *I*). In contrast, the establishment of suberin lamellae was not affected by the treatment (Fig. S6*A*). Exactly the same effects were observed when using a different lignin biosynthetic inhibitor, 2-aminoindan-2-phosphonic acid (AIP) (20) (Fig. S6*B*), acting on a different target in the pathway. Although PA and AIP certainly block monolignol biosynthesis, their early action in the pathway will also lead to a block of other parts of the phenylpropanoid metabolic network. We therefore attempted to complement the inhibitor-induced defects by simultaneous addition of the two canonical components of Angiosperm lignin, coniferyl-, and sinapyl alcohols. Strikingly, the exogenous application of these two compounds allowed the formation of autofluorescent Casparian strips and a functional diffusion barrier, with coniferyl alcohol being the most effective (Fig. 4 *C*–*H* and Fig. S7). This complementation indicates that functional Casparian strips can be made exclusively of the typical monomers found in other lignified tissues, such as xylem vessels.

We then tried to more specifically interfere with monolignol biosynthesis by a genetic approach. This process is very challenging because of the high redundancy within the enzyme families involved (21). However, once a sufficient number of biosynthetic mutants were combined, we expectedly observed pleiotropic germination and growth defects. In independent allelic combinations of a triple and a quintuple insertion mutant, we could nevertheless observe a clear delay in the formation of the PI diffusion barrier (Fig. 4*J* and Fig. S6*C*). Taken together, our results provide strong evidence that the Casparian strip polymer is made from monolignols and that it consists either of conventional lignin or a very similar, lignin-like structure. We therefore sought for ways that would allow a direct chemical analysis of exclusively Casparian strips. Because of the small size of *Arabidopsis* roots, we considered a direct separation of the early Casparian strip network from lignified xylem vessels to be unfeasible. As an alternative, we decided to make use of an *Arabidopsis* mutant, *arabidopsis histidine transfer protein 6* (*ahp6*) (22), which we treated with low amounts of cytokinin. This combination causes strongly delayed xylem differentiation but does not affect formation of Casparian strips (Fig. 5 *A*–*D*). In this way, we generated a root zone, sufficiently long for dissection, that harbors Casparian strips as the only lignified structures. We prepared sufficient material from the first 5 mm of root tips and subjected the samples to thioacidolysis, followed by GC-MS analysis. In this way, we could obtain direct, chemical data on the composition of Casparian strips. As expected, total amount of lignin in these samples was very low. Nonetheless, we were able to unambiguously identify the typical lignin units from their

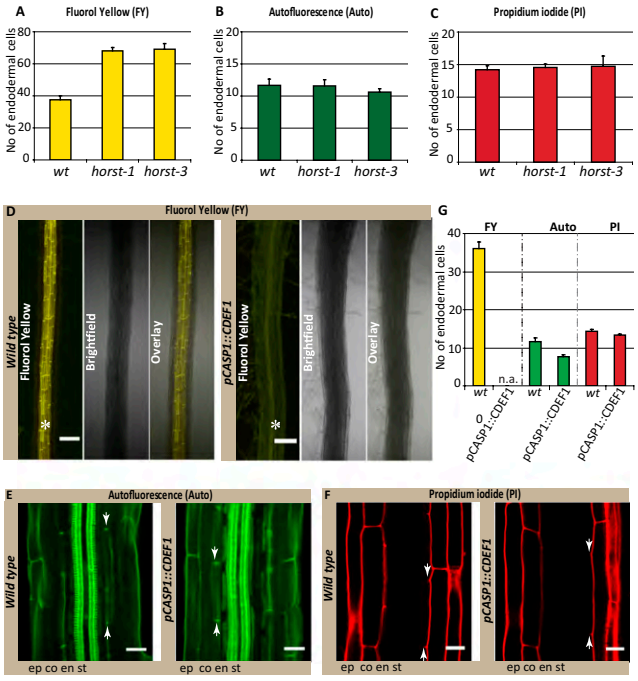

Fig. 3. Suberin degradation has no effect on the formation of functional Casparian strips. (*A*) Fluorol yellow staining reveals significant delay in the appearance of suberin lamellae formation in *horst-1* and *horst-3* insertion lines compared with wild-type (*wt*); (*B*) *horst* mutants do not affect formation of Casparian strips, visualized by autofluorescence. (*C*) Establishment of a functional diffusion barrier, visualized by PI, is also not affected in *horst* mutants. (*D*) No Fluorol yellow signal observed in the *pCASP1::CDEF1* transgenic line, compared with wild-type seedlings; asterisks show the presence (wt, *Left*) and lack of Fluorol yellow signals in endodermis (*Right*). (Scale bar, 100 μm.) (*E*) Casparian strip autofluorescence is not affected by suberin degradation in *pCASP1::CDEF1* transgenic line. (*F*) PI stainings also shows no difference in the formation of a functional diffusion barrier between *pCASP1::CDEF1* and wild-type. n = 16 roots counted. (Scale bars *E* and *F*, 20 μm.) (*G*) Quantification of data in *D*–*F*. Stele (st), endodermis (en), cortex (ct), epidermis (ep), not applicable (n.a).

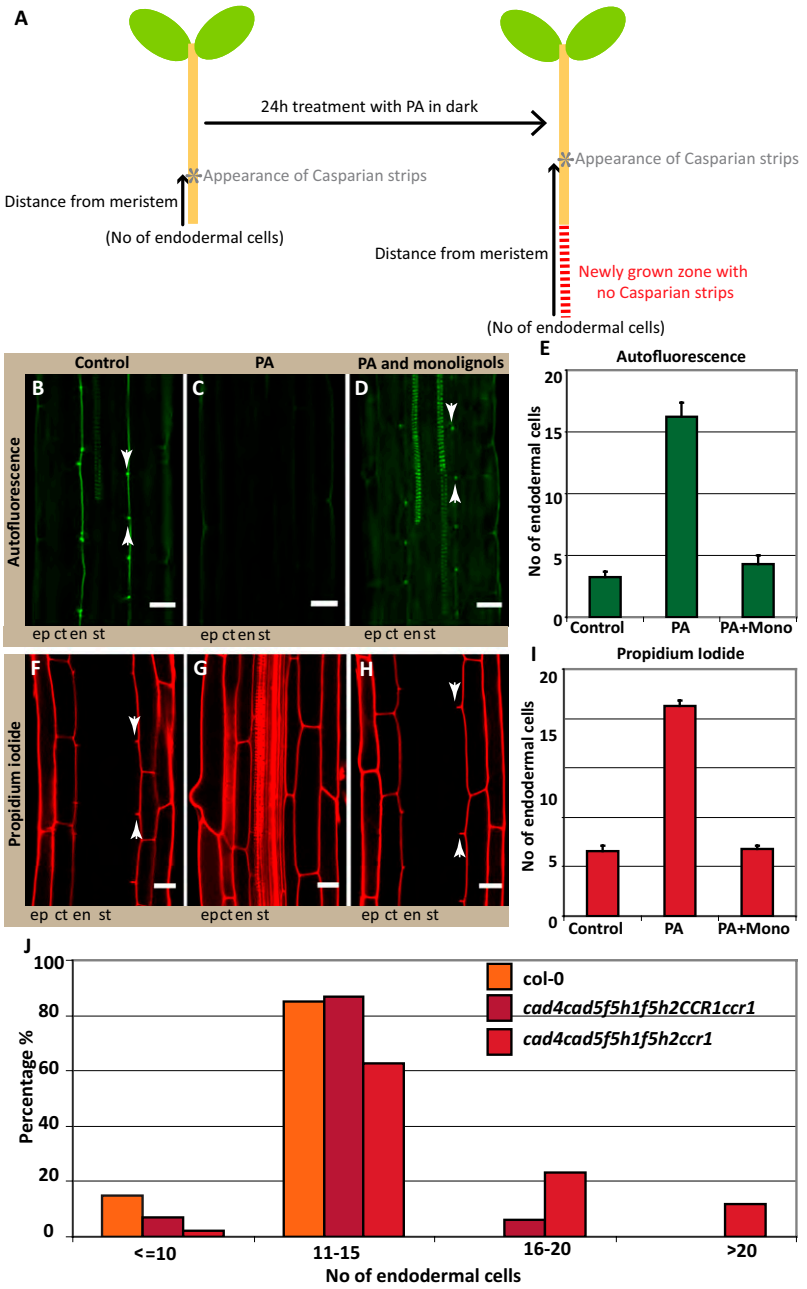

Fig. 4. Interference with monolignol biosynthesis abrogates Casparian strip formation. (*A*) Schematic representation of a seedling explaining how continued root growth after lignin inhibitor treatment results in an apparent "upward shift" of Casparian strip appearance when the cellular distance to the meristem is counted after 24 h. (*B–D*) Autofluorescence after clearing shows the suppression of Casparian strip formation in seedlings treated for 24 h with lignin biosynthesis inhibitor (PA) (*C*), compared with the control (*B*). This effect is complemented by the exogenous application of two monolignols: 20 μM of each coniferyl alcohol and sinapyl alcohol, which allows for the formation of functional Casparian strips (*D*). (*E*) Quantification of *B–D* shows that in the control samples green autofluorescent signal appears around three cells, whereas PA treatment results in the apparent upward-shift of autofluorescent signal to 16 cells, and monolignols complement this inhibitor induced-effect. Signals appear around four cells; close to the control value (*F–H*) PA also blocks the establishment of the diffusion barrier in newly forming cells (*G*) compared with the control (*F*), and this effect is also complemented by monolignol addition (*H*). (*I*) Quantification of *F–H* shows that PA treatment also shifts the block of PI uptake to 21 cells compared with the control samples where PI penetration is blocked around 6 cells. Monolignol addition complements this inhibitor-induced effect and block of PI uptake again appears around 6 cells, matching with the control samples. Arrowheads points to the seventh endodermal cell after onset of elongation. (*J*) Genetic interference using multiple insertion mutants (*ccr1;cad4;cad5;f5h1;f5h2*) of lignin biosynthetic genes reveals a delay in the formation of the diffusion barrier, visualized by PI. In a population of quadruple homozygous (*cad4;cad5;f5h1;f5h2*), segregating for *ccr1*, a delay in the formation of the diffusion barrier is observed in the quadruple mutants, which is further increased in the quintuple mutant. Wild-type (Col): $n = 60$; quadruple mutant *(cad4;cad5;f5h1;f5h2* with *CCR1* either *CCR1/CCR1* or *CCR1/ccr1)*: $n = 227$ and the quintuple mutant *(cad4,cad5,f5h1,f5h2;ccr1)*: $n = 41$. Stele (st), endodermis (en), cortex (ct), epidermis (ep). *B–D* and *F–H*: $n = 20$ roots counted. (Scale bars, 20 μm.)

specific thioacidolysis monomers in ratios that are very similar to that of the xylem-containing wild-type sample (Fig. 5 *E* and *F*). As typical for angiosperm lignin, more than 90% of the monomers in the sample consisted of coniferyl alcohol-derived units, nicely fitting with our exogenous monolignol applications (Fig. 4). Finally, the occurrence of coniferaldehyde end-groups, estimated from

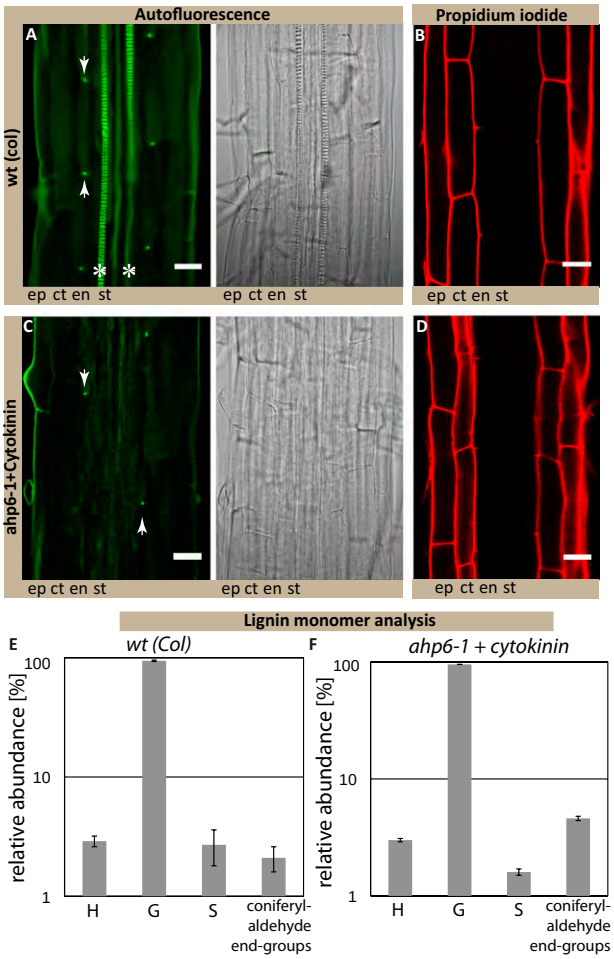

Fig. 5. Casparian strips are made of lignin or a closely related, lignin-like polymer. (*A*) Autofluorescence after clearing shows the appearance of Casparian strip formation (dot-like) and the protoxylem formation. (*B*) PI staining shows functional diffusion barrier. (*C*) Autofluorescence after clearing shows only the dot-like appearance of Casparian strips but no protoxylem formation in *ahp6-1* mutant treated with 10 nM of the cytokinin benzyl-adenine (*ahp6+ck*). (*D*) PI staining confirms presence of a functional diffusion barrier. (Scale bars, 20 μm.) (*E* and *F*) Similar presence and relative abundance of thioacidolysis monomers specifically released from *p*-hydroxyphenyl (H), guaiacyl (G), and syringyl (S) lignin units and from lignin coniferaldehyde end-groups is observed in *wt* (*E*) and *ahp6+ck* root tips (*F*). Total lignin monomers released by thioacidolysis are 208 ± 49 nmol/g for wt and 449 ± 48 nmol/g for *ahp6+ck* root tips. Asterisks mark the presence of xylem vessels in wild-type; arrowheads point to the dot-like structures of the Casparian strips in wt and *ahp6-1*. Stele (st), endodermis (en), cortex (ct), epidermis (ep), wild-type (wt), Cytokinin (ck).

their diagnostic thioacidolysis monomers, fits the phloroglucinol lignin staining observed in Fig. S1*A* and additionally support the idea that genuine lignins are present in the *ahp6* (Casparian strip only) samples. Thus, Casparian strips appear to be made of a polymer that is identical or closely related to the typical lignin found in other cell types in the plant.

Discussion

In summary, our work greatly advances our understanding of the chemical nature and function of Casparian strips. Although it could have been concluded from earlier works that some lignin-like polymer is one of the components of Casparian strips, none of the previous studies did any experimental manipulations that could have established the function and relative importance of lignin and suberin in the Casparian strips. Our work now unambiguously demonstrates that suberin biosynthesis and accumulation occurs much later than the formation of an endodermal barrier and that completely abrogating suberin accumulation still allows the establishment of an efficient barrier to PI penetration. In contrast, monolignol synthesis is absolutely required for establishment of a functional barrier and our reconstitution experiments and chemical analysis both indicate that the Casparian strip is made of lignin or a closely related lignin-like polymer. Our results have important consequences for our thinking about the mechanisms of Casparian strip formation. We can now assume that the localized formation of Casparian strips comes about by confining lignin-polymerizing activity into a meridional ring around the cell. This process could be achieved by localizing lignin-polymerizing enzymes, such as peroxidases or laccases, by confining production of reactive oxygen species or by localized transport of monolignol substrates. The recently identified CASPs are necessary for the correctly localized formation of Casparian strips and appear to form an extensively scaffolded domain within the plasma membrane (the Casparian strip membrane domain, CSD) that precedes and predicts the formation of the Casparian strips themselves. We speculate that the CSD provides a protein platform that allows localization, or localized activation, of the above-mentioned peroxidases/laccases, reactive-oxygen species-producing enzymes, transporters, or combinations of those. Late processes of lignin biosynthesis, such as lignin-polymerization and monolignol transport to the apoplast, remain badly understood. Even more limited is our understanding of the mechanisms that allow the precise subcellular localization of lignin that is seen in many cell types. Our work establishes the endodermis as a promising cellular model for the investigation of lignin formation per se, as well as its subcellular localization. The advantage of the endodermis might be that it is less required for plant survival than xylem vessels, which could be useful for identification and characterization of mutants. In addition, only subsets within the big families of lignin biosynthetic enzymes might be used in the endodermis, which could alleviate problems of redundancy. Finally, the endodermis is a relatively large and peripheral cell layer, compared with many other lignifying tissues. Moreover, it shows a very localized and restricted lignification and stays alive during this process, which should make *in planta* localization studies and cell biological analysis of lignin formation much more straightforward.

Materials and Methods

Plant Material and Growth Conditions. *Arabidopsis thaliana* ecotype Columbia were used for all experiments. For detail of knockout mutants, see Tables S1 and S2. The *ahp6-1* seeds were obtained from Y. Helariutta (University of Helsinki, Helsinki, Finland). Plants expressing the cutinase gene (DEX-CUTE) were generated by a dexamethasone-inducible promoter (18, 23). Plants were germinated on 1/2 MS (Murashige and Skoog) agar plates after 2 d in dark at 4 °C. Seedlings were grown vertically in Percival chambers at 22 °C, under long days (16-h light/8-h dark), and were used at 5 d after shift to room temperature.

Chemicals. PI was purchased from Invitrogen. AIP was kindly provided by Jerzy Zon (Wroclaw Technical University, Wroclaw, Poland). All other dyes, inhibitors, solvents, and chemicals were purchased from Sigma-Aldrich.

Microscopy, Histology, and Quantitative Analysis. Confocal laser scanning microscopy was performed on an inverted Leica SP2 or Zeiss LSM 700 confocal microscope. Excitation and detection windows were set as follows: GFP 488 nm, 500–600 nm; PI 488 nm, 500–550 nm. Autofluorescence and Fluorol yellow were detected with standard GFP filter under wide-field microscope (Leica DM5500). Fluorol yellow staining was performed according to ref. 13. Casparian strips were visualized, as described in refs. 24 and 25. For visualization of the apoplastic barrier, seedlings were incubated in the dark for 10 min in a fresh solution of 15 μM (10 μg/mL) PI and rinsed two times in water (24). For quantification, "onset of elongation" was defined as the point where an endodermal cell in a median optical section was more than twice its width. From this point, cells in the file were counted until the respective signals were detected, see also ref. 24.

Inhibitor Assays. For lignin inhibitor assays, 5-d-old seedlings were incubated in 10 μM PA or 50 μM AIP for 24 h in dark and washed with 1/2 MS before histochemical analysis.

Lignin Quantification. Lignin content in roots was determined by the thioglycolic extraction method as described in ref. 26. The absorbance was measured at 280 nm, lignin alkali (Sigma-Aldrich) was used for generation of a standard.

Evaluation of Lignin Level and Composition in Root Tips by Thioacidolysis. Lignin structure was evaluated by thioacidolysis performed from 6 to 25 mg of the collected samples (air-dried, duplicate experiments). Samples were collected from 5-d-old seedlings. For *Columbia* and cytokinin-treated *ahp6* roots, ~200 mg fresh weight from the first 5 mm of root tips were collected, as the zone that contained no xylem vessels in *ahp6*. Samples were subjected to thioacidolysis, together with 0.083 mg of C21 and 0.12 mg C19 internal standards. After the reaction, the lignin-derived monomers were extracted as usually done (27), the combined organic extracts were concentrated to about 0.2 mL and then 10 μL of the sample were silylated by 50 μL BSTFA and 5 μL pyridine before injection onto a DB1 supelco capillary columns (carrier gas helium, constant flow rate 1 mL/min) operating from 40 to 180 °C at +30 °C/min, then 180–260 °C at +2 °C/min and combined to an ion-trap mass spectrometer (Varian Saturn2100) operating in the electron impact mode (70 eV), with ions detected on the 50–600 *m/z* range. The surface area of the internal standard peaks, measured on reconstructed ion chromatograms [at *m:z* (57+71+85)] and the surface area of the H, G, and S monomers (measured at *m/z* 239, 269, and 299 respectively), were measured.

Vector Construction and Transgenic Lines. For cloning and generation of expression constructs, Gateway Cloning Technology (Invitrogen) was used. For primer details, see Tables S1–S3. Transgenic plants were generated by introduction of the plant expression constructs into a pSOUP containing *Agrobacterium tumefaciens* strain GV3101. Transformation was done by floral dipping (28).

GUS-Staining. For promoter::GUS analysis, 5-d-old seedling were incubated in 5-bromo-4-chloro-3-indolyl-β-D-glucuronide (X-Gluc) staining buffer solution (10 mM EDTA, 0.1% Triton X-100, 2 mM Fe2+CN, 2 mM Fe3+CN, 1 mg/mL X-Gluc) in 50 mM sodium phosphate buffer (pH7.2) at 37 °C for 3~5 h in darkness.

Generation and Analysis of Multiple Monolignol Biosynthesis Mutants. For generation of quintuple monolignol mutants, T-DNA insertion lines from the SALK or GABI-KAT collection were used (all in Columbia). Analysis was done on a quadruple mutant, segregating for *ccr1*. Each seedling was analyzed for the cellular distance from the meristem at which PI diffusion becomes blocked. The same seedlings were then transferred to soil and genotyped. The results were confirmed in an independent crossing in which all alleles (except *ccr1*) were different. In this second cross, *CAD4* and *CAD5* insertion mutants were from the Versailles collection (in Wassilewskija). Here, a *cad5 ccr1* double mutant, segregating for *cad4*, was analyzed as above. See Tables S1 and S2 for additional information.

ACKNOWLEDGMENTS. We thank Dr. J. Zon for providing 2-aminoindan-2-phosphonic acid; Y. Helariutta for *ahp6* seeds; L. Jouanin for the ccc triple mutant; Nicolaus Amrhein for sharing unpublished results; E. Pesquet for proposing the mono-lignol complementation experiments; F. Beisson, Y. Li-Beisson, and Lukas Schreiber for discussions and sharing of material; and J. Alassimone, D. Roppolo, and J. Vermeer for critically reading the manuscript. This work was funded by a European Research Council Young Investigator grant and grants from the Swiss National Science Foundation (to N.G.), and a European Molecular Biology Organization long-term fellowship (to Y.L.).

1. Roppolo D, et al. (2011) A novel protein family mediates Casparian strip formation in the endodermis. *Nature* 473:380–383.
2. Caspary R (1865) Remarks on the protective sheath and the formation of stem and root (translated from German). *Jahrbücher für wissenschaftliche Botanik* 4:101–124.
3. Espelie KE, Kolattukudy PE (1979) Composition of the aliphatic components of suberin of the endodermal fraction from the first internode of etiolated sorghum seedlings. *Plant Physiol* 63:433–435.
4. Vanfleet DS (1961) Histochemistry and function of the endodermis. *Bot Rev* 27: 165–220.
5. Taiz L, Zeiger E (2006) *Plant Physiology* (Sinauer Associates, Sunderland, MA), 4th Ed.
6. Esau K (1977) *Anatomy of Seed Plants* (Wiley, New York), 2nd Ed.
7. Raven PH, Evert RF, Eichhorn SE (2005) *Biology of Plants* (W.H. Freeman, New York), 7th Ed.
8. Hopkins WG (1999) *Introduction to Plant Physiology* (J. Wiley, New York), 2nd Ed.
9. Schreiber L, Hartmann K, Skrabs M, Zeier J (1999) Apoplastic barriers in roots: Chemical composition of endodermal and hypodermal cell walls. *J Exp Bot* 50: 1267–1280.
10. Zeier J, Ruel K, Ryser U, Schreiber L (1999) Chemical analysis and immunolocalisation of lignin and suberin in endodermal and hypodermal/rhizodermal cell walls of developing maize (*Zea mays* L.) primary roots. *Planta* 209:1–12.
11. Zeier J, Schreiber L (1997) Chemical composition of hypodermal and endodermal cell walls and xylem vessels isolated from *Clivia miniata* (Identification of the biopolymers lignin and suberin). *Plant Physiol* 113:1223–1231.
12. Wilson CA, Peterson CA (1983) Chemical-composition of the epidermal, hypodermal, endodermal and intervening cortical cell-walls of various plant-roots. *Ann Bot (Lond)* 51:759–769.
13. Lux A, Morita S, Abe J, Ito K (2005) An improved method for clearing and staining free-hand sections and whole-mount samples. *Ann Bot (Lond)* 96:989–996.
14. Molina I, Li-Beisson Y, Beisson F, Ohlrogge JB, Pollard M (2009) Identification of an *Arabidopsis* feruloyl-coenzyme A transferase required for suberin synthesis. *Plant Physiol* 151:1317–1328.
15. Gou J-Y, Yu X-H, Liu C-J (2009) A hydroxycinnamoyltransferase responsible for synthesizing suberin aromatics in *Arabidopsis*. *Proc Natl Acad Sci USA* 106:18855–18860.
16. Höfer R, et al. (2008) The *Arabidopsis* cytochrome P450 CYP86A1 encodes a fatty acid omega-hydroxylase involved in suberin monomer biosynthesis. *J Exp Bot* 59: 2347–2360.
17. Takahashi K, et al. (2010) Ectopic expression of an esterase, which is a candidate for the unidentified plant cutinase, causes cuticular defects in *Arabidopsis* thaliana. *Plant Cell Physiol* 51:123–131.
18. Chassot C, Nawrath C, Métraux JP (2007) Cuticular defects lead to full immunity to a major plant pathogen. *Plant J* 49:972–980.
19. Schalk M, et al. (1998) Piperonylic acid, a selective, mechanism-based inactivator of the trans-cinnamate 4-hydroxylase: A new tool to control the flux of metabolites in the phenylpropanoid pathway. *Plant Physiol* 118:209–218.
20. Amrhein N, Frank G, Lemm G, Luhmann HB (1983) Inhibition of lignin formation by L-alpha-aminooxy-beta-phenylpropionic acid, an inhibitor of phenylalanine ammonia-lyase. *Eur J Cell Biol* 29:139–144.
21. Thévenin J, et al. (2011) The simultaneous repression of CCR and CAD, two enzymes of the lignin biosynthetic pathway, results in sterility and dwarfism in *Arabidopsis thaliana*. *Mol Plant* 4:70–82.
22. Mähönen AP, et al. (2006) Cytokinin signaling and its inhibitor AHP6 regulate cell fate during vascular development. *Science* 311:94–98.
23. Aoyama T, Chua NH (1997) A glucocorticoid-mediated transcriptional induction system in transgenic plants. *Plant J* 11:605–612.
24. Alassimone J, Naseer S, Geldner N (2010) A developmental framework for endodermal differentiation and polarity. *Proc Natl Acad Sci USA* 107:5214–5219.
25. Malamy JE, Benfey PN (1997) Organization and cell differentiation in lateral roots of *Arabidopsis thaliana*. *Development* 124:33–44.
26. Bruce RJ, West CA (1989) Elicitation of lignin biosynthesis and isoperoxidase activity by pectic fragments in suspension cultures of castor bean. *Plant Physiol* 91:889–897.
27. Lapierre C, et al.; De Nadai V (1999) Structural alterations of lignins in transgenic poplars with depressed cinnamyl alcohol dehydrogenase or caffeic acid O-methyltransferase activity have an opposite impact on the efficiency of industrial kraft pulping. *Plant Physiol* 119:153–164.
28. Clough SJ, Bent AF (1998) Floral dip: A simplified method for *Agrobacterium*-mediated transformation of *Arabidopsis thaliana*. *Plant J* 16:735–743.

Supporting Information

Naseer et al. 10.1073/pnas.1205726109

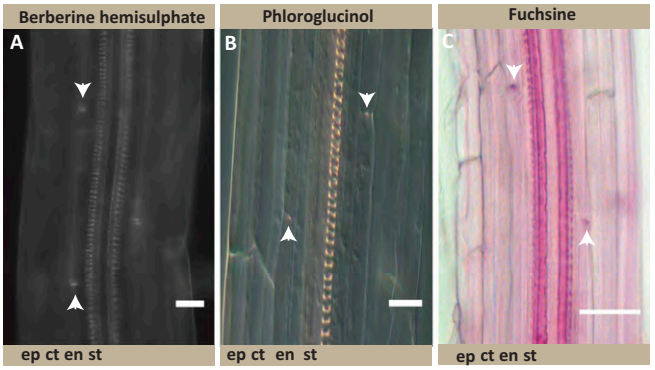

Fig. S1. Casparian strip detection with additional dyes. (*A*) Dot-like appearance of Casparian strips as visualized by Berberine hemisulfate staining. (*B*) Phloroglucinol staining and (*C*) Fuchsine staining. Stele (st), endodermis (en), cortex (ct), epidermis (ep). $n = 16$ (Scale bars: *A* and *B*, 20 μm; *C*, 50 μm.)

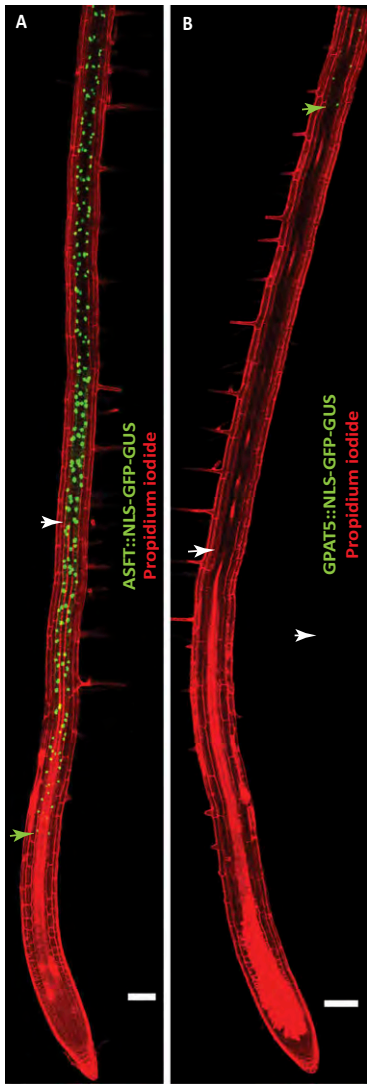

Fig. S2. Comparison of onset of ALIPHATIC SUBERIN FERULOYL TRANSFERASE (ASFT) and GPAT5 promoter activities. (*A*) *ASFT::NLS-GFP-GUS*: beginning of promoter activity in the elongation zone (green arrowhead) before establishment of a functional diffusion barrier, as visualized with propidium iodide (PI, white arrowhead). (*B*) *GPAT5::NLS-GFP-GUS*: beginning of activity late in the differentiated zone (green arrowhead), appears long after establishment of the diffusion barrier (white arrowhead). n = 10. (Scale bars, 100 μm.)

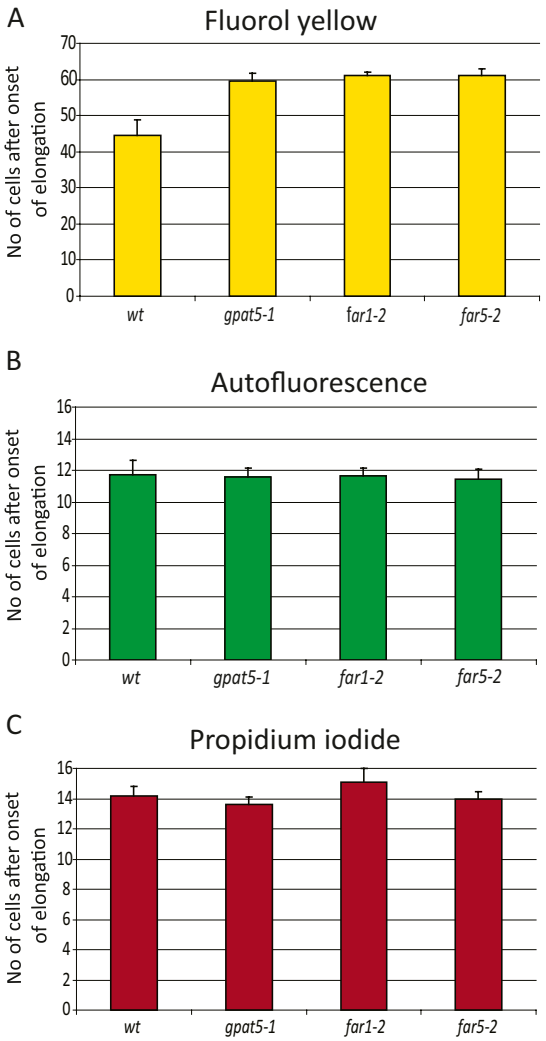

Fig. S3. Additional suberin biosynthetic mutants delay in suberin lamellae formation without affecting Casparian strips. (*A*) Fluorol yellow staining shows the significant delay in the formation of suberin lamellae; first signal was observed at around 44.5 endodermal cells after the onset of elongation in wild-type (*wt*), 59 endodermal cells in *gpat5-1*, 61 endodermal cells in *far1-2*, and 61 endodermal cells in the *far5-2* mutant. (*B*) Autofluorescence after clearing shows that both both insertion mutants do no significantly affect the appearance of Casparian strips, compared with wild-type. (*C*) PI staining shows no effect on the establishment of functional difussion barrier in both insertion mutants and *wt* (n = 16). "Onset of elongation" was defined as the zone where an endodermal cells was clearly more than twice its width.

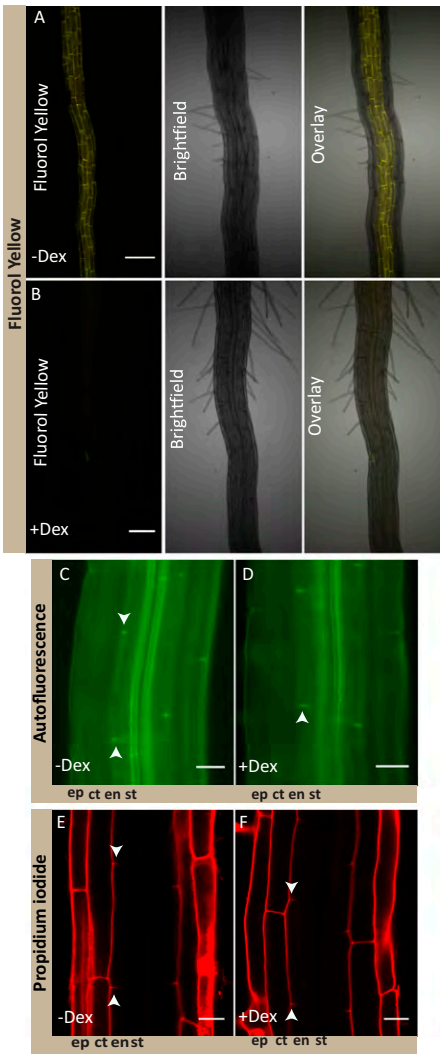

Fig. S4. Inducible suberin degradation does not affect formation of Casparian strips or diffusion barrier establishment. (*A* and *B*) Fluorol yellow staining reveals presence of suberin lamellae formation in the untreated seedling (−Dex), whereas no staining is observed in seedlings treated with 10 μM dexamethasone (+Dex). (*C* and *D*) Autofluorescence shows no effect on the formation of Casparian strips in both −Dex and +Dex seedlings. (*E* and *F*) PI shows that suberin degradation does not affect formation of a diffusion barrier in both −Dex and +Dex-treated seedlings. Stele (st), endodermis (en), cortex (ct), epidermis (ep). $n = 20$ (Scale bars: *A* and *B*, 100 μm; *C*–*F*, 20 μm.)

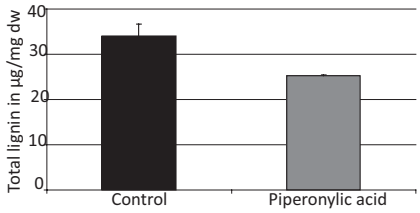

Fig. S5. Piperonylic acid (PA) significantly lowers overall lignin contents in young seedling roots. Quantitative analysis shows significant difference in the total amount of lignin extracted from 5-d-old seedling roots treated with 10 μM PA for 24 h compared with the control (untreated) samples.

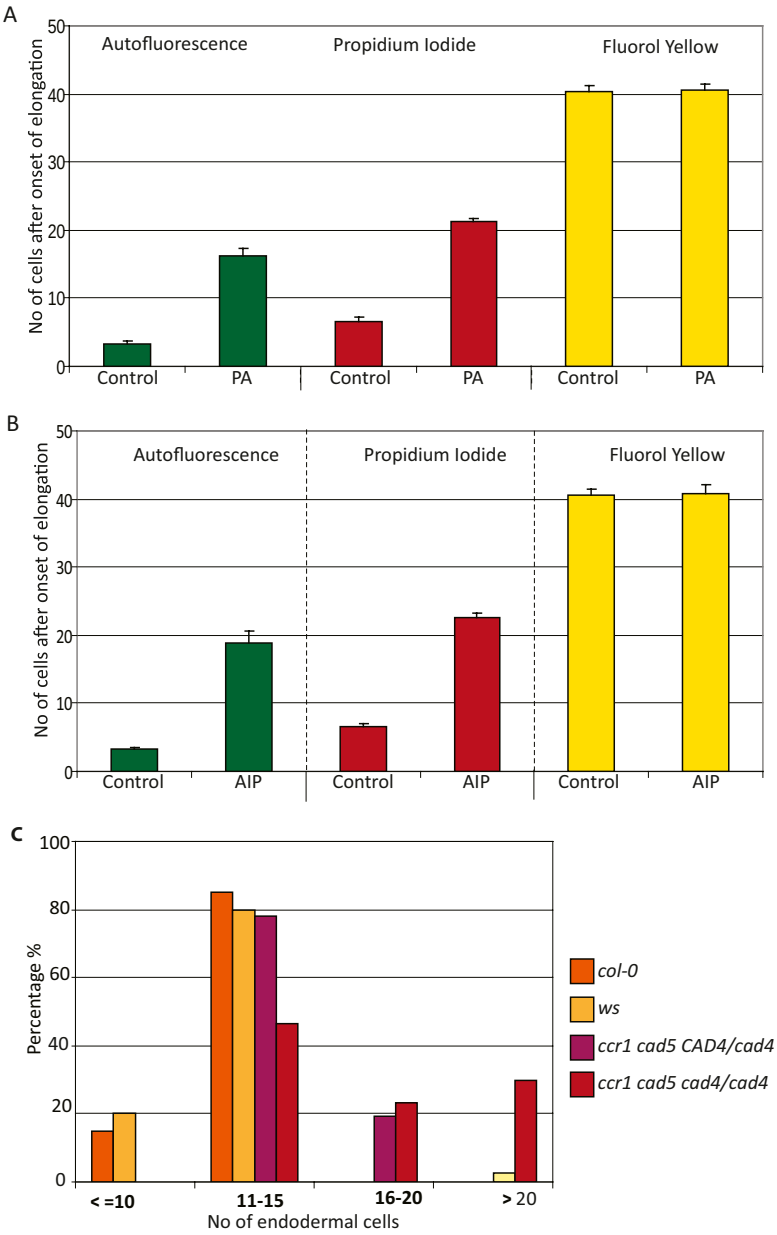

Fig. S6. Interference with lignin biosynthesis affects Casparian strip formation, but not suberin lamellae. (*A* and *B*) Quantification of seedling treated with two different lignin biosynthesis inhibitors (10 μM PA and 50 μM 2-aminoindan-2-phosphonic acid, AIP) blocks the appearance of green autofluorescent signal and of PI uptake in the newly formed cells, compared with control seedlings. However, suberin lamellae formation was not affected by the inhibitors. (*C*) Genetic interference using triple insertion mutants (*ccr1;cad4;cad5*) of lignin biosynthetic genes reveals a delay in the formation of the diffusion barrier, visualized by PI. In a population of double homozygote (*cad4;cad5*), segregating for *ccr1*, a delay in the formation of the diffusion barrier is observed in the double mutant, which is further increased in the triple mutant. Wild-type (*Col*): $n = 60$ and Wassilewskija (*Ws*), double mutant *(cad5;ccr1* with *CAD4* either *CAD4/CAD4* or *CAD4/cad4): n* = 82 and the triple mutant *(cad5;ccr1;cad4): n* = 30. Data of autofluorescence and PI in *A* the same as in Fig. 4 *D* and *H*.

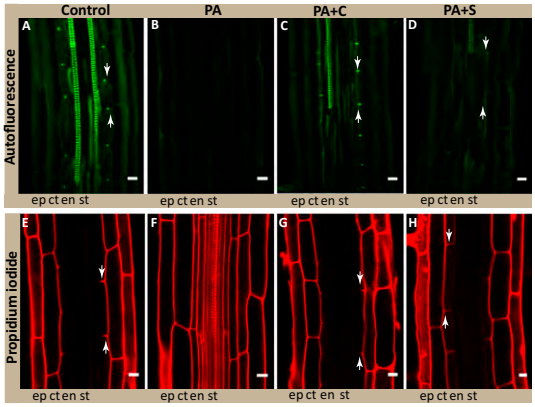

Fig. S7. Exogenous treatment with only coniferyl alcohol can lead to Casparian strip formation in lignin inhibitor-treated roots. (*A*) Autofluorescence after clearing shows the dot-like appearance of Casparian strips in control seedlings. (*B*) Block of Casparian strip formation in the PA-treated seedling. (*C*) Formation of functional Casparian strips by exogenous application of 20 μM coniferyl alcohol. (*D*) Formation of Casparian strips by exogenous application of 20 μM of sinapyl alcohol. (*E*) PI staining shows block of PI uptake in untreated (control) seedling. (*F*) Penetration of PI in the seedling treated with PA. (*G*) Establishment of functional diffusion barrier because of the complementation of the inhibitor-induced defect with coniferyl-alcohol. (*H*) Sinapyl-alcohol is less functional in the formation of a functional diffusion barrier than coniferyl alcohol. Stele (st), endodermis (en), cortex (ct), epidermis (ep). *n* = 20 roots counted. (Scale bars, 20 μm.)

Table S1. Sequences of primers used for genotyping

Primer name	Primer sequence
horst-1-LP	AAGAACCAGCTCAAGGCCACC
horst-1-RP	AGCAAAAAGCCTAAACCGGGA
horst-3-LP	AGGTAGCAACATCTGCTTCCC
horst-3-RP	ACCAGGATTTCAAATACGTCG
*gpat*5–1-LP	TTGGTTACTATATGCTCCTATTTTGG
*gpat*5–1-RP	TTCGGACAAATGGTGAATTTC
far 1–2 -LP	TTGTTGCAATAAATGAAATGAACAG
far 1–2 -RP	TACCTTGCACGACTATGTCCC
far 5–2-LP	TTCTTGCAACGTCCTTAGCTG
far 5–2-RP	AAAGGTGGTATATAAAATTTCTTGTAGC
ccr1- LP	CCGTAACAATACCAATTCTACAAAAC
ccr1-RP	TTTTATTGTTTTGATTGACAATTTGG
f5h1-LP	ATGTCGGATTCTTCAACTCGTCTGTCA
f5h1-RP	GGCTTCAGTTCGTGATGAAGTGGAC
f5h2-LP	TATGTGGGAGTCGTGAAATTTATATG
f5h2-RP	AACTCACCAAAGAGCTTAGAGAACTC
cad4-LP	GCTCAGAACTTGAGCAGTATTGTAAC
cad4-RP	TTAACAAATTTGAGTTCAAGTGGAAG
cad4-ccc -LP	GCCACCTTGAGTAGGTTTTCC
cad4-ccc -RP	CTGCAAGAGATCCTTCTGGTG
cad5-LP	AATACACACACATAAACAGCAAAAGC
cad5-RP	CTCTCTTCTTGTTTGATGAGCTTATG
cad5-ccc -LP	GATCTTGCAATGCCTCTTCTC
cad5-ccc -RP	GAAGTAGTGGAGGTGGGATCA
LBb1	ATTTTGCCGATTTCGGAAC
GABI-LB	ATATTGACCATCATACTCATTGC
Versailles-LB	CTACAAATTGCCTTTTCTTATCGAC

Table S2. Details of knock-out mutants associated with suberin biosynthesis

Gene number	Accession	Salk number	Mutant name	References
AT5G58860	Col	SALK_107454	*horst*-1	Hofer et al. (1)
AT5G58860	Col	SALK_050126.55.50.x	*horst*-3	Present work
AT3G11430	Col	SALK_018117	*gpat*5–1	Beisson et al. (2)
At5g22500	Col	SALK_149469	*far* 1–2	Domergue et al. (3)
At3g44550	Col	SALK_070363	*far* 5–2	Domergue et al. (3)
At1g15950	Col	GABI_622C01	*ccr1*	Ruel et al. (4)
At4g36220	Col	SALK_063792	*f5h-1*	Huang et al. (5)
At5g04330	Col	SALK_093419	*f5h-2*	Present work
At3g19450	Col	SAIL_1265_A06	*cad4-c*	Present work
At3g19450	Ws	Versailles collection	*cad4-c*	Sibout et al. (6)
At4g34230	Col	SALK_040062	*cad5-d*	Kim et al. (7)
At4g34230	Ws	Versailles collection	*cad5-d*	Sibout et al. (6)

1. Hofer R, et al. (2008) The Arabidopsis cytochrome P450 CYP86A1 encodes a fatty acid omega-hydroxylase involved in suberin monomer biosynthesis. *J Exp Bot* 59(9):2347–2360.
2. Beisson F, Li Y, Bonaventure G, Pollard M, Ohlrogge JB (2007) The acyltransferase GPAT5 is required for the synthesis of suberin in seed coat and root of Arabidopsis. *Plant Cell* 19(1): 351–368.
3. Domergue F, et al. (2010) Three Arabidopsis fatty acyl-coenzyme A reductases, FAR1, FAR4, and FAR5, generate primary fatty alcohols associated with suberin deposition. *Plant Physiol* 153(4):1539–1554.
4. Ruel K, et al. (2009) Impact of CCR1 silencing on the assembly of lignified secondary walls in Arabidopsis thaliana. *New Phytol* 184(1):99–113.
5. Huang J, et al. (2009) Pleiotropic changes in Arabidopsis f5h and sct mutants revealed by large-scale gene expression and metabolite analysis. *Planta* 230(5):1057–1069.
6. Sibout R, et al. (2003) Expression pattern of two paralogs encoding cinnamyl alcohol dehydrogenases in Arabidopsis. Isolation and characterization of the corresponding mutants. *Plant Physiol* 132(2):848–860.
7. Kim SJ, et al. (2004) Functional reclassification of the putative cinnamyl alcohol dehydrogenase multigene family in Arabidopsis. *Proc Natl Acad Sci USA* 101(6):1455–1460.

Table S3. Primer sequences used for construction of promoter::GUS fusions

At number	Gene name	Enzyme name	Bp before ATG	Primer name	Primer sequence
at1g04220	*DAISY*	3-ketoacyl CoA synthase	2,084 bp	prKCS2-attB4(12bp) Sense	ATAGAAAAGTTGCTCTCATGGTTG AGTAGTTGAATGTTG
				prKCS2-attB1r(12bp) AS	TTGTACAAACTTGCGGTAGGTTTT TTGGTTTTAAATGATA
at1g67730	*KCR1*	Ketoacyl CoA reductase	2,027 bp	prKCR1-attB4(12bp) Sense	ATAGAAAAGTTGCTCAAATGTGC AGGTTGCTCTATTAT
				prKCR1-attB1r(12bp) AS	TTGTACAAACTTGCTAGAGAAGAA AGGTTGAGACTTTGG
at5g58860	*HORST*	Fatty acid ω-hydroxylase	2,165 bp	prHORST-attB4(12bp) Sense	ATAGAAAAGTTGCTGAGTAGTACC CTCAGAGGAACTTGCA
				prHORST-attB1r(12bp) AS	TTGTACAAACTTGCTATCCCGGTTT AGGCTTTTTGCT
at5g23190	*CYP86B1*	Fatty acid ω-hydroxylase	1,734 bp	prCYP86B1-attB4(12bp) Sense	ATAGAAAAGTTGCTCACACCCAGTA AGAGATCAAACACA
				prCYP86B1-attB1r(12bp) AS	TTGTACAAACTTGCTGTGACAAAGA GAAGAGAGAGCGA
at4g15330	*CYP705A1*	Other CYP450 enzymes	1,917 bp	prCYP705A1-attB4(12bp) Sense	ATAGAAAAGTTGCTGTTCATCGTGCTG CCAAAGTAGTGA
				prCYP705A1-attB1r(12bp) AS	TTGTACAAACTTGCTGTTGCTGAAA AGCAAAGAAGAGGC
at3g11430	*GPAT5*	Glycerol-acyl-transferase	2,146 bp	prGPAT5-attB4(12bp) Sense	ATAGAAAAGTTGCTTGATCGCAA ACGTCAATGGTCTAT
				prGPAT5-attB1r(12bp) AS	TTGTACAAACTTGCTTCTTTTGTTT TTTGCTCGAATATTA
at5g41040	*ASFT*	Feruloyl-acyl-transferase	2,049 bp	prACT-attB4(12bp) Sense	ATAGAAAAGTTGCTGAAGATCAG CAGCAGAGTGCAGAG
				prACT-attB1r(12bp) AS	TTGTACAAACTTGCTTTGATCCAAA TGGAGAAAACAGC
at3g44540	*FAR4*	Alcohol-forming fatty acyl-CoA reductase	2,300 bp	prFAR4-attB4(12bp) Sense	ATAGAAAAGTTGCTGGAACCTAT GTCCGAACTCCG
				prFAR4-attB1r(12bp) AS	TTGTACAAACTTGCTGAAGAAA CTTATATCTATCCAATTAAT

For construction of transgenic line expressing CDEF1 (At4g30140), Gateway Directional TOPOentry vector(U15010) was used (Invitrogen). Fragments of entry clones were transferred into the destination vector pB7m34GW.

3 Chapter III: Understanding patterning, differentiation, and functioning of endodermal passage cells

3.1 Collaborators and contributions

I contributed to the conception of the study. All the main experiments were done by me. I generated all the fluorescent marker lines in order to highlight the passage cells. I performed all the microscopic experiments. Passage cells reporter constructs with plasma membrane marker (pPassage cell:3XmCherry-SYP122) were generated and transformed by Joop Vermeer. I generated all the transgenic lines by remixing the INTACT and affinity tagging of ribosomal binding protein for gene expression profiling. I would like to thank Christian Fankhauser (University of Lausanne) for providing the pGAT-HF-RPL18 for the amplification of coding sequence of FLAG tagged RPL18 and Dolf Weijers (Wageningen University, Laboratory of Biochemistry) for providing the GIIK LIC-BirA and GIIB LIC-BirA vectors for the amplification of Biotin ligase (BirA). I also would like to thank the student helpers Deborah Mühlemann and Christophe Sahli in their contribution in harvesting transgenic lines.

3.2 Introduction

In *Arabidopsis,* endodermal differentiation is characterized by the formation of two developmental stages. Establishment of the Casparian Strip (CS) apoplastic barrier is the primary differentiation stage (State I) and it is generally followed by a suberin deposition, forming thin lamellae that eventually coat the entire cell (State II). However, this secondary differentiation is not occurring in all the endodermal cells. There is an intermediate zone where the cells in the secondary stage are intermixed with cells in the primary stage. The latter do contain the CS but formation of suberin lamellae is absent or delayed. These cells are termed as “passage cells” because of the absence of secondary differentiation that allows them to retain uptake capacity. Interestingly, these cells are always positioned adjacent to the protoxylem poles (Fig. 1) (Enstone et al. 2002).

Occurrence of passage cells has been reported to decrease with age. As the root grows older, these cells may form suberin lamellae (sometimes-tertiary walls) and thus their number decreases. Position of passage cells in the endodermis (adjacent to the xylem poles) is explained in terms of function of these cells. As shown in chapter I, walls of the intact endodermis act as an efficient barrier to the passage of ions due to the formation of the CS. This is coupled with the capacity of the cytoplasm to retain ions, meaning that

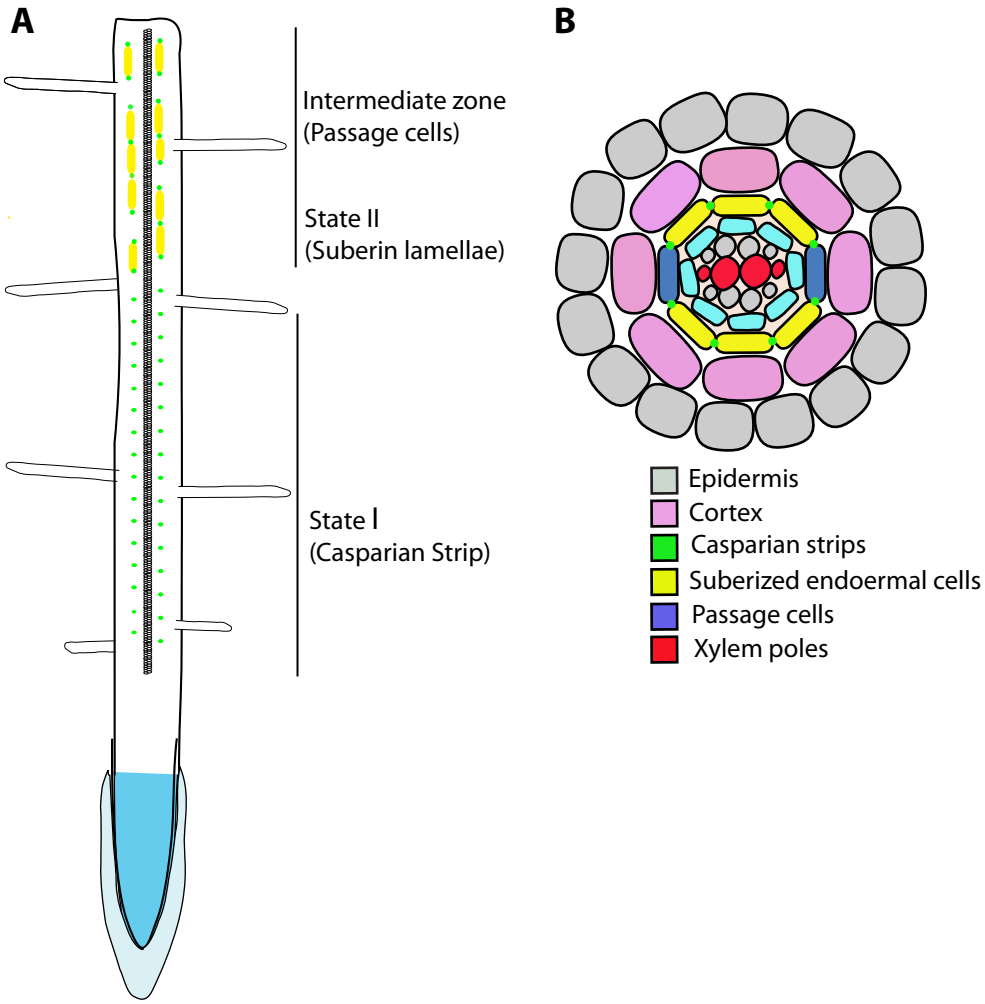

Figure: 1 Schematic representation of *Arabidopsis* root showing the different developmental stages of endodermis.

(A) Two different developmental states of endodermis, State I is characterized by the dot-like appearance of Casparian Strip(CS), which is followed by the formation of Suberin lamellae on the inner surfaces of entire endodermal cell (State II). Intermediate zone represent the region where the some cells in the state I are surrounded by the state II cells, shown with only dot-like appearance of CS without the formation of Suberin lamellae.

(B) Schematic representation of Non-suberized passage cells in blue positioned at the xylem poles of the underlying vasculature.

most of the ions that enter the stele use the symplastic path to cross the endodermis. Later on, development of suberin lamellae may prevent movement of ions through the symplast. It has been shown that the transfer of calcium across the endodermis declined markedly with suberin lamellae formation (Ferguson and Clarkson 1976). Furthermore, as the transfer of calcium into the root is shared by magnesium, Peterson and Enstone (1996) pointed out that these ions were transferred into the stele through the passage cells. Suggesting that the symplastic transfer of ions already in the cytoplasm may take place in passage cells. In contrast, it has been reported that, in barley roots, movement of radiolabelled phosphate ions across the endodermis was not inhibited by development of suberin lamellae (Clarkson et al. 1971). The passage cells are also reported to be present in the tannin zone of jack pine roots and these would represent the only ion-absorbing cell membrane surface area in this region of the root (McKenzie and Peterson 1995). Therefore, passage cells in the roots appear to be areas at which solutes present at the cortex can pass to the stele.

Passage cells are up to now defined as:

- Non-suberized endodermal cells
- Cells associated with the xylem pole.

This definition has two problems:

- It defines passage cells in the negative way (absence of cell wall)
- It cannot really distinguish passage cells from primary endodermal cells.

Since passage cells only contain the CS but not the suberin lamellae formation, it has been assumed that may these cells preserve lower resistance pathway for water flow into the stele (Peterson and Enstone1996). Ultrastructural studies of these cells failed to show any special modification of protoplasts of passage cells. However, it has been reported that the plasmodesmata of the state I endodermal cells are probably retained by the passage cells (Bonnet 1968; Clarkson et al.1971). If these cells are not morphologically different from primary stage cells, what are the characteristic features of these cells that will make them distinguish from the neighboring cells. In past few centuries, lots of effort was done in order to describe the development of endodermis in different plant

species. However, passage cells were always ignored or exclusively defined in a negative way (by an absence of suberin lamellae).

3.3 Rationale of the study

The various histochemical tools and transgenic lines that I developed (see chapter II) allow for precise measurement of different endodermal stages and provided us with a platform to further characterize the endodermal development. In this context, it would be important to define the passage cells in positive and molecular terms and possibly distinguish them from primary-stage endodermal cells in the model plant *Arabidopsis.* The aim of this work is to define the patterning and development of passage cells as well as their physiological role in the root endodermis. A direct approach is to use some available genes that specifically express in these cells and describe their role in molecular and physiological terms. However, if we look in the literature, only PHO1, a phosphate efflux transporter is reported to be expressed both in the stele and in single endodermal cells that were proposed to be passage cells because of their location adjacent to the protoxylem poles (Fig. 2) (Hamburger et al. 2002). When reviewing the literature, other stele-expressed transporters, like YSL2 (Yellow Strip-Like Protein), IRT3 (Zinc/Iron transporter) and SKOR (Shaker-like outward channels involved in potassium release into the xylem sap) show a similar extended expression in some endodermal cells. Those, very probably, represent passage cells (Di Donato et al. 2004; Gaymard et al. 1998). However, in these publications, it is never mentioned that these endodermal cells could be passage cells and the extended expression in some of the endodermal cells has never been discussed.

To better characterize the formation of passage cells, it would be crucial to first identify some genes that are exclusively expressed in passage cells. In order to do identify such genes, we decided to first make the fluorescent marker lines with stele-expressed transporters that are reported to be expressed in passage cells for an indirect approach. This helps us to highlight the passage cells in a non-specific way and may provide an entry point into defining endodermal passage cells.

Furthermore, in order to find the passage cell specific genes, our aim is to develop a technique through which we can uniquely mark passage cells. For this purpose, our strategy is to use and adapt a two-component system based on the previous published

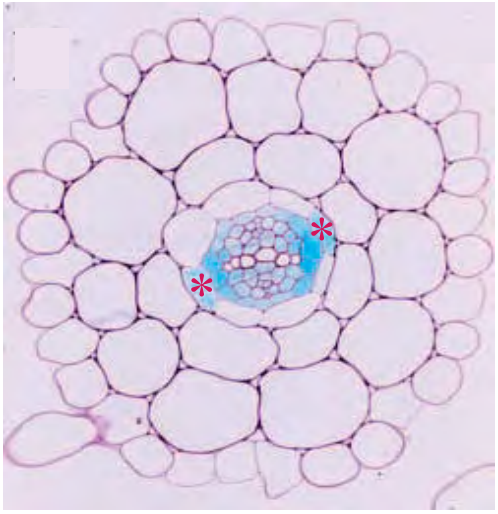

Figure: 2 Expression pattern of PHO1 promoter.
Cross section of *Arabidopsis* root showing the GUS staining in the stele and only in two endodermal cells positioned at the xylem poles of vasculature, shown by Asterisk.
(Adopted from Hamburger et al, The Plant Cell, 2002)

methods, mainly used to study the gene expression profiles of individual cell types. In future, this would allow us to study the gene expression profile in these cells specifically.

3.4 Results and discussion

3.4.1 Passage cells presence revealed by Fluorol yellow (FY) in young roots

As mentioned in Chapter II, suberin deposition in the endodermis occurs long after the formation of Casparian Strip (CS). However, not all the endodermal cells at this stage formed suberin lamellae at the same time. First, it starts in some cells and later on, it becomes homogenous in all the cells (except for passage cells). FY staining is shown to be a reliable marker for the presence of suberin (see Chapter II). In order to identify the zone where the Passage cells/non-suberized cells formation occur, we tested 5-days old seedling with whole-mount FY staining assay. We observed that there are two zones in the state II which are characterized by the presence of state I cells. There is a transition zone, where the cells of state I are in the process of being suberized, exhibiting a patchy pattern in which some stained cells lie next to others that do not show any suberin deposition (Fig. 3A). The second zone is characterized as a zone where most of the cells have become suberized with the presence of single cells or some times, clusters of non-suberized cells. These cells are always surrounded by strongly stained cells (Fig. 3B). We also noticed that the endodermal cells that do not form suberin lamellae are always positioned at the xylem poles of the underlying vasculature (Fig. 3C).

This data, firstly, confirm the presence of non-suberized endodermal cells in the young root. In addition, these cells are observed to be located adjacent to the protoxylem poles, suggesting that they might be the passage cells. Secondly, suggests that the number of passage cells decreased with increasing distance from the root tip. This may be because, as mentioned earlier, lateral root (LRs) formation is initiated from the xylem pole associated pericycle cells, which suggest that, may be due to LRs initiation in the older part of the root, frequency of passage cells become decreased or less pronounced.

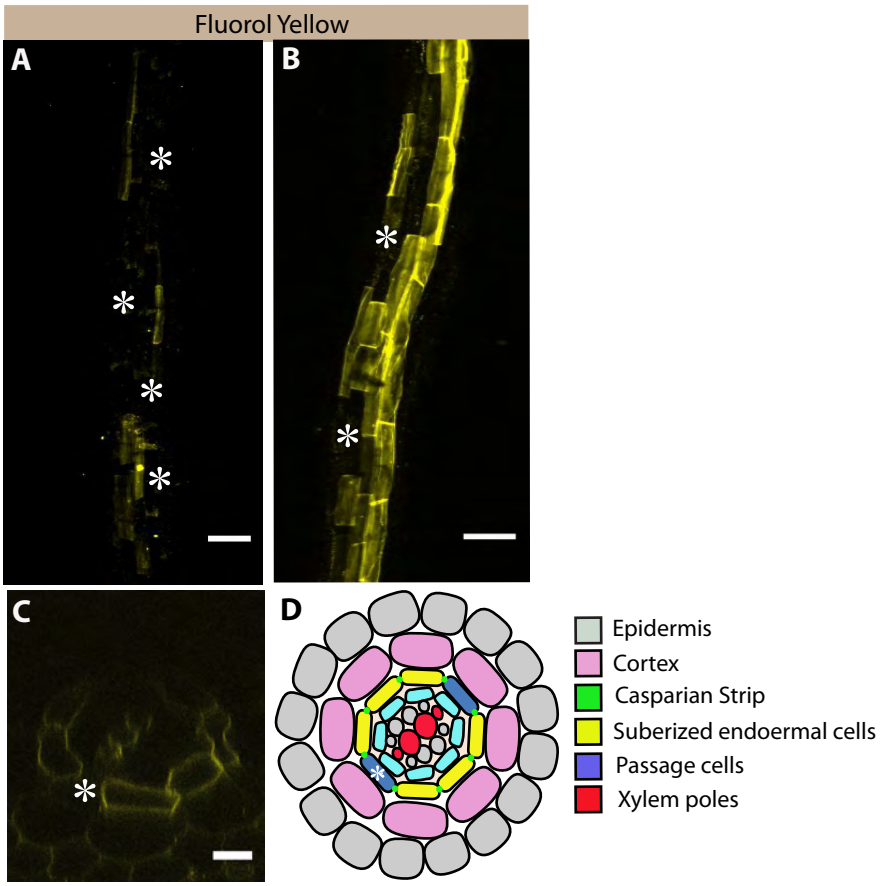

Figure: 3 Passage cells formation revealed by Fluorol Yellow (FY) staining in 5-days old seedlings.

(A) Early patchy appearance of suberin lamellae formation in individual interspersed cells with number of cells that do not shows any suberin staining. Asterisk mark the position of non-suberized cells.

(B) State II of endodermal development where suberin staining becomes eventually homogenized with some non-suberized. Asterisks mark the position of non-suberized cells surrounded by the strongly stained suberized cells.

(C) Transversal view of young root at state II that shows the presence of non-suberized cell/passage cells positioned at the xylem pole of underlying vasculature.

(D) Schematic depicting the presence of xylem pole-associated non-suberized/passage cells, mark by asterisk (Scale bars, 20µM).

3.4.2 Stele-expressed transporters are also expressed in the passage cells but exhibit different expression pattern

Identification of genes that are specifically expressed in passage cells is crucial to define the passage cells and to separate them from the state I endodermal cells of the root. GUS reporter analysis shows that some stele specific transporters are also expressed in a subset of endodermal cells. Because of their position on the xylem poles, these cells can be seen as passage cells, as described in Hamburger 2002. Based on this GUS expression pattern, I created the fluorescent marker lines using the promoter region of the following transporters; PHO1 (mediates phosphate efflux), YSL2 (involve in iron and zinc homeostasis), IRT3 (involve in iron and zinc transport) and SKOR (mediates potassium release into the xylem sap) (See Annex chapter VIII.B; Table 1 for all available transgenic lines).

Analysis of 5-days old seedling of these fluorescent marker lines show that in addition to the stele all theses transporters are also expressed in some endodermal cells (presumable passage cells). However, the expression pattern is varying among all these transporters. pIRT3::NLS-3XVenus analysis demonstrates that IRT3 expression was mainly restricted to stele at state I and in some cortical cells. Nevertheless, expression in the stele was very weak (Fig. 4A). Later, expression extended to some of the endodermal cells at state II, when endodermal cells become suberized. We also observed that in the zone where IRT3 was expressed in some endodermal cells its expression in the stele disappeared or became very weak (Fig. 4E). Observation of pPHO1: NLS-3XVenus transgenic lines demonstrate that at state I of endodermal development it is only expressed in the stele (Fig. 4B). However, later on its expression starts to extend to some of the endodermal cells (Fig. 4F). PHO1 expression is mainly observed in endodermal cells located in the transition zone between primary and secondary stage cells (sometimes in clusters of 3 or 4 cells) (Fig. 5B). This correlates with the pattern of suberin deposition, as shown by the Fluorol Yellow staining and later on in some cells located in the state II of endodermis (Fig 4B). Analysis of pSKOR: NLS-3XVenus shows that it is expressed in all the endodermal cells and the stele at both state I (Fig. 4C) and state II (Fig. 4G) of endodermis development, which is contrary to the expression pattern shown in the literature. This expression pattern is interesting, but eliminates the SKOR promoter as a potential marker for passage cells. Analysis pYSL2: NLS-3XVenus shows that, first

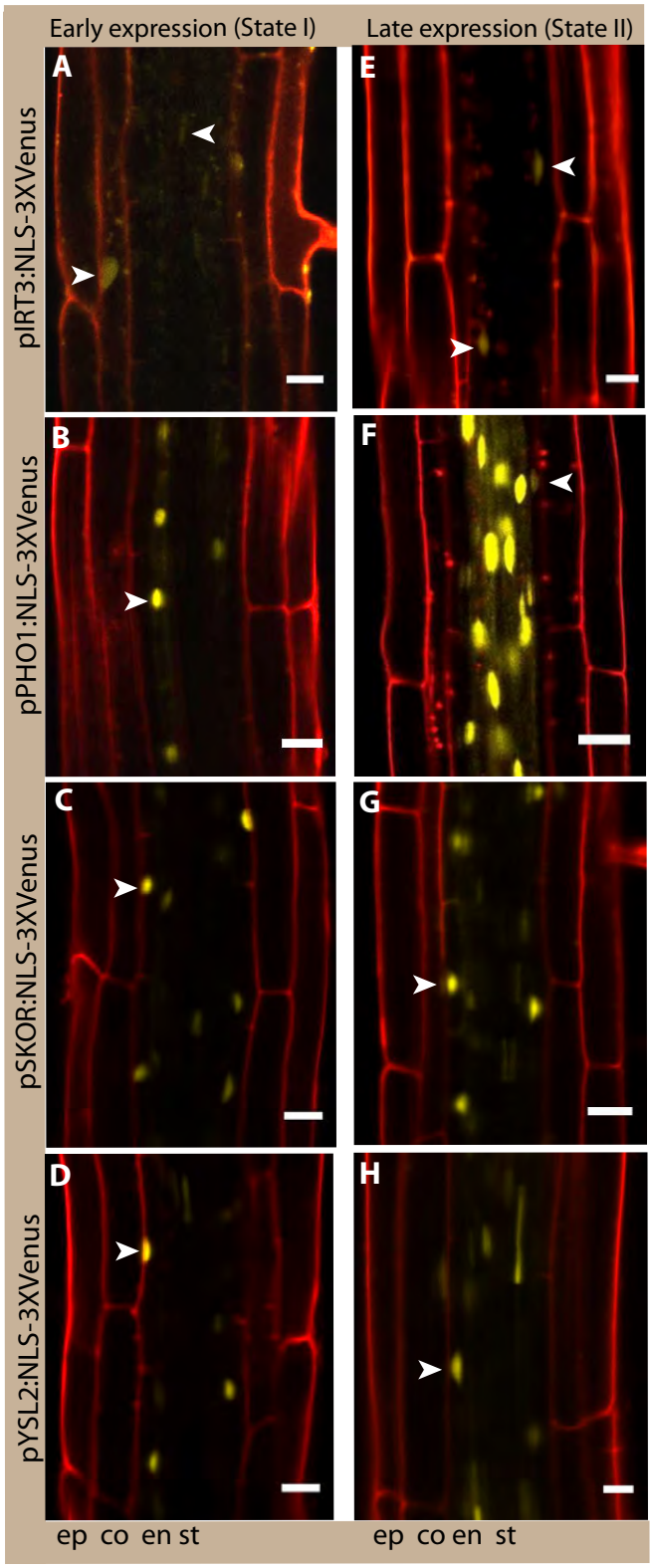

Figure: 4 Expression patterns of stele-specific transporters at state I (Primary stage) and state II (Secondary stage) of endodermis.

(A-D) Expression pattern of pIRT3: NLS-3XVenus, pPHO1:NLS-3XVenus, pSKOR:NLS-3XVenus and pYSL2 :NLS-3XVenus at state I of endodermis shown by arrowheads. pIRT3: NLS-3XVenus was expressed in some cortical cells and in stele. pPHO1:NLS-3XVenus expression was restricted to stele. pSKOR:NLS-3XVenus and pYSL2 :NLS-3XVenus expression were observed in all the cells of endodermis and in the stele.

(E-H) Expression pattern of pIRT3:NLS-3XVenus, pPHO1:NLS-3XVenus, pSKOR:NLS-3XVenus and pYSL2 :NLS-3XVenus at state II of endodermis. All show expression in some of endodermal cells (shown by arrowheads) except pSKOR:NLS-3XVenus which expressed in all the endodermal cells at both state I and state II.

(Scale bars, 20μM). epidermis (ep),cortex (co), endodermis (en) and stele (st).

nuclear localized signals (NLS) were observed in the stele and all the endodermal cells (Fig. 4D). Later on at state II, however, signals were restricted to stele and some of the endodermal cells (Fig. 4H).

Together, these data suggests that all these transporters except SKOR are potential, non-specific markers for endodermal passage cells. However, their expression pattern is different from one another; PHO1 and IRT3 are expressed only in some endodermal cells of state II, whereas YSL2 seems to be initially expressed in all primary state (non-suberized) endodermal cells and then becomes restricted to a subset of endodermal cells. It has to be borne in mind that we performed all the analysis on seedlings grown on standard MS media and the expression pattern of all these transporters might depend on the availability of ions that they transport. Furthermore, from the reference papers of these transporters, we cannot state at which zone of the root transversal sections were made. For example, in the Fig 2 regarding the GUS expression pattern of PHO1, endodermis is surrounded by the two cortical layer, showing that the analysis done on older seedlings. In this way, the interest of making passage cell marker lines is not only the confirmation of the published results in live-seedlings, but also the scoring of expression in young roots and in a developmental progression. Because of the different expression pattern of all these transporters in the endodermis, we also crossed the passage cells marker lines with each other (See Annex VIII.B; Table 4).

By using all these different fluorescent marker lines, we were unable to identify whether the endodermal cells that show NLS expression are located exclusively above the xylem pole. It has been reported that lateral roots (LRs) originate from a small number of differentiated pericycle cells adjacent to xylem poles, called pericycle founder cells (Laskowski etal. 1995). We therefore checked, for example, PHO1 expression in the older part of the root where lateral root primordial were initiated. We observed a NLS signal in the endodermal cells located above the pericycles cells from where the lateral root is coming out (Fig. 5A).

However, we appreciate the sensitivity of the 3X nuclear localized markers but we noticed that, firstly it was very hard to distinguishing the endodermis from the outer cortical or inner pericycle cell layers in the presence of stele expression. Secondly, the extended nuclear localized signals in endodermal cells were very weak as compared to

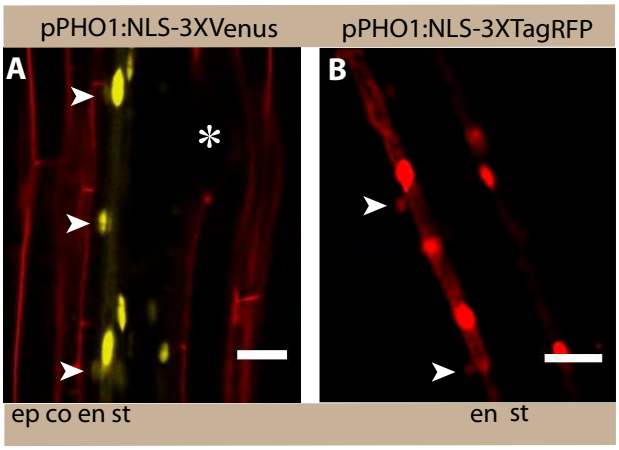

Figure: 5 Expression pattern of pPHO1 at LR initiation site and transition zone between states I and II of endodermis.
(A) Expression of pPHO1 in the endodermal cells positioned opposite of site of lateral root (LR) initiation. Arrows show the expression of PHO1 in endodermal cells and the asterisk marks the LR initiation site. **(B)** Expression pattern of pPHO1 in the number of endodermal cells at the transition zone shown by arrows, where the endodermal cells are in process of being suberized (Scale bars, 20μM).

the stronger NLS expression in the stele. This weaker expression also makes it very difficult to characterize the endodermal passage cells. Under this context, in order to highlight passage cells differently and make it easier to show the radial patterning, I also made the fluorescent plasma membrane marker lines with all these transporters (See Annex VIII.B; Table1).

In addition, I also generated GUS reporters lines with all these transporters to check the expression pattern by making transversal cuts (See Annex VIII.B; Table 1). These GUS reporter lines will be also useful in the future for "overview studies" of passage cells, such as defining the zone and number of passage cell formation in young roots.

3.4.3 Stele-expressed transporters are expressed in some cortical cells located adjacent to the xylem pole endodermal cells

During the expression pattern analysis of the passage cell fluorescent marker lines, we observed that in addition to the stele and the xylem pole endodermal cells all these transporters are expressed in a subset of cortical cells. Detailed observation of these expression patterns shows that these cortical cells are always located opposite to the xylem pole endodermal cells (Fig. 6A-E). However, IRT3 expression was also observed in some epidermal cells in addition to the cortex and endodermis. These results are very interesting, as published data mainly mentions "bilateral" or "bisymmetric" cellular patterning associated with the vascular tissues and the pericycle. Bisymmetric patterning of the endodermis has largely been ignored in the *Arabidopsis* literature, whereas bisymmetric differential expression within cortical cells has, to our knowledge, never been reported.

This preliminary data suggests that, as deposition of suberin on the entire endodermal cells during the secondary development should make nutrient uptake more difficult, passage cells may still allow for some direct nutrient uptake into the vasculature either from xylem pole located cortical and endodermal cells that are in proximity to xylem vessels. Specialized endodermis and cortex cells could provide a sort of a funnel in older roots that ushers nutrients directly into the xylem vessels.

We also made fluorescent marker lines specific for suberized endodermal cells ("non-passage cell") with the promoter of suberin biosynthetic genes mention in chapter II (See

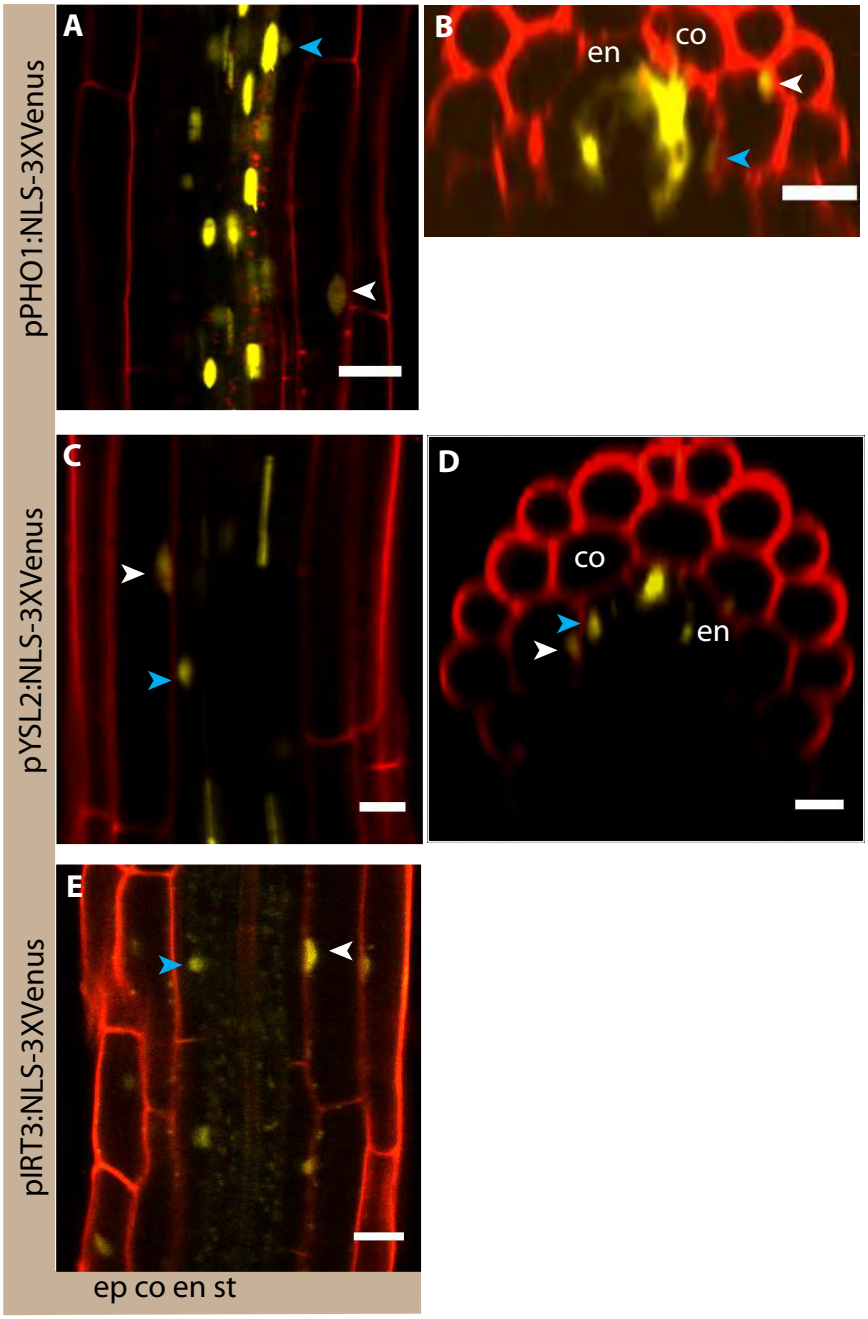

Figure: 6 Expression of pPHO1,pYSL2 and pIRT3 in some cortical cells that are positioned at the xylem pole –associated endodermal cells.

(A-B) pPHO1: NLS-3XVenus expression in cortex and endodermis shown in both longitudinal and transversal cut.

(C-D) pYSL2:NLS-3XVenus expression in cortex and endodermis shown in both longitudinal and transversal cut.

(E) Expression of pIRT3:NLS-3XVenus in some cortical and enodermal cells.

Blue arrowheads mark the expression in xylem pole–associated endodermal cells whereas white arrowheads mark the expression in cortical cells aligned with xylem pole – associated endodermal cells.

(Scale bars, 20μM) epidermis (ep),cortex (co), endodermis (en) and stele (st).

Annex VIII.B; Table 1). The main idea is to see the separation, or mutually exclusive expression, between the suberin biosynthetic gene and PHO1. This would confirm that endodermal cells that show transporter expression are non-suberized. In order to observe this, we made a double marker line using the potential passage cell markers (all transporters mentioned above) and the suberized cell marker line (pGPAT5: NLS 3X Tag RFP) (See Annex VIII.B; Table 4). Co-expression analysis of one of these lines (pPHO1: NLS 3XVenus; pGPAT5: NLS 3X Tag RFP) shows that PHO1 expression was only observed in endodermal cells of the state II where most of the cells become suberized. Despite this, no pGPAT expression was observed in the cells expressing PHO1 (Fig. 7A-F). This data firstly suggests that there is indeed a complementary gene expression between suberized and non-suberized cells. Secondly, passage cells indeed have their own identity and that they can be distinguished by expression from primary stage endodermal cells.

This preliminary data is only based on the analysis of PHO1 and GPAT co-expression pattern, but it shows that PHO1 is solely expressed in passage cells (non-suberized endodermal cells). In the future, it could be used as a candidate gene in order to define the physiological role of passage cells and to find the passage cells specific genes through cell-type specific gene expression profiling.

3.4.4 Patterning and differentiation of passage cells

In order to characterize the passage cells as cell with their own identity, it is important to define the physiological role of these cells that make them different from the primary stage endodermal cells and the surrounding suberized cells. As mentioned above that, the position of passage cells overlying the xylem poles is part of their definition and might be associated with their function. It also suggests that the position of passage cells could be defined by the vascular bundle organization. We therefore asked what would be the results of altered vascular patterning on the position of passage cells formation. It has been reported that cytokinins and auxin have been implicated in controlling vascular morphogenesis. For example: *wooden leg* (*wol*, a low cytokinin signaling mutant), *auxin resistant 3 (axr3,* a low auxin signaling mutant) and *Arabidopsis histidine transfer protein 6 (ahp6,* a mutant of an inhibitor of cytokinin signaling) display a markedly reduced number of cell files within the vascular bundle. This results in extreme

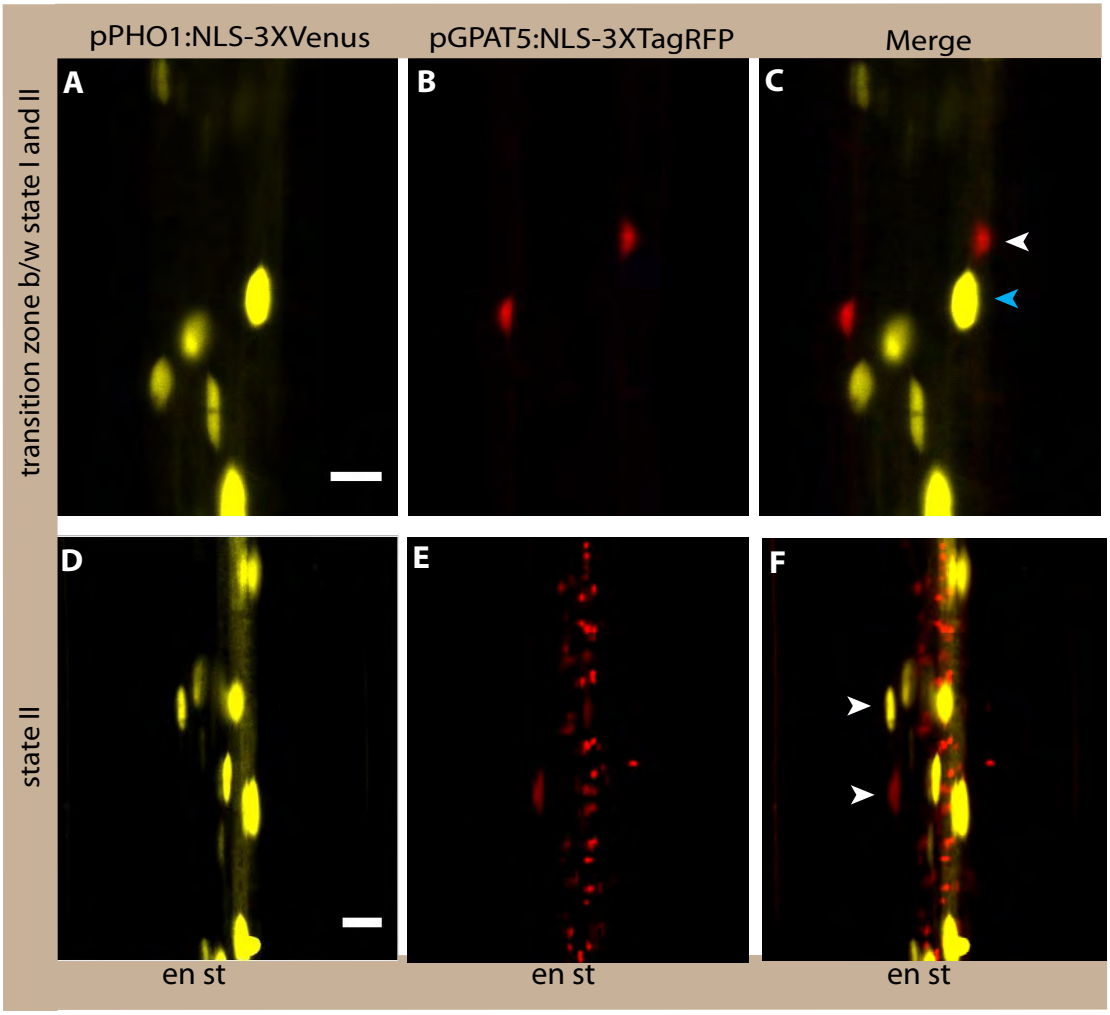

Figure: 7 Complementary gene expression between passage cell/non-suberized cells and suberized cells.

(A-C) Co-expression of pPHO1 and pGPAT5 at transition zone between state I and state II; pPHO1 is only expressed in the stele (yellow) shown by blue arrowhead and pGPAT5 expressed only in the endodermal cells shown by white arrowhead (red).

(D-F) Co-expression of pPHO1 and pGPAT5 at the state II of endodermal development, where suberin lamellae is completely formed. pPHO1 expressed in the stele and non-suberized/passage cell, (yellow) whereas pGPAT5 is only expressed in the suberized endodermal cells (red) shown by arrowheads.

(Scale bars, 20μM) endodermis (en) and stele (st).

phenotypes with the formation of either all protoxyelm elements or lack of only protoxylem. The most severe phenotype results in no xylem formation at all *(axr3)* (Fig. 8A-D) (Scheres et al.1995; Bishopp et al.2011; Mähönen et al. 2006).

Considering this, we did crossings of passage cells marker lines with different set of mutants that either have defects in protoxylem formation or completely lack the xylem vessels. (See Annex VIII.B; Table 2 and 4). In the future, our aim is to check how the transit from bisymmetric to radial symmetric pattern of vascular cells affects the passage cell positioning.

3.4.5 Physiological importance of passage cells

In addition to investigate passage cells in terms of their patterning and development, we would also like to define the physiological importance of passage cells in term of nutrient transport. Nutrients can cross the endodermis either through the symplastic or through the apoplastic pathway. The plasma membrane acts as the first soil/plant interface by selecting ion uptake through specific transporters reported to be present in the epidermis and can counteract the presence of undesired molecules (Marschner et al. 1995). However, controlling external compound entrance via the apoplastic space is more complicated since free diffusion occurs within cell walls. The presence of CS allow an efficient and selective uptake of nutrients, making passage through endodermal cells a essential step for molecules to reach the stele. Therefore, the role of CS is to stop the apoplastic pathway and to force the symplastic passage of compounds. Later on, formation of suberin lamellae between the plasma membranes and primary cell walls of endodermal cells makes nutrient uptake into the stele more difficult. As suberin deposition occurs on the entire endodermal cell, it may be responsible for blocking nutrient uptake across the plasma membrane of suberized cells into the endodermis, thus forcing entry of nutrients at the level of cortex and epidermis, and forcing a symplastic passage of nutrients. If symplastic passage of nutrients is possible, then why do some of the endodermal cells (passage cells) not seal off with suberin deposition? Are these cells in some way specialized for direct transport of some essential nutrients directly into the xylem vessels? In order to answer these questions we crossed all our passage cells marker lines with *esb1* mutant previously describe as an enhanced suberin mutant (See Annex VIII.B; Table 4). *esb1* mutant shows stronger and earlier deposition of suberin

with the complete lack of passage cells formation (See Chapter V.A). Our aim is to observe if suberization will also interfere with the expression of PHO1 in the xylem pole associated endodermal cells. As shown above, PHO1 expression and suberization in wild type plants are mutually exclusive, but it remains to be seen whether this is also the case in the *esb1* background.

3.4.6 Do all the endodermal cells become passage cells in the absence of suberin lamellae formation?

Finally, as introduced in chapter II, we created a line expressing the plant cutinase under endodermis specific promoter (pCASP1::CDEF1), which specifically degrades the endodermal suberin formation but has no effect on the formation of a functional CS. This is a tool of great utility for studying the role of suberin lamellae in root nutrient uptake. We will use this line to answer the question whether all the cells will behave like passage cells (i.e. show PHO1 expression) if suberin lamellae are absent. We have crossed all the potential passage cells marker lines with pCASP1::CDEF1 transgenic line. We would also like to test the uptake of different nutrient into the stele in the plants with no suberin lamellae formation (only containing CS) in comparison with one having normal endodermal development with CS, passage cell and suberin lamellae formation (Fig. 8E-F). Marie Barberon in our lab is trying to solve this issue regarding the role of suberin. In the future, this will provide us with direct evidence for the role of suberin in regulating water and nutrient uptake into the stele.

3.4.7 Identification of genes specific to passage cells using a two-component system

Identification of genes specific to passage cells would be important for defining them clearly as a distinct root cell type. Current methods for the study of pure individual cell types include the laser capture microdissection (LCM) of sectioned tissues (Brunskill et al. 2008; Jiao et al. 2009), cell type-specific chemical modification of RNA (Miller et al. 2009) and fluorescence-activated cell sorting (FACS) of fluorescently labeled cell lines or isolation of GFP-marked protoplasts (Birnbaum et al. 2003). Unfortunately, we cannot proceed with any of these techniques for several reasons. Firstly, as mentioned above, all our transporters are not exclusively expressed in passage cells. Secondly, among all techniques, LCM and FACS are the only ones applicable to *in vivo* studies, but both are limited in that they involve extensive tissue manipulation, require complex and

expensive equipment and it is hard to get enough pure tissue, specially in the case of LCM. We considered protoplasting followed by FACS, which is now a day is being used on a large scale for transcript analysis in cell-type specific manner. However, as mentioned in chapter I that upon plasmolysis, the protoplast of endodermal cell remains tightly attached to the cell wall. Therefore, protoplasting may only allow obtaining endodermal cells before the formation of CS.

Regarding these problems, we decided to develop a simple and generally applicable method for studying gene expression profiles exclusively in the passage cells. Considering this we selected two recently introduced methods: affinity tagging of ribosomal proteins or poly (A)-binding proteins (Mustroph et al. 2009) and INTACT, for isolation of nuclei tagged in specific cell types ((Deal and Henikoff 2010). During the past few years, both of these methods have been adapted and successfully applied to measure the gene expression profiles of individual cell types within a complex tissue. We choose them because both are robust and simple in many aspects: they do not require any extensive tissue manipulation or use of expensive instrumentation, are easy to perform and do not require any specialized skills for gene expression profiling of individual cell types. Both of these procedures are much faster and gentler, allowing us to obtain sufficient material without artifacts arising from specific tissue manipulation. An additional advantage is that nuclei isolation/ribosome extraction can be simply perform by fast freezing and grinding of whole tissues without any harsh treatment to separate the specific cells.

How these two-system work?

INTACT: Isolation of nuclei tagged in specific cell types

This system is based on two-step process; the first one is the biotin tagging of nuclei by expressing an outer nuclear envelope targeted fusion protein under desired cell-specific promoter. This nuclear targeting fusion (NTF) protein consisted of three parts:

1: The WPP domain of *Arabidopsis* RAN GTPASE ACTIVATING PROTEIN 1 (RanGAP1), which is necessary and sufficient for envelope association (Rose and Meier 2001)

2: Green fluorescent protein (GFP) for visualization,

3: Biotin ligase recognition peptide (BLRP), which acts as a substrate for the *E. coli* biotin ligase BirA (Beckett et al.1999).

The second one is the expression of BirA under a cell-specific promoter to provide a biotinylation of NTF in the desired cell type. The expression of the both NTF and BirA in the same cell type produces biotinylated nuclei exclusively in that cell type (Fig. 9A). Initially, the INTACT system was used to measure the cell type-specific expression of the NTF protein in hair and non-hair cell types of the *Arabidopsis* root epidermis. Both of these transgenic lines also expressed BirA constitutively, in order to generate the biotinylation of the NTF in the hair or non-hair cell types (Deal and Henikoff 2010).

Affinity tagging of ribosomal binding proteins

This method allows capturing of ribosomes associated mRNA in high throughput studies. It involves the generation of transgenic lines that express ribosomal proteinL18 (RPL18) with a His-FLAG (HF) dual epitope tag. These transgenic lines facilitate the isolation of a sub-population of mRNA complexes from specific cell types by a one-step immunoprecipitation method. Finally, ribosomes, with their associated mRNAs, could be used for the measurement of the gene expression profiles (Fig. 9B). This method was used to monitor the rapid remodeling of gene expression in response to specific environmental stresses such as hypoxia in *Arabidopsis thaliana*. This is accomplished by producing transgenic lines in which the ribosomal protein gene is driven by the near-constitutive cauliflower mosaic virus 35S promoter and under different cell-type-specific promoters. The profiling of total cellular mRNA is done by immunoprecipitation from a specific cell population (Zanetti et al. 2005 and Mustroph et al. 2009).

"Remix" of Intact and affinity tagging of ribosomal binding proteins methods

Both of the above-mentioned methods were demonstrated to be biologically and technically reproducible. As our candidate genes are also highly expressed in the stele, we cannot only use the affinity tagging of ribosomal binding proteins method. This would isolate the mRNA population not only from passage cells, but also from the stele. The INTACT system allows *in vivo* biotin labeling and provides a solution for our

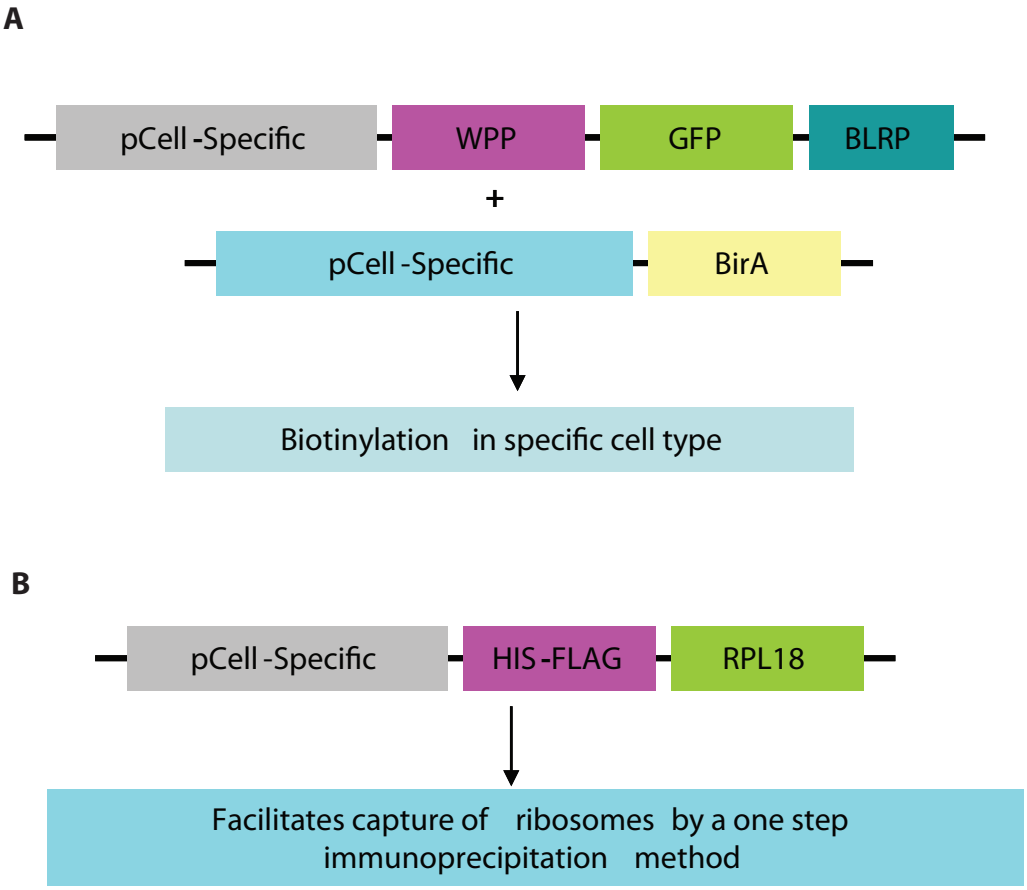

Figure 9: Schematic representation of nuclear envelope targeted fusion protein (NTF), E. coli Biotin ligase A (BirA) and epitope tagged ribosomal binding protein (RPL18) under cell-specific promoter.

(A) Together, NTF and BirA provide biotinylation in the specific cell type in the presence of Biotin ligase recognition peptide (BLRP).

(B) Schematic depicting the epitope tagged ribosomal binding protein RPL18 under cell-specific promoter: facilitates the epitope-tagged ribosomes capturing to study the gene expression profiling.

problem. We can first express the NTF under a passage cell/stele specific promoter and then to express BirA under an endodermis-specific promoter in order to biotinylate the NTF. Finally, the expression of both NTF and BirA will produce the biotinylation specifically in only the passage cells (Fig. 10). However, we also decided to remix both INTACT and ribosomal pull down systems in a way to keep the advantages of each one and use them to solve our problem.

For example, The INTACT method appears to be simple, fast, and potentially, widely applicable. Compared to the affinity tagging of ribosome, the INTACT system has an advantage: it allows having a cell population from the overlap or intersection of two expression profiles, which is what we need at present: to get a specific labeling of passage cells. On the other hand, affinity tagging of ribosomal binding protein allows the targeting of ribosomes exclusively from the desired cell type only if the right promoter, expressed only in the cells of interest, is used. However, this system has an advantage as it facilitates the capture of the actively translated, ribosome-associated mRNA, compared to INTACT that only uses nuclear RNA, which contains only a fraction of the total mRNA. As our candidates genes are only expressed in a few endodermal cells, obtaining sufficient RNA might be a problem and we will check whether purifying nuclei or ribosome-associated RNA makes a difference.

We therefore combined the two systems in such a way that we would use the advantage of INACT system to produce a biotinylation specifically in the passage cells, with the possible advantage of the ribosome pull down system in delivering more mRNA per cell. This was achieved by expressing the Biotin ligase recognition peptide (BLRP)-FLAG tagged RPL18 under passage cell or non-passage cell. In order to facilitate the biotinylation exclusively in the passage cells, we expressed BirA under the endodermis specific promoter. Finally, the intersection of both BLRP-FLAG tagged RPL18 (expressed in stele and passage cell endodermis) and BirA (in all endodermal cells) will allows biotinylation only in passage cell and to obtain an mRNA population only from those specific cells.

This far, we have been able to produce two types of transgenic lines, one expressing BLRP-FLAG tagged RPL18 under different sets of passage cell and suberized cell promoters. Moreover, a second line expressing the BirA under endodermal cell specific

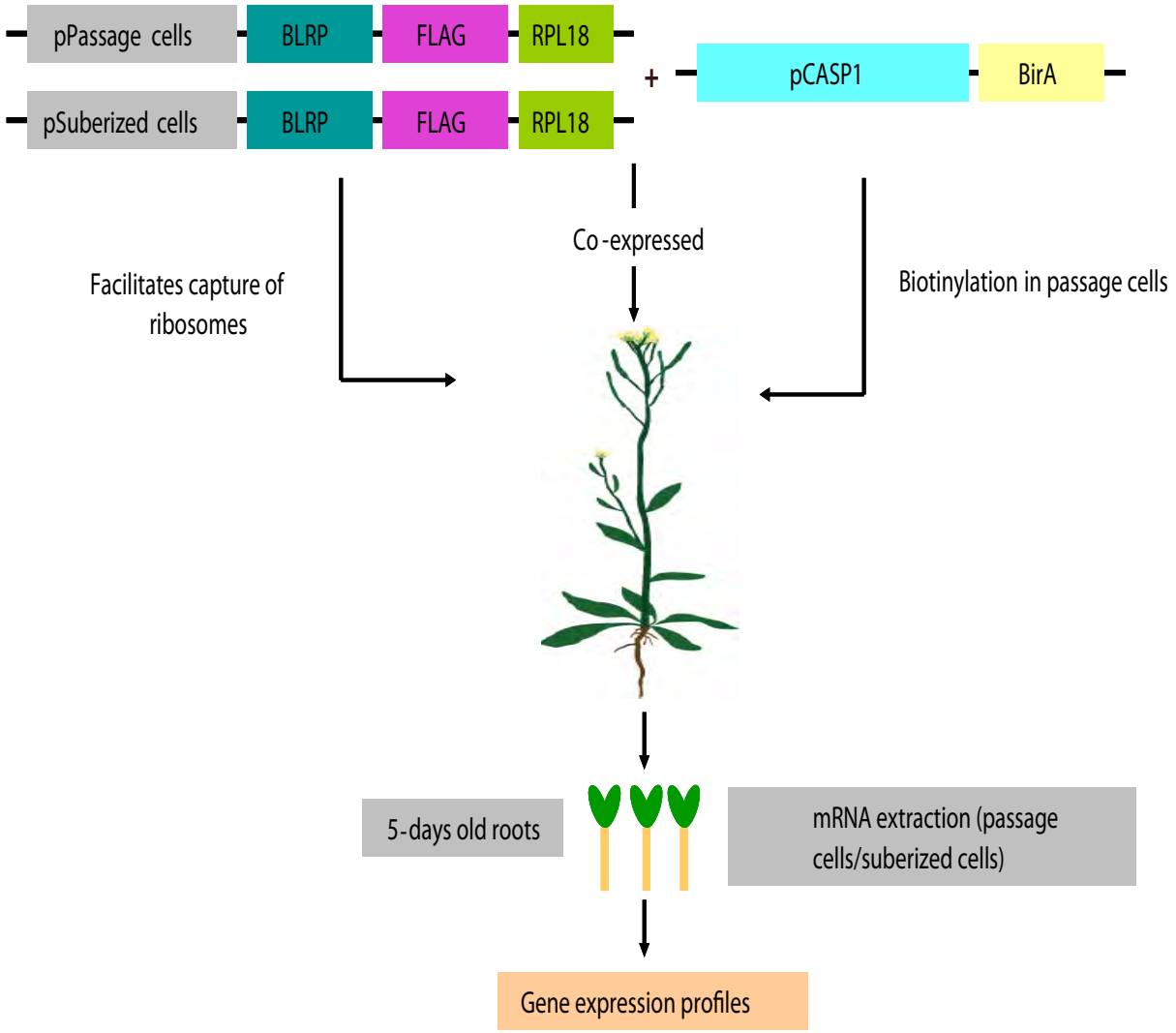

Figure 10: Schematic representation of "Remix" of INTACT and Affinity tagging of ribosomal binding protein.

Expression of *E. coli* biotin ligase A (BirA) under endodermis specific promoter CASP1 will produce the biotinylation exclusively in the passage cells or suberized cells in the presence of Biotin ligase recognition peptide (BLRP-FLAG tagged ribosomal binding protein; RPL18) under the passage cell (pPHO1) or suberized cell specific promoter (pGPAT5).

BLRP-FLAG tagged RPL18 enables the targeting of tagged ribosomes only in these specific cells.

Finally the intersection of both BLRP-FLAG tagged RPL18 and BirA in the passage cells allow the targating of ribosome-associated mRNA and measurement of gene expression profiles exclusively from passage cells.

promoter allows the biotinylation only in the endodermis. Crossing of both transgenic lines will provide us a tool to perform gene expression profiling exclusively of passage cells (Fig. 10).

As mentioned above, both of these systems work very well independently and we are quite ambitious to attempt to make both systems work in a combined form. However, in case this combination will not work, we will also be able to just go for the unaltered INTACT system. For this purpose, I also made the transgenic lines specifically for this system. It involves one line expressing NTF under passage or non-passage cells promoter and a second expressing BirA under endodermis specific promoter. Together, these lines will produce biotin labeled nuclei only in the passage cells (See Annex VIII. B; Table 3 for all the transgenic lines generated for this system).

3.5 Conclusion and Perspectives

Altogether, our preliminary data mainly demonstrates our efforts to define the endodermal passage cells better than just as endodermal cells that “stay young”. However, in order to characterize passage cells, we needed to find genes that are specifically expressed in those cells. Although we succeeded in the identification of some stele-specific transporters that are expressed in passage cells, but we did not obtain strictly passage cell specific promoters. Nevertheless, we showed that all of these transporters exhibit different expression patterns during the development of endodermis. For example, YSL2 is expressed only in the non-suberized cells of both states I and II. By contrast, PHO1 is expressed only in the state II non-suberized cells. According to the co-expression analysis with lines expressing suberin biosynthetic genes, PHO1 appears to be expressed in passage cells and is considered our best candidate for future manipulations.

We also developed a new strategy for cell-type specific expression profiling by “remixing” two independent systems. This two-component system will be useful in the future in order to characterize passage cell identity. A better description of passage cells occurrence and differentiation might provide a breakthrough in our understanding of root physiology. These findings will also guide our efforts in understanding the barrier properties of different developmental stages of endodermis in term of nutrient or water uptake and protecting cells against pathogen attacks.

Most of the work regarding this project in terms of generating transgenic lines, crossings, and propagation was done and all the transgenic lines will soon be ready to use. However, I will not be able to finish this project myself because of time restrictions.

3.6 Experimental procedures

3.6.1 Plant Material and Growth Conditions

All used transgenic lines were generated in an *Arabidopsis thaliana* ecotype Columbia-0 background. For detail of knockout mutants and transgenic lines, See Annex VIII.B: Table 1, 2, and 3. *ahp6-1* seeds were obtained from Y. Helariutta (University of Helsinki, Helsinki, Finland). esb1 seeds were obtained from David Salt (University of Aberdeen)

Seeds of *wol* were kindly provided by Helariutta Y and *axr3* by Leyser O. Plants were germinated on 1/2 MS agar plates after 2 days in the darkness at 4°C. Seedlings were grown vertically in percival chambers at 22°C, under long days (16 hr light/8 hr dark) and were used at 5 days after shift to room temperature.

3.6.2 Chemicals

PI was purchased from Invitrogen. Fluorol yellow was purchased from Sigma-Aldrich.

3.6.3 Vector Construction and Transformation

In order to check the promoter activity of stele-expressed transporters in the passage cells transgenic lines regarding Promoter: NLS-3XmVenus and Promoter: NLS-3XTagRFP were made by classical cloning methods. The pJV120pGREEN229-NLS-3XmVenus and pJV184pGREEN229-NLS-3XTagRFP vectors containing OCS3' terminator site were used for the insertion of cell-type specific promoters upstream of NLS3XVenus or TagRFP into the *KpnI* restriction sites. The obtained vector confers bacterial kanamycin resistance and plant Hygromicin (Suberized cell marker lines) and Basta resistance (Passage cell marker lines). (See Annex VIII.B: Table 1 for detail of fluorescent marker lines and Table 5 for primer details). All constructs were electroporated into pSOUP containing *Agrobacterium tumefaciens strain* GV3101. Plant transformation was done by floral dipping method (Clough SJ and Bent AF 1998).

Transgenic lines for the two-component system and for INTACT were generated by using Gateway Cloning Technology (Invitrogen).

For generation of pEnBLRP-FLAG-RPL18 clone, coding region of ATRPL18 was amplified from pGATA:HF-RPL18 vector (Zanetti *et al.,* 2005 and Mustroph *et al.,* 2009) by PCR using primers Osn039AS and Osn040S, that encode for BLRP-FLAG tags, followed by a spacer of seven Gly residues, were annealed. The resulting fused fragment was recombined into pDONR221 by using BP clonase enzyme (Invitrogen). For pEnMyc-BirA clone the coding region of 3xMyc tagged biotin lygase A (BirA) were amplified from Lab 530 GIIK LIC-BirA vector (Bert De Rybel et al. 2011; Dealand Henikoff 2010) by PCR using primers Osn042S and Osn043AS. The resulting fragment was recombined into pDONR221 by using BP clonase enzyme (Invitrogen). The nuclear tagging protein (NTF) for the INTACT system was amplified from Lab 444 pGL2: NTF INTACT by using Osn044S and Osn045AS primers through PCR. The resulting fragment was recombined into pDONR221 using BP clonase enzyme (Invitrogen). The resulting pEntry clones were named as pEn-L1-BLRP-FLAG-RPL18-L2 (pSN031) and pEnL1-3x MycBirA- L2 (pSN032) and pEntry-L1-NTF-L2 (pSN037) (See Annex VIII. B; Table 6 for primer details).

In order to generate the Promoter: BLRP-FLAG-RPL18, Promoter:Myc-BirA transgenic lines the following pEntry clones; pEntry Clone kpnIL4- IRT3 -kpnIR1(pSN033), pEntry Clone-KpnIL4-PHO1-KpnI-R1(pSN034),pEntryClone-kpnIL4-SKOR-KpnI-R1(pSN035), and pEntry Clone KpnIL4- YSL2-KpnI-R1(pSN036) were generated as follow. The 2.1kb fragment located upstream of PHO1 gene, 597 bp fragment of IRT3 including the 528 bp upstream sequence of AtIRT3 5′-UTR containing the promoter and partial 5′-UTR regions, 1.8kb promoter region of SKOR gene and 1.12kb promoter region of AtYSL2 gene were amplified from genomic DNA. Restriction sites KpnI were added by amplification. The amplified fragments for each gene were digested with kpnI restriction enzyme and cloned into the Lab479 pUC L4-KpnI-XmaI-R1 vector (containing Gateway binding specific attL4-attR1 specific sites).

To recombined promoter specific pENTRY clones and pEn-L1-BLRP-FLAG-RPL18-L2 (pSN031) for two-component system and pEn-L1-NTF-L2 (pSN037) for INTACT Lab 176 pB7m24GW, 3 were used as destination vector. Destination vector Lab 190

pK7m24GW, 3 were used to recombined promoter specific pENTRY clones and pEnL1-3x MycBirA- L2 (pSN032) using LRclonase (Invitrogen) (For details see Annex VIII. B; Table 3). Transgenic plants were generated by introduction of the plant expression constructs into *Agrobacterium tumefaciens* strain GV3101 and transformation was carried out by floral dipping (Clough and Bent. 1998).

All the promoter:NLS-GFP-GUS lines were generated by Gateway Cloning Technology (Invitrogen). PYL-037Gateway (attR4-R1)::NLS-GFP-GUS vector was used as destination vector (For detail see Annex VIII.B: Table 1).

pCASP1: CDEF1 (pSN007) and pELTP::CDEF1 (pSN017) transgenic line used were described in Chapter IV.

3.6.4 Microscopy and Histology

Confocal laser scanning microscopy was performed on a Zeiss LSM 700 confocal microscope. Excitation and detection windows were set as follows: GFP 488 nm, 500–600 nm; mCherry 594 nm, 600–700 nm; Propidium iodide 488 nm, 600–700 nm; mVenus and mCherry 514 and 594, 520–560, and 600–700 nm. Fluorol yellow staining was performed, as described in chapter II (Naseer *et al.,* 2012). For Propidium iodide, seedlings were incubated in the dark for 10 min in a fresh solution of 15 mM (10 mg/ml) PI and rinsed two times in distilled water (For detailed protocols see chapter VII.A).

3.7 Literature cited

Alassimone J, Naseer S, Geldner N. 2010. A developmental framework for endodermal differentiation and polarity. Proc. Natl. Acad. Sci. USA, 107:5214–19.

Anthony Bishopp, Hanna Help, Sedeer El-Showk, Dolf Weijers, Ben Scheres, Jiří Friml, Eva Benková, Ari Pekka Mähönen, Ykä Helariutta. 2011. A Mutually Inhibitory Interaction between Auxin and Cytokinin Specifies Vascular Pattern in Roots. Current Biology, 21: 917–926.

Baxter I, Hosmani P.S, Rus A., Lahner B., Borevitz J.O, Muthukumar B, Mickelbart M.V, Schreiber L, Franke R.B, Salt D.E. 2009. Root suberin forms an extracellular barrier that affects water relations and mineral nutrition in *Arabidopsis*. PLoS Genet, 5(5):492.

B. Scheres *et al.,* 1995. Mutations affecting the radial organization of the *Arabidopsis* root display specific defects throughout the embryonic axis, Development, 121: 53.

Beckett D, Kovaleva E, Schatz PJ. 1999. A minimal peptide substrate in biotin holoenzyme synthetasecatalyzed biotinylation. Protein Sci, 8:921–929.

Bhattacharya B, Puri S, Puri RK.2009. A review of gene expression profiling of human embryonic stem cell lines and their differentiated progeny. Curr Stem Cell Res, 4:98–106.

Bishopp A, Help H, El-Showk S, Weijers D, Scheres B, Friml J, *et al.,* 2011. A mutually inhibitory interaction between auxin and cytokinin specifies vascular pattern in roots. Curr. Biol, 21:917-926.

Bonnett, H. T. Jr. 1968. The root endodermis: fine structure and function.J. Cell Biol, 37: 109-205.

Brunskill EW, Aronow BJ, Georgas K, Rumballe B, Valerius MT, Aronow J, Kaimal V, Jegga AG, Yu J, Grimmond S, *et al.,*2008. Atlas of gene expression in the developing kidney at microanatomic resolution. Dev Cell, 15:781–791.

Clarkson, D.T, Robards, A.W, and Sanderson, J.1971. The tertiary endodermis in barley roots: Fine structure in relation to radial transport of ions and water. Planta, 96: 292–305.

Clarkson DT, Robards AW. 1975. The endodermis, its structural development and physiological role. In the development and function of roots. Academic Press, London, 415-436.

Clough S.J., Bent A. 1998. Floral dip: A simplified method for *Agrobacterium*-mediated transformation of *Arabidopsis thaliana*. Plant J, 16:735–743.

De Rybel B, van den Berg W, Lokerse AS, Liao CY, van Mourik H, *et al.,* 2011. A versatile set of Ligation-Independent Cloning vectors for functional studies in plants. Plant Physiol, 156:1292–1299.

Di Donato, R. J., L. A. Roberts, *et al.,* 2004. *Arabidopsis* Yellow Stripe-Like2 (YSL2) : a metal-regulated gene encoding a plasma membrane transporter of nicotianamine-metal complexes. The Plant Journal, 393: 403-414.

Enstone, D.E, Peterson, C.A. and Ma, F.2002. Root endodermis and exodermis: structure,

function, and responses to the environment. Journal of Plant Growth Regulation, 21: 335–351.

Esau K. 1965. Plant Anatomy. 2nd edition. John Wiley and Sons, Inc., New York.

Ferguson, I. B. and Clarkson, D. T. 1976. Simultaneous uptake and translocation of magnesium and calcium in barley (*Hordeum vulgare*) roots. Planta, 128: 267-269.

Gaymard F, Pilot G, Lacombe B, Bouchez D, Bruneau D, Boucherez J, *et al.,* 1998. Identification and disruption of a plant Shaker-like outward channel involved in K^+ release into the xylem sap. Cell, 94: 647–655.

Geldner, N. 2013. "The Endodermis." Annual Review of Plant Biology, 64(1): 531-558.

Hamburger, D. 2002. Identification and Characterization of the *Arabidopsis* PHO1 Gene Involved in Phosphate Loading to the Xylem. The Plant Cell Online, 14(4): 889-902.

Irion S, Nostro MC, Kattman SJ, Keller GM.2008. Directed differentiation of pluripotent stem cells: from developmental biology to therapeutic applications. Cold Spring Harb Symp Quant Biol ,73:101–110.

4 Chapter IV: Interference of CDEF1 (Plant Cutinase) with suberin accumulation in the periderm

4.1 Collaborators and Contribution

I contributed to the conception of the study and mainly did all the experiments. I generated the transgenic lines expressing plant Cutinase. For analysis of promoter GUS activity, transgenic lines pCASP1: NLS-GFP-GUS and pGPAT5:NLS-GFP-GUS were previously described in Roppolo *et al.,* 2011 and Naseer *et al.,* 2012. Daniele Roppolo, a former postdoc in our lab, generated peLTP::GUS (AT2G48130-prom) line. Rochus Franke (Institute of Cellular and Molecular Botany, University of Bonn, Germany) performed suberin monomer analysis.

4.2 Introduction

The roots of many dicotyledonous plants undergo secondary growth; the onset and extent of this process, however, exhibits remarkable variation between different species. Cell layers forming within the stele drive secondary growth in roots, result in the formation of secondary meristems (lateral meristems) called “vascular cambium” and “cork cambium” (phellogen). The phellogen is a meristematic tissue from which the periderm originates. However, secondary growth is mainly the result of the activity of the vascular cambium. The vascular cambium divides to produce secondary xylem and phloem cells. This growth increases the girth of the plant root rather than its length. As long as the vascular cambium continues to produce new cells, the root will continue to grow in diameter. For a certain period, outer primary cell layers such as the epidermis, cortex, and endodermis can adapt to this growth in girth by cell division and circumferential extensions of cells. Nevertheless, at a certain point, they break down and become sloughed off. Thus, continued secondary growth eventually ruptures the outer primary cell layers.

The cork cambium divides and produces two different tissue layers. The first layer is a thin layer of parenchyma cells (phelloderm) that forms in the interior of the cork cambium. The second layer is a thick layer of cork cells (phellem), which accumulate at the exterior of the cambium. Thus, cork, cork cambium, and phelloderm collectively form the suberized, multilayered, secondary dermal tissue termed as the “periderm” that replaces the protective role of primary dermal tissues (Fig. 1). The periderm serves both functional and structural roles, controlling the loss of water and solutes to the

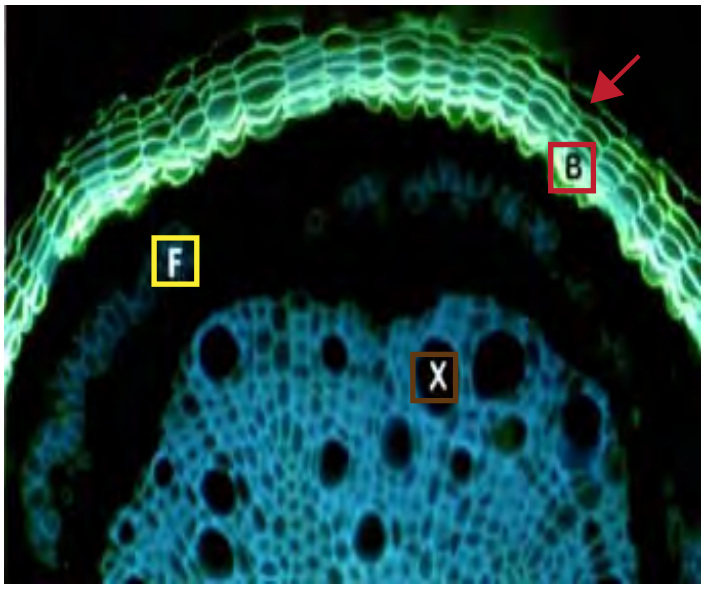

Figure 1: Root cross section of *Quercus* after secondary growth showing multilayered periderm (red arrow).
(B) Fluorescent staining of suberised periderm
(X) Blue autofluorescence of lignified xylem
(F) phloem fibre
(Adopted from mycorrhizas.info/root.htm).

environment, restricting the entrance of pathogens, and keeping plants firm due to their rigidity and stability (Dolan and Robert 1995; Geldner 2012).

In this chapter, further investigations of the transgenic lines expressing plant Cutinase (CDEF1) under an endodermis specific promoter are discussed. CDEF1 is a member of the GDSL lipase/esterase family of proteins, which are mainly expressed in pollen. Subcellular analysis showed that the CDEF1 protein is secreted to the extracellular space when expressed in leaves (Takahashi et al. 2010). Cutinase is an enzyme that degrades cutin, the major polymer present in plant cuticle. Both cutin and suberin share the same monomer composition with some differences in the chain length. Therefore, we thought that CDEF1 could also have the ability of degrading suberin. The main purpose of generating this line expressing CDEF1 was to specifically degrade the suberin deposited in the endodermis.

4.3 Rationale of the study

As mentioned in Chapter II, through the line expressing CDEF1, we were able to show that CDEF1 strongly degrades the endodermal suberin and this degradation has no effect on the formation of functional Casparian Strip (CS). However, in order to gain more insights and to confirm these results, we would like to study the suberin compositional changes in plants devoid of suberin in comparison with wild type individuals. As shown in Chapter II, Fluorol Yellow staining (FY) is a reliable reporter for the presence or absence of suberin and in the transgenic plants expressing CDEF1 no FY signals was observed at all. Thus, we would expect the complete reduction in the different monomers of suberin.

For this purpose, our collaborator Rochus Franke, from the University of Bonn, analyzed the quantity and composition of the aliphatic root suberin in these plants by using GC and GC-MS (Gas chromatography–mass spectrometry) analysis. However, instead of using 5-days old seedlings for suberin monomer analyses, 4 to 5 weeks old roots were used. In these, the periderm, which characteristically possesses several layers of suberin lamellae, is completely formed. Interestingly, suberin monomer composition was significantly reduced in the pCASP1::CDEF1 plants. To the best of our best knowledge, CASP1 is specifically expressed exclusively in the endodermis, but not in the periderm even in young roots, its expression starts to be weaker in the older part (Roppolo et al.

2011). This posed the problem of how CDEF1 under an endodermis specific promoter could be able of degrading suberin deposited in the periderm. In order to start to solve this conundrum, I first performed a Fluorol Yellow assay on 4 to 5 weeks-old roots of pCASP1::CDEF1 plants to check the presence or absence of suberin deposition in the periderm. Then I checked the expression of CASP1 in the periderm.

4.4 Results and Discussion

4.4.1 pCASP1::CDEF1 transgenic line exhibits a significant reduction in root suberin deposited in the periderm

In Chapter II, we introduced different experimental manipulations of lignin and suberin production, combined with histochemical and functional assays for the apoplastic barrier formation. This combination of methods demonstrated that suberin is produced much toolate and is not required for formation of functional CS in the *Arabidopsis.* During this study, in order to obtain a stronger interference with suberin accumulation in the endodermis, we generated plants that are devoid of any detectable suberin. This was done by expressing the gene CUTICLE DESTRUCTING FACTOR 1 (CDEF1), a plant-encoded cutinase under the endodermis specific promoter pCASP1 (CASPARIAN STRIP DOMAIN PROTEIN 1). Strikingly, in 5-days old seedlings we observed a complete lack of suberin staining (FY) in these transgenic lines as compared to the wild type plants (Fig. 2A-2B). Based on these histochemical results we further analyzed these transgenic plants through GC and GC-MS analysis. To analyze the composition of root suberin, 4 to 5-weeks old soil-grown roots were subjected to depolymerization of suberin and subsequently analyzed using GC and GC-MS. Surprisingly, pCASP1::CDEF1 suberin exhibited significant reductions in monomers of all compound classes except for alcohols (Fig. 2C). The most pronounced reductions were detected in ω-hydroxyacids of chain length C16 and C18 and α, ω-diacids with chain length C16–C18:1. However, significant reductions could also be detected in C20 and C22 fatty acids.

These results were interesting for two reasons. Firstly, as discussed above, we generated this transgenic line in order to specifically degrade the suberin deposited in the endodermis in 5 days-old roots. The monomer analysis mentioned above was performed on roots of fully developed plants. In these roots, suberin deposition occurs mainly in the multilayered periderm and not only in the endodermis. This raises the question of how a

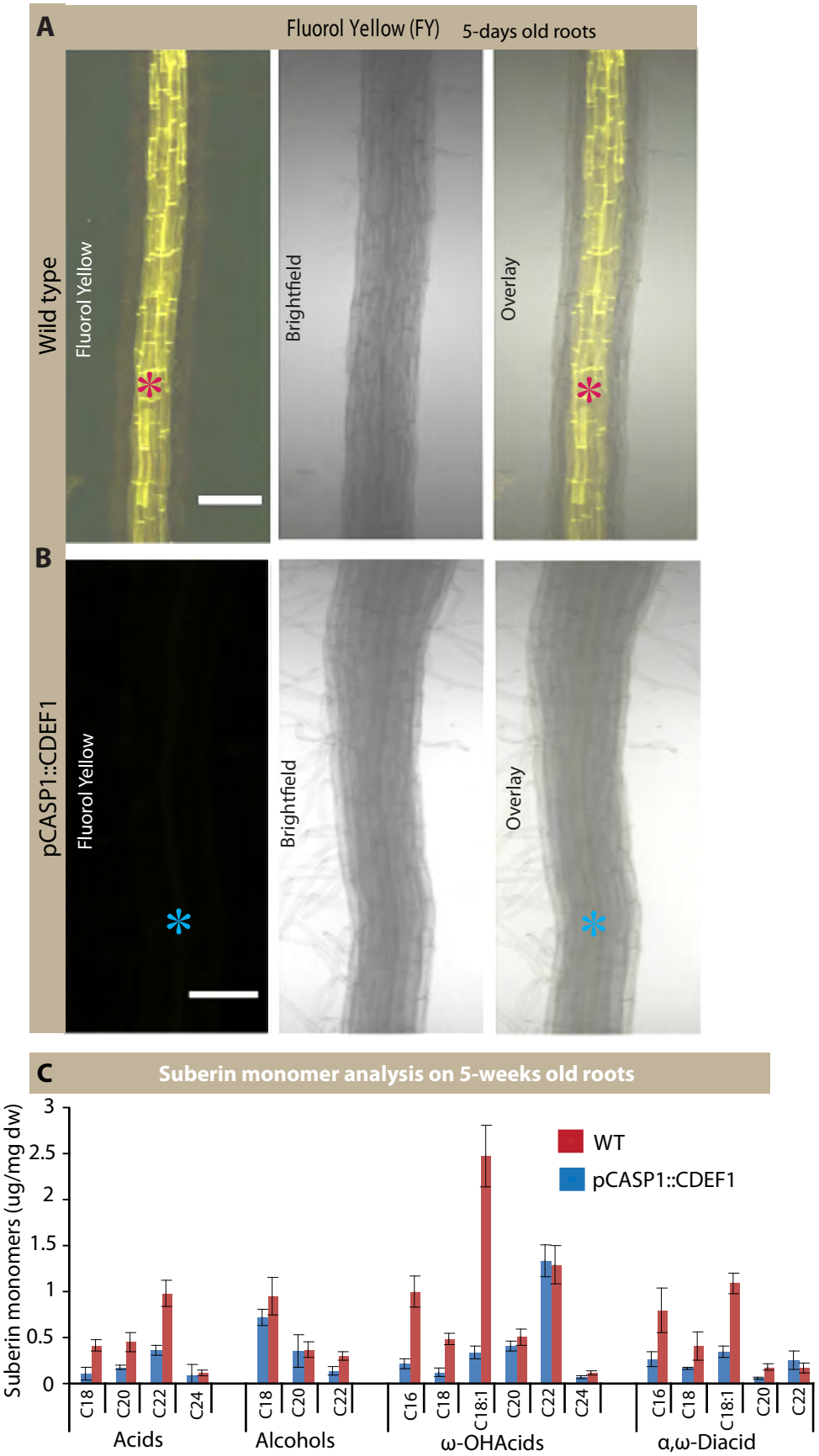

Figure 2: Amount of suberin monomers is significantly altered in 5-weeks old roots of pCASP1::CDEF1.

(A-B) Fluorol Yellow (FY) staining reveals the complete degradation of endodermal suberin in 5-days old seedlings of the pCASP1::CDEF1 transgenic line when compared to wild type individuals. Asterisks mark the presence (pink) and absence (blue) of FY staining in the endodermis (Scale bars 20 µm).

(C) Suberin monomer composition in 5-week old pCASP1::CDEF1 (Blue) and wild type (Pink) plants in µg /mg dry weight ±SD of four or five replicates. Significant reduction observed in C18, C20, C22 fatty acids and C16, C18, C18:1 α,ω-diacids . More pronounced reduction was detected in the ω-hydroyacids of chain length C16 and C18.

plant cutinase under an endodermis specific promoter could strongly interfere with the accumulation of suberin in the periderm? To our knowledge, such a strong reduction in suberin amount in the periderm has never been reported. Secondly, as mentioned in Chapter II, FY appears to be a good reporter for suberin deposition. Yet, as shown in Figure 1A, CDEF1 transgenic plants show complete absence of FY signals, while chemical suberin analysis only reports a strong reduction, but not the complete lack, of different suberin monomers? It would be important to understand the reasons for this discrepancy.

When we analyzed pCASP1::CDEF1 lines in further generations, we found that all the analyzed, independent transgenic lines were stable until T2 generation. Afterwards, we observed silencing with varying frequency in these transgenic lines, as we further propagated them. We noticed the appearance of a weak FY signal in T3 and T4 segregating lines as compared to the T2 transgenic lines. Suberin monomer analysis was carried out on T4 transgenic lines that started to accumulate detectable levels of suberin. This could explain the strong reduction, but not an absence, of suberin monomers in the chemical analysis.

As discussed in Chapter II, a strong and specific interference with suberin accumulation was never previously reported. I believe that in the future the pCASP1::CDEF1 transgenic line will be extremely useful to assess the numerous supposed physiological roles of suberin in roots. Taking this importance into account, and in order to solve the silencing problem, we generated transgenic line by expressing the CDEF1 under another endodermis specific promoter (AT2G48130-prom; LIPID TRANSFER PROTEIN). Strong degradation of suberin was observed in these lines with FY staining as compared to the wild type plants (Fig. 3A and B). Interestingly, no silencing was observed among these independent transgenic lines.

4.4.2 Fluorol Yellow (FY) staining reveals complete degradation of suberin accumulation in the periderm

In order to confirm the suberin monomer analysis with the histochemical analysis and to verify that suberin accumulation is indeed absent in the periderm in the CDEF1 expressing transgenic lines, we performed FY assays on 4 to 5 weeks-old roots. Strikingly, no FY signal was observed in the periderm in any of the transgenic lines,

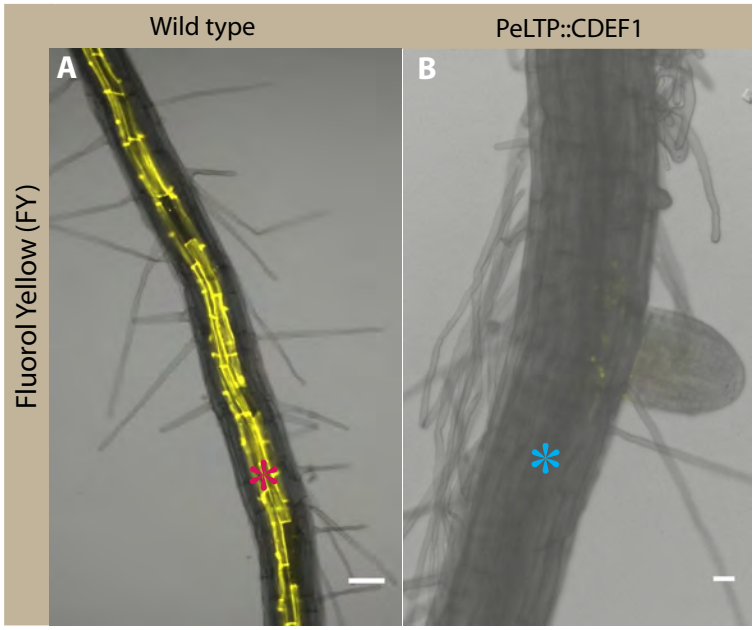

Figure 3: Fluorol yellow (FY) staining reveal the complete degradation of endodermal suberin in peLTP::CDEF1 (T3 individual transgenic line).
(A-B) Complete lack of suberin staining in the 5-days old seedling of peLTP::CDEF1 as compared to the wild type. Asterisks mark the presence (pink) and absence (blue) of FY staining in the endodermis (Scale bars 50µm).

either expressing CDEF1 under CASP1 or ELTP promoter (Fig. 4B and 4C). On the other hand, a strong FY signal was observed in the periderm of wild type roots (Fig. 4A). The complete lack of FY signal in our histochemical analysis when compared to the merely strong reduction in suberin monomer composition during GC-MS analysis was due the fact that FY assay was done on the T2 segregating lines and T4 silenced transgenic lines were used for suberin monomer analysis.

4.4.3 Neither CASP1 nor ELTP promoters are active in the periderm

In order to understand why pCASP1 driven CDEF1 would interfere with suberin accumulation in the periderm, we first observed the expression of CASP1 in 4 to 5 week-old roots, when the periderm becomes fully developed. No pCASP1::GUS reporter activity was observed in the older part of the root where the periderm is fully developed (Fig. 5C). Nevertheless, a strong GUS expression pattern was observed in the young part of the main root and in the lateral roots, specifically in the endodermis (Fig. 5D). We then also observed the GUS expression pattern of pELTP in older roots. In this case, no significant periderm specific GUS activity of pELTP was observed (Fig. 5E). However, some patchy GUS expression was observed in the older part of the root. This may be an artifact of the GUS staining procedure. A strong endodermis specific GUS expression was observed in the younger part of the root (Figure 3F). The pGPAT5: GUS reporter fusion (gene involved in the suberin biosynthesis) was used as a positive control to check the functionality of the GUS assay in periderm. GUS analysis shows that pGPAT5 was strongly expressed in the periderm and only in the base of the lateral root initiation site (Fig. 5A and 5B).

These results show that both CASP1 and LTP promoters are only expressed in the young parts of the root, specifically in the endodermis, but not in the periderm. Nevertheless, CASP1 or ELTP-driven CDEF1 is able to interfere with periderm suberin accumulation.

4.5 Concluding Remarks and Perspective

Our work suggests that even in the absence of CASP1 and LTP expression in the periderm, CDEF1 can significantly altered the composition of suberin monomers in the periderm. Unfortunately, with the previously mentioned data we were unable to solve this mystery. Probably, cutinase are able of diffusing and causing the degradation of

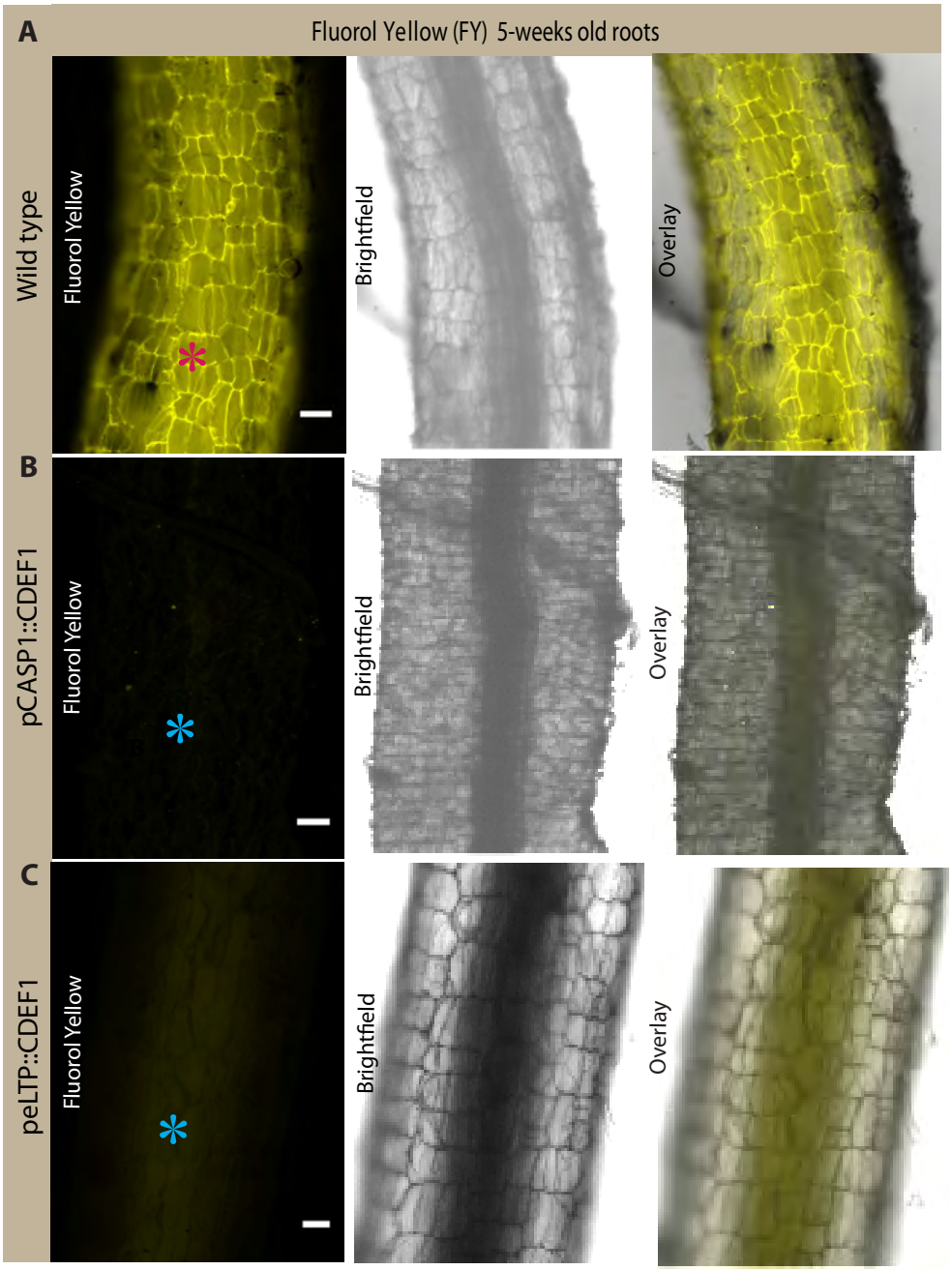

Figure 4: Plant Cutinase (CDEF1) completely degrades the suberin deposited in the periderm.

(A-C) Fluorol Yellow (FY) staining shows the complete lack of suberin deposition in the periderm in both pCASP1::CDEF1and peLTP::CDEF1 transgenic lines as compared to wild type.

Asterisk mark the presence (pink) of suberin on the cellular surface of periderm (A) and lack of suberin staining (blue) in the periderm (B-C) (Scale bars 10 µm).

suberin, even in the tissues where it is not expressed. As a future perspective, we are planning to check the cutinase activity in older roots of CDEF1 expressing transgenic lines with the fully developed periderm. The enzyme activity could be measured spectrophotometrically at 405 nm, following the hydrolysis of the artificial substrate PNB *(*p-nitrophenyl butyrate) (Dantzlg et al.1996).

A suberized periderm provides the root with an additional outer barrier. At this point, the endodermis might become dispensable. In fact, once secondary growth has occurred in mature roots, the endodermis will eventually disappear and a multi-layered suberized periderm derived from the epidermis will be the only apoplastic barrier. As there is no detailed data available about the timing and development of these secondary barriers, I attempted to analyze timing and development of these suberized layers and their relationship with the establishment of barriers in *Arabidopsis*. We are planning to observe consecutively the process of formation of periderm from pericycle cells in the 7-days old roots until the periderm forms. Development of suberized periderm will be monitor by fluorescent suberin dyes like Fluorol yellow or by transgenic reporter lines based on the expression of genes involved in suberin biosynthesis. Our main aim is to observe the effects of secondary growth on the endodermis apoplastic barrier by using the apoplastic tracer Propidium Iodide (PI). Most of the previously published work demonstrated that the endodermis would eventually break off during secondary growth. However, if we consider the primary cell wall modification of endodermis as a lignified network than the question arises of how the breaking of lignified CS might be facilitated. Is it purely the result of mechanical stress? Another question is if and how the CS manages to keep an apoplastic barrier during the process of secondary growth.

In this context, I succeeded to collect some preliminary data regarding the start of periderm formation, rupture of epidermis, cortex and endodermis and its effect on protective function of the endodermis. In summary, my data shows that in agar plate-grown seedlings the periderm formation starts in about 9 to 11 days under our growth conditions. As a result division in the pericycle cells start to push the endodermis, cortex, and epidermis to the outside. However, this cell divisions have no effect on the functionality of the barrier that was created by the CS. Approximately at 12 to 14 days-old seedlings, epidermis and cortex suddenly collapsed or were sloughed off, making it impossible to identify intermediary stages. Notwithstanding this, the apoplastic barrier

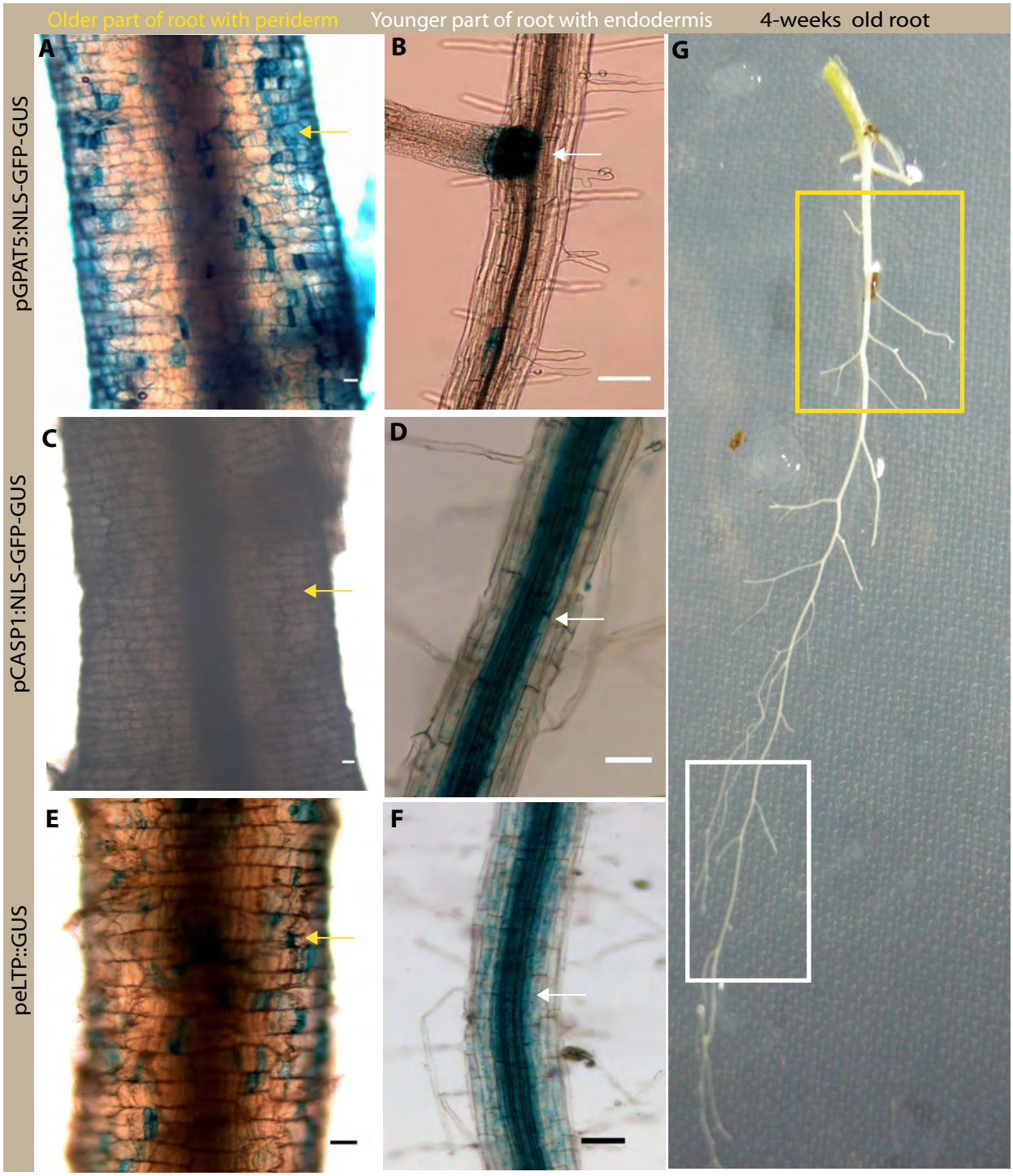

Figure 5: Neither CASP1 nor eLTP are expressed in the periderm.
(A-F) Promoter Gus fusion activity of pGPAT5: NLS-GFP-GUS, peLTP::GUS and pCASP1:NLS-GFP-GUS in the older part of the root containing fully developed periderm (A, C and E) and in the younger part of the root containing epidermis, cortex and endodermis (B, D and F). Arrows mark the Gus-expression pattern in the periderm (Yellow) and in the endodermis (White).
(Scale bars B-D 100µm and E-G 50 µm).
(G) Overview of 5 weeks-old root; younger part of the root containing the epidermis, cortex and endodermis (White) and older part of the root containing the multilayered periderm (Yellow).

apparently still remained intact. No Propidium Iodide penetration was observed in 14 to 18-days old roots (Fig. 6A and B). On the other hand, phloroglucinol staining (dye specifically staining lignin) was only observed in xylem vessels and in the outermost layer of the 14-days old root specifically in the radial walls of these cells (Fig. 6C and D). However, if we looked at the root with fully developed periderm (4-weeks old), autofluorescence after clearing shows a mild fluorescent signal in the outermost layer of periderm (phellem) at the uppermost zone of the root. This is the zone where multilayered periderm is fully developed without any remained of primary root tissues (Fig. 6F). However, at the middle zone of the 4-week old root, where the periderm is not yet fully formed or in the process of being formed, well-localized fluorescent signals were also observed in the outermost layer of the root which is the layer of endodermal cells before sloughed off or fall apart (Fig. 6E). Moreover, at that zone, I was able to observe a ruptured epidermis/cortex. These results, once more, support the existence of an endodermis as an intermediate outer protective layer before the formation of periderm, as it was shown by PI and phloroglucinol data. This preliminary data suggests that before the outermost layers of the roots become fully sloughed off and replaced by the phellogen; the endodermis with more-or-less well-localized CS stays functional for a certain time and is maintained as a functional barrier.

To date, there is no data available, which demonstrates the existence of a CS also in the periderm in *Arabidopsis*. However, recently CS-like structures were characterized in the mature phellem cells in both stems and roots of *Pelargonium hortorum* and in the wound-induced periderm in the shoot (Meyer et al. 2010). According to this study, CS was detected in the radial walls of the mature phellem cells and as upon acid digestion; these cells remain intact suggesting the presence of CS-like structures in the primary walls.

In the future, the molecular dissection and control of endodermal breakage during secondary growth initiation might lead to an important and novel perception into how plants reorganize lignified cell walls and keep the root apoplastic barrier intact. These studies will enrich our understanding of the dynamics of root growth and development. However, it is enigmatic that before the endodermis dies or sloughs off, it is able to increase its girth, either by cell divisions or by extension of individual endodermal cells.

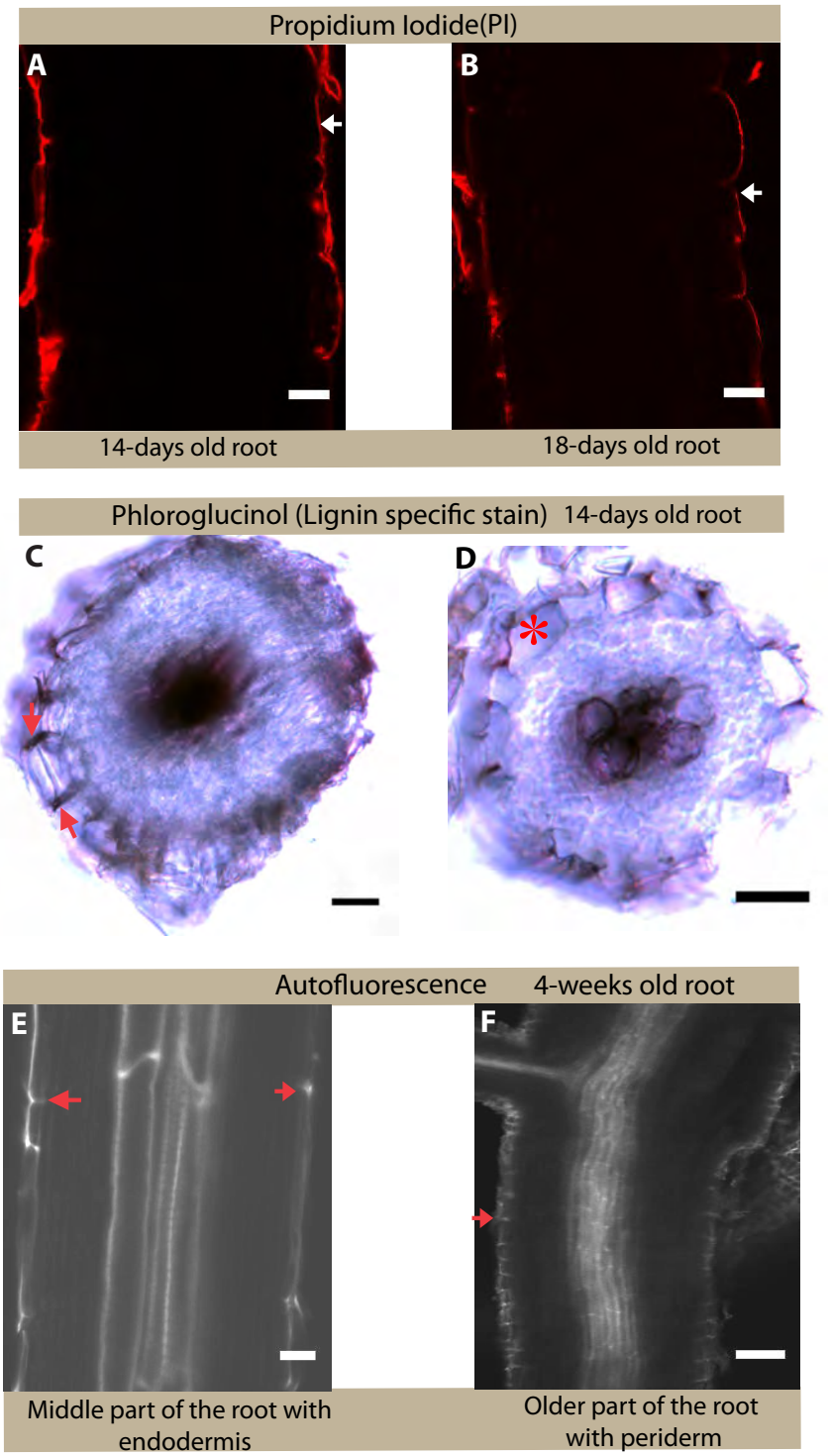

Figure 6: Secondary growth and its effect on endodermis.
(A-B) Block of apoplastic tracer PI during the formation of periderm in 14-days and 18-days old roots. Arrows mark the PI blocked in the outermost layer of root.
(C-D) Phloroglucinol staining reveals the presence of CS in the radial walls of outermost layer of the root, shown by a red arrows. Asterisk marks an individual endodermal cell.
(E-F) Autofluorescence after clearing shows the endodermis with CS as outermost layer of the root (middle zone of the root) and periderm with fluorescence signal in the outer most layer of the periderm (upper zone of the root). Red arrows mark the presence of fluorescence signal corresponds to more-or -less localized CS. (Scale bars A-C 20µm; D 100 µm and E-F 1 µm).

As major function of the periderm is to prevent water loss and pathogen entry from its surroundings, specifically through the primary walls of the cork cells, thus the addition of lignin to the suberin may improve the overall function of the periderm. However, as we show that in the young roots suberin formation alone is not able to block apoplastic diffusion. This raises the question whether suberin alone is responsible for the formation of the apoplastic barrier in the periderm or whether there is also the formation of a more-or-less localized, Casparian Strip-like structure, or simply a non-localized impregnation of the primary cell wall with lignin that contributes to the barrier properties of periderm.

4.6 Experimental procedures

4.6.1 Plant Material and Growth Conditions

Arabidopsis thaliana ecotype Columbia-0 were used for all experiments. For analysis of 5-days old seedlings, seeds were germinated on 1/2 MS agar plates after 2 days in darkness at 4°C. Seedlings were grown vertically in Percival chambers at 22 °C, under long days (16-h light/8-h dark), and were used at 5 days after shift to room temperature. For periderm analysis, plants were grown in soil for 4 to 5 weeks. Seeds were germinated directly in soil. After 2 days in darkness at 4°C, pots were transferred to the culture chamber with the following growth conditions: light/dark cycle 16 h/8 h, irradiance 100 μmol s–1 m–2, temperature 23°C/19°C, humidity 70 to 80%.

4.6.2 Chemicals

Propidium Iodide (PI) was purchased from Invitrogen. All other dyes, solvents, and chemicals were purchase from Sigma-Aldrich.

4.6.3 Vector Construction and Transgenic Lines

For cloning and generation of plants, expressing the cutinase gene, Gateway Cloning Technology (Invitrogen) was used. For construction of pCASP1:: CDEF1(pSN007) transgenic line pEntry clones Lab 482pEn/SD/D-TOPO-CDEF1(attL1 and attL2 sites) and Lab 300 pEN L4-pCASP1-R1 were recombined into Lab 176 pB7m24GW,3 destination vector by using LR clonase (Invitrogen). To generate pELTP::CDEF1 (pSN017) transgenic line Lab 482pEn/SD/D-TOPO-CDEF1 (attL1 and attL2 sites) and pJV134pEN-L4-pAT2G48130-R1 were recombined into Lab 176 pB7m24GW,3 destination vector by using LR clonase (Invitrogen). The obtained vector confers

bacterial spectinomycine resistance and plant Basta resistance. All the constructs were electroporated into *Agrobacterium tumefaciens strain* GV3101. Plant transformation was done by floral dipping method (Clough and Bent 1998). Transgenic plants were selected on soil by spraying with BASTA.

4.6.4 Microscopy and Histology

Confocal laser scanning microscopy was performed on an inverted Leica SP2 confocal

Microscope. The excitation and detection window for PI was set as 488 nm, 500–550 nm. Fluorol yellow was detected with standard GFP filter under wide-field microscope (Leica DM5500). Fluorol yellow and autofluorescence staining assays were performed according to Naseer *et al* 2012 (see Annex VIII. A. for detail protocol). Phloroglucinol staining was performed as follows: two drops of freshly prepared phloroglucinol- HCl reagent (25mg of phloroglucinol were fully dissolved in 25 ml of 100% ethanol and 25 ml of 37% HCl) were added one minute prior to visualization directly on a glass slide containing the root cross-sections. For visualization of the apoplastic barrier, seedlings were incubated in the darkness for 10 min in a fresh solution of 15 μM (10 μg/mL) PI and rinsed twice in water (See Annex VIII.A for detailed protocols).

4.6.5 Suberin monomer analysis

The suberin monomer analysis was carried out after isolation and depolymerization of suberin as described in Franke et al. 2005. Quantitative determination of suberin monomers were carried out with GC system coupled with a flame ionization detector based on the internal standard. Analyses are presented as means ± standard deviation of three to five replicates.

4.6.6 GUS Staining assay

For promoter::GUS fusion assay, 4-week old soil-grown roots were used. Gus activity assay was perform as follows: roots were incubated in 5-bromo-4-chloro-3-indolyl-β-D-glucuronide (X-Gluc) staining buffer solution (10mM EDTA, 0.1% Triton X-100, 2 mM Fe2+CN, 2 mM Fe3+CN, 1 mg/mL X-Gluc) in 50 mM sodium phosphate buffer (pH7.2) at 37 °C for 30 hours in complete darkness (See Annex VIII. A. for detailed protocol).

4.7 Literature cited

Clough S.J., Bent A. 1998. Floral dip: A simplified method for Agrobacterium-mediated transformation of *Arabidopsis thaliana*. Plant J, 16:735–743.

Chris J. Meyer and Carol A. Peterson. 2010. Casparian bands occur in the periderm of *Pelargonium hortorum* stem and root. Annals of Botany, 1-8.

Dantzlg, A.H., Zuckerman, S.H., and Andonov-Roland. 1986. lsolation of a *Fusarium solani* mutant reduced in cutinase activity and virulence. J. Bacteriol, 168: 911-916.

Dolan L, Roberts K.1995. Secondary thickening in roots of *Arabidopsis thaliana*: anatomy and cell surface changes. New Phytol, 131:121–128.

Franke R, Briesen I, Wojciechowski T, Faust A, Yephremov A, Nawrath C, Schreiber L.2005, Apoplastic polyesters in *Arabidopsis* surface tissues: a typical suberin and a particular cutin. Phytochemistry, 66:2643–2658

Geldner, N. 2013. "The Endodermis." Annual Review of Plant Biology, 64(1): 531-558.

Murashige T and Skoog F. 1962. A revised medium for rapid growth and bioassays with tobacco tissue cultures. Physiol. Plant. 15:473-97.

Roppolo D, DeRybel B, Tendon VD, Pfister A, Alassimone J, *et al.*, 2011. A novel protein family mediates Casparian strip formation in the endodermis. Nature, 473:380–83

Takahashi K, *et al.*, 2010. Ectopic expression of an esterase, which is a candidate for the unidentified plant cutinase, causes cuticular defects in *Arabidopsis thaliana*. Plant Cell Physiol, 51:123–131.

5 Chapter V: Co-author publications

5.1 A developmental framework for endodermal differentiation and polarity

Alassimone J, Naseer S, Geldner N. 2010. A developmental framework for endodermal differentiation and polarity. Proc. Natl. Acad. Sci. USA, 107:5214–19.

5.1.1 Own contribution

Dr. Julien Alassimone, former Ph. D student in our lab, identified molecular markers that localize exclusively to the inner or outer sides (i.e. toward the cortex or toward the stele) of endodermal plasma membrane. The main aim of the work presented in this chapter was firstly to establish the developmental sequence of events that lead to a differentiated endodermal cell. Secondly, to develop marker lines and tools that would allow studying this process in a mechanistic and developmental manner in *Arabidopsis*.

Dr. Julien Alassimone designed this study and did most of the experiments. I contributed to this paper by analyzing the data shown in Figure 1D and quantifying the autofluorescence appearance (Figure 1H).

5.1.2 Original article

For details, the article is attached herewith.

A developmental framework for endodermal differentiation and polarity

Julien Alassimone, Sadaf Naseer, and Niko Geldner[1]

Department of Plant Molecular Biology, University of Lausanne–Sorge, Lausanne 1015, Switzerland

Edited* by Maarten J. Chrispeels, University of California at San Diego, La Jolla, CA, and approved December 16, 2009 (received for review September 22, 2009)

The endodermis is a root cell layer common to higher plants and of fundamental importance for root function and nutrient uptake. The endodermis separates outer (peripheral) from inner (central) cell layers by virtue of its Casparian strips, precisely aligned bands of specialized wall material. Here we reveal that the membrane at the Casparian strip is a diffusional barrier between the central and peripheral regions of the plasma membrane and that it mediates attachment to the extracellular matrix. This membrane region thus functions like a tight junction in animal epithelia, although plants lack the molecular modules that establish tight junction in animals. We have also identified a pair of influx and efflux transporters that mark both central and peripheral domains of the plasma membrane. These transporters show opposite polar distributions already in meristems, but their localization becomes refined and restricted upon differentiation. This "central–peripheral" polarity coexists with the apical–basal polarity defined by PIN proteins within the same cells, but utilizes different polarity determinants. Central–peripheral polarity can be already observed in early embryogenesis, where it reveals a cellular polarity within the quiescent center precursor cell. A strict diffusion block between polar domains is common in animals, but had never been described in plants. Yet, its relevance to endodermal function is evident, as central and peripheral membranes of the endodermis face fundamentally different root compartments. Further analysis of endodermal transporter polarity and manipulation of its barrier function will greatly promote our understanding of plant nutrition and stress tolerance in roots.

Casparian strips | cell polarity | root development | endodermis | Arabidopsis

The endodermis is one of the fundamental cell layers found in the roots of higher plants (1). It sets up a diffusion barrier between the extracellular space of the root cortex, connected to the soil, and that of the vascular tissue, connecting the root with the aboveground organs. The endodermis is thought to be crucial for the efficient and selective uptake and sequestering of nutrients from the soil, necessary for plant survival (1). Specification of endodermal cells is very well understood and thought to depend on the SHR transcription factor. SHR acts as an evolutionary conserved short-range signal that moves out from the inner tissues of the stele, thereby promoting asymmetric cell division and specification of the innermost cortical tissue layer into endodermis (2). It is entirely unknown, however, how and when this initial specification event is translated into differentiation of the endodermis. The best known feature of a differentiated endodermal cell is the "Casparian strip," a highly localized cell wall deposition in the transversal and anticlinal walls of the cell, which surrounds the cell like a belt and is tightly coordinated with respect to neighboring cells (Fig. 1*I*). The Casparian strip thereby forms a supracellular network between cells within the layer, sealing the extracellular space (3). It has been known for a long time that this cell wall modification is associated with special features of the underlying plasma membrane (PM), which was shown to be very electron dense and to be tightly attached to the cell wall upon plasmolysis (4).

Because of the central position of the endodermis, its PM is exposed to two very different compartments. One domain faces the periphery of the root, the cortex, because it is peripheral to the Casparian strip barrier. The other domain faces the central part of the root, the stele, because it lies central to the barrier defined by the Casparian strip. Accordingly, transporters in the endodermis should localize either to the outer (peripheral) or the inner (central) domain of the endodermal PM, depending on their function in uptake or loading of nutrients. Indeed, it has recently been shown in rice that a pair of silicon transporters localize either to the outer or to the inner domain of the PM of differentiated exodermal and endodermal cells, in accordance with their function in influx or efflux (xylem loading) of silicon (5). Currently, most of our knowledge about endodermal structure and function comes from studies in organisms other than Arabidopsis and has mostly been concerned with a description of already differentiated endodermal cells through electron micrographs and histochemical staining procedures. Because of this limitation, we are ignorant about when and how an endodermal cell differentiates and we lack the marker lines and tools that would allow us to study this process in a mechanistic and developmental fashion.

Here we report the establishment and use of molecular markers for the analysis of endodermal polarity and Casparian strip (CS) formation in Arabidopsis. Using these markers in a quantitative analysis, we establish the developmental sequence of events that leads to a differentiated endodermal cell. We demonstrate establishment of a PM subdomain that coincides with the formation of the Casparian strip. This subdomain diffusionally separates inner from outer PM domains and mediates tight adherence to the cell wall: the plant extracellular matrix. In addition, we show that endodermal polarity is defined independently of this subdomain, is present already in meristems, and becomes established early during embryogenesis. Inner and outer polar markers appear to have distinct trafficking requirements, but use common polar cues that are different from those establishing apical–basal PIN polarity. PIN proteins are efflux carriers for the plant hormone auxin, often localize to the apical or basal plasma membrane domains of cells, and define their orientation with respect to the organ or body axis (6).

Results and Discussion

Endodermal Differentiation Occurs in a Narrow Developmental Window. We established a PM marker line with endodermis-specific expression to allow a precise visualization of exclusively endodermal cells in live imaging. We measured both the speed and the duration of elongation of cells after their exit from cell division, as well as their position with respect to their length (Fig. 1 *A* and *B*,

Author contributions: N.G. designed research; J.A., S.N., and N.G. performed research; J.A. analyzed data; and J.A. and N.G. wrote the paper.

The authors declare no conflict of interest.

*This Direct Submission article had a prearranged editor.

[1]To whom correspondence should be addressed. E-mail: niko.geldner@unil.ch.

This article contains supporting information online at www.pnas.org/cgi/content/full/0910772107/DCSupplemental.

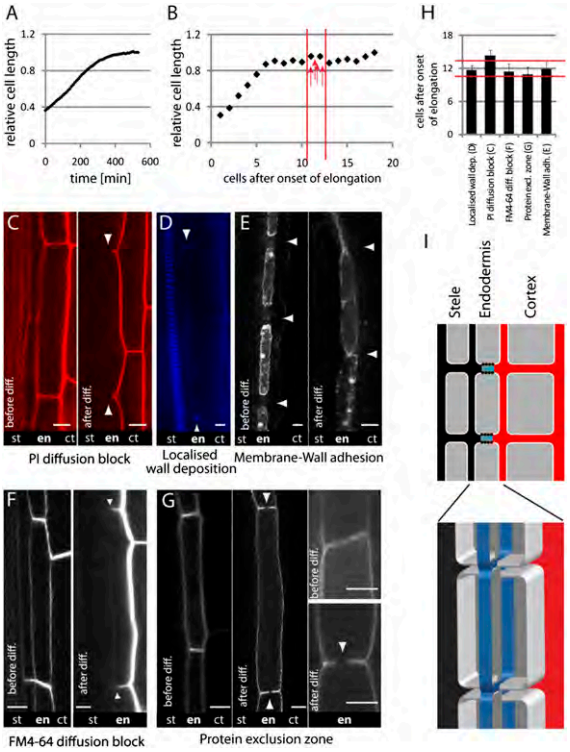

Fig. 1. Molecular and quantitative analysis of endodermal differentiation. (*A*) Average rate and duration of endodermal cell elongation in 9-h time-series/10-min intervals (13 cells/6 roots). (*B*) Average cell length vs. position in the cell file ($n = 25$). Red arrows mark the position of the differentiation events depicted in *D*–*G*. (*C*) Penetration of propidium iodide (PI) into the stele (*Left*) is blocked in differentiated roots (*Right*). Block at 14.4 cells ($n = 30$) is shown. (*D*) Casparian strip presence visualized by autofluorescence is observed at 11.7 cells ($n = 25$). (*E*) Cell-wall adhesion of the CSD membrane upon plasmolysis. Attachment to transversal walls is observed at 11.9 cells ($n = 21$) (*Right*). Before that, protoplasts retract from each other (*Left*). (*F*) The membrane tracer FM4-64 highlights all surfaces of endodermal and inner cells (*Left*), but becomes restricted to the outer domain of the endodermis in differentiated roots (*Right*) at 11.4 cells ($n = 30$). (*G*) Exclusion of PM marker NPSN12 from the Casparian strip domain (CSD), observed at 10.9 cells ($n = 31$). *Left* and *Upper Right* are before differentiation, and *Middle* and *Lower Right* are after differentiation. (*H*) Graph of the positioning of the different differentiation events, as shown in *C*–*G*. Red lines mark the narrow zone (~11–13 cells) in which differentiation events occur. Propidium iodide is probably observed later due to some upward diffusion or mass flow from undifferentiated tissue. (*I*) Cartoon depicting the compartments of the endodermis: inner apoplastic space of vasculature (black), outer apoplastic space of cortex (red), Casparian strip blocking extracellular diffusion (blue), PMs (white), PM region (CSD) mediating cell wall attachment, and protein exclusion and suppression of FM4-64 (black dots). 3D representation in the same color code visualizes how two "dots" in median longitudinal sections in *C*–*G* relate to ring structures of the CS in three dimensions. en, endodermis; ct, cortex; st, stele. Arrowheads in *C*–*G* indicate position of the CS/CSD, and in *E* they indicate the presumptive transversal borders between cells. (Scale bars: *C*–*G*, 10 μm; *G Right*, 5 μm.)

Movie S1, and Fig. S1). These two data sets allowed us to determine that an endodermal cell elongates for ~6–7 h under our growth conditions and that it ceases elongation at ~500 μm away from the end of the meristematic zone. In addition, we estimated from the linear part of the curves that a new cell enters cell elongation approximately every hour.

Having quantified these parameters, we established a number of assays to describe the onset of endodermal differentiation. We decided to describe the timing of differentiation events by counting the "number of cells after onset of elongation" as a robust and easily quantified parameter. One hallmark of endodermal function is the establishment of an apoplastic diffusion barrier between the cortex and the vascular cylinder. We tested a number of fluorescent apoplastic tracer molecules that have been described in the literature (7). It turned out that the most efficient apoplastic tracer by far was propidium iodide (PI), which is extensively used to visualize cell walls in Arabidopsis roots (8). We noticed that in median confocal sections of differentiated roots, PI penetrates only until the outer half of the endodermis, being blocked precisely at the expected position of the Casparian strip (Fig. 1*C Right*), whereas it penetrates readily in younger root parts (Fig. 1*C Left*). Using PI, we determined that the apoplastic barrier is established on average at 14.4 cells after onset of elongation (Fig. 1*H*), right about the time when xylem vessels also appear. We then searched for a direct way to visualize the Casparian strip itself as a localized cell wall modification. The CS is thought to be composed of both suberin and lignin-like compounds (6). After testing a number of staining methods, we found that the most reliable way to visualize the CS in Arabidopsis was to simply detect its autofluorescence after clearing of the roots (9) (Fig. 1*D*). With this method, we observed the first localized cell wall depositions to occur at 11.7 cells, preceding the observed block in apoplastic diffusion (Fig. 1*H*). It is evident that such localized deposition of wall material has to be preceded by the establishment of a membrane domain that would allow localized secretion or retention of wall precursors or biosynthetic enzymes. It is known from numerous electron micrographs of differentiated endodermal cells that the membrane domain underlying the Casparian strip (in the following called the Casparian strip domain, CSD) is distinct from the rest of the PM in being very electron dense and in remaining tightly attached to the cell wall after plasmolysis (4, 10). Using our endodermal-specific PM-marker lines, we show that endodermal cells close to the meristem retract from all cell walls after plasmolysis (Fig. 1*E Left*), whereas they become firmly attached to their transversal walls at later stages (Fig. 1*E Right*). We quantified onset of membrane attachment to occur at ~11.9 cells, which precisely coincides with the appearance of the CS (Fig. 1*H*). The high electron density of the CSD in mature endodermal cells certainly suggests a dense, scaffolded arrangement of proteins in this region. We tested whether this arrangement would lead to a suppression of lateral diffusion of membrane material between outer and inner membrane domains. Such a suppression has been reported for tight junctions in animal epithelia (11), but has not been reported for any plant cell type. To our surprise, FM4-64, a lipid tracer that inserts and highlights PMs in meristematic and elongating cells (Fig. 1*F Left*), can penetrate only until the presumptive position of the CSD, but does not show any significant lateral diffusion into the inner (stele-facing) PM domain (Fig. 1*F Right*). Again, this lateral diffusion barrier was found to be established at 11.4 cells, simultaneous with the onset of membrane adhesion (Fig. 1*H*). A strong suppression of lateral diffusion of lipids should also have the effect of excluding PM localized proteins from this region. Indeed, we found a strikingly strong exclusion of our PM marker YFP-NPSN12 at this region, leading to a sort of negative image of the CSD (Fig. 1*G Center*). This finding is observed only in older endodermal cells and cannot be seen closer to the meristem (Fig. 1*G Left*). The first appearance of this "depletion zone" closely matches the position where FM4-64 diffusion is blocked (10.9 cells) (Fig. 1*H*).

Our analysis shows that Casparian strips form a functional endodermal barrier already very close to the meristem, 11–12 cells adding to ≈900 μm. Importantly, differentiation of the Casparian strip membrane domain into a cell wall-adhesion and lateral diffusion barrier, as well as the formation of the cell wall modification itself, appears to occur in a very narrow time window, suggesting that endodermal differentiation proceeds as a "burst" of interdependent events rather than as a gradual process

of stepwise maturation. The finding that the CSD causes diffusional separation between the inner and outer domains of the PM highlights a very distinct feature of the endodermis, which should have strictly separated polar domains, very unlike the situation found in the apical–basal polarity of PINs.

Endodermal Polarity Is Already Present in Meristems and Is Organized with Respect to the Central Stele. The only proteins shown to mark outer and inner domains of the endodermis are the silicon transporters Lsi1 and Lsi2 in rice (5). As in the case of our generic PM marker YFP-NPSN12, we used the cell-layer-specific *SCARECROW* (*SCR*) promoter that drives expression exclusively in the endodermis. This allows good image acquisition of this inner cell layer and endodermal signals are not confounded with signals from neighboring cells. We tested fluorescent protein fusions of a number of candidates that were reported to have a function in the endodermis or to localize to an outer membrane domain in other cell types. The rice silicon transporters did not display a polar localization in Arabidopsis. OsLsi1 accumulated in the ER, whereas OsLsi2 showed a weak, apolar localization (Fig. S2). Proteins reported to localize to the outer domain of epidermal cells in Arabidopsis, such as BOR4 (12), or that showed weak, apolar signals in the endodermis, such as other transporters (AHA4, NRT1;1, DSP/WBC11), did not accumulate and show also weak apolar signals (Fig. S2). Yet, two boron transporters, NIP5;1 and BOR1, were additional good candidates for polarity markers, on the basis of their reported function in uptake and xylem loading (efflux) of boron (13–15). Indeed, in these cases, a clear polar localization to the inner and outer domains of the PM was observed for BOR1 and NIP5;1, respectively (Fig. 2 *A* and *B*). Thus, we have identified markers that define two complementary plasma membrane domains within the endodermis of Arabidopsis. These findings are also reported in an independent work on BOR1/NIP5;1 polarity in an accompanying paper by Takano et al. (16).

As expected from our analysis, signals of both proteins showed a sharp drop in intensity across the transversal PM at the position of the CSD (Fig. 1 *G* and *I*). We then investigated whether the CSD is necessary for the establishment of this polarity. The SCR promoter used also drives expression in meristematic proendodermal cells, initials, and the quiescent center (QC) cells. To our surprise, both boron transporters also accumulated in a polar fashion in these undifferentiated cells (Fig. 2 *C* and *D*). However, localization in these cases was less restricted and extended in a gradient across the entire transversal PM. This result suggests that the Casparian strip domain is not needed for establishment or maintenance of polarity per se, but rather is "built into" an already polarized setting and acts to refine and separate partially overlapping polar domains. To visualize this separation directly, we generated a line expressing the two proteins fused to spectrally distinct fluorophores. The two proteins indeed showed significant overlap in transversal cell sides in undifferentiated cells (Fig. 2*E*), but became completely separate at the point of CSD establishment (Fig. 2*F*).

In a median optical cut, BOR1 polarities in the cells to the left and the right of the stele are facing each other. The *SCR* promoter allows observation of what happens to polarity in the quiescent center cells, where cells of the left and right cell files meet and might show an opposite or apolar localization. Contrary to our expectations, polarity of BOR1 was maintained, but gradually changed to apical when approaching the quiescent center (Fig. 2*G*). The reverse happened in the case of NIP5;1, which gradually changed to a more basal localization (toward the base of the plant, the root tip) (Fig. 2*H*). These observations are strongly suggestive of a scenario in which polarity in the endodermis does not follow global coordinates, such as left and right, apical or basal, but always orients toward or away from the center of the root, the stele. We tested if orientation of polarity toward the stele is a special feature

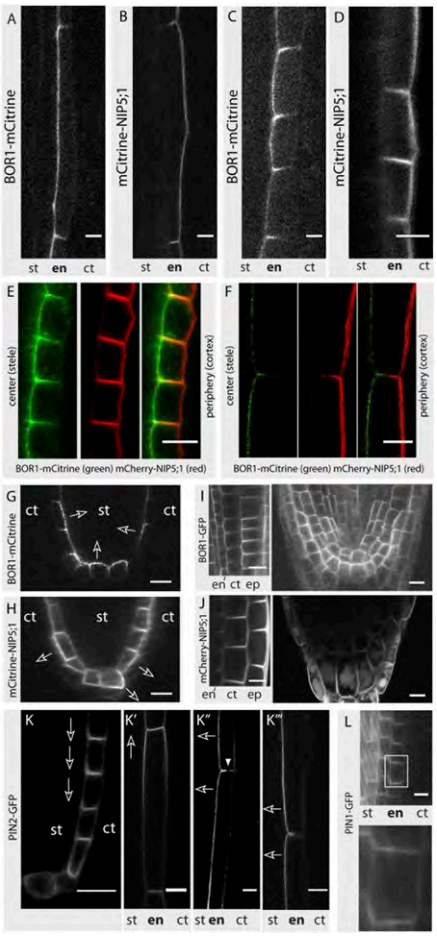

Fig. 2. Endodermal polarity is different from PIN polarity and organizes with respect to the stele. (*A–D*) Signals of BOR-mCit and mCit-NIP5;1 at opposite cell sides in differentiated (*A* and *B*) and meristematic (*C* and *D*) cells. (*E* and *F*) Colocalization of BOR1-mCit (*Left*), mCherry-NIP5;1 (*Center*), and overlay (*Right*). Colocalization can be observed in meristematic (*E*), but not in differentiated cells (*F*). (*G* and *H*) Localization of BOR1-mCit and mCit-NIP5;1 in quiescent center and initials and proendodermal cells. BOR1 signals polarize toward NIP5;1 signals away from the stele. (*I* and *J*) Signals of BOR1 and NIP5;1 in nonendodermal cells, expressed from 35S or UBQ10 promoter, respectively. Signals from neighboring cells are confounded, and the same orientation of polarity is observed as in the endodermis. (*K*) Localization of PIN2-GFP is apolar in quiescent center and basal in initials and proendodermal cells. Localization switches to apical in elongating cells (*K′*) and to the central side in differentiated cells (*K″* and *K‴*). (*L*) PIN1-GFP shows basal localization in endodermis. Overview (*Upper*) and zoom in (*Lower*) are shown. ct, cortex; en, endodermis; ep, epidermis; st, stele. Open arrows indicate direction of polarity of individual cells. Arrowhead indicates position of the CSD (Scale bar: 10 μm.)

of the endodermis, which is immediately bordering and enclosing the stele. We therefore used lines expressing BOR1 and NIP5;1 under constitutive promoters. Polarity of individual cells is more difficult to observe, because of signals from neighboring cells. However, careful inspection of cortical, epidermal, and root cap initial cells also revealed a polar accumulation toward or away from the stele (Fig. 2 *I* and *J*). In our opinion, our observations are explained most readily in a scenario in which signals emanating from the stele act as polarizing cues for more peripheral tissue layers of the root.

The observed polar localization of the boron transporters in the quiescent center also illustrates that the polar cues and machinery used to orient boron carriers in the endodermis are different from those orienting PIN proteins, because PINs are

mostly apolar in these cells (17, 18). To further investigate this difference, we used a line expressing PIN2 from the SCR promoter (19). We observed a weak, but completely apolar signal of PIN2 in the quiescent center (Fig. 2*K*). Outside the quiescent center, it did not polarize like either of the boron transporters, but showed a basal localization, as reported for PIN2 in the cortex (Fig. 2*K*). This polarity then switched to a very shallow localization gradient toward the upper (apical) side of the cell (Fig. 2*K′*). A similar switch was reported previously for PIN2 localization in cortical cells (20). In a differentiated endodermis, PIN2 signals became weaker and the signal started to preferentially accumulate at inner sides (Fig. 2 *K″* and *K‴*). Like YFP-NPSN12, PIN2-GFP was excluded from the CSD (Fig. 2*K″*, arrowhead). Thus, PIN2 expressed in the endodermis showed a very different localization pattern from that of either BOR1 or NIP5;1, in QC, meristematic, and elongating cells, showing that it follows different polarization cues in those cells. PIN2 retains a propensity to localize in a polar fashion along the apical–basal axis. Its eventual accumulation at the central side of cells might simply be due to a slightly delayed turnover of protein from the central side. We observed similar polar accumulation with DSO/WBC11 and BOR4 immediately before their complete disappearance (Fig. S2 *I* and *L*).We also investigated PIN1, a protein that shows a weak expression in the endodermis under its endogenous promoter. Using PIN1-GFP, we were able to observe a basal polarity of PIN1-GFP, as observed for PIN2 (Fig. 2*L*). On the basis of this observation, we conclude that endodermal cells in the meristem are able to define at least three different polar distributions of PM proteins: toward the center (stele), toward the periphery (cortex), and toward the base of the plant. PIN3 has been reported to localize differently from PIN1 and PIN2 in proendodermal cells, in a way that more resembles the center-oriented polarity of BOR1, suggesting that BOR1 and PIN3 might be able to use the same trafficking pathway in endodermal cells, distinct from that of other PINs (21).

The Polarity Realized in the Endodermis Is Established Early During Embryogenesis. Our finding that the "central–peripheral" polarity of endodermal cells is not a feature of differentiated endodermal cells, but preexists in the meristem, begged the question at which point endodermal polarity is initially established. We therefore investigated at which point polar localization of BOR1 and NIP5;1 can be observed during embryogenesis. To our surprise, we found that both BOR1 and NIP5;1 are already localized in a polar fashion in heart and triangular-stage embryos (Fig. 3 *B*, *C*, *F*, and *G*). In globular-stage embryos we observed polar localization in the lens-shaped precursor cell of the quiescent center in most embryos (Fig. 3 *A* and *E*). No signals were observed in earlier embryo stages for BOR1 and occasional NIP5;1 signals in the undivided hypophysis were apolar. Thus, polarity cues are apparently becoming established at the time when the formative divisions of the provasculature are taking place. Again, these findings suggest a clear difference between PIN polarity and the polarity visualized by the boron transporters. PIN1, PIN4, and PIN7 are expressed in the lens-shaped cell, but their localization appears mostly apolar, although some degree of polarization cannot be excluded (18, 22). Our markers now provide a clear indication of the presence of complementary polar domains within the lens-shaped cell. This cell is produced by an asymmetric division, gives rise to the stem cell organizing center, and faces a clonal boundary (23). Therefore, the ability to visualize its orientation and polarity might be of importance for understanding its function.

Polarity in the Endodermis Does Not Require a Polarized Cytoskeleton, but Needs Endocytic Trafficking. We then investigated the cellular basis of the endodermal polarity and subdomain establishment. We first asked whether there are any specific arrangements of the actin cytoskeleton associated with either the CSD or any of

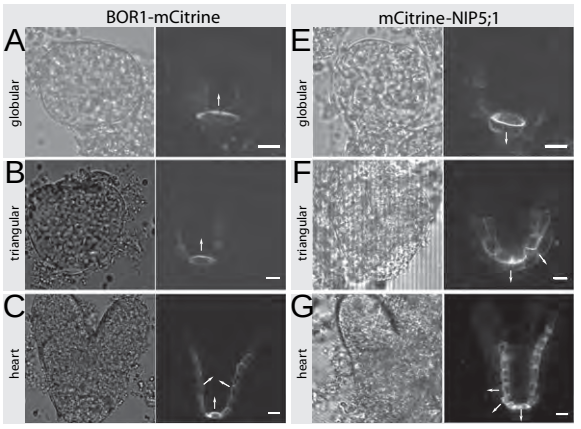

D

embryo stage	embryos polar signals
pre-globular	*no signal*
globular	19/25
triangular	18/18
heart	31/31

H

embryo stage	embryos polar signals
pre-globular	0
globular	13/15
triangular	9/9
heart	12/12

Fig. 3. Central–peripheral polarity becomes established early in embryogenesis. (*A–C*) BOR1-mCit signals in quiescent center precursor cells, initials, and proendodermal cells display polarity oriented toward the *center* of the embryo. Arrows point to cell sides with visible polar accumulation. (*Left*) Transmitted light image. (*Right*) Confocal image. (*D*) Number of embryos observed with polar BOR1-mCit signals over total number of embryos inspected. (*E–G*) mCit-NIP5;1 signals in quiescent center precursor cells, initials, and proendodermal cells display polarity oriented toward the *periphery* of the embryo. Arrows point to cell sides with visible polar accumulation. (*Left*) Transmitted light image. (*Right*) Confocal image. (*H*) Number of embryos observed with polar mCit-NIP5;1 signals over total number of embryos inspected. (Scale bar: 10 μm.)

the two polar (central vs. peripheral) domains. Polar actin accumulation is involved in polarity establishment in a number of different cellular systems (24). We again expressed an actin microfilament reporter (YFP-Fimbrin) specifically in the endodermis, to obtain images of sufficient quality. Fig. 4 *A–C* shows sequences of images from equivalent stages in the epidermis and endodermis. No evident accumulation or special arrangements of microfilaments were observed in endodermal cells at any developmental stage (Fig. S3), either toward one or the other PM domain or at the site of CSD formation. This observation contrasts, for example, with the easily observable sites of root hair outgrowth in epidermal cells (Fig. 4*A*). Thus, in contrast to many cell types in other organisms, endodermal cells are apparently able to polarize and establish the CSD without using a polarized actin cytoskeleton for vesicle delivery.

Consequently, interfering with actin polymerization in the endodermis by Latrunculin B (LatB) treatment (Fig. 4*D*) had no effect on the polar localization of either BOR1 or NIP5;1 (Fig. 4 *G* and *H*). The Casparian strip domain was also maintained in the presence of the actin depolymerizer (Fig. 4*E Lower*). To determine whether the actin cytoskeleton is required during the establishment of the CSD, we quantified the cellular distance from the meristem at which the depletion zone of the CSD appeared. A shift away from the meristem would indicate that nondifferentiated cells at the beginning of the treatment (Fig. 4*E Upper*) did not form a new CSD. No significant shift was observed after a 5-h treatment (Fig. 4*F*), which would suggest that the actin cytoskeleton is also not needed for establishment of the CSD. A similar analysis was done for the microtubule cytoskeleton, with similar results; i.e., we did not observe any specific microtubular structures in the endodermis or any effect of MT depolymerization (Fig. S4).

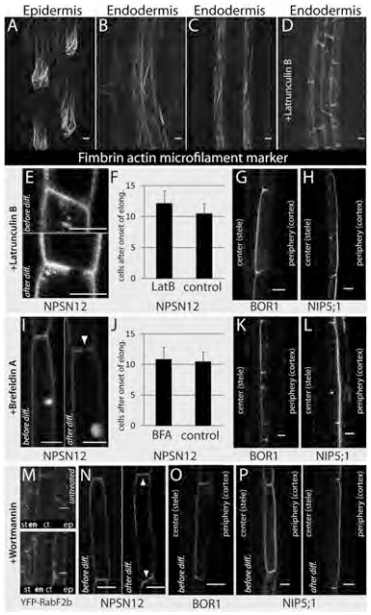

Fig. 4. Dependence of endodermal differentiation and polarity on actin and vesicle trafficking. (*A*) 35S::YFP-Fimbrin highlights actin during root hair formation in epidermis. (*B* and *C*) Surface (*B*) and median optical section (*C*) of SCR::YFP-Fimbrin. No localized accumulation of actin can be seen. (*D*) Signals after 1 h treatment with 10 μM LatB. (*E*, *G*, and *H*) Localization of BOR1, NIP5;1, or NPSN12 before and after differentiation (top and bottom) at the PM is unaffected after LatB treatment (10 μM, 1 h). (*F*) No shift in meristem distance is observed for the NPSN12 depletion zone after LatB treatment (10 μM, 5 h). (*I*) PM localization of NPSN12 is unaffected after BFA treatment (50 μM, 90 min) before (*Left*) and after (*Right*) differentiation. (*J*) No shift in meristem distance for the NPSN12 depletion zone is observed after BFA treatment (50 μM, 5 h). (*K* and *L*) BOR1 and NIP5;1 polarity is unaffected by BFA treatment (50 μM, 90 min). (*M*) WM treatment (50 μM, 1 h) effects of YFP-RabF2b, a WM-sensitive compartment marker in endodermis and stele, as seen by the higher background, irregular dots, and ring-like structures (*Lower*), compared to control (*Upper*). (*N*) WM treatment (50 μM, 1 h) leaves the NPSN12 depletion zone (CSD) intact (*Left*) and does not affect localization before differentiation (*Left*). (*O*) WM treatment (50 μM, 1 h) does not affect BOR1 polarity in elongating cells. (*P*) WM treatment (50 μM, 1 h) leads to complete depolarization of NIP5;1 in cells before differentiation (*Left*), but does not affect polarity in differentiated cells (*Right*). Arrowheads indicate position of the CSD. (Scale bars: 10 μm and (*E*) 5 μm.)

We then tested two widely used inhibitors of membrane trafficking in plants, the endosomal recycling inhibitor Brefeldin A (BFA) and the endocytic inhibitor Wortmannin (WM). BFA treatment led to accumulation of BOR1, NIP5;1, and NPSN12 in endosomal aggregates (BFA compartments) in differentiating endodermal cells (Fig. 4 *I*, *K*, and *L*). This result showed that all three proteins are trafficked at least partially through BFA-sensitive endosomes and that BFA accumulated and was active in the endodermis. However, BOR1 and NIP5;1 still retained their polar accumulation at the PM, both before and after CSD establishment (Fig. S5). This result is unlike the depolarization observed for PIN1, for example, but resembles the BFA-resistant localization of apically localized PIN2 in the epidermis (25, 26). In contrast to our results, a BFA sensitivity of BOR1 polarity in meristematic epidermal cells was observed by Takano et al. (16) in an accompanying paper. It remains to be seen whether this observation points to some underlying difference in endodermal vs. epidermal transport pathways or reflects some subtle differences in the experimental setup. No shift was observed in the onset of the depletion zone after BFA treatment (Fig. 4*J*).

WM treatment, by contrast, led to strong depolarization of NIP5;1 at the PM before CSD establishment (Fig. 4*P Left*), whereas it left BOR1 polarity and the CSD unaffected (Fig. 4 *N* and *O*). Intriguingly, NIP5;1 polarity became resistant to WM in cells that had established Casparian strips (Fig. 4*P Right*). Again, we could show that WM penetrates and acts in inner cell layers, using a marker line for a WM-sensitive compartment (Fig. 4*M*) (27). One straightforward explanation for this striking difference in WM sensitivity is based on our observation that the CSD suppresses lateral diffusion and separates the two polar domains. It has repeatedly been reported that WM affects internalization of proteins from the PM, which might be independent—or an indirect consequence—of its action on the endosomal PI-3 kinase (28–30). Lower WM concentrations expectedly induced accumulation of BOR1 and NIP5;1 in aberrant endosomes, revealing that a certain fraction of both proteins became endocytosed and trapped in these compartments. However, no accumulation was observed at the higher concentrations that led to depolarization of NIP5;1 (Fig. S5). This observation can only be explained by Wortmannin acting on an earlier step of endocytosis at higher concentrations, most probably inhibiting internalization from the PM. Indeed, inhibition of PM internalization would explain depolarization of NIP5;1 by allowing it to distribute within the entire PM by lateral diffusion, even if polar targeting would remain intact. Such a case has been observed for a polar PM SNARE in budding yeast, for example (31). The resistance to WM in differentiated cells would then simply be due to the suppressed lateral diffusion by the CSD, which confines NIP5;1 within its polar domain, even if endocytosis is blocked. The relevance of the CSD in maintaining polarized distributions of proteins is also highlighted by independent findings of Takano et al. (16) in the accompanying paper.

Conclusion and Perspectives. The hormonal and transcriptional networks that determine meristem size and progression into elongation have started to become unraveled in recent years (32). However, much less is known about the actual differentiation that is the end result of the patterning processes in the meristem. This lack is reflected in the vague term "elongation and differentiation zone" (EDZ) that is often employed for this region. We have now defined a set of differentiation readouts for the endodermis. This set, in combination with long-term in vivo tracking of endodermal cells, now places endodermal differentiation in a precise time window and at a defined cellular distance from the meristem. Our work provides the basis for identifying genuine endodermal differentiation genes and contributes to connecting the current gap between cell-fate specification and actual cellular differentiation (32). The orientation of polarity of peripheral cell layers with respect to the stele suggests a scenario whereby the stele provides polar cues to the peripheral root region. In our view, the terms central (facing the center of the root/plant) and peripheral (facing the periphery) are well suited to describe this polarity. They are generally applicable to all cell types and probably best encompass the function underlying this polarity, i.e., vectorial transport of substances toward the center or their expulsion toward the periphery. Alternative terms in the literature are "proximal" and "distal" (16). We demonstrate that the CSD has features of both tight and adherens junctions. It therefore resembles polarized epithelia of animals. Yet, the endodermis lacks all of the central factors that establish polarized epithelia in animals, such as PAR proteins, Claudins, E-Cadherins, ZO proteins, or others (33–36. We are now identifying and characterizing the factors that make up the plant tight-junction equivalent, the CSD. It will be intriguing to understand how plants have independently evolved the capacity to organize a selective and polarized cellular barrier, one of the first and most fundamental features of multicellular organisms (33). Both polarity and CSD domain establishment are immediately relevant to the cellular barrier function of the endodermis. Other cell types also maintain a central–peripheral polarity, which will contribute to the vectorial transport of nutrients toward or away from the stele (12) (ref. 16 and our

work). It is only the endodermis, however, where central and peripheral PM domains face different extracellular spaces, as is the case for polarized animal epithelia. We predict that understanding and manipulating endodermal CSD formation and polarity will provide us with a new level of understanding of how plants manage to selectively take up and reject substances from the soil and how they ascertain plant integrity and homeostasis in the face of various biotic and abiotic stresses.

Materials and Methods

Plasmid Construction and Transformation. Standard cloning procedures were used for plasmid construction. For information about constructs, see *SI Materials and Methods*.

Plant Material and Growth Conditions. Columbia background was used for all experiments. Plants were germinated after 2 days at 4 °C in the dark. Seedlings were grown in Percival chambers at 22 °C, under long days (16 h light/8 h dark), and were used at 4–6 days after germination. For growth conditions for live imaging see *SI Materials and Methods*.

Microscopy, Quantitative Analysis, and Image Processing. Confocal laser scanning microscopy was performed on an inverted Leica TCS SP2 AOBS confocal microscope. Image processing was done with ImageJ from the National Institutes of Health using plug-ins from the MBF ImageJ bundle (http://www.macbiophotonics.ca/imagej/). "Onset of elongation" was defined as the point when an endodermal cell in a median optical section was clearly more than twice its width. From there, cells in the file were counted until the respective differentiation feature was observed. For live imaging experiments, different *z*-axis pictures (minimum of three) were collected to be able to follow cells through *z*-axis drift.

Detection of Casparian Strip Autofluorescence. Autofluorescence of Casparian strips was detected with standard GFP filter sets after clearing of roots according to ref. 9.

Embryo Analysis. Analysis was done as described in ref. 37.

Tracer, Drug, and Plasmolysis Assays. For incubation conditions and dye and inhibitor concentrations, see *SI Materials and Methods*.

ACKNOWLEDGMENTS. We thank G. Vert for thoughtful discussions on the endodermis; M. Bennett, G. Jürgens, E. M. N. Dohmann, and D. Roppolo for critical reading of the manuscript; P. Dhonukshe, J. Friml, T. Fujiwara, C. Lloyd, J. Long, S. Savaldi-Goldstein, B. Scheres, and J. Takano for providing material; and J. Takano and T. Fujiwara for discussion and sharing of unpublished data. Imaging was done with equipment from the Central Imaging Facility at the University of Lausanne. This work was financed by grants from the European Research Council and the Swiss National Science Foundation (to N.G.).

1. Enstone DE, Peterson CA, Ma F (2002) Root endodermis and exodermis: Structure, function, and responses to the environment. *J Plant Growth Regul* 21:335–351.
2. Cui H, et al. (2007) An evolutionarily conserved mechanism delimiting SHR movement defines a single layer of endodermis in plants. *Science* 316:421–425.
3. Zeier J, Schreiber L (1997) Chemical composition of hypodermal and endodermal cell walls and xylem vessels isolated from Clivia miniata (identification of the biopolymers lignin and suberin). *Plant Physiol* 113:1223–1231.
4. Bonnett HT, Jr (1968) The root endodermis: Fine structure and function. *J Cell Biol* 37: 199–205.
5. Ma JF, et al. (2007) An efflux transporter of silicon in rice. *Nature* 448:209–212.
6. Kleine-Vehn J, Friml J (2008) Polar targeting and endocytic recycling in auxin-dependent plant development. *Annu Rev Cell Dev Biol* 24:447–473.
7. Enstone DE, Peterson CA (1992) A rapid fluorescence technique to probe the permeability of the root apoplast. *Can J Bot* 70:1493–1501.
8. van den Berg C, Willemsen V, Hage W, Weisbeek P, Scheres B (1995) Cell fate in the Arabidopsis root meristem determined by directional signalling. *Nature* 378:62–65.
9. Malamy JE, Benfey PN (1997) Organization and cell differentiation in lateral roots of Arabidopsis thaliana. *Development* 124:33–44.
10. Behrisch R (1926) Zur Kenntnis der Endodermiszelle. *Ber Dtsch Bot Ges* 44:162–164.
11. van Meer G, Simons K (1986) The function of tight junctions in maintaining differences in lipid composition between the apical and the basolateral cell surface domains of MDCK cells. *EMBO J* 5:1455–1464.
12. Miwa K, et al. (2007) Plants tolerant of high boron levels. *Science* 318:1417.
13. Takano J, Miwa K, Yuan L, von Wirén N, Fujiwara T (2005) Endocytosis and degradation of BOR1, a boron transporter of Arabidopsis thaliana, regulated by boron availability. *Proc Natl Acad Sci USA* 102:12276–12281.
14. Takano J, et al. (2002) Arabidopsis boron transporter for xylem loading. *Nature* 420: 337–340.
15. Takano J, et al. (2006) The Arabidopsis major intrinsic protein NIP5;1 is essential for efficient boron uptake and plant development under boron limitation. *Plant Cell* 18: 1498–1509.
16. Takano, et al. (2010) *Proc Natl Acad Sci USA*, in press.
17. Blilou I, et al. (2005) The PIN auxin efflux facilitator network controls growth and patterning in Arabidopsis roots. *Nature* 433:39–44.
18. Friml J, et al. (2003) Efflux-dependent auxin gradients establish the apical-basal axis of Arabidopsis. *Nature* 426:147–153.
19. Xu J, et al. (2006) A molecular framework for plant regeneration. *Science* 311: 385–388.
20. Kleine-Vehn J, et al. (2008) Cellular and molecular requirements for polar PIN targeting and transcytosis in plants. *Mol Plant* 1:1056–1066.
21. Sorefan K, et al. (2009) A regulated auxin minimum is required for seed dispersal in Arabidopsis. *Nature* 459:583–586.
22. Friml J, et al. (2002) AtPIN4 mediates sink-driven auxin gradients and root patterning in Arabidopsis. *Cell* 108:661–673.
23. Weijers D, et al. (2006) Auxin triggers transient local signaling for cell specification in Arabidopsis embryogenesis. *Dev Cell* 10:265–270.
24. Geldner N (2009) Cell polarity in plants: A PARspective on PINs. *Curr Opin Plant Biol* 12:42–48.
25. Geldner N, Friml J, Stierhof YD, Jürgens G, Palme K (2001) Auxin transport inhibitors block PIN1 cycling and vesicle trafficking. *Nature* 413:425–428.
26. Kleine-Vehn J, et al. (2008) ARF GEF-dependent transcytosis and polar delivery of PIN auxin carriers in Arabidopsis. *Curr Biol* 18:526–531.
27. Tse YC, et al. (2004) Identification of multivesicular bodies as prevacuolar compartments in Nicotiana tabacum BY-2 cells. *Plant Cell* 16:672–693.
28. Reichardt I, et al. (2007) Plant cytokinesis requires de novo secretory trafficking but not endocytosis. *Curr Biol* 17:2047–2053.
29. Emans N, Zimmermann S, Fischer R (2002) Uptake of a fluorescent marker in plant cells is sensitive to brefeldin A and wortmannin. *Plant Cell* 14:71–86.
30. Stevenson-Paulik J, Love J, Boss WF (2003) Differential regulation of two Arabidopsis type III phosphatidylinositol 4-kinase isoforms. A regulatory role for the pleckstrin homology domain. *Plant Physiol* 132:1053–1064.
31. Valdez-Taubas J, Pelham HR (2003) Slow diffusion of proteins in the yeast plasma membrane allows polarity to be maintained by endocytic cycling. *Curr Biol* 13: 1636–1640.
32. Iyer-Pascuzzi AS, Benfey PN (2009) Transcriptional networks in root cell fate specification. *Biochim Biophys Acta* 1789:315–325.
33. Cereijido M, Contreras RG, Shoshani L (2004) Cell adhesion, polarity, and epithelia in the dawn of metazoans. *Physiol Rev* 84:1229–1262.
34. Martin-Belmonte F, Mostov K (2008) Regulation of cell polarity during epithelial morphogenesis. *Curr Opin Cell Biol* 20:227–234.
35. Tsukita S, et al. (2009) Roles of ZO-1 and ZO-2 in establishment of the belt-like adherens and tight junctions with paracellular permselective barrier function. *Ann N Y Acad Sci* 1165:44–52.
36. Fujiwara T, Hirai MY, Chino M, Komeda Y, Naito S (1992) Effects of sulfur nutrition on expression of the soybean seed storage protein genes in transgenic Petunia. *Plant Physiol* 99:263–268.
37. Takada S, Jurgens G (2007) Transcriptional regulation of epidermal cell fate in the Arabidopsis embryo. *Development* 134:1141–1150.

Supporting Information

Alassimone et al. 10.1073/pnas.0910772107

SI Materials and Methods

Plasmid Construction and Transformation. Vectors are based on pGREENII series (http://www.pgreen.ac.uk). The upstream region 2.5 kb directly preceding the start of *SCR* (At3G54220) and the upstream region 1,986 bp directly preceding the ATG of *UBQ10* (At4G05320) were amplified and sequence verified. Cloning introduced KpnI between promoter and ORF for N-terminal fusions and the sequence 5′-ggtaccccgggtgatc-3′ for C-terminal fusions. Open reading frames of BOR1 (At2G47160), BOR4 (At1g15460), NIP5;1 (At4G10380), WBC11/DSO (At1g17840), OsLSI1 (Os02g0745100), OsLSI2 (Os03g0107300), AHA4 (At3g47950), NRT1.1 (At1g12110), and EB1a (At3G47690) were amplified from the clones PDA06190, PDA05366, pU84226, PDA07839, AK069842, AK101092, PDA11117, pU15475, and pU23125, respectively, and sequence verified. Clones were obtained from ABRC, RIKEN BRC, and the Rice Genome Resource Center. Fimbrin Actin Binding Domain2 (FABD2) (AT4G2670) was amplified as defined and described in ref. 1. N-terminal fusions were done for NIP5;1 and Fimbrin and C-terminal fusion for BOR1, BOR4, WBC11/DSO, OsLSI1, OsLSI2, AHA4, NRT1.1, and EB1a constructs. The fluorescent protein coding sequences used are mCitrine (mCit) and mCherry (2) and the linkers are tctagaggaaccggaggt for BOR1, BOR4, WBC11/DSO, OsLSI1, and OsLSI2; ggtctagataagatatcggatcac for AHA4, NRT1.1, and EB1a; and tcgtacggcgccgatatc for mCherry and mCit NIP5;1. For NPSN12 (AT1G48240), YFP-NPSN12 fusion was directly amplified and sequenced verified from Wave line 131Y (3). Agrobacterium-mediated plant transformation was performed as described (4). pSOUP containing GV3101 Agrobacteria (http://www.pgreen.ac.uk) was used. mCherry containing plasmids carry kanamycin resistance, whereas YFP or mCit recombined plasmids contain Basta resistance for plant selection. The 35::GFP-MAP4 line used is as described in ref. 5.

Tracer, Drug, and Plasmolysis Assays. Seedlings were incubated in the dark for 10 min in a fresh solution of 4 μM FM4-64 and 15 μM (10 μg/mL) propidium iodide (Invitrogen) and rinsed two times in water. Stock solutions were 100× for PI (in water) and 400× for FM4-64 (in DMSO). For plasmolysis assays, seedlings were incubated in 50% glycerol for 90 min in the dark. Inhibitors were diluted from DMSO stocks (EtOH for Oryzalin). Stocks were 100 mM (BFA), 50 mM (WM), and 10 mM (LatB and Oryzalin). Final concentrations were 50 μM (BFA and WM) and 10 μM (LatB and Oryzalin). Incubations were performed in 24-well plates in the light, except for WM. Incubations were performed in the dark for 5 h for counting appearance of NPSN12 depletion zone after drug treatment. Mounting was done in drug solution.

Plant Material and Growth Conditions. Live imaging experiments seedlings were grown in the Lab-Tek II Chambered Coverglass (Nalge Nunc) with 200 μL 0.5 Murashige and Skoog (MS) medium, 1.5% Agar, pH 5.7. Seedlings were grown horizontally for 4–5 days then oriented vertically for 1 day. For other experiments plants were grown vertically on 0.5 MS, 0.8% Agar, pH 5.7. The line expressing pSCR::BOR1-mCit was grown vertically on MGRL media (6) containing 0.3 μM boron. The 35S::BOR1-GFP line was grown vertically on MGRL media containing 3 μM boron for 5 days then transferred for 2 days on MGRL media containing 0.1 μM boron.

1. Voigt B, et al. (2005) GFP-FABD2 fusion construct allows in vivo visualization of the dynamic actin cytoskeleton in all cells of Arabidopsis seedlings. *Eur J Cell Biol* 84: 595–608.
2. Shaner NC, Steinbach PA, Tsien RY (2005) A guide to choosing fluorescent proteins. *Nat Methods* 2:905–909.
3. Geldner N, et al. (2009) Rapid, combinatorial analysis of membrane compartments in intact plants with a multicolor marker set. *Plant J* 59:169–178.
4. Clough SJ, Bent AF (1998) Floral dip: A simplified method for Agrobacterium-mediated transformation of Arabidopsis thaliana. *Plant J* 16:735–743.
5. Dhonukshe P, Gadella TW, Jr (2003) Alteration of microtubule dynamic instability during preprophase band formation revealed by yellow fluorescent protein-CLIP170 microtubule plus-end labeling. *Plant Cell* 15:597–611.
6. Fujiwara T, Hirai MY, Chino M, Komeda Y, Naito S (1992) Effects of sulfur nutrition on expression of the soybean seed storage protein genes in transgenic Petunia. *Plant Physiol* 99:263–268.

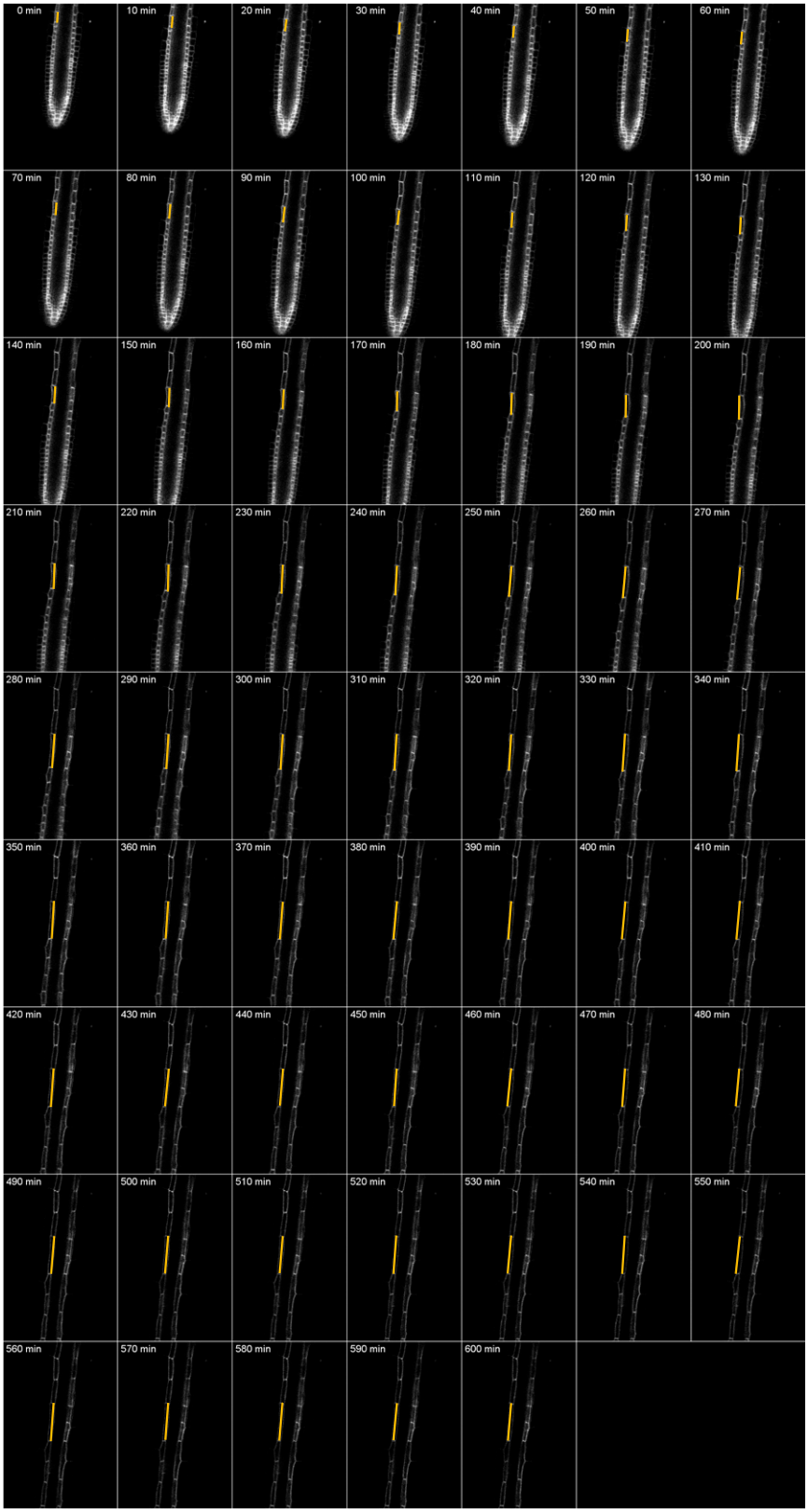

Fig. S1. Tracing elongation of individual endodermal cells in time stacks. Picture tile of Movie S1 is shown. The yellow line indicates length and division of an individual cell in each 10-min time frame. Note the initial displacement toward the bottom due to elongation of cells above and the displacement of the meristem due to division/elongation of cells below.

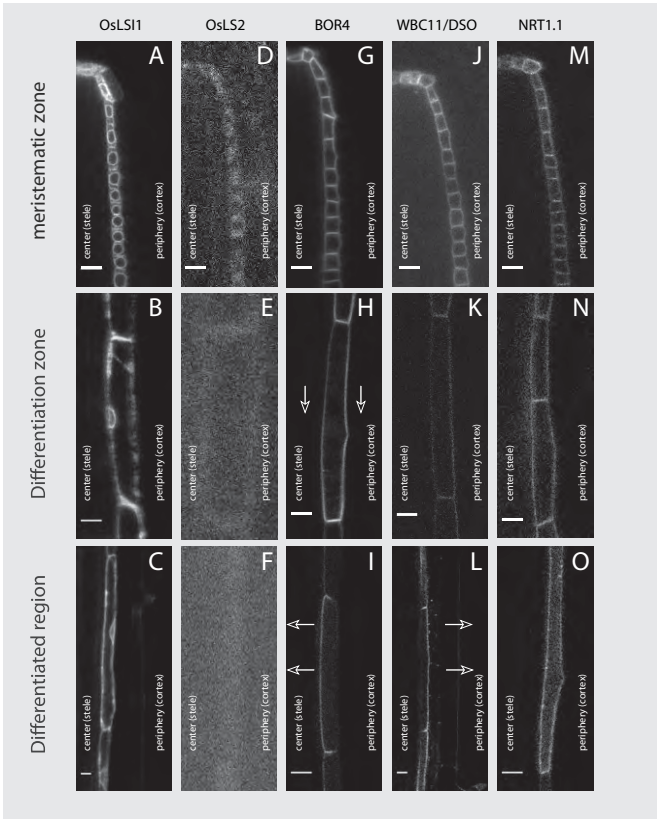

Fig. S2. Localization of additional polar marker candidates in the endodermis. Pictures show median optical cuts of candidate reporter lines in the meristematic zone, the differentiation zone, and the differentiated zone. (*A*–*C*) Localization of SCR::OsLSI1-mCitrine signal in endodermal cells. Signal resembles endoplasmic reticulum. (*D*–*F*) Weak signal was observed for the SCR::OsLSI2-mCitrine line, apparently at the plasma membrane. No signal was observed in differentiated cells. (*G*–*I*) BOR4 is localized to the plasma membrane in a nonpolar fashion in meristematic cells and becomes localized toward the upper (apical) side of the cell in differentiating cells. In differentiated cells a residual signal exclusively in the central domain is observed. (*J*–*L*) Plasma membrane localization of SCR::DSO-mCitrine signal in endodermal cells is apolar in undifferentiated cells and becomes localized exclusively to the peripheral domain in differentiated cells. (*M*–*O*) Plasma membrane localization of SCR::NRT1.1-mCitrine. The weak signal in endodermal cells is apolar in all investigated stages of endodermal development. Open arrows indicate direction of polarity of individual cells. (Scale bar, 10 μm.)

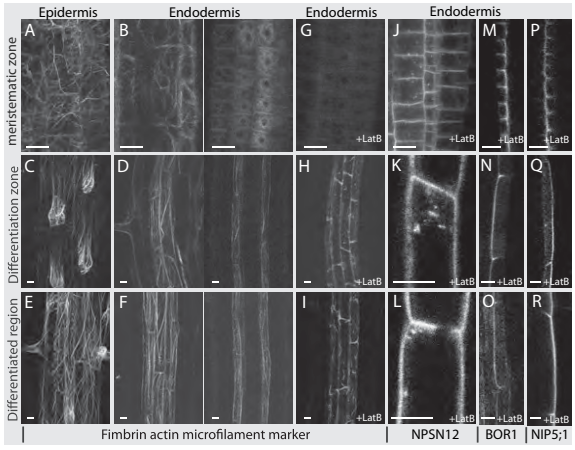

Fig. S3. Localization of the actin marker YFP-Fimbrin in the endodermis. (*A*, *C*, and *E*) 35S::YFP-Fimbrin marker highlights actin accumulation in epidermal cells during different developmental stages. (*B*, *D*, and *F*) Surface (*Left*) and median optical section (*Right*) in a SCR::YFP-Fimbrin line at different developmental stages. No polar or localized accumulation of actin can be observed. (*G*–*I*) SCR::YFP-Fimbrin signals after 1 h treatment with 10 μM Latrunculin B. Only surface cuts are shown. The absence of long strands and the appearance of stubs and patches indicate that Latrunculin B act in endodermal cells. (*J*–*L*) Localization of NPSN12 in meristematic cells, before and after differentiation (*J*, *K*, and *L*, respectively) at the plasma membrane, is unaffected after Latrunculin B treatment (10 μM, 1 h). (*M*–*O*) Polar localization of BOR1 in meristematic cells, before and after differentiation (*M*, *N*, and *O*, respectively), is unaffected after Latrunculin B treatment (10 μM, 1 h). (*P*–*R*) Polar localization of NIP5;1 in meristematic cells, before and after differentiation (*P*, *Q*, and *R*, respectively), is unaffected after Latrunculin B treatment (10 μM, 1 h). *C*, *D*, *H*, *I*, *K*, *L*, *N*, *O*, *Q*, and *R* are the same as in Fig. 4 in the main text. LatB, Latrunculin B. (Scale bar, 10 μm.)

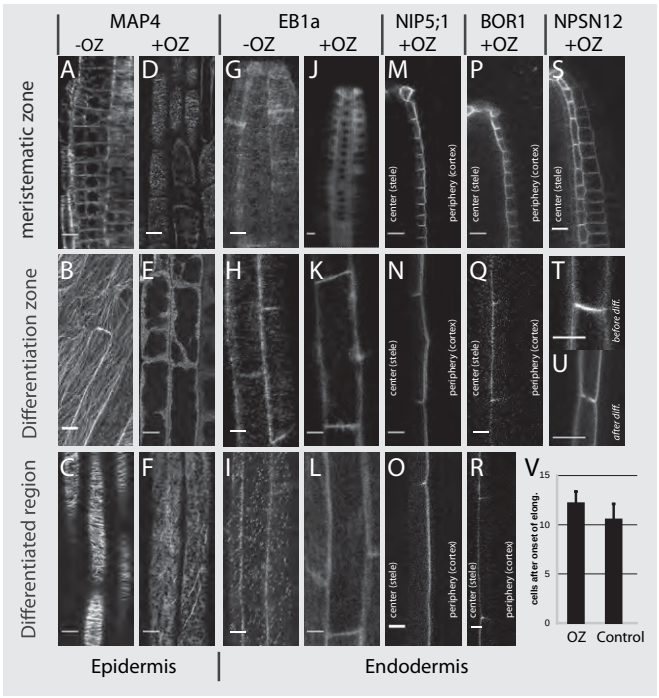

Fig. S4. Organization and function of microtubules in the endodermis. (*A–C*) 35S::GFP-MAP4 marker line highlights microtubule organization in epidermal cells during different developmental stages. (*D–F*) 35S::GFP-MAP4 signals after 90 min 10 μM Oryzalin treatment. Only surface cuts are shown. Microtubule filament structure is disorganized by Oryzalin. (*G–I*) SCR::EB1a-Citrine marker line at different developmental stages. The small dots highlight the microtubule plus ends of the endodermal cell surface. (*J–L*) SCR::EB1a-Citrine signals after 90 min 10 μM Oryzalin treatment. The dotty microtubule plus end structure is not visible after Oryzalin treatment, indicating that Oryzalin treatment is efficient in endodermal cells. (*M–O*) Median optical section in a SCR::mCitrine-NIP5;1 line at different developmental stages after Oryzalin treatment (10 μM, 90 min). Polar localization of NIP5;1 is unaffected by the Oryzalin treatment. (*P–R*) Polar localization of BOR1 in meristematic cells, before and after differentiation, is unaffected by Oryzalin treatment (10 μM, 90 min). (*S*) Median optical section in SCR::NSNP12 in the meristematic zone still indicates plasma membrane signal after Oryzalin treatment (10 μM, 90 min). (*T* and *U*) NPSN12 localization, before and after differentiation, at the plasma membrane is unaffected after Oryzalin treatment (10 μM, 90 min). (*V*) No significant shift in the distance from the meristem at which the NPSN12 depletion zone appears can be observed after Oryzalin treatment (10 μM, 5 h). OZ, Oryzalin. (Scale bar, 10 μm.)

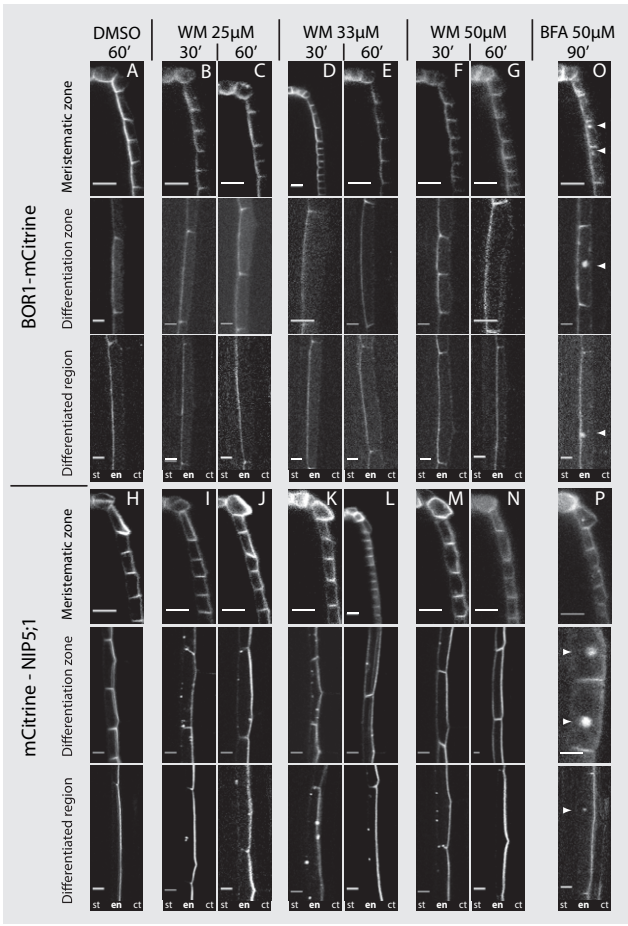

Fig. S5. Effect of Wortmannin concentration and BFA treatment on polarity markers. (*A–G*) BOR1-mCitrine signal and (*H–N*) mCitrine-NIP5;1 are shown after 30 or 60 min Wortmannin (WM) treatment (25, 33, or 50 μM) in meristematic cells and in cells before and after differentiation. No defect in polar localization of BOR1 was observed after 25 μM (*B* and *C*), 33 μM (*D* and *E*), or 50 μM (*F* and *G*) Wortmannin treatment compared to the control (*A*). (*H–N*) The polar localization of NIP5;1 is affected by Wortmannin treatments. (*H*) Peripheral polarity is clearly observed in the control treatment. Applying 25 μM Wortmannin during 30 or 60 min (*I* and *J*) and 33 μM Wortmannin during 30 min (*K*) provokes the appearance of endosomal dots, but the polarity remains intact. After 33 μM during 60 min (*L*) or under higher Wortmannin concentration such as 50 μM (*M* and *N*), the NIP5;1 signal seems to be depolarized before the differentiation. Polar localization of BOR1 in meristematic cells is observed (*I–K*) but becomes less defined (*L* and *M*). (*N*) A strict depolarization is observed after 60 min 50 μM Wortmannin treatment before, but not after differentiation. (*O* and *P*) Polar localization of BOR1 (*O*) and NIP5;1 (*P*) at the plasma membrane is unaffected after Brefeldin A treatment (50 μM, 90 min) in meristematic cells, as well in cells before and after differentiation. However, BFA patches are observed in the three developmental stages investigated. Arrowheads in *O* and *P* indicate BFA patches. BFA, Brefeldin A; WM, Wortmannin. (Scale bar, 10 μm.)

Other Supporting Information Files

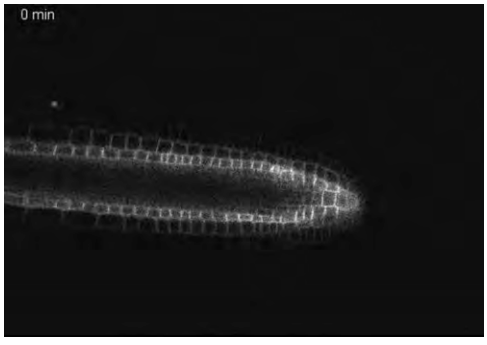

Movie S1 (AVI)

5.2 Dirigent domain-containing protein is part of the machinery required for formation of the lignin-based Casparian Strip in the root

Hosmani P, Takehiro Kamiya, John Danku, Sadaf Naseer, Niko Geldner, Mary Lou Guerinot, and David E. Salt. 2013. Dirigent domain-containing protein is part of the machinery required for formation of the lignin-based Casparian Strip in the root. PNAS, 110:14498-14503.

5.2.1 Own contribution

Recently, the group of David Salt (University of Aberdeen) characterized the dirigent -domain containing protein named as ESB1 (enhanced suberin 1), which localized to the Casparian Strip (CS). This Chapter presents the molecular characterization of this protein and its role in the Casparian Strip formation.

Prashant Hosmani and colleagues in the lab of Prof. Dr. David Salt carried out most of the molecular characterization of ESB1 protein. I particularly participated in this study by analyzing the effect of loss of ESB1 function on the formation of CS and functional diffusion barrier formation (Figure 3G, H, J and I). I also quantified the ectopic deposition of suberin using Fluorol Yellow (Figure 5 E, F, G, and H). In order to observe the effect of loss of ESB1 function on the CASP1 (Casparian Strip membrane domain protein 1) localization, I also generated the line described in the supplementary figure 4 by transformation of available pCASP1:CASP1-GFP construct into *esb1-1* mutant. I prepared all the above-mentioned figures.

5.2.2 Original article

For details, the article is attached herewith.

Dirigent domain-containing protein is part of the machinery required for formation of the lignin-based Casparian strip in the root

Prashant S. Hosmani[a], Takehiro Kamiya[b], John Danku[b], Sadaf Naseer[c], Niko Geldner[c], Mary Lou Guerinot[a], and David E. Salt[b,1]

[a]Department of Biological Sciences, Dartmouth College, Hanover, NH 03755; [b]Institute of Biological and Environmental Sciences, University of Aberdeen, Aberdeen AB24 3UU, United Kingdom; and [c]Department of Plant Molecular Biology, University of Lausanne–Sorge, 1015 Lausanne, Switzerland

Edited by Philip N. Benfey, Duke University, Durham, NC, and approved July 22, 2013 (received for review May 7, 2013)

The endodermis acts as a "second skin" in plant roots by providing the cellular control necessary for the selective entry of water and solutes into the vascular system. To enable such control, Casparian strips span the cell wall of adjacent endodermal cells to form a tight junction that blocks extracellular diffusion across the endodermis. This junction is composed of lignin that is polymerized by oxidative coupling of monolignols through the action of a NADPH oxidase and peroxidases. Casparian strip domain proteins (CASPs) correctly position this biosynthetic machinery by forming a protein scaffold in the plasma membrane at the site where the Casparian strip forms. Here, we show that the dirigent-domain containing protein, enhanced suberin1 (ESB1), is part of this machinery, playing an essential role in the correct formation of Casparian strips. ESB1 is localized to Casparian strips in a CASP-dependent manner, and in the absence of ESB1, disordered and defective Casparian strips are formed. In addition, loss of ESB1 disrupts the localization of the CASP1 protein at the casparian strip domain, suggesting a reciprocal requirement for both ESB1 and CASPs in forming the casparian strip domain

The root is the central plant organ required for water and mineral nutrient uptake from the soil. Understanding the mechanisms underlying root function is therefore central for developing plants with the improved root systems required for the more efficient water and mineral nutrient utilization needed to drive sustainable increases in food production and quality. The rate limiting step in water and mineral nutrient transport to the shoot is radial transport across the root (1). Radial transport involves movement of water and dissolved solutes from the soil, through the epidermis, cortex, and endodermal cell layers and into the vascular system (1). Transport occurs through the cell wall continuum (apoplasm) or cell to cell by using symplastic or transmembrane pathways. The differentiation of the endodermis is marked by the formation in the cell wall of the Casparian strip, a belt-like structure surrounding the cell and running parallel to the root surface in the anticlinal cell wall. This structure is composed of a fine band of lignin (2) tightly adhered to the plasma membrane and spanning the apoplastic space between adjacent endodermal cells. Casparian strips form a physical barrier to extracellular diffusion (3, 4), allowing endodermal cells to exert control over passage of water and solutes into the stele and the vascular system for transport throughout the plant (5). Lignin-forming Casparian strips is polymerized by oxidative coupling of monolignols through the action of specific localized NADPH oxidase and peroxidases (6). The Casparian strip membrane domain proteins (CASPs) (7) form a protein scaffold at the Casparian strip domain, the region of the plasma membrane where the Casparian strip will form. This scaffold is thought to be involved in correctly positioning the biosynthetic machinery involved in building the Casparian strip. However, the proteins required for the precise control of lignin deposition to a fine band spanning the cell wall between adjacent endodermal cells to form the Casparian strip are unknown.

Results and Discussion

Enhanced suberin1 (*ESB1*) was originally identified in a forward genetic screen of *Arabidopsis thaliana* for mutants with altered mineral nutrient and trace element contents (8, 9). The *esb1* mutant displays changes in the leaf accumulation of various elements, including a significant reduction in calcium, which are proposed to be caused by the observed increase of suberin deposition in the roots of this mutant (8, 10). *ESB1* encodes a protein containing a predicted 154-aa residue dirigent domain (Pfam 26.0 PF03018) (11). Dirigent proteins have been characterized to act as nonenzymatic templates guiding bond formation between two monolignols to define the stereochemistry of the resulting dimeric lignin (12). It has been suggested that dirigent proteins can guide synthesis of lignin by providing a template for a specific order of monolignol subunits during lignin deposition in the cell wall (13), but these observations need to be reconciled with biochemical evidence that lignin polymerization can occur in the absence of proteinaceous control (14). Here, we demonstrate that the dirigent domain containing protein ESB1 is required for the correct patterning of lignin deposition in Casparian strips. Use of a stably expressed protein fusion of ESB1 with red fluorescent mCherry under the transcriptional control of the *ESB1* native promoter revealed that *ESB1* is uniquely expressed in the endodermis (Fig. 1 *A*–*C*) and localizes in a band-like structure around the endodermal cells in a similar pattern to Casparian strips (Fig. 1 *D* and *E*). Interestingly, ESB1-mCherry appears to initially localize along the equatorial line of the endodermal cell in patches, which then coalesce to form

Significance

The endodermis acts as a "second skin" in plant roots by providing the cellular control necessary for the selective entry of water and mineral nutrients into the vascular system. To enable such control, Casparian strips span the cell wall of adjacent endodermal cells to form a tight junction that blocks diffusion across the endodermis in the cell wall. This junction is composed of a fine band of lignin, the polymer that gives wood its strength. Here, we characterize a dirigent protein (from Latin, *dirigere*: to guide or align) as playing a vital role in the patterning of lignin in the Casparian strip, identifying a new component of the molecular machinery that builds Casparian strips.

Author contributions: D.E.S. designed research; P.S.H., T.K., J.D., and S.N. performed research; N.G. contributed new reagents/analytic tools; P.S.H., T.K., J.D., S.N., N.G., M.L.G., and D.E.S. analyzed data; and P.S.H. and D.E.S. wrote the paper.

The authors declare no conflict of interest.

This article is a PNAS Direct Submission.

Freely available online through the PNAS open access option.

[1]To whom correspondence should be addressed. E-mail: david.salt@abdn.ac.uk.

This article contains supporting information online at www.pnas.org/lookup/suppl/doi:10.1073/pnas.1308412110/-/DCSupplemental.

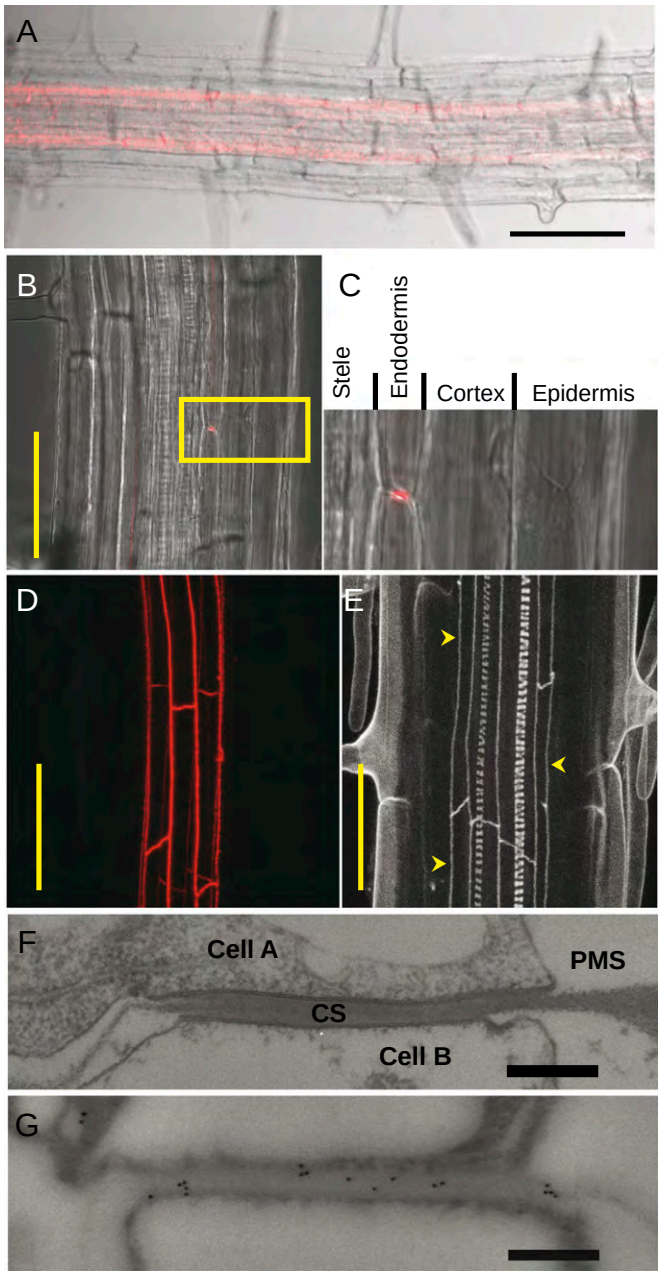

Fig. 1. The dirigent domain containing protein ESB1 accumulates uniquely in the root endodermis at the Casparian strips. (*A–D*) *ESB1-mCherry* expression from native *ESB1* promoter in roots of *esb1-1*. Confocal image (red) merged with transmission image (*A–C*). (*C*) Enlargement of area boxed in *B*. (*D*) *Z*-stack confocal image (red) in the same area as *B*. (*E–G*) Casparian strips in wild-type roots. (*E*) *Z*-stack confocal image of lignin autofluorescence (arrows indicate Casparian strips). (*F*) Transmission electron micrograph of a representative Casparian strip. (*G*) Representative image of immunogold-electron micrograph at the anticlinal wall of an endodermal cell by using anti-ESB1 antibodies. CS, Casparian strip; PMS, space generated by plasmolysis. (Scale bars: *A*, 100 μm; *B*, *D*, and *E*, 50 μm; *F* and *G*, 500 nm.)

a continuous band (Fig. 2). This ESB1-mCherry localization process is similar to that previously observed for CASP1-GFP (7) and for the deposition of the Casparian strip (6), which both pass through a patchy stage before coalescing into continuous strips. Immunogold electron microscopy confirmed that native ESB1 protein is specifically localized to the Casparian strip (Fig. 1 *F* and *G*), and this localization was lost in *esb1-1* (Fig. S1*A*). Significantly, ESB1 localization to the Casparian strip requires CASPs because immunogold labeling of ESB1 at the Casparian strip is reduced in the *casp1-1casp3-1* double mutant (Fig. S1*A*). Further, in the *casp1-1casp3-1* mutant, immunogold particles specific for ESB1 appear to accumulate in the cytoplasm (Fig. S1*B*), supporting the mistargeting of ESB1 in this double mutant.

Loss of *ESB1* function in *esb1-1* causes a complete loss of the well-organized structure of Casparian strips as revealed by electron microscopy (Fig. 3 *A* and *B*). Confocal imaging of Casparian strips using autofluorescence confirms this malformation (Fig. 3 *D* and *E*). The Casparian strips of wild-type endodermal cell walls are replaced in *esb1-1* with deposition of fluorescent material in patches in the equatorial region of the endodermal cells, and also in the corners of the cells on both the cortex and pericycle faces (Fig. 3 *D* and *E* and Movie S1). Raman confocal microscopy (15) establishes that the disrupted Casparian strips in *esb1-1* are composed of an enhanced deposition of lignin-like material with a similar chemical composition to wild-type Casparian strips and xylem lignin (Fig. 4). This disrupted Casparian strip morphology is fully complemented by expression of wild-type *ESB1* or an *ESB1-mCherry* construct from the native *ESB1* promoter (Figs. S2*A* and S3*A*). Propidium iodide (PI) is a fluorescent dye used as an apoplastic tracer whose movement into the inner cell layer of the stele is blocked by Casparian strips (2). Staining with PI revealed that *esb1-1* shows delayed barrier development (Fig. 3 *G* and *H*) that is complemented by expression of wild-type *ESB1* from its native promoter (Fig. S2 *B* and *C*). The enhanced deposition of lignin in *esb1-1* could be explained in several different ways. In the

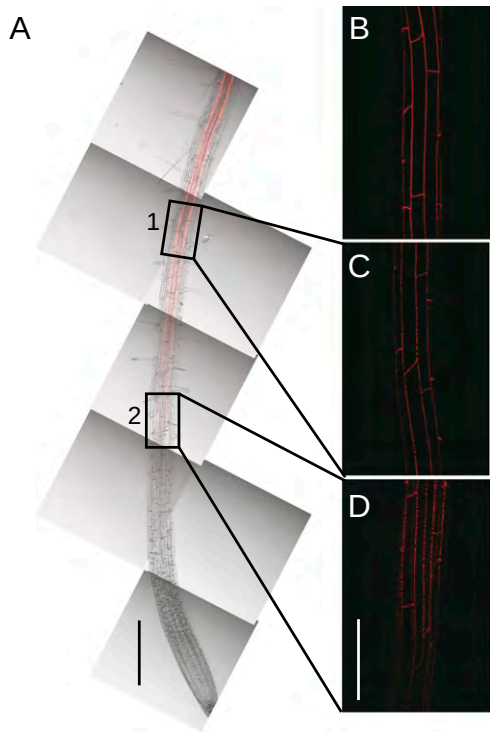

Fig. 2. The dirigent domain containing protein ESB1 localized at the endodermis in equatorially located patches that coalesce into a continuous strip. (*A–D*) *ESB1-mCherry* expression in *esb1-1* transgenic plants were grown for 6 d, and mCherry fluorescence was observed by confocal microscope. (*A*) ESB1-mCherry observed in a 5-mm section of root. Confocal image (red) was merged with transmission image, and multiple merged images were tiled to form a combined image. Higher magnification *Z*-stack confocal images taken 6 mm from the root tip (*B*), in boxed area 1 (*C*), and in boxed area 2 (*D*). (Scale bars: *A*, 500 μm; *B–D*, 100 μm.)

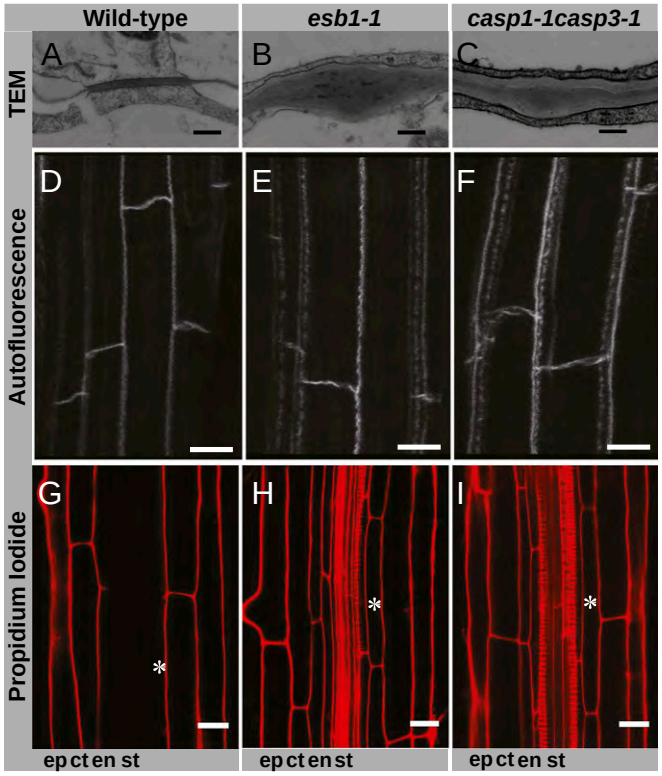

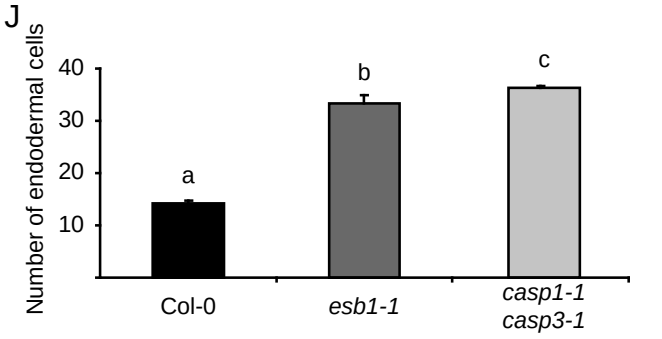

Fig. 3. The dirigent-domain protein ESB1 is required for the normal morphology and function of the lignin Casparian strip. Transmission electron micrographs showing Casparian strip in wild-type (*A*), *esb1-1* (*B*), and *casp1-1casp3-1* (*C*). Autofluorescence visualization after clearing root in wild-type (*D*), *esb1-1* (*E*), and *casp1-1casp3-1* (*F*). PI penetration in wild-type (*G*), *esb1-1* (*H*), and *casp1-1casp3-1* (*I*). Asterisks mark the 30th endodermal cell after onset of elongation. Onset of elongation is defined as the zone where the length of an endodermal cell was observed to be more than twice its width. (*J*) Quantification of PI penetration into the stele quantified as number of endodermal cells from the first fully expanded cell in wild-type, *esb1-1*, and *casp1-1casp3-1*. Casparian strips in wild-type plants form a barrier to apoplastic diffusion of PI starting at the 13th endodermal cell from the onset of elongation, whereas in *esb1-1*, this barrier does not form until the 32nd endodermal cell. Different letters (a, b, and c) indicate statistically significant differences between means by one-way analysis of variance (ANOVA) with Tukey–Kramer separation of means ($P < 0.05$), $n = 15$ roots. (Scale bars: *A*–*C*, 250 nm; *D*–*F*, 10 μm; *G*–*I*, 20 μm.) ct, cortex; en, endodermis; ep, epidermis; st, stele.

absence of ESB1, it is possible that polymerization of monolignols, usually directed by localized NADPH oxidases and peroxidases (6), does not proceed normally, as indicated by the islands of lignin observed in *esb1-1*. Unpolymerized monolignols could accumulate in the corners of the cells where they are activated by nonspecific peroxidase and polymerize to form ectopic lignin deposits. This process would occur in an unregulated manner, forming a sink for monolignols and allowing increased levels of lignin to accumulate. It is also possible that to repair the disrupted Casparian strip in *esb1-1*, release of monolignols into the cell wall is stimulated, providing substrate for enhanced lignifications. In *esb1-1* the development of an effective barrier to apoplastic diffusion of PI at the endodermis is delayed but not completely blocked. A functional barrier develops in more mature endodermal cells (30 cells from the root tip) (Fig. 3*J*), supporting the idea that the enhanced lignification observed in *esb1-1* is a Casparian strip repair mechanism.

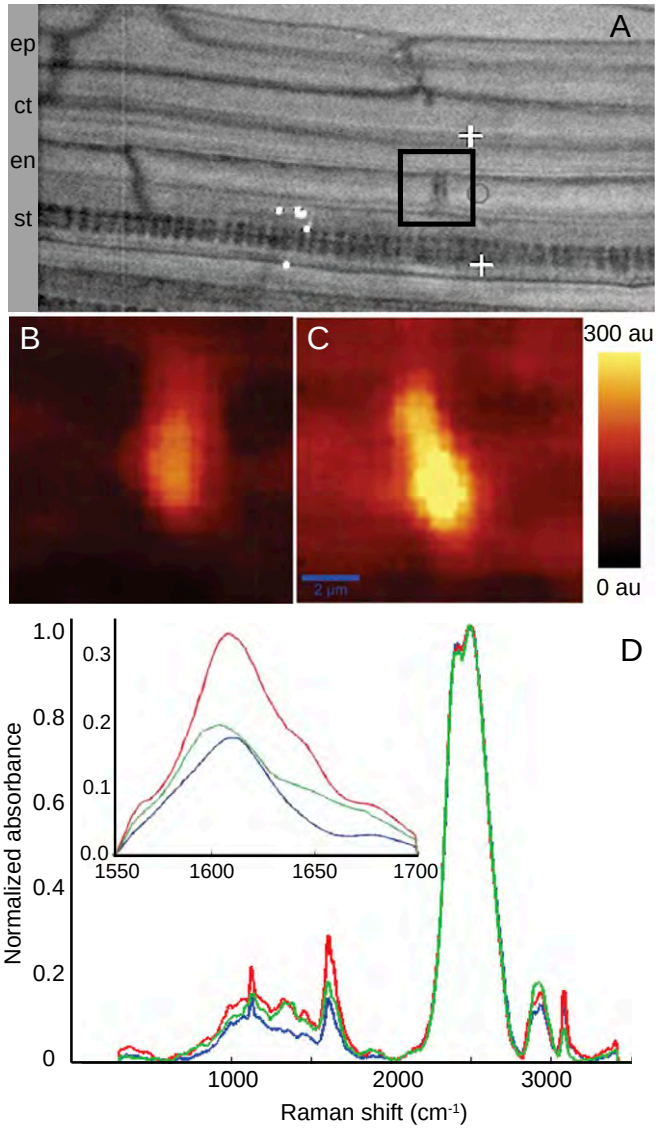

Fig. 4. Chemical imaging using Raman confocal microscope showing increased deposition of lignin at the disrupted Casparian strip in *esb1-1* mutant. (*A*) Representative image showing an endodermal cell junction used for acquiring 2D Raman spectra (marked with a black square box signifying a 10×10 μm^2 area). Raman images showing the modification of lignin deposition at the Casparian strip were obtained by integrating absorption intensities between 1,550 and 1,700 cm^{-1} in wild-type (*B*) and *esb1-1* (*C*). (*D*) Raman spectra extracted from the wild-type Casparian strip (blue), wild-type xylem (green), and *esb1-1* Casparian strip (red). *D Insert* shows the lignin spectra (1,550–1,700 cm^{-1}). Intensities were normalized to the peak height of D_2O at ~2,500 cm^{-1}, representing the O-D stretching band intensity. au, arbitrary units; ct, cortex; en, endodermis; ep, epidermis; st, stele.

From this evidence, we conclude that ESB1 is essential for the correct deposition of lignin-based Casparian strips and for their normal barrier function. In particular, ESB1 appears to be involved in the deposition of lignin patches that occurs early in the development of the Casparian strip (6) and also in the coalescence of these patches to form a continuous fine band of lignin as the Casparian strip matures. These conclusions are supported by the fact that ESB1 localization mirrors this coalescence process (Fig. 2), and in the absence of ESB1, malformed lignin patches form that fail to coalesce into a mature Casparian strip (Fig. 3). Lignin polymerization in the corners of cells in the *esb1-1* mutant (Fig. 3) may represent a default pathway that occurs when coalescence of the equatorial lignin patches is blocked. The CASP complex likely scaffolds the machinery for the precise localization of the lignification required to create the Casparian strip. This machinery includes ESB1 and the NADPH oxidase/peroxidase required for monolignol activation (6). During the initial development of the Casparian strip, this machinery occurs as equatorially located islands that produce patchy lignifications (6, 7). As Casparian strip development continues, these assembly islands coalesce, perhaps through the delivery of ESB1 and other components through cellular trafficking pathways, to eventually form a continuous strip. As functional units of this machinery are assembled, new lignin is laid down, bridging the gap between the initial lignin islands to finally form a precisely deposited lignin band sealed to the plasma membrane and spanning the cell walls of adjacent endodermal cells.

Importantly, the localization of ESB1 to the correct position in the cell wall for formation of the Casparian strip requires the function of the CASPs. The loss of ESB1 localization to the Casparian strip in the *casp1-1casp3-1* mutant (Fig. S1) could therefore account for the *casp1-1casp3-1* phenotypes, which show similar defects to *esb1-1* in both the morphology (7) and function of Casparian strips (Fig. 3 and Movie S1). Interestingly, we also observe that ESB1 is required for the correct localization of CASP1-GFP to the plasma membrane (Fig. S4). In the absence of ESB1, the localization of CASP1-GFP appears to stall at the "string-of-pearls" stage (7) with CASP1-GFP remaining localized in patches that do not coalesce into a mature Casparian strip domain.

Although its role in building Casparian strips is clear, the biochemical function of ESB1 remains obscure. When tested, dirigent proteins lack oxidative activity (12). However, in vitro in the presence of an oxidase, a dirigent protein has been shown to be able to direct the stereoselective coupling of the monolignol coniferyl alcohol to form the dimeric lignan pinoresinol (12). In this assay, the dirigent protein played no catalytic role in coupling but it was proposed to "bind and orientate" the monolignol before coupling (12). In vitro recombinant ESB1 in the presence of a fungal laccase appears to lack the capacity for stereoselective coupling of coniferyl alcohol to produce the dimeric lignin pinoresinol, although other potential monomers such as sinapyl alcohol and ρ-coumaryl alcohol were not tested (16). In the absence of any known activity for ESB1, its biochemical function remains speculative. It is possible that ESB1 plays a role in locating the lignin polymer of the Casparian strip by nucleating lignin polymerization at specified sites, and this suggestion is supported by the colocalization of ESB1 and the Casparian strip. Given the requirement of ESB1 for the correct localization of the CASPs, it is also possible that ESB1 has a role in bridging between the plasma membrane Casparian strip domain and lignin to allow a tight seal between the Casparian strip and the plasma membrane. Further experiments are required to test these hypotheses.

In wild-type plants suberin, a waxy material composed of both polyaliphatic and polyaromatic domains (17), is deposited between the plasma membrane and cell wall of endodermal cells in mature regions of the root. These suberin deposits are thought to act as an extracellular barrier to water and solutes (17). It is now clear that in *esb1*, suberin is ectopically deposited in endodermal cells close to the root tip, a region that is normally not suberized, and where Casparian strips first develop (2). This ectopic deposition can be clearly seen as alternating light and dark bands of suberin lamellae between the plasma membrane and cell wall (Fig. 5 *A*–*C*). The presence of suberin closer to the root tip in *esb1-1* can also be quantified by counting the first appearance of endodermal cells stained with Fluorol yellow, a suberin staining fluorescent dye (Fig. 5*E*). In addition, *esb1-1* lacks the unsuberised passage cells normally observed in more mature regions of the root (Fig. 5 *F* and *G*), suggesting that suberin is also ectopically deposited in these cells. Endodermal passage cells are thought to be specialized for ion transport in more mature regions of the root where suberin deposition blocks transport in normal endodermal cells (18). We observe a similar ectopic deposition of suberin in the *casp1-1casp3-1* double mutant (Fig. 5 and Fig. S5), consistent with the loss of ESB1 from the Casparian strip in this double mutant. Additionally, ectopic suberin deposition in *esb1-1* and *casp1-1casp3-1* also correlates with similar changes in the mineral nutrient composition of the leaves of both mutants, with significant reductions in the concentration of magnesium, calcium (strontium chemical analog), manganese, and iron, and increases in sulfur, potassium (rubidium chemical analog), and molybdenum (Dataset S1). Because suberin lamellae are deposited between the plasma membrane and the cell wall, they potentially limit transmembrane transport into cells, but are unable to block diffusion between cells in the cell wall. This function is unlike Casparian strips that span the cell wall and effectively block apoplastic transport. Suberin lamellae and Casparian strip formation at the endodermis are therefore expected to have different effects on nutrient uptake by roots. In *esb1*, both processes are affected together, revealing a fascinating interaction and providing an important tool to understand root function.

We propose that the ectopic deposition of suberin in *esb1-1* is a consequence of the defect in Casparian strip formation, revealing an intriguing cross-talk between formation of lignin and suberin-based cell wall modifications. The existence of such a mechanism is supported by the observation that in wild-type roots, suberin deposition occurs in a pocket of endodermal cells surrounding the developing lateral root primordium (19), and this deposition is congruent with the primordium penetrating the endodermis and disrupting the Casparian strip network (20). This knowledge raises the intriguing possibility that the ectopic deposition of suberin in *esb1* is being driven by a cell wall surveillance system normally responsible for coordinating the deposition of suberin as Casparian strips are disrupted during lateral root emergence. Surveillance systems that monitor primary cell walls has been reported. For example, the lack of cellulose synthesis in the *cesa* mutants initiates ecotopic deposition of lignin (21, 22), and this response appears to be mediated by the plasma membrane bound receptor-like kinase THESEUS1 (23).

In conclusion, our analysis indicates that the dirigent domain containing protein ESB1 plays an essential role in building the extracellular lignin-based Casparian strip in endodermal cells of *A. thaliana* roots. ESB1 requires the CASP complex for its correct localization to the region of the cell wall where Casparian strips form, because the *esb1-1* knockout phenocopies *casp1-1casp3-1*. However, ESB1 is also required for the coalescence of the CASP complex into the continuous Casparian strip domain that underlies the Casparian strip. In the absence of ESB1, the barrier function of Casparian strips is impaired, causing ectopic deposition of suberin lamellae between the plasma membrane and the cell wall in both endodermal cells close to the root tip and endodermal passage cells. Such ectopic suberin deposition

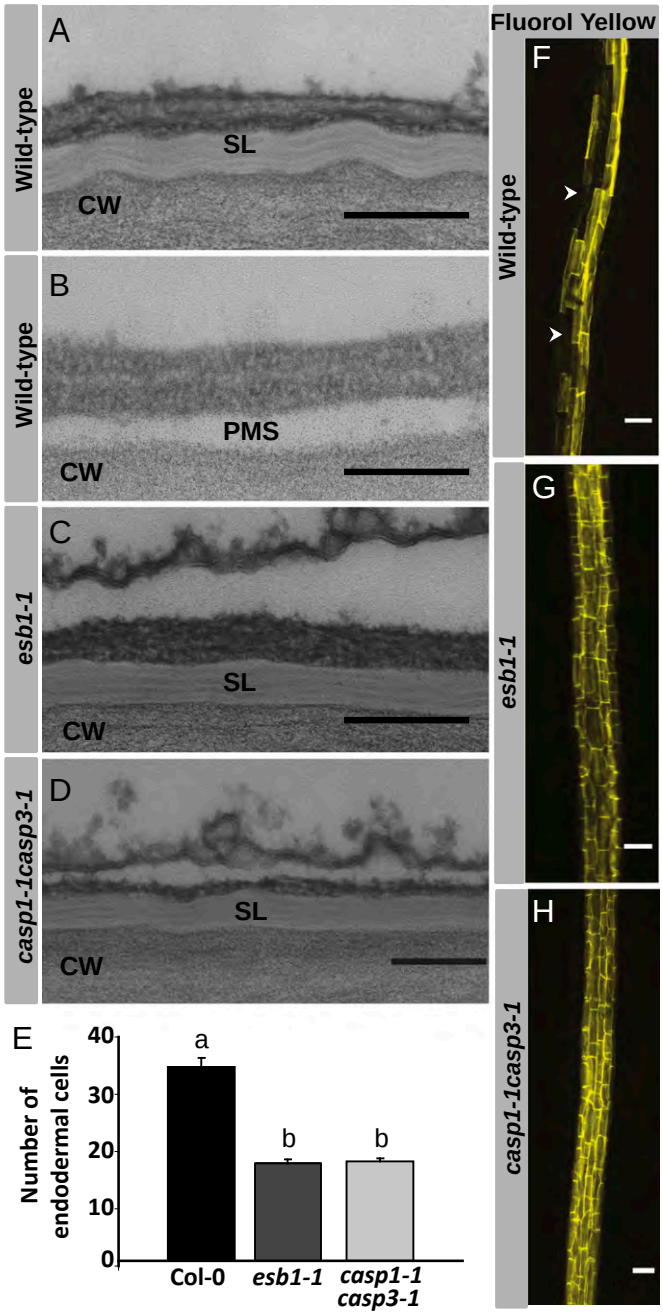

Fig. 5. Disruption of the Casparian strip through loss of *ESB1* function leads to ectopic deposition of suberin lamellae closer to the root tip and around passage cells in the endodermis. Transmission electron micrographs at periclinal wall of endodermal cells in wild-type mature region (*A*), wild-type young region (*B*), *esb1-1* young region (*C*), and *casp1-1casp3-1* young region (*D*). (*F–H*) Suberin deposition in roots detected by Fluorol Yellow staining of wild-type (*F*), *esb1-1* (*G*), and *casp1-1casp3-1* (*H*). Counting of the number of endodermal cells from the first fully expanded cell shows the early appearance of suberin in both *esb1-1* and *casp1-1casp3-1* double mutant compared with the wild type, with Fluorol yellow staining starting at the 17th endodermal cell after onset of elongation in *esb1-1*, and *casp1-1casp3-1* compared with the 33rd endodermal cell in wild-type (*E*). Different letters (a and b) indicate statistically significant differences between means by one-way analysis of variance (ANOVA) with Tukey–Kramer separation of means ($P < 0.05$), $n = 15$ roots. Arrowheads represent unsuberised passage cells. CW, cell wall; PMS, space generated by plasmolysis; SL, suberin lamellae. (Scale bars: *A–D*, 200 nm; *F–H*, 50 μm.)

reveals cross-talk between Casparian strips and suberin biosynthesis and suggests the existence of a cell wall surveillance system capable of perceiving the integrity of Casparian strips. The ectopically deposited suberin in *esb1-1* likely blocks transmembrane uptake of calcium and other ions into endodermal cells, limiting xylem loading and causing the reduction in leaf calcium and other minerals observed in plants with a disrupted ESB1 function. Our discoveries start to dissect the molecular mechanisms involved in endodermal control of solute entry into plants. Further, we provide in vivo evidence for proteins in the dirigent family functioning as part of the machinery that builds extracellular lignin-based structures, opening an avenue to determine the elusive role of this protein family *in planta*.

Methods

Plant Materials. *A. thaliana* Col-0 wild-type seeds were purchased from Lehle Seeds. The mutant *esb1-1* was identified in an ionomics screen of fast neutron mutagenized plants and was twice backcrossed to wild-type Col-0 (8, 9). The *casp1-1casp3-1* was generated by Roppolo et al (7).

Plant Growth Conditions. Plants were grown on agar solidified half-strength Murashige and Skoog (Caisson Laboratories) (24) with 1% sucrose (wt/vol) in sterile square (100 × 15 mm) Petri dishes (BD Falcon). Seeds were surface sterilized (10% bleach/0.1% Tween20 and 70% ethanol treatments), washed six times with sterile 18 MΩ H_2O and stratified for 3 d at 4 °C in 0.1% agarose solution. Petri dishes were kept in a growth room at 16-h light (90 μmol $m^{-2}·s^{-1}$): 8-h dark at a temperature of 19 °C to 22 °C. Plants were grown for either 7 or 14 d as required.

Elemental Analysis. Shoots of plants grown on agar plates were harvested into labeled Pyrex digestion tube (16 × 100 mm) sets by using surgical knife, plastic forceps, Teflon rod, and a beaker filled with 18 MΩ water. The tissues were dried in an oven at 88 °C for 20 h. Seven samples of the shoots were weighed (these were used to calculate the weights of all of the others on the basis of their averaged elemental concentrations; ref. 9). Concentrated nitric acid (0.7 mL per tube) (Trace metal grade; T.J. Baker) with indium internal standard (20 ppb) was added and samples digested at 115 °C for 5 h by using digital dry block heaters inside a fume hood. The acid-digested samples were diluted to a final volume of 6 mL with 18 MΩ water. Aliquots were transferred from the digestion tubes into 96-well deepwell plates for analysis. Elemental analysis was performed on an ICP-MS (inductively coupled plasma mass spectrometry) (Elan DRC II; PerkinElmer) equipped with Apex sample introduction system and SC-2 autosampler (Elemental Scientific). Twenty elements (Li, B, Na, Mg, P, S, K, Ca, Mn, Fe, Co, Ni, Cu, Zn, As, Se, Rb, Sr, Mo, Cd) were monitored; their concentrations were obtained by using calibration standards with blanks and the external calibration method of the Elan software (version 3.4). Normalized concentrations of the samples were obtained by using the solution concentrations and the calculated weights (9).

Plasmid Construction and Transformation. The −2,245-bp region from the first ATG was used as the promoter for construction of the *pESB1::ESB1::mCherry* construct. Genomic DNA was amplified (forward primer 5′-CACCCAACAATGAGGACACTGAGC-3′ and reverse primer 5′-GTAAGAAAGATAAACGGTAC-3′. mCherry was amplified (forward primer 5′-GTTGTTGAGTGTACCGTTTATCTTTCTTACGGAGGAGGAGGAGCTATGGTGAGCAAGGCGAGGA-3′ and reverse primer 5′-TCACTTGTACAGCTCGTCCATGC-3′). The amplified DNA fragment from genomic DNA and mCherry was fused by fusion PCR (forward primer 5′-GAGAATTCCAACAATGAGGACACTGAGC-3′ and reverse primer 5′- GAGCTCGAGTCACTTGTACAGCTCGTCCATGC-3′). The resulting fused fragment was digested with EcoRI and XhoI and cloned into the EcoRI and XhoI site of pENTR2B Dual Selection Vector (Invitrogen) followed by the destination vector GWB510 (25) by using LR Clonase (Invitrogen). The −1,172-bp region from the first ATG of *ESB1* was used for complementation of *esb1-1* with wild-type *ESB1*. Genomic DNA was amplified (forward primer 5′- AAAATATTTCTTCTAAATTTATTGAGAATCCATACGAT -3′ and reverse primer 5′- TCTACGTCTCTTTTTATTGTAGAAAATTTTAATCTGC -3′) with gateway adapters and recombined into pDONR 221 by using BP clonase enzyme (Invitrogen). The resulting entry clone was recombined with the promoterless binary destination vector pCC1136 by using LR Clonase (Invitrogen). All constructs were transformed into electro competent *Agrobacterium tumefaciens* GV3101 cells. Positive clones were selected by using suitable antibiotic resistance and used for plant transformation by using the floral dip method (26). Plants were selected by using resistance to glufosinate-ammonium (Basta) in soil. We note

that ESB1 used in the mCherry experiment contained a mutation (Ala^{137}, which is not conserved among ESB1 homologs, is substituted with Thr) because we could not obtain nonmutated ESB1. Although ESB1-mCherry in this work has the mutation, the construct fully complemented the *esb1-1* mutant (Fig. S3), indicating that the protein activity of ESB1 is the same as that of wild-type ESB1.

Optical Microscopy. Autofluorescence of the Casparian strip was observed on cleared roots (27) by using a Zeiss LSM700 confocal microscopy. Briefly, 5- to 6-d-old seedlings (Col-0, *esb1-1*, and *casp1-1casp3-1*) were transferred to a Petri dish containing 0.24 M HCl and 20% methanol and incubated for 15 min at 57 °C. The solution was replaced with 7% NaOH and 60% ethanol and incubated for 15 min at room temperature. After these clearing steps, roots were rehydrated at room temperature by sequential replacement of the solution using 40% ethanol for 5 min, 20% ethanol for 5 min, 10% ethanol for 5 min, 5% ethanol for 15 min, and finally 25% glycerol was added. For mounting root on glass slides, 50% glycerol was used. Cleared roots were visualized for autofluorescence with excitation at 488 nm and with band path filter of 500–600 nm. *Z*-stack images were obtained by imaging several slices with 0.95 μm thickness. Fluorol yellow was detected with a standard GFP filter under a wide-field microscope (Leica DM5500). Fluorol yellow staining was performed as described (28). For assay of the apoplastic barrier, seedlings were incubated in the dark for 10 min in a fresh solution of 15 μM (10 μg/mL) PI and rinsed twice in water (29). For quantification, "onset of elongation" was defined as the point where an endodermal cell in a median optical section was more than twice its width. From this point, cells in the file were counted until the respective signals were detected (27).

Electron Microscopy. The state I endodermis was visualized by using root sections taken 6 mm from the root tip. The state II endodermis was visualized by using root sections taken at the mature region of the root (in the region of the root where lateral roots start to develop) ∼30 mm from the root tip in 14-d-old seedling. Transmission electron microscopy (TEM) was conducted by using a described protocol (30). Ultrathin sections were prepared by using a microtome from London resin white-embedded samples. Samples were visualized with an FEI/Philips CM-10 transmission electron microscope (FEI Company) at an accelerating voltage of 80 kV.

Immunogold Labeling. Subcellular localization was performed by using transmission electron microscopy (TEM) after immunogold labeling of root sections taken 6 mm from the root tip in 7-d-old *A. thaliana* seedlings grown in plates on agar solidified medium. Ultrathin section were prepared from London resin white-embedded root samples and transferred on to nickel grids (Electron Microscopy Science). After transfer immunocytochemistry (ICC) was performed by using standard procedures (30). ICC involved the anti-ESB1 primary antibody with a dilution of 1:250 in Tris-buffered saline (TSB) containing 0.5% bovine serum albumin (TSB-B) overnight and secondary antibody goat anti-rabbit IgG EM grade 10 nm gold conjugate (Ted Pella) at a 1:50 dilution in TBS containing 0.5% Tween-20 and 1% BSA (TBS-TB). Samples were stained with 2% uranyl acetate in 70% methanol for 10 min. Custom affinity-purified polyclonal anti-ESB1 antibodies were made by Genscript USA and were used as a primary antibody. Anti-ESB1 antibodies were generated in rabbits against a synthetic peptide (CGTQQNQPHQFTDGL) designed from the C terminus of the ESB1 protein. Root sections were visualized with an FEI/Philips CM-10 transmission electron microscope (FEI Company) by using an accelerating voltage of 80 kV.

Raman Confocal Microscopy. Confocal Raman microscopy was performed for lignin imaging by using a described method (15) on cleared root samples. After clearing, roots were suspended and subsequently mounted in deuterium oxide. Two-dimensional Raman spectra were obtained by using a confocal Raman microscope (WITec CRM200) for chemical imaging with a 50× objective and a 514 nm polarized light source. Using a piezoelectric scan stage, spectral data were acquired every 200 nm. Images were obtained by using an integration time of 1 s for each spectrum. Image analysis was performed by using the WITec project software (version 1.88). Different spectral map intensities were normalized by using the reference peak (oxygen-deuterium stretching band ∼2,500 cm^{-1}) using a Raman spectrum processing program (31).

ACKNOWLEDGMENTS. We thank Dr. Charles Daghlian (Dartmouth College Microscopy Facility), Dr. Aaron Taylor (Purdue University Bioscience Imaging Facility), and the University of Aberdeen and University of Lausanne for technical support. This work was supported by grants from the US National Science Foundation Arabidopsis 2010 Program to D.E.S and M.L.G (Award IOB 0419695), the European Commission Marie Curie Career Integration to D.E.S. (Award FP7-PEOPLE-2011-CIG), and the Japan Society for the Promotion of Science (T.K.).

1. Steudle E (2001) The cohesion-tension mechanism and the acquisition of water by plant roots. *Annu Rev Plant Physiol Plant Mol Biol* 52:847–875.
2. Naseer S, et al. (2012) Casparian strip diffusion barrier in Arabidopsis is made of a lignin polymer without suberin. *Proc Natl Acad Sci USA* 109(25):10101–10106.
3. Steudle E (2000) Water uptake by plant roots: An integration of views. *Plant Soil* 226: 45–56.
4. White PJ (2001) The pathways of calcium movement to the xylem. *J Exp Bot* 52(358): 891–899.
5. Geldner N (2013) The endodermis. *Annu Rev Plant Biol* 64:531–558.
6. Lee Y, Rubio MC, Alassimone J, Geldner N (2013) A mechanism for localized lignin deposition in the endodermis. *Cell* 153(2):402–412.
7. Roppolo D, et al. (2011) A novel protein family mediates Casparian strip formation in the endodermis. *Nature* 473(7347):380–383.
8. Baxter I, et al. (2009) Root suberin forms an extracellular barrier that affects water relations and mineral nutrition in Arabidopsis. *PLoS Genet* 5(5):e1000492.
9. Lahner B, et al. (2003) Genomic scale profiling of nutrient and trace elements in Arabidopsis thaliana. *Nat Biotechnol* 21(10):1215–1221.
10. Ranathunge K, Schreiber L (2011) Water and solute permeabilities of Arabidopsis roots in relation to the amount and composition of aliphatic suberin. *J Exp Bot* 62(6): 1961–1974.
11. Finn RD, et al. (2010) The Pfam protein families database. *Nucleic Acids Res* 38(Database issue):D211–D222.
12. Davin LB, et al. (1997) Stereoselective bimolecular phenoxy radical coupling by an auxiliary (dirigent) protein without an active center. *Science* 275(5298):362–366.
13. Davin LB, Lewis NG (2000) Dirigent proteins and dirigent sites explain the mystery of specificity of radical precursor coupling in lignan and lignin biosynthesis. *Plant Physiol* 123(2):453–462.
14. Ralph J, et al. (2009) Lignification: Are lignins biosynthesized via simple combinatorial chemistry or via proteinaceous control and template replication? *Rec Adv Polyphen Res* 1:36–66.
15. Schmidt M, Perera P, Schwartzberg AM, Adams PD, Schuck PJ (2010) Label-free in situ imaging of lignification in plant cell walls. *J Vis Exp* (45):2064.
16. Kim KW, et al. (2012) Opposite stereoselectivities of dirigent proteins in Arabidopsis and schizandra species. *J Biol Chem* 287(41):33957–33972.
17. Franke R, Schreiber L (2007) Suberin—a biopolyester forming apoplastic plant interfaces. *Curr Opin Plant Biol* 10(3):252–259.
18. Peterson CA, Enstone DE (1996) Functions of passage cells in the endodermis and exodermis of roots. *Physiol Plant* 97:592–598.
19. Martinka M, Dolan L, Pernas M, Abe J, Lux A (2012) Endodermal cell-cell contact is required for the spatial control of Casparian band development in Arabidopsis thaliana. *Ann Bot (Lond)* 110(2):361–371.
20. Lucas M, et al. (2013) Lateral root morphogenesis is dependent on the mechanical properties of the overlaying tissues. *Proc Natl Acad Sci USA* 110(13):5229–5234.
21. Caño-Delgado AI, Metzlaff K, Bevan MW (2000) The eli1 mutation reveals a link between cell expansion and secondary cell wall formation in Arabidopsis thaliana. *Development* 127(15):3395–3405.
22. Caño-Delgado A, Penfield S, Smith C, Catley M, Bevan M (2003) Reduced cellulose synthesis invokes lignification and defense responses in Arabidopsis thaliana. *Plant J* 34(3):351–362.
23. Hématy K, et al. (2007) A receptor-like kinase mediates the response of Arabidopsis cells to the inhibition of cellulose synthesis. *Curr Biol* 17(11):922–931.
24. Murashige T, Skoog F (1962) A revised medium for rapid growth and bio assays with tobacco tissue cultures. *Physiol Plant* 15:473–497.
25. Nakagawa T, et al. (2007) Improved Gateway binary vectors: High-performance vectors for creation of fusion constructs in transgenic analysis of plants. *Biosci Biotechnol Biochem* 71(8):2095–2100.
26. Clough SJ, Bent AF (1998) Floral dip: A simplified method for Agrobacterium-mediated transformation of Arabidopsis thaliana. *Plant J* 16(6):735–743.
27. Malamy JE, Benfey PN (1997) Organization and cell differentiation in lateral roots of Arabidopsis thaliana. *Development* 124(1):33–44.
28. Lux A, Morita S, Abe J, Ito K (2005) An improved method for clearing and staining free-hand sections and whole-mount samples. *Ann Bot (Lond)* 96(6):989–996.
29. Alassimone J, Naseer S, Geldner N (2010) A developmental framework for endodermal differentiation and polarity. *Proc Natl Acad Sci USA* 107(11):5214–5219.
30. Kolosova N, Sherman D, Karlson D, Dudareva N (2001) Cellular and subcellular localization of S-adenosyl-L-methionine:benzoic acid carboxyl methyltransferase, the enzyme responsible for biosynthesis of the volatile ester methylbenzoate in snapdragon flowers. *Plant Physiol* 126(3):956–964.
31. Reisner LA, Cao A, Pandya AK (2011) An integrated software system for processing, analyzing, and classifying Raman spectra. *Chemometr Intell Lab* 105:83–90.

Supporting Information

Hosmani et al. 10.1073/pnas.1308412110

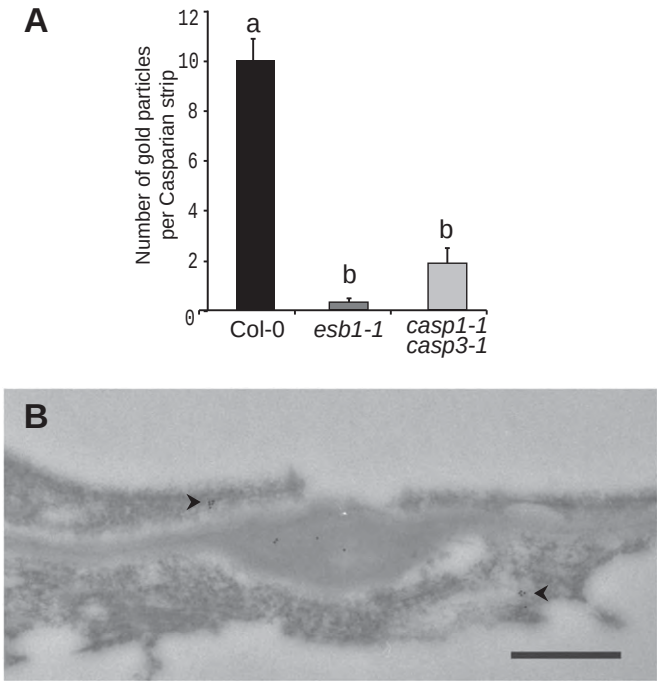

Fig. S1. Casparian strip domain proteins (CASPs) are necessary for correct localization of dirigent-domain protein ESB1. (*A*) Plot of number of gold particles per Casparian strip from an immunogold localization experiment by using anti-ESB1 antibodies. Different letters (a and b) indicate statistically significant differences between means by one-way analysis of variance (ANOVA) with Tukey–Kramer separation of means ($P < 0.05$), $n = 8–16$. (*B*) ESB1 mislocalized in *casp1-1casp3-1*. Immunogold-electron micrograph of the Casparian strip in *casp1-1casp3-1* using anti-ESB1 antibodies. Arrowheads show gold particles corresponding to ESB1 protein in the cytosol of endodermal cells. (Scale bar: 500 nm.)

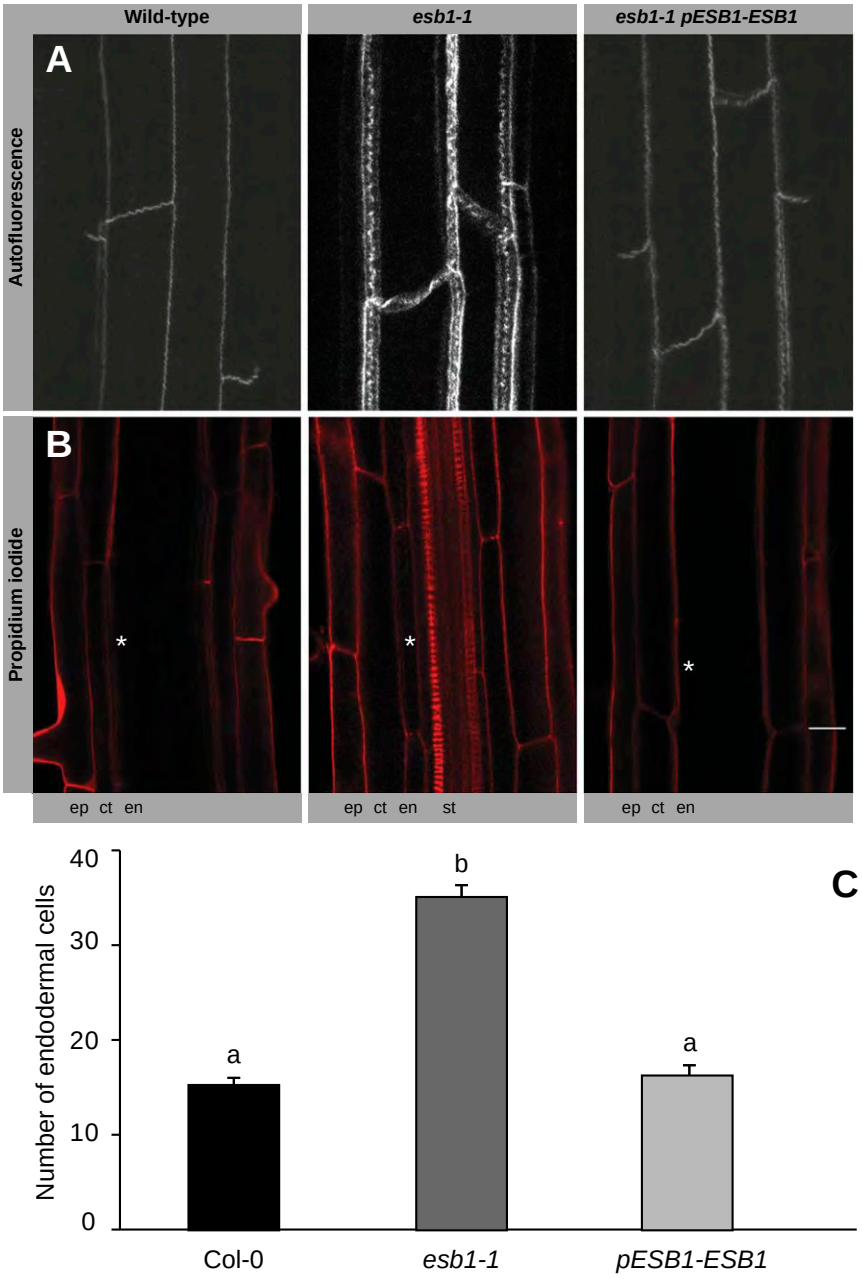

Fig. S2. Wild-type *ESB1* complements *esb1-1* Casparian strip defects including morphology and diffusion barrier properties. Casparian strip morphology defect of *esb1-1* is complemented by wild-type *ESB1* expressed from its native promoter. (*A*) Casparian strips visualized by autofluorescence of lignin. Delayed establishment of a functional barrier to propidium iodide diffusion observed in *esb1-1* is complemented by wild-type *ESB1*. (*B*) Propidium iodide fluorescence. Asterisks mark the 30th endodermal cell after onset of elongation. (*C*) Propidium iodide penetration into the stele of roots quantified as number of endodermal cells after onset of elongation. Different letters (a and b) indicate statistically significant differences between means by one-way ANOVA with Tukey–Kramer separation of means ($P < 0.05$), $n = 5$ roots. (Scale bar: 10 μm.) ct, cortex; en, endodermis; ep, epidermis; st, stele.

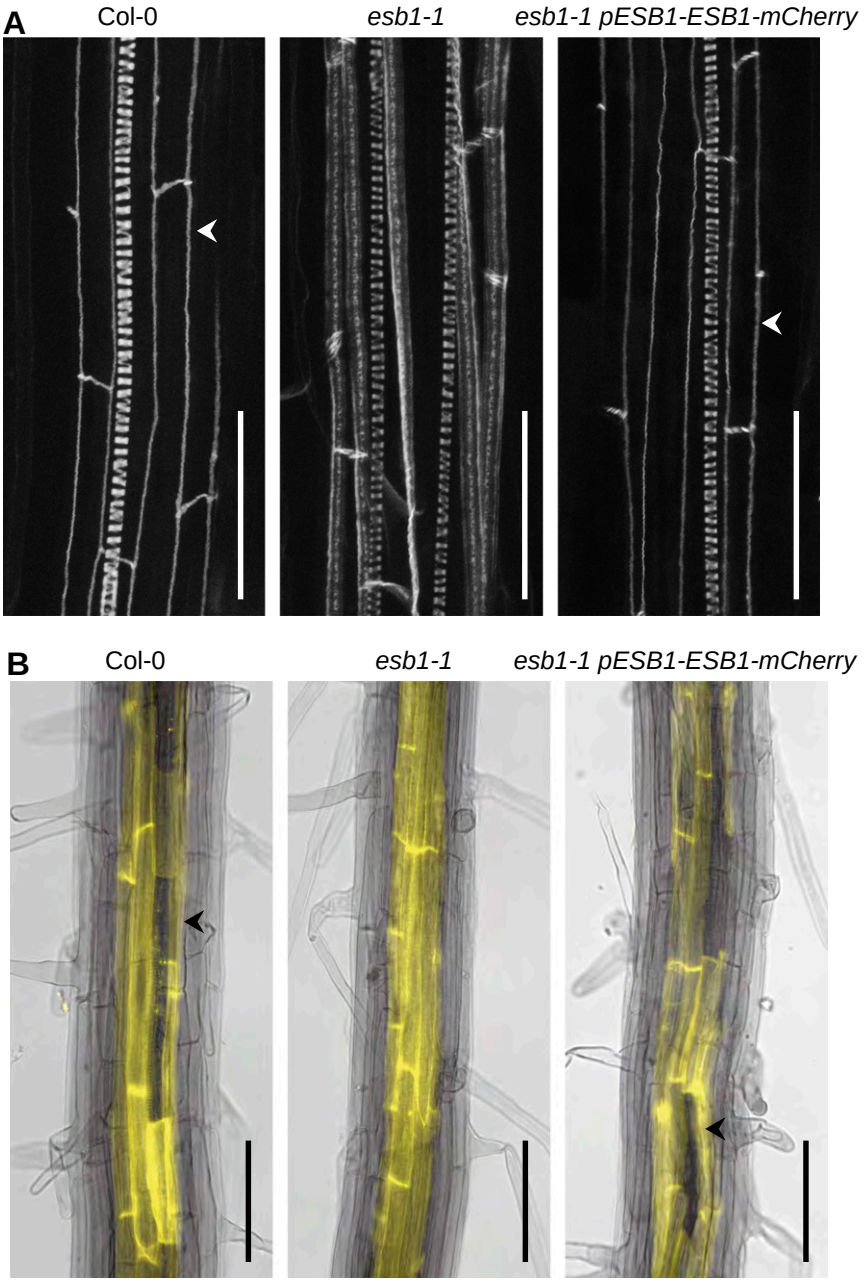

Fig. S3. *ESB1-mCherry* fusion construct complements *esb1-1* Casparian strip morphology defect and the loss of unsuberised endodermal passage cells. (*A*) Casparian strips imaged by confocal microscopy of lignin autofluorescence. Arrows indicate wild-type Casparian strip morphology. (*B*) Endodermal suberin lamella formation detected by Fluorol Yellow 088 staining. Arrowheads marks transfer cells. (Scale bars: *A*, 50 μm; *B*, 100 μm.)

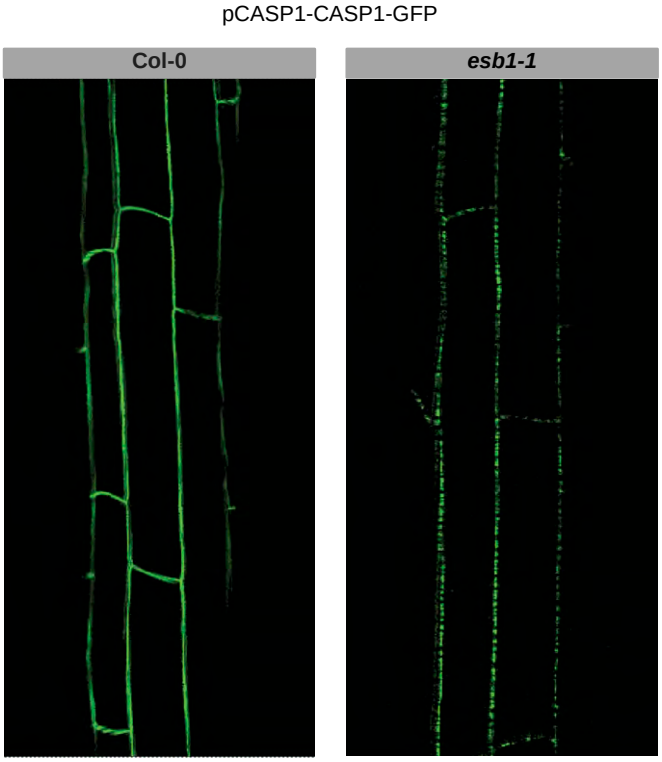

Fig. S4. CASP1 localization is disrupted in *esb1-1*. *Z*-stack confocal image (green) of plants expressing *CASP1-GFP* from the *CASP1* native promoter in *esb1-1* shows a patchy distribution of CASP1-GFP along the Casparian strip domain.

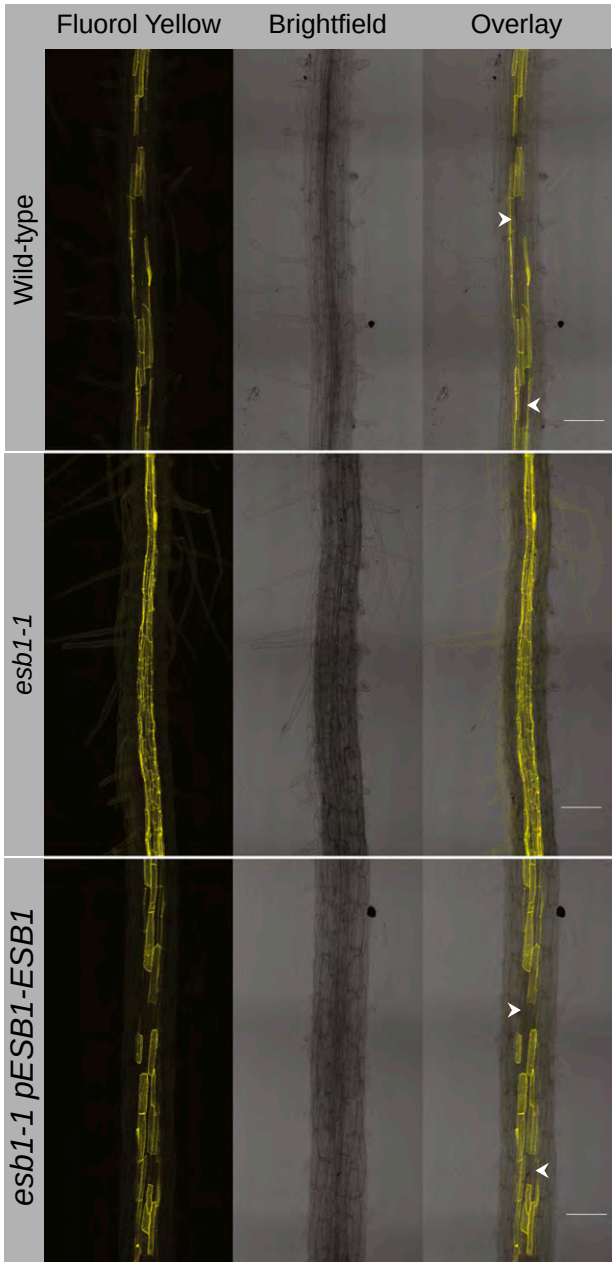

Fig. S5. Wild-type *ESB1* complements *esb1-1* loss of unsuberised passage cells. Fluorol Yellow staining of suberin in wild-type, *esb1-1*, and *esb1-1* expressing *pESB1-ESB1*. Arrowheads indicate passage cells. (Scale bars: 100 μm.)

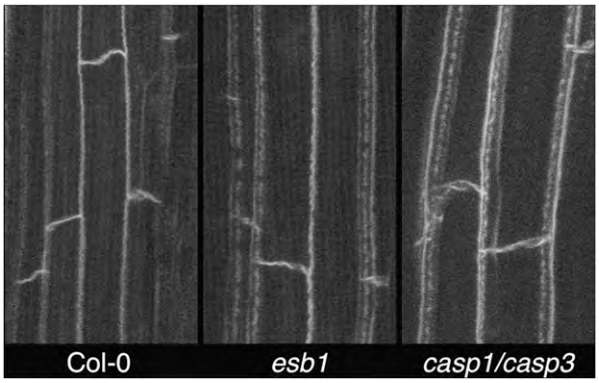

Movie S1. Autofluorescence of wild type Col-0, *esb1-1*, and *casp1-1casp3-1*. Three-dimensional view of the Casparian strip in wild-type (*Left*), *esb1-1* (*Center*), and *casp1-1casp3-1* (*Right*) visualized as autofluorescence after root clearing. For constructing 3D animation images were acquired every 0.95 μm with a depth of at least one endodermal cell.

Movie S1

Dataset S1. Elemental profile of *esb1-1* is similar to that of *casp1-1/casp3-1*

Dataset S1

Plants were grown for 2 wk on MGRL medium (1) with 1% sucrose solidified with 1.2% type E agar (Sigma). Shoot element concentrations were determined by inductively coupled plasma mass spectrometry. *P* values were calculated by Dunnett's multiple comparison with wild-type Col-0. Element concentrations significantly different from wild-type are colored with red (decrease in mutant) and blue (increase in mutant). $n = 10$ biological replicates.

1. Fujiwara T, Hirai MY, Chino M, Komeda Y, Naito S (1992) Effects of sulfur nutrition on expression of the soybean seed storage protein genes in transgenic petunia. *Plant Physiol* 99(1): 263–268.

5.3 RETINOBLASTOMA RELATED1 Regulates Asymmetric Cell Divisions in *Arabidopsis*

Annika K. Weimer, Moritz K. Nowack, Daniel Bouyer, Xin'Ai Zhao, Hirofumi Harashima, Sadaf Naseer, Freya e Winter,Nico Dissmeyer, Niko Geldner, Arp Schnittger.2012. Retinoblastoma related 1 regulates asymmetric cell divisions in *Arabidopsis*. Plant Cell, 24: 4083–4095.

5.3.1 Own contribution

Annika K.Weimer from the group of Arp Schnittger (University of Strasbourg, France) did most of the work presented in this paper. The main aim of the study was to describe the general mechanism by which RBR1 (RETINOBLASTOMA RELATED1 (*Arabidopsis* homolog of the human tumor suppressor Retinoblastoma) regulates cell cycle and cell differentiation genes. In *Arabidopsis* CDKs (Cyclin –dependent kinases) were identified as the major core cell cycle regulators. This study reports that the RBR1 activity was predominantly regulated by CDKA; 1.

I contributed to this study by analyzing the data shown in supplementary Figure 1. Its purpose was to observe the effect of the generation of additional initial daughter cells and the delayed formation of separate endodermis and cortex files on the subsequent formation of functional Casparian Strips in different loss of function alleles of CDKA;1.

5.3.2 Original article

For details, the article is attached herewith.

This article is a *Plant Cell* Advance Online Publication. The date of its first appearance online is the official date of publication. The article has been edited and the authors have corrected proofs, but minor changes could be made before the final version is published. Posting this version online reduces the time to publication by several weeks.

RETINOBLASTOMA RELATED1 Regulates Asymmetric Cell Divisions in *Arabidopsis*[C][W][OA]

Annika K. Weimer,[a,1] Moritz K. Nowack,[b,c,1] Daniel Bouyer,[a] Xin'Ai Zhao,[a] Hirofumi Harashima,[a,d] Sadaf Naseer,[e] Freya De Winter,[b,c] Nico Dissmeyer,[a,2] Niko Geldner,[e] and Arp Schnittger[a,d,3]

[a] Department of Molecular Mechanisms of Phenotypic Plasticity, Institut de Biologie Moléculaire des Plantes du Centre National de la Recherche Scientifique, IBMP, Unité propre de recherche 2357, Université de Strasbourg, F-67084 Strasbourg cedex, France
[b] Department of Plant Systems Biology, Vlaams Instituut voor Biotechnologie, B-9052 Ghent, Belgium
[c] Department of Plant Biotechnology and Bioinformatics, Ghent University, B-9052 Ghent, Belgium
[d] Trinationales Institut für Pflanzenforschung, Institut de Biologie Moléculaire des Plantes du Centre National de la Recherche Scientifique, IBMP, F-67084 Strasbourg cedex, France
[e] Department of Plant Molecular Biology, University of Lausanne, CH-1015 Lausanne, Switzerland

Formative, also called asymmetric, cell divisions produce daughter cells with different identities. Like other divisions, formative divisions rely first of all on the cell cycle machinery with centrally acting cyclin-dependent kinases (CDKs) and their cyclin partners to control progression through the cell cycle. However, it is still largely obscure how developmental cues are translated at the cellular level to promote asymmetric divisions. Here, we show that formative divisions in the shoot and root of the flowering plant *Arabidopsis thaliana* are controlled by a common mechanism that relies on the activity level of the Cdk1 homolog CDKA;1, with medium levels being sufficient for symmetric divisions but high levels being required for formative divisions. We reveal that the function of CDKA;1 in asymmetric cell divisions operates through a transcriptional regulation system that is mediated by the *Arabidopsis* Retinoblastoma homolog RBR1. RBR1 regulates not only cell cycle genes, but also, independent of the cell cycle transcription factor E2F, genes required for formative divisions and cell fate acquisition, thus directly linking cell proliferation with differentiation. This mechanism allows the implementation of spatial information, in the form of high kinase activity, with intracellular gating of developmental decisions.

INTRODUCTION

The development of multicellular organisms requires a tight coordination of cell proliferation with growth and differentiation (Harashima and Schnittger, 2010). A paradigm for the need of this coordination are formative, also called asymmetric or unequal, cell divisions in which one cell will give rise to two cells each with different cell fates (Abrash and Bergmann, 2009; Knoblich, 2010; De Smet and Beeckman, 2011). Formative divisions are typically found in stem cell niches and the cell lineages originating from stem cells. A typical example is found in the *Arabidopsis thaliana* root meristem, where stem cells are grouped around a quiescent center (Benfey and Scheres, 2000). While most root tissues are organized into files of cells that are derived each from one of these stem cells, the cell files of both the endodermis and the cortex layers originate from one common cortex-endodermis initial. Thus, instead of an anticlinal division that is perpendicular to the surface of the root and contributes to the length of a cell file, the division plane in the cortex-endodermis initial daughter cell is shifted by 90°, resulting in a periclinal cell division (i.e., a division that generates two cells parallel to the surface of the root with different fates, namely, cortex and endodermis).

Formative divisions can also be found during the development of aerial plant structures, and a representative case are the cell divisions in the stomata lineage. This cell lineage produces stomata, gas exchange pores formed by two guard cells, as well as epidermal pavement cells (Bergmann and Sack, 2007). Stomata are produced via a series of asymmetric divisions, the first of which occurs in a parent meristemoid mother cell to produce a meristemoid cell. The meristemoid cell is a transit-amplifying cell that may divide asymmetrically several times, each time producing a new epidermal cell and regenerating the meristemoid. The meristemoid ultimately differentiates into a guard mother cell that divides symmetrically to produce two guard cells.

Formative divisions, like any other type of division, rely on the cell cycle machinery with centrally acting cyclin-dependent kinases (CDKs) and their cyclin cofactors to promote S phase and mitosis. In *Arabidopsis*, five CDKs have been identified to be the core cell cycle regulators. CDKA;1 controls entry into M phase and especially entry into S phase by phosphorylating RETINOBLASTOMA RELATED1 (RBR1), the *Arabidopsis* homolog of the human tumor suppressor Retinoblastoma (Nowack et al.,

[1] These authors contributed equally to this work.
[2] Current address: Leibniz Institute of Plant Biochemistry, Weinberg 3, D-06120 Halle (Saale), Germany.
[3] Address correspondence to arp.schnittger@ibmp-cnrs.unistra.fr.
The author responsible for distribution of materials integral to the findings presented in this article in accordance with the policy described in the Instructions for Authors (www.plantcell.org) is: Arp Schnittger (arp.schnittger@ibmp-cnrs.unistra.fr).
[C] Some figures in this article are displayed in color online but in black and white in the print edition.
[W] Online version contains Web-only data.
[OA] Open Access articles can be viewed online without a subscription.
www.plantcell.org/cgi/doi/10.1105/tpc.112.104620

2012). In the nonphosphorylated state, RBR1 represses the action of the transcription factor E2F that activates the expression of many genes required for DNA replication, such as F-BOX PROTEIN17 (FBL17), PROLIFERATING CELL NUCLEAR ANTIGEN (PCNA), and MINICHROMOSOME MAINTENANCE PROTEIN5 (MCM5) (Gutzat et al., 2012; Zhao et al., 2012). CDKA;1 action for S phase entry is backed up by the two redundantly acting CDKB1s (CDKB1;1 and CDKB1;2) (Nowack et al., 2012). CDKB1s also function in the control of M phase and the analysis of loss-of-function as well as dominant-negative alleles have in particular revealed a role in the last (i.e., symmetric) division during stomata development (Boudolf et al., 2004; Xie et al., 2010). CDKB2s (CDKB2;1 and CDKB2;2) appear to be M phase specific, as judged by their strong cell cycle phase-dependent expression pattern (Boudolf et al., 2004; Menges et al., 2005; Xie et al., 2010). CDKB2 action was found to be specifically required for the function of the shoot apical meristem (Andersen et al., 2008). CDKs by themselves have almost no kinase activity and require the binding of a cyclin partner. In *Arabidopsis*, there are 30 cyclins and almost all of them can bind to each of the five core CDKs (Van Leene et al., 2011). However, the number of functional pairs might be smaller, as suggested by in vitro kinase assays (Harashima and Schnittger, 2012).

Recent evidence indicated a special role for some core cell cycle regulators in asymmetric cell divisions. *CYCLIN D6;1* (*CYCD6;1*) was found to be specifically expressed in the cortex-endodermis initial daughter cells, and in *cycd6;1* mutants, this division is delayed (Sozzani et al., 2010). Conversely, CYCD4;1 appears to modulate divisions that initiate a stomata lineage and overexpression stimulated the production of stomata (Kono et al., 2007). However, how cell cycle regulators can translate developmental cues at the cellular level to promote formative divisions has remained largely obscure.

Here, we present a general mechanism of how extracellular information can be integrated with an intracellular gene regulatory network to execute formative divisions. We show that RBR1 regulates both cell cycle and cell differentiation genes. RBR1 activity is predominantly regulated by CDKA;1, giving rise to a CDKA;1 dose-dependent model of symmetric versus asymmetric cell divisions that hence allows the developmentally programmed activation of the cell cycle machinery to promote formative cell divisions.

RESULTS

Reduction of CDKA;1 Activity Affects Formative Cell Divisions in the Root

Weak loss-of-function (hypomorphic) alleles and allelic series, especially of essential regulators, are powerful tools to dissect developmental processes and to infer gene function in vivo. Previously, we addressed the posttranslational regulation of the central cell cycle kinase CDKA;1 in *Arabidopsis* by exchanging amino acids that are known from work in yeast and metazoans to be subject to inhibitory and stimulatory phosphorylation events in CDKA;1 homologs (Pines, 1995; Morgan, 1997). Of key importance for the activation of this type of kinase is the phosphorylation in the activation loop, also called the T-loop, at residue Thr-161 of CDKA;1 in *Arabidopsis*, or at the corresponding position (e.g., Thr-169 of CDC28 in *Saccharomyces cerevisiae* or Thr-167 of Cdc2 in *Schizosaccharomyces pombe*). Conversely, phosphorylation of the residues Thr-14 and Tyr-15 and the corresponding positions in the regulatory loop, also called the P-loop, has a strong inhibitory function. The expression of a *CDKA;1* variant in which Thr-161 was replaced with the nonphosphorylatable amino acid Val (*cdka;1*$^{-/-}$ *Pro*$_{CDKA;1}$:*CDKA;1*^{T161V}) could not rescue *cdka;1* mutants, consistent with a requirement of Thr-161 phosphorylation for kinase activation (Dissmeyer et al., 2007). A variant that mimicked a phosphorylated amino acid (i.e., one in which Thr-161 was replaced with the negatively charged amino acid Asp; *cdka;1*$^{-/-}$ *Pro*$_{CDKA;1}$:*CDKA;1*^{T161D}) could rescue the *cdka;1* mutant, albeit only partially, giving rise to a hypomorphic *cdka;1* mutant designated *D* in the following (Dissmeyer et al., 2007). Conversely, the exchanges of Thr-14 and Tyr-15 with Asp and Glu mimicked an inhibited CDKA;1 and, after transformation of the respective cDNA expression construct into *cdka;1* mutants, resulted in a second hypomorphic mutant (*cdka;1*$^{-/-}$ *PRO*$_{CDKA;1}$:*CDKA;1*$^{T14D;Y15E}$), designated *DE* in the following (Dissmeyer et al., 2009).

While null mutants of *CDKA;1* are severely compromised and not viable on soil (Nowack et al., 2006, 2012), hypomorphic *CDKA;1* mutants *D* and *DE* are much less affected and in general form all of the organs and cell types of wild-type plants (Figure 1A). However, when analyzing in detail the root architecture of these hypomorphic mutants, we found specific developmental defects. Whereas the formative division of a cortex-endodermis initial daughter is rapidly executed in the wild type, the division was delayed in weak loss-of-function *cdka;1* mutants, resulting in a unique phenotype with files of up to three additional cells between the initial and the beginning of two separated endodermis and cortex layers (Figures 2A to 2C, Table 1; see Supplemental Table 1 online). Initial daughter cells are marked by the expression of *CYCD6;1* (Sozzani et al., 2010), and we observed that a *CYCD6;1* reporter was active in the newly arising cell files between the quiescent center and the eventually forming endodermis and cortex cell files of weak *cdka;1* loss-of-function alleles, implying that they have initial daughter fate (Figures 2D and 2E).

The generation of additional initial daughter cells and the delayed formation of separate endodermis and cortex files, however, did not interfere with subsequent differentiation steps, as seen by the proper formation of the Casparian strip, the hallmark of the endodermis layer (see Supplemental Figures 1A to 1F online). In addition, we found that the endodermis marker SCARECROW (SCR) and the cortex marker CORTEX2 (CO2) become expressed in the respective cell files in both hypomorphic *cdka;1* mutants (Figures 2F and 2G; see Supplemental Figures 2A and 2B online). Thus, the appearance of daughter cell files in hypomorphic *cdka;1* represents a specific defect in formative cell division of the cortex-endodermis initial daughter cell.

The Phenotype of Weak *cdka;1* Loss-of-Function Alleles Becomes Stronger over Time

The *Arabidopsis* root meristem is established during embryo development, and wild-type embryos at maturity contain

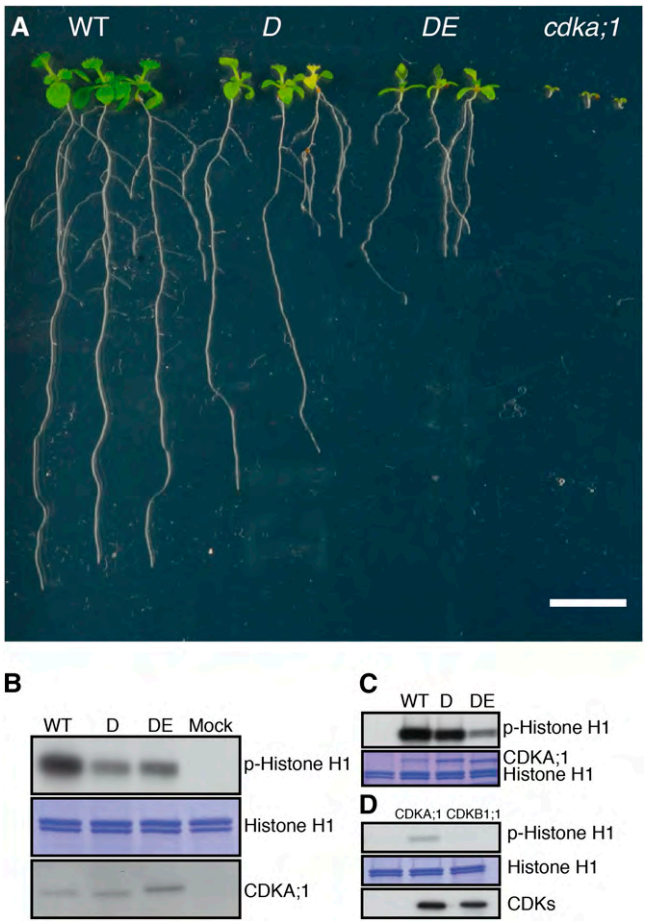

Figure 1. Allelic Series of *cdka;1* Mutants.

(A) Ten-day-old wild-type (WT), *D*, *DE*, and homozygous *cdka;1* mutant plants (from left to right). Bar = 1 cm.

(B) p13^{suc1}-associated protein kinase activity is strongest in wild-type extracts, while extracts from D plants have higher activity than those from DE extracts as revealed by autoradiography (top panel). Coomassie blue staining (middle panel) shows equal loading of the substrate histone H1. Equal purification levels of CDKs were quantified by protein blot with the anti-PSTAIR antibody (bottom panel). Protein extraction buffer was incubated with p13^{suc1} beads as a mock.

(C) In vitro kinase assays show that the hypomorphic *cdka;1* mutant *D* has less activity than the wild type but more than the hypomorphic *cdka;1* mutant *DE* (autoradiography top). Coomassie blue staining (bottom) shows equal loading of the substrate histone H1 and the different CDKA;1 versions.

(D) In vitro kinase assays of CDK-CYCD6;1 complexes reveal that CYCD6;1 has activity with CDKA;1 but not with CDKB1;1 against histone H1 (autoradiography top). Coomassie blue staining (middle) shows equal loading of the substrate histone H1. Quantification with Strep-Tactin HRP (bottom) reveals equal amounts of CDKA;1 and CDKB1;1 bound to CYCD6;1.

a cortex-endodermis initial and a cortex-endodermis initial daughter cell. After germination, root meristems of *Arabidopsis* expand in the following 5 to 6 d and then plateau (Ubeda-Tomás et al., 2009). When analyzing the embryonic root meristem in both hypomorphic *cdka;1* mutants, we found that the pattern of the formative division of the cortex-endodermis initial daughter was indistinguishable from that of the wild type, suggesting that the mutant phenotype would become more severe over time (Figures 3A to 3C). Indeed, roots analyzed at 10 d after germination showed significantly ($P < 0.001$) longer files of undivided initial daughter cells than roots examined at 5 d after germination (Figure 3D). Remarkably, we never observed that any cell but the top-most cell within the single file of initial daughter cells divided asymmetrically, suggesting that the specific position neighboring the already established separated cortex and endodermis files provides spatial cues for the asymmetric division (Figure 2C). This top-most cell never divided anticlinally (i.e., symmetrically), as judged by the continuously increasing cell sizes in the files of mutant initial daughter cells. Thus, we conclude that in *cdka;1* mutants, the different cell division programs within the root meristem are uncoupled: The initials continue to divide and produce daughter cells, but the formative division of the initial daughter cell occurs in *cdka;1* mutants with a lower rate, resulting in growing files of daughter cells and a separation of cell production and differentiation.

Formative Divisions in the Root Meristem Depend on CDKA;1 Dosage

The stronger phenotype of the *DE* versus *D* hypomorphic *cdka;1* mutant plants suggested that the asymmetric division of a cortex-endodermis initial daughter correlates with the activity levels of CDKA;1. In vitro kinase reactions with both mutant kinase versions and CDK activities extracted from both hypomorphic mutants revealed that *D* has higher activity than *DE*, although still markedly less activity than wild-type CDKA;1 (Figures 1B and 1C). This series of kinase activity also correlated with overall plant growth (i.e., wild-type plants are bigger than *D*, and *D* plants grows larger than *DE*) (Figure 1A). To further test a possible CDKA;1 kinase dose dependency of the formative division of an initial daughter cell, we analyzed roots of homozygous *cdka;1* null mutants that can be grown on agar plates but are even smaller than *DE* plants (Figure 1A) (Nowack et al., 2012). In homozygous mutants, the root meristem architecture is severely compromised, hampering quantitative morphological analyses, but in several optical sections, the formative division of the initial daughter was more strongly delayed than in the weak loss-of-function mutants or even failed completely (Figure 2H; see Supplemental Figures 2C and 2F online). Thus, the formative divisions of the initial daughter cells depend on the dose of CDKA;1 activity.

Since the embryonic root meristem was correctly established in hypomorphic *cdka;1* mutants, and even in *cdka;1* null mutants the initial daughter cells occasionally divided asymmetrically, we asked whether other CDKs than CDKA;1 are also involved in this cell division. Based on the finding that *CDKB1* can partially compensate for the loss of *CDKA;1* (Nowack et al., 2012), we first analyzed homozygous *cdka;1* mutants in which *CDKB1* was expressed from the *CDKA;1* promoter. Along with a general restoration of the root meristem, the formative division of the initial daughter cells was partially restored (Figure 2J, Table 1). Accordingly, we found that *cdkb1;1 cdkb1;2* double mutants showed a mild delay in the division of the initial daughter (Table 1; see Supplemental Table 1 online). However, we never observed

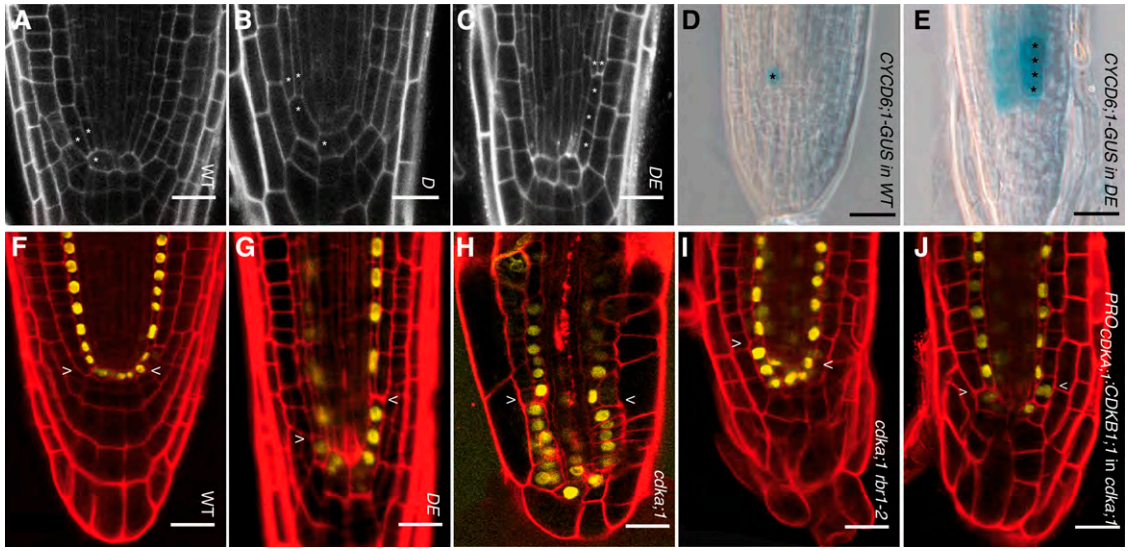

Figure 2. Formative Divisions in the Root Correlate with CDKA;1 Activity Levels.

(A) In wild-type (WT) roots, the cortex-endodermis initial next to the quiescent center produces a cortex-endodermis initial daughter cell that rapidly divides asymmetrically, giving rise to a cortical and endodermal cell.
(B) and **(C)** In weak loss-of-function *cdka;1* mutants, the initial daughter division is delayed so that an initial daughter is present for a longer time **(B)**, or due to continued divisions of the initial **(C)**, files of undivided initial daughter cells are generated.
(D) CYCD6;1:GUS marks the initial daughter in the wild type.
(E) The additional cell files in DE are also marked by CYCD6;1:GUS, indicating their fate as initial daughters.
(F) to **(J)** The expression pattern of Pro_{SCR}:*SCR*:*YFP*, marking quiescent center, cortex-endodermis initial, cortex-endodermis initial daughter, and endodermal cells, is similar in the wild type **(F)**, weak loss-of-function *cdka;1* mutants **(G)**, null *cdka;1* mutants **(H)**, and *cdka;1 rbr1-2* **(I)** and $Pro^{CDKA;1}$:CDKB1;1 **(J)**.
In **(A)** to **(C)**, a single asterisk indicates cortex-endodermis initials and their daughter cells. The formative division gives rise to an endodermis and cortex cell, which is marked by two asterisks. Bars = 20 μm.

files of undivided initial daughter cells in the *cdkb1* double mutant, and even the loss of both *CDKB1* genes in hypomorphic *cdka;1* mutants (*cdka;1*$^{-/-}$ $Pro_{CDKA;1}$*CDKA;1*$^{T14D;Y15E+/+}$ *cdkb1;1*$^{-/-}$ *cdkb1;2*$^{-/-}$) did not enhance the mutant phenotype of the weak *cdka;1* loss-of-function alleles (Table 1). Thus, we conclude that it is CDKA;1 and not CDKB1;1/CDKB1;2 that plays a central role during formative divisions. However, CDKB1s contribute to the fast execution of the initial daughter division, additionally

Table 1. Division of Cortex-Endodermis Initial Daughter Cells until Differentiation of Cortex and Endodermis

	No. of Divisions of a Cortex-Endodermis Initial Daughter Cell until Differentiation (in %)				
Genotype	1	2	3	4	*n*
The wild type	100	0	0	0	50
cdka;1	n.a.[a]	n.a.	n.a.	n.a.	0[b]
DE	25	42	25	8	72
D	53	42	5	0	72
cdkb1;1 cdkb1;2	98	2	0	0	40
DE cdkb1;1 cdkb1;2	17	50	28	5	36
$Pro_{CDKA;1}$:*CDKB1;1* in *cdka;1*	60	25	5	10	40
rbr1-2	100	0	0	0	92
DE rbr1-2	79	14	7	0	28
rbr1-2 cdka;1	86	0	7	7	28
cycd6;1	94	6	0	0	36
D cycd6;1	65	23	9	3	40
cdkb1;1 cdkb1;2 cycd6;1	98	2	0	0	43

[a]n.a.,not analyzable
[b]Twenty-five roots/50 cortex-endodermis initial daughter divisions analyzed.

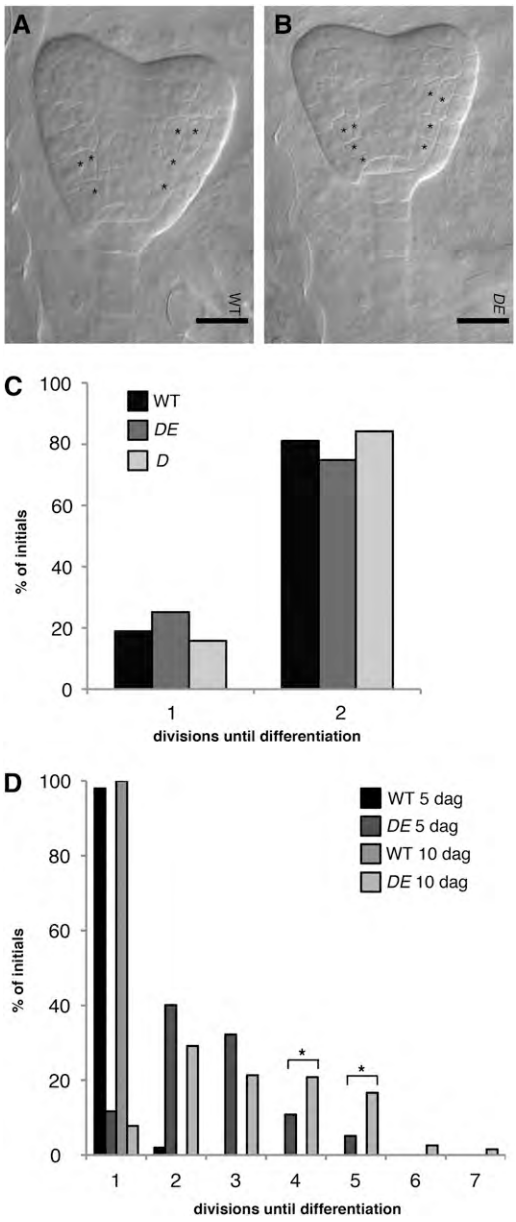

Figure 3. Time Course of Initial Daughter Division in Weak *cdka;1* Alleles.

(A) Mature wild-type (WT) embryos contain an initial and an initial daughter.

(B) The weak loss-of-function *cdka;1* mutant *DE* is indistinguishable from the wild type with respect to the embryonic initial and initial daughter pattern.

(C) Quantification revealed no significant difference of initial daughter division between wild-type and DE plants.

(D) The mutant phenotype of *DE* becomes stronger over time. At day 5, DE is significantly different from the wild type ($P < 0.001$). Files between QC and the endodermis-cortex specification contain up to five cells at 5 d after germination (dag) but up to seven cells after the 10th day. Asterisks indicate significant differences within a 5% confidence interval.

In **(A)** and **(B)**, a single asterisk indicates cortex-endodermis initials and their daughter cells. The formative division gives rise to an endodermis and cortex cell, which is marked by two asterisks.

[See online article for color version of this figure.]

stressing the importance of a CDK activity-dependent mechanism for this division.

Since CYCD6;1 is specifically involved in the formative division of the initial daughter cells in *Arabidopsis* (Sozzani et al., 2010), we next asked whether CDKA;1 or CDKB1s operates together with CYCD6;1. Although both kinases coprecipitated in vitro with CYCD6;1, only the combination with CDKA;1 showed kinase activity, underscoring the central function of CDKA;1 in the division of the initial daughter (Figure 1D). However, removal of CYCD6;1 activity in hypomorphic *cdka;1* mutant plants did not significantly enhance the *cdka;1* mutant phenotype, indicating that additional cyclins are involved in this asymmetric division, likely each with a small contribution to the overall CDKA;1 activity (Table 1; see Supplemental Table 1 online). The assisting role of CDKB1s and CYCD6;1 to the asymmetric division of the initial daughter was further supported by the observation that the *cdkb1;1 cdkb1;2 cycd6;1* triple mutant did not show undivided initial daughter cells (Table 1; see Supplemental Table 1 online).

Formative Divisions Are Regulated by RBR1

The requirement of high CDK activity levels argued that one or more CDK substrates are responsible for the formative division of the cortex-endodermis initial daughter. Recently, some CDKA;1 substrates were identified in *Arabidopsis*, and especially RBR1 was found to be a crucial target of CDKA;1 (Nowack et al., 2012; Pusch et al., 2012). If the inactivation of RBR1 by CDKA;1-mediated phosphorylation is of central importance for the execution of the formative division of the initial daughter cell, a reduction of RBR1 levels should at least partially restore the mutant phenotype of weak *cdka;1* loss-of-function mutants. Therefore, we introgressed a *rbr1* mutant into hypomorphic *cdka;1* mutants; indeed, we found that *DE rbr1* double mutants showed a strong restoration of the wild-type division pattern of the initial daughter cell (Table 1; see Supplemental Table 1 online). Strikingly, formative division of the initial daughter was, even in homozygous *cdka;1*$^{-/-}$ null mutants, largely restored when *RBR1* was depleted (Figure 2I, Table 1; see Supplemental Figure 2D and Supplemental Table 1 online). As RBR1 exerts many of its functions as a transcriptional regulator, our results suggest a transcriptional base of the observed delay in the formative division of an initial daughter cell.

Intensive work over the last few years has revealed that the transcription factors *SHORTROOT* (*SHR*) and *SCR* regulate the asymmetric division and subsequent fate specification of the initial daughter cells (Ten Hove and Heidstra, 2008; De Smet and Beeckman, 2011). Thus, the direct regulation of the asymmetric cell division by RBR1 could conceivably operate by modulating the *SHR* and *SCR* pathway. We therefore tested whether RBR1 would bind to the promoter regions of a cluster of six genes that were recently identified as SHR targets: *At4g01330*, *CYCD6;1*, *MAGPIE* (*MGP*), *NUTCRACKER* (*NUC*), *SCARECROW LIKE3* (*SCL3*), and *SCR* itself (see Supplemental Figure 3 online) (Sozzani et al., 2010). To this end, we performed chromatin immunoprecipitation (ChIP) experiments using an antibody directed against red fluorescent protein (RFP) in transgenic plants that produce an RBR1:RFP fusion protein (Ingouff et al., 2006). As expected, we observed in ChIP-PCR experiments RBR1 binding to the known RBR1 targets

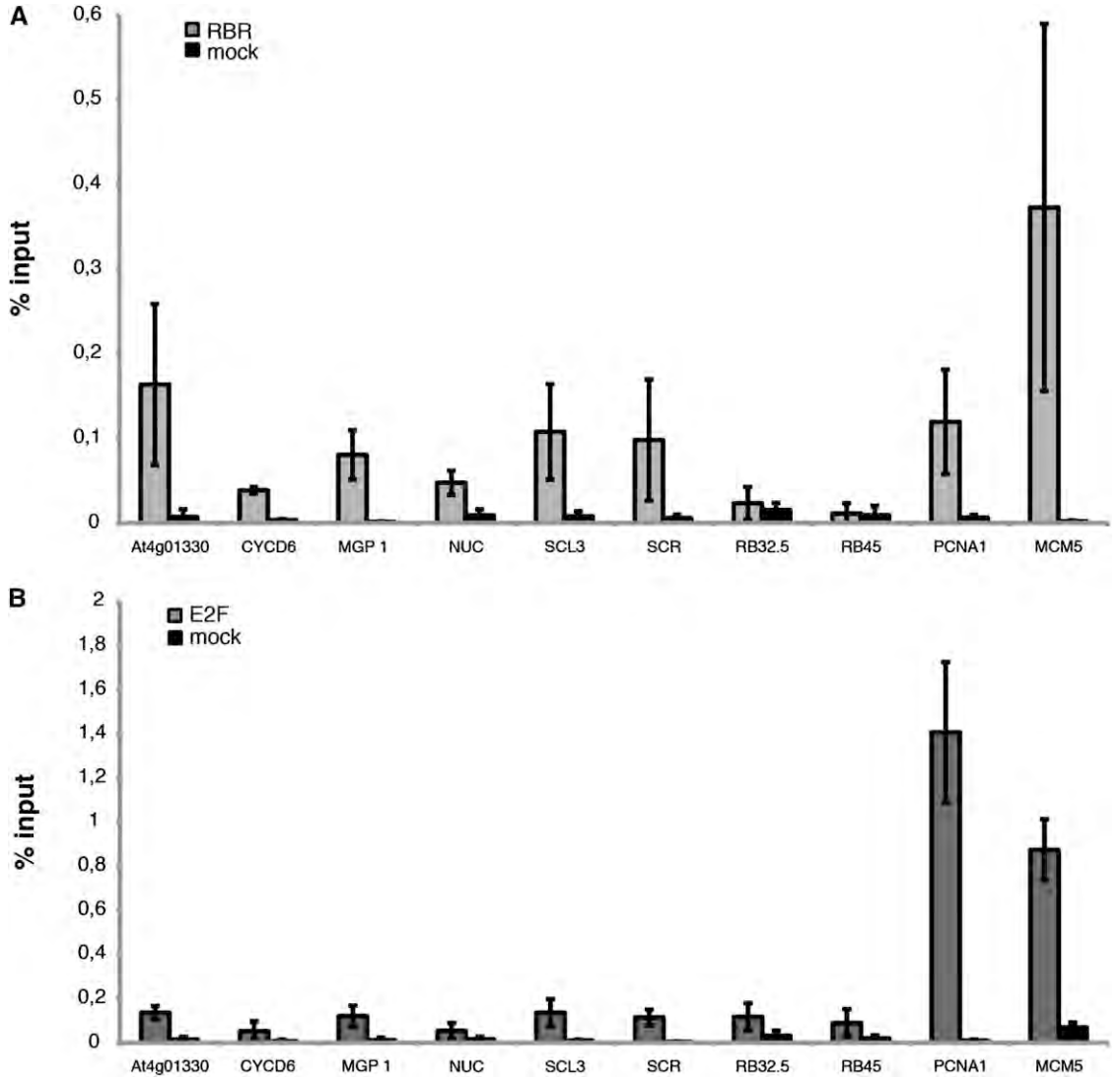

Figure 4. RBR1 Binds to Cell Cycle Genes and Genes Involved in Cell Differentiation in the Root.

(A) ChIP of Pro_{RBR1}:*RBR1*:*RFP* seedlings using an anti-RFP antibody. The promoter regions of *At4G01330*, *MGP1*, *SCL3*, *SCR*, and the cell cycle genes *PCNA1* and *MCM5* are bound by RBR1, whereas the heterochromatic regions (RB32.5 and RB45) show no difference between mock and treatment. **(B)** RBR1 targets MCM5 and PCNA1 can also be detected with an E2FA antibody. However, no enrichment could be observed for the SHR targets tested in **(A)**.

[See online article for color version of this figure.]

FBL17, *MCM5*, and *PCNA1* (Nowack et al., 2012; Zhao et al., 2012). Fragments further upstream or downstream of the known RBR1 binding site could not be amplified. Remarkably, the promoter region that was previously identified as being bound by SHR could be specifically amplified for *At4g01330* and *SCL3*. However, we could not find evidence for binding of RBR1 to the promoter region of the presumptive SHR/SCR target gene *CYCD6;1* (see Supplemental Figure 3 online).

Next, we quantified the binding of RBR1 to the promoter fragments containing a SHR binding site by ChIP–quantitative PCR (Figure 4A; see Supplemental Figure 3 online). Two heterochromatic loci were used as negative controls and showed no enrichment in our ChIP assays. A weak enrichment was obtained for *CYCD6;1* and *NUC*. Although we cannot exclude a weak binding of RBR1 to these genes, we conclude that the here-seen weak enrichment is due to unspecific binding of the antibody based on the failure to amplify the same fragments in the more stringent ChIP-PCR. Notably, *At4g01330*, *MGP*, *SCL3*, and *SCR* were at least 5 times more enriched than the negative control and showed enrichment similar to the known RBR1 target PCNA1, corroborating them as RBR1 targets.

RBR1 generally counteracts E2F function in cell cycle regulation (Weinberg, 1995), and the RBR1 targets *MCM5* as well as *PCNA1* could also be precipitated with an antibody recognizing

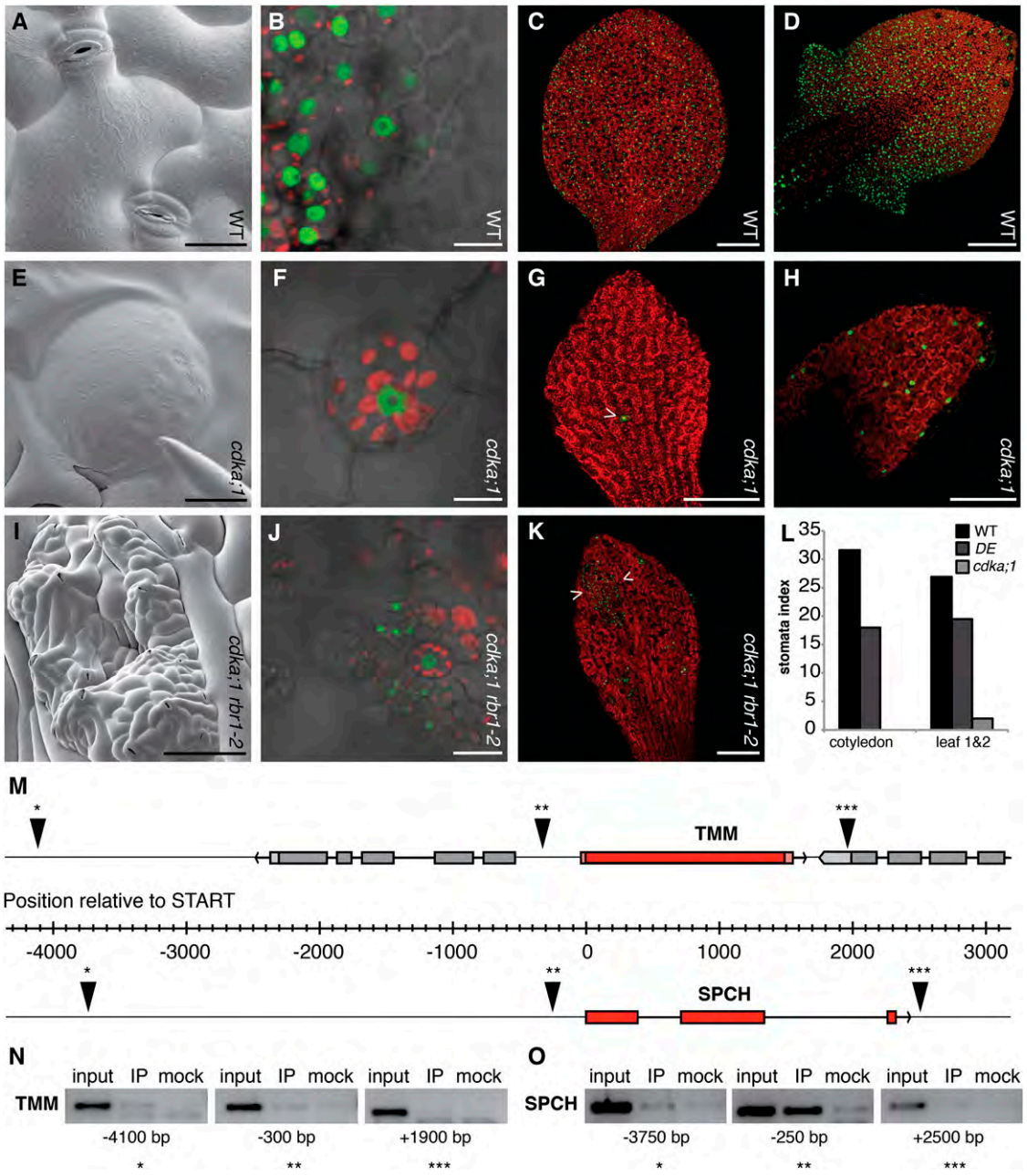

Figure 5. The Interplay between CDKA;1 and RBR1 Regulates Formative Divisions in the Stomata Lineage.

(A) Scanning electron micrographs of two stomata each comprised of two guard cells in the wild type (WT).
(B) Expression of the stomatal lineage marker *Pro$_{TMM}$:YFP* (green fluorescence) in the stomata lineage. Guard mother cells and guard cells contain chloroplasts as seen by red fluorescence.
(C) and **(D)** The stomata lineage marked by *TMM* expression in wild-type cotyledons **(C)** and in young wild-type rosette leaves **(D)**.
(E) and **(F)** Scanning electron micrographs of an arrested guard mother cell **(E)** in *cdka;1$^{-/-}$* as indicated by *TMM* expression and the presence of chloroplasts **(F)**.
(G) and **(H)** The stomata lineage is not or rarely (arrowhead) activated in cotyledons of *cdka;1$^{-/-}$* mutants as revealed by *TMM* expression (green) **(G)** and very rarely established in true leaves of *cdka;1$^{-/-}$* mutants **(H)**.
(I) Scanning electron micrographs of *cdka;1 rbr1;2* double mutants, in which the activation of the stomatal lineage is partly restored in cotyledons.
(J) The *TMM* marker is strongly expressed in islands of overproliferating cells in *cdka;1 rbr1;2* double mutants.
(K) These islands can be surrounded by areas of *TMM*-negative cells and consist of stomata mixed with small meristematic cells.
(L) Stomata indices decrease from the wild type, to the weak loss-of-function *cdka;1* mutant *DE* and are very low in homozygous *cdka;1$^{-/-}$* null mutants.

E2FA (Figure 4B). However, no enrichment beyond the level of the negative control could be obtained for the six above-tested SHR and SCR target genes using the E2FA antibody in ChIP experiments (Figure 4B). Thus, while genes with a direct role in cell cycle regulation are controlled by both RBR1 and E2F, the regulation of genes involved in cell differentiation was an E2F-independent function of RBR1. Thus, cell proliferation and cell differentiation are directly connected by RBR1.

The Interplay between CDKA;1 and RBR1 Also Regulates Formative Divisions in Aerial Structures

Finally, we wanted to know whether the role of RBR1 in the asymmetric cell division is specific to the cortex-endodermis initial daughter divisions or represents a general principle of formative cell divisions in *Arabidopsis*. Therefore, we analyzed stomata development in hypomorphic and *cdka;1* null mutants. Indeed, the number of stomata per mm^2 was significantly reduced in *cdka;1* mutants (see Supplemental Table 2 online). In addition, *DE* hypomorphic *cdka;1* mutant plants showed 4% undivided guard mother cells of all stomata as identified by their round shape, the presence of chloroplast, and the expression of stomatal lineage marker *TOO MANY MOUTHS* (*TMM*) that marks meristemoids and their progeny (Nadeau and Sack, 2002) (Figures 5A to 5D; see Supplemental Table 2 online). The occurrence of undivided guard mother cells increased to 80% of all stomata and guard mother cells in homozygous *cdka;1* null mutants, demonstrating that CDKA;1 is involved in the last symmetric cell division during stomatal development (Figures 5E to 5H; see Supplemental Table 2 online). This function was confirmed by the observation that expression of *CDKA;1* from the *TMM* promoter could partially rescue the previously reported arrest of guard mother cell division in *cdkb1;1 cdkb1;2* double mutants (see Supplemental Figures 4A to 4C online) (Xie et al., 2010).

To address whether asymmetric divisions that occur early during stomatal development are also affected by a reduction of CDKA;1 activity, we determined the stomatal indices in *DE* hypomorphic *cdka;1* mutants and *cdka;1* null mutants. The stomatal index is the percentage of stomata per all epidermal cells (including stomata). If symmetric and asymmetric divisions were equally affected in the mutants, the stomatal index should stay the same as that of the wild type or is even expected to slightly increase, since the stomatal lineage contributes to ~70% of all epidermal cells (Geisler et al., 2000). However, the stomatal index of the *DE* hypomorphic mutant was 18 for cotyledons and 19 for the first two rosette leaves and, hence, significantly lower ($P < 0.001$) than that of wild-type plants with a stomatal index of 32 for cotyledons and 27 for the first two rosette leaves (Figure 5L). This effect became even more striking in homozygous *cdka;1* mutants: In contrast with the wild type, the stomatal lineage was not activated in cotyledons (Figures 5G and 5L). On true leaves, few *TMM*-positive cells could be identified and stomata were only rarely formed (Figures 5H and 5L). Similar to the root, the defects during stomatal development could be reduced by expression of *CDKB1;1* under the *CDKA;1* promoter (see Supplemental Table 2 online). Importantly, the mutant phenotype was rescued when RBR1 was depleted (Figures 5I to 5K; see Supplemental Table 2 online). Thus, the interplay between CDKA;1 and RBR1 also regulates formative cell divisions during stomatal development.

Next, we asked whether RBR1 would also bind to genes involved in stomata differentiation. A key candidate would be the transcription factor SPEECHLESS (SPCH), which acts early in setting up a stomata lineage and is necessary and sufficient for the formation of stomata (MacAlister et al., 2007). While promoter fragments for the receptor kinase TMM could not be amplified by ChIP-PCR, one fragment of the SPCH promoter that was close to the transcriptional start site could readily be amplified after precipitation of RBR1-bound chromatin (Figures 5M and 5N). Thus, similar to the root, formative divisions in aerial structures are regulated by the interplay between CDKA;1 and RBR1, with RBR1 binding to differentiation genes.

DISCUSSION

Here, we have shown that formative divisions in the root and shoot depend on the level of CDKA;1 activity. This gives rise to a threshold model for formative cell divisions (Figure 6A). At low CDK levels, for instance, in the triple *cdk* mutant *cdka;1 cdkb1;1 cdkb1;2*, cell cycle progression is completely blocked (Nowack et al., 2012). At medium levels (e.g., in hypomorphic *cdka;1* mutants), RBR1 can be sufficiently inhibited to allow symmetric cell divisions. However, this reduced CDK activity is not enough to fully liberate cell differentiation genes from the repression of RBR1; hence, asymmetric divisions are specifically compromised. At high levels of CDK activity (i.e., in plants with functional CDKA;1 and CDKB1s), RBR1 can be completely inactivated, allowing the rapid execution of asymmetric divisions.

In turn, this mechanism allows asymmetric divisions to be developmentally programmed by providing positional cues for high kinase activity levels (Figure 6B). In the root meristem, this might be seen in the specific expression of *CYCD6;1* in the

Figure 5. (continued).

(M) The genomic region of *TMM* (top) and *SPCH* (below), both in red with neighboring genes in gray, exons depicted as filled rectangles and introns as lines. The orientation of the genes is given in the 5′ to 3′ direction and indicated with an arrowhead. The origin of the ruler indicates the translational start. ChIP fragments are shown by a triangle with one, two, or three asterisks corresponding to the PCR fragments shown in **(N)** and **(O)**.

(N) RBR1 does not bind to the promoter of the receptor kinase, as judged by ChIP of three different elements in the *TMM* genomic region. Amplified fragments corresponding to the genomic region shown in **(M)** are indicated with one, two, or three asterisks.

(O) RBR1 specifically binds to a promoter element shortly before the translational start of *SPCH*. Amplified fragments corresponding to the genomic region shown in **(M)** are indicated with one, two, or three asterisks.

Bars = 20 μm in **(A)**, **(E)**, and **(J)**, 10 μm in **(B)** and **(F)**, 100 μm in **(D)**, **(H)**, and **(I)**, and 250 μm in **(C)**, **(G)**, and **(K)**. IP = immuno precipitation in **(N)** and **(O)**.

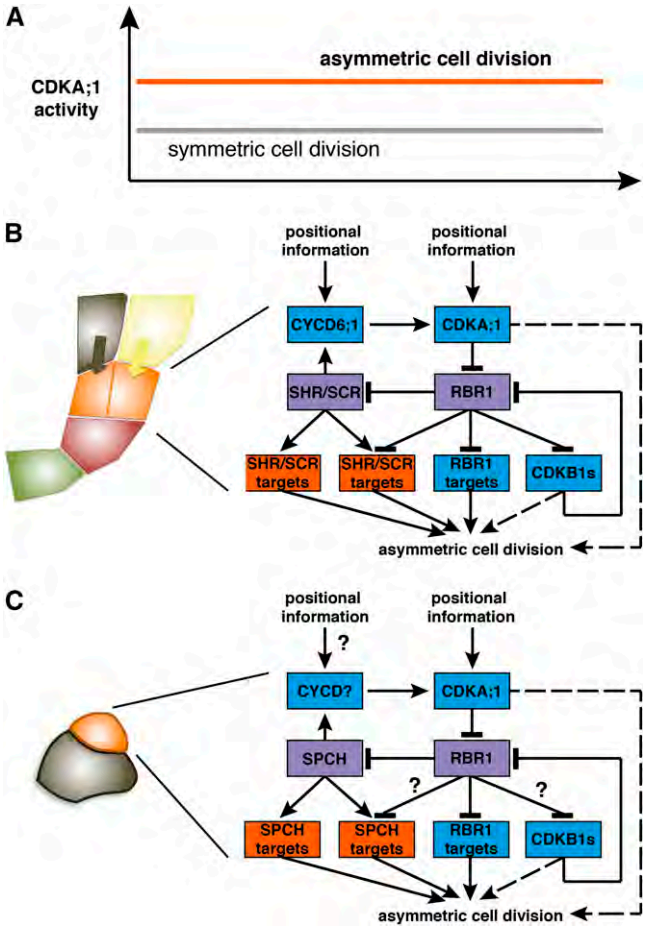

Figure 6.

(A) Model of asymmetric cell division in *Arabidopsis*. Of central importance is RBR1, which inhibits both cell cycle genes, such as *MCM5*, and cell differentiation genes, such as *SCL3*. At low levels of CDKA;1 activity (i.e., low levels of RBR1 inactivation), symmetrical cell divisions can occur, but inhibition of cell differentiation genes is only released at high levels of CDKA;1 activity (i.e., high levels of RBR1 inactivation), leading to asymmetric divisions.

(B) High levels of CDK activity in the initial daughter (orange) are directed by developmental cues (e.g., by the position-dependent activation of *CYCD6;1* that is also regulated by SCR and SHR). In addition, other positional cues appear to guide CDKA;1 activity to promote the division of the upper-most initial daughter and thus likely involve cues from the already specified endodermis (black) and cortex (yellow) layers. Green shading, quiescent center cell; red, initial. Model of molecular circuitry during asymmetric divisions in the cortex-endodermis initial daughter cell. RBR1 and SHR/SCR (violet boxes) integrate cell differentiation (genes with orange boxes) with cell cycle control (genes in blue boxes). The activation of genes required for asymmetric cell divisions involves double negative-feedback loops, resulting in a feed-forward mechanism that is likely to generate hysteresis. SHR/SCR activate CYCD6;1, which then inactivates their repressor (RBR1). Whether CDKs (i.e., CDKA;1 and CDKB1) also participate directly in the regulation of the symmetric division, for instance, by regulating the spindle orientation, is not clear and is indicated by a hatched line.

(C) Model of formative division during the stomata lineage. The formative division restores the meristemoid cell (orange) and generates a neighboring epidermal cell (black). High levels of CDKA;1 activity in the meristemoid mother cell and/or meristemoid (orange) are required to initiate formative divisions in the stomata lineage. Similar to the root, the major substrate appears to be RBR1. Whereas CDKB1s have a role during the symmetric division of a guard mother cell, it is not clear whether they also participate during formative divisions (question mark). The basic helix-loop-helix transcription factor SPCH is regulated by RBR1. In analogy to the function of SHR and SCR, it seems likely that SPCH directly regulates the expression of cell cycle genes, such as D-type cyclins. However, there is currently no molecular evidence for this (question mark). It is also not clear whether SPCH targets are regulated by RBR1 (question mark). Similar to the root, it is remains to be seen whether CDKs regulate other aspects of asymmetric divisions (e.g., the polar localization of cell fate determinants) (hatched line).

cortex-endodermis initial daughter cell (Sozzani et al., 2010) and in the fact that the formative division of the cortex-endodermis initial daughter cell is rapid. *CYCD6;1* is regulated by the SHR/SCR pathway (Sozzani et al., 2010), but notably, we identified SCR itself as an RBR1 target. Thus, SHR/SCR acts in a double negative feedback loop, since CYCD6;1 activates CDKA;1, which in turn phosphorylates and inhibits RBR1, which itself acts as a transcriptional repressor of SCR (Figure 6B).

This wiring resembles the recently identified wiring of RBR1 in a pathway that regulates entry into S phase in which RBR1 directly represses the expression of the F-box protein FBL17 that mediates the degradation of CDK inhibitors (Zhao et al., 2012). A central feature of this S phase regulatory cascade is hysteresis that arises through the connection of at least two negative feedback loops (Ferrell, 2002). Thus, it is conceivable that the here-identified wiring during formative division will generate hysteresis. Hysteresis is important to reach stable decisions in biology, since the activity levels to initiate a process (e.g., DNA replication) are higher than the levels to continue this process. In the case of the cell cycle, hysteresis contributes to its unidirectionality (i.e., the replication of nuclear DNA only once per cell cycle and an ordered progression of mitosis in which chromosomes typically do not fluctuate between condensation and decondensation) (Tyson and Novak, 2008).

In addition, a second double negative feedback loop centered on B1-type CDKs appears to operate during S-phase entry and the execution of formative divisions. CDKB1s were found to have some activity against RBR1 and can partially compensate for the loss of CDKA;1 (Nowack et al., 2012). The *cdkb1;1 cdkb1;2* double mutant also showed a delayed division of the cortex-endodermis initial daughter cell, underlining their contribution for the formative division. Remarkably, *CDKB1;1* and *CDKB1;2* are also under the control of RBR1 (Nowack et al., 2012), hence contributing, although to a lesser extent than CDKA;1, to the hysteretical behavior of the system.

The importance of RBR1 for stomata formation has already previously been demonstrated (Borghi et al., 2010). Our finding that SPCH is also bound by RBR1 suggests that a similar regulatory cascade controls formative divisions during stomata lineage, although it remains to be seen whether SPCH directly regulates the expression of cell cycle regulators. By analogy, key candidates here are D-type cyclins, such as *CYCD4;1* and

CYCD4;2, that have already been implicated in the regulation of the divisions that initiate the stomata lineage (Figure 6C) (Kono et al., 2007).

A central question is how the regulatory cascade is initiated that then results in a formative division of the cortex-endodermis initial cell. One cue comes from the observation that *CYCD6;1* becomes expressed in the additional cells between initial and endodermis/cortex in hypomorphic *cdka;1* mutants. Consistently, we see that the promoter of *CYCD6;1* is not, or at least not strongly, bound by RBR1. Again, this resembles known patterns of cell cycle regulation. In mammals, entry into S phase is initiated by phosphorylation of Rb by the two kinases Cdk4 and Cdk6 that pair with D-type cyclins (Weinberg, 1995; Dyson, 1998; Sherr and Roberts, 1999). Partially phosphorylated Rb cannot sufficiently repress CycE, and CycE in conjunction with Cdk2 will then fully phosphorylate Rb, causing the derepression of many genes required for DNA replication, such as *PCNA*. Thus, it seems likely that such a two-step process also operates in root meristems, but it remains to be seen which other cyclin or cell cycle regulator is in charge of RBR1 inactivation.

In addition to the expression of *CYCD6;1* in the daughter cell, positional information appears to direct the formative division, since only the uppermost cell, which was in direct contact with the already specified endodermis and cortex layers, eventually divided asymmetrically, although *CYCD6;1* was expressed in all additional daughter cells in hypomorphic *cdka;1* mutants. Thus, it is tempting to speculate that the system is further biased by a cue that comes from the endodermis and/or cortex layer. Evidence for local signaling in the root in which a direct cell-to-cell contact provides fate information comes from ablation experiments (van den Berg et al., 1997). Such a cue could lead to the expression/activation of another cell cycle regulator, especially since *cycd6;1* mutants only showed a slight retardation in the execution of a formative divisions. Although a delay of the formative division did not interfere with later differentiation steps as seen in *cycd6;1* mutants or, more pronouncedly, in hypomorphic *cdka;1* alleles, a fast execution of the formative division assures that meristem integrity is maintained (i.e., that the different populations of proliferating cells within the meristem coordinate their cell division rates and that cell differentiation proceeds with the same pace as cell production).

Interestingly, asymmetric cell divisions in *Drosophila melanogaster* have been previously found to depend on the dose of Cdk1 that is homologous to CDKA;1 (Tio et al., 2001). However, the underlying mechanisms of Cdk action in *Drosophila* versus *Arabidopsis* appear to be different. Cdk1 in *Drosophila* is required for the asymmetric localization of an apical-cortical complex at interphase, which then directs the apical-basal orientation of the mitotic spindle as well as the basal/cortical localization of cell fate determinants during mitosis. By contrast, we found here that CDKA;1 operates through a transcriptional regulatory system. However, we currently cannot exclude that CDK activity is also required for proper spindle orientation in the cortex-endodermis initial daughter cell, and it remains to be seen how the generation of a local peak in kinase activity through the double-negative feedback loops identified in this study is further used in the regulation of asymmetric cell divisions (e.g., by affecting cell polarity and/or the cytoskeleton).

METHODS

Plant Material and Growth Conditions

The *Arabidopsis thaliana* plants used in this study were either grown on soil (16 h light) or in vitro on half-strength Murashige and Skoog medium (MS; Sigma Aldrich) containing 0.5% Suc (16 h light) in a growth chamber. The accession Columbia-0 was used as the wild type. *cdka;1* and *rbr1*-2 mutant alleles were described previously (Ebel et al., 2004; Nowack et al., 2006). The hypomorphic *cdka;1* mutants (*D* and *DE*) have been characterized (Dissmeyer et al., 2007, 2009). T-DNA insertion lines for CDKB1;1 and CDKB1;2 have been described (Nowack et al., 2012). The T-DNA allele for CYCD6;1 was described previously (Sozzani et al., 2010). The Pro_{RBR1}:*RBR1-mRFP*–expressing plants have been described (Ingouff et al., 2006). The *TMM* promoter was described previously (Nadeau and Sack, 2002). The Pro_{SCR}:*SCR:YFP* (for yellow fluorescent protein) and PRO_{CO2}:*H2B:YFP* lines were presented previously (Heidstra et al., 2004). All genotypes were determined by PCR, and primers are indicated in Supplemental Table 3 online.

Microscopy

For whole-mount embryo preparation, siliques were dissected with needles, in such a manner that the ovules remained connected to the placenta. Dissected siliques were fixed on ice in FAA (10:7:2:1 ethanol:distilled water: acetic acid:formaldehyde; 37%) for 30 min. After that, the siliques were hydrated in a graded ethanol series to 50 nM $NaPO_4$, pH 7.2, and mounted on microscope slides in a clearing solution of 8:2:1 chloral hydrate:water: glycerol. Embryo phenotypes were analyzed with a Zeiss Imager.Z1 with AxioCam MRm. The software used was AxioVision Rel. 4.8.2.

For root cell wall staining, entire 5- to 12-d-old seedlings were stained with propidium iodide (Invitrogen; stock 1 mg/mL, 100× dilution) in water for 3 to 4 min and rinsed afterwards once in water. Confocal laser scanning microscopy was performed on an inverted Zeiss LSM 510 confocal microscope. Excitation and detection windows were set as follows: YFP, 488 nm, 500 to 600 nm; propidium iodide, 488 nm, 500 to 550 nm.

For visualization of the Casparian strips, roots of 10- to 12-d-old seedlings were used. Seedlings were incubated in 0.24 N HCl in 20% methanol at 57°C for 15 min. This solution was replaced with 7% NaOH in 60% ethanol for 15 min at room temperature. Roots were then rehydrated for 5 min each in 40, 20, and 10% ethanol and infiltrated for 15 min in 5% ethanol and 25% glycerol. Roots were mounted in 50% glycerol for microscopy analysis. To detect the apoplastic barrier, seedlings were incubated in the dark for 10 min in a fresh solution of 15 μM (10 μg/mL) propidium iodide and rinsed two times in water (Alassimone et al., 2010). Confocal laser scanning microscopy was performed on an inverted Leica SP2 and Zeiss LSM 700 confocal microscope. Excitation and detection windows were set as follows: green fluorescent protein, 488 nm, 500 to 600 nm; propidium iodide 488 nm, 500 to 550 nm.

Stomata numbers were determined on cotyledons or the two first true leaves of wild-type or mutant plants as indicated. Plants were grown well-spaced on agar plates with half-strength MS medium containing 0.5% Suc, pH 5.8. Cotyledons and true leaves were collected 21 d after germination, fixed in a 100% watery ethanol solution, and cleared and mounted in lactic acid. The samples were viewed using a Zeiss Axiophot microscope with Nomarski optics. Stomata density was determined by counting the stomata on two defined areas per leaf. The stomata index was calculated as described before by dividing the number of guard cells (number of stomata multiplied by two to correct for the presence of two guard cells) by the total number of cells (pavement cells + guard cells) (Rymen et al., 2010).

Histology

For GUS (for β-glucuronidase) assays, 5-d-old seedlings were directly collected in staining buffer with X-Gluc and infiltrated under vacuum for

5 to 10 min at room temperature. The samples were incubated at 37°C overnight. After one washing step in ethanol (70%) for 30 min, the seedlings were mounted in chloral hydrate for 3 h. Staining buffer was prepared as follows: 0.2% Triton, 50 mM $NaPO_4$, 2 mM Ferro-K, 2 mM Ferri-K, and 2 mM X-Gluc, filled up with water.

Expression Constructs

The Gateway Entry clone of CDKA;1-YFP (Nowack et al., 2007) was recombined into the destination vector pAM-PAT-GW-ProTMM (Weinl et al., 2005). The resulting binary plant expression vector, which confers phosphinotricine (BASTA; Bayer Cropscience) resistance, was retransformed into *Agrobacterium tumefaciens* GV3101-pMP90RK. Heterozygous plants for *cdka;1-1* and *rbr1-2* and homozygous plants for *cdkb1;1 cdkb1;2* were transformed.

Kinase Assay

To clone *CYCD6;1*, total RNA was extracted from flower buds using NucleoSpin RNA Plant (Macherey-Nagel). First-stranded cDNA was synthesized using SuperScript III reverse transcriptase (Invitrogen) with oligo (dT)-AP_M13 according to the manufacturer's instructions (all primer sequences are in Supplemental Table 3 online). *CYCD6;1* cDNA was amplified first with primers CYCD6;1_s1 and M13-forward, followed by primers CYCD6;1_s1 and CYCD6;1_as2. The resulting PCR products were cloned using a CloneJET PCR cloning kit (Fermentas) and sequenced. To express CYCD6;1 in *E.scherichia coli*, cDNA was amplified by sequential PCR first using attB1Ad-CYCD6;1_s and attB2Ad-CYCD6;1_as, followed by the attB1 adapter primer and attB2 adapter primer. The PCR product was cloned into the pDONR223 vector (Invitrogen). A recombination reaction was performed between the resulting entry clone and a destination vector pHMGWA (Busso et al., 2005). To express CDKA;1 hypomorphic alleles in *E. coli*, site-directed mutagenesis was performed using StrepIII-CDKA;1 in *pCDFDuet-Cak1* (Harashima and Schnittger, 2012) as a template of PCR. For D, the 5′ half was amplified with the ACYCDuetUP1 primer and the ND35; 3′ half was amplified with ND34 and the DuetDOWN1 primer. For DE, the ACYCDuetUP1 primer and ND04 and ND03 and the DuetDOWN1 primer were used. The 5′ and 3′ half of StrepIII-CDKA;1 were fused by PCR using the ACYCDuetUP1 and DuetDOWN1 primers. The resulting PCR products were digested by *Nco*I and *Not*I and cloned into the *Nco*I-*Not*I site of *pCDFDuet-Cak1*. CDK-cyclin complexes were expressed and purified from *E. coli* as described previously (Harashima and Schnittger, 2012). $p13^{suc1}$-associated kinases were purified as described previously (Harashima and Sekine, 2011) from 14-d-old Col-0, *D*, and *DE* seedlings grown on half-strength MS plates containing 0.5% Suc. CDK-cyclin complexes were processed for kinase assays as described previously (Harashima and Sekine, 2011) using Histone H1 as a substrate.

ChIP

ChIP was performed as previously described (Berr et al., 2010; Bouyer et al., 2011; Zhao et al., 2012). Two-week-old seedlings of Pro_{RBR1}:*RBR1*:*mRFP* growing on 0.5 MS plates were used. Chromatin was sheared with a Bioruptor sonicator (Cosmo Bio) twice for 15 min with a 50% duty cycle and high power output to obtain 200- to 1000-bp DNA fragments. Immunoprecipitation was performed using the DsRed polyclonal antibody (Clontech) together with Protein A-magnetic beads (Millipore). The E2FA antibody was described previously (Heyman et al., 2011). Negative controls were performed without antibody. DNA was recovered using Magna ChIP spin filters according to the manufacturer's instructions (Millipore). Then, 0.5 or 1 μL of a one-fifth dilution of ChIP DNA was analyzed by ChIP PCR or quantitative real-time PCR using gene-specific primers, respectively (see Supplemental Table 3 online). Two biological and three technical replicates were performed for ChIP–quantitative PCR using PCNA1 and MCM5 as positive controls and heterochromatic region primers as a negative control (see Supplemental Table 3 online).

Statistical Analyses

A multinomial distribution was generated by taking the sum of the count data, followed by fitting a generalized linear model, incorporating a log-linear link function to test for the difference of the supernumerary cortex-endodermis initial daughter cells in hypomorphic mutants versus wild-type plants. For the comparison of different time points (Figure 3), multinomial distributions were determined for each of the multinominate values. For statistical analyses of stomata indices (Figure 3), a binomial distribution was generated by taking the sum of the count data, followed by fitting a generalized linear model, incorporating a logit link function.

Accession Numbers

Sequence data from this article can be found in the Arabidopsis Genome Initiative or GenBank/EMBL databases under the following accession numbers: CDKA;1 has the Arabidopsis Genome Initiative code At3g48750. The T-DNA insertion line for the *cdka;1* mutant allele used (cdka;1-1) is Salk_106809.34.90.X. For RBR1 (At3g12280), the T-DNA insertion line used was SALK_002946. CDKB1;1 (At3g54180) mutants from the SALK_073457 line and CDKB1;2 (At2g38620) mutants from the SALK_133560 line were used. For the ChIP experiments, the following genes with their respective Arabidopsis Genome Initiative code were used: CYCD6;1 (At4g03270), MCM5 (At2g07690), MGP (At1g03840), NUC (At5g44160), PCNA1 (At1g07370), SCL3 (At1g50420), SCR (At3g54220), SPCH (At5g53210), and TMM (At1g80080).

Supplemental Data

The following materials are available in the online version of this article.

Supplemental Figure 1. Casparian Strip Formation Is Not Affected in Weak *cdka;1* Alleles.

Supplemental Figure 2. Cortex and Endodermis Differentiation.

Supplemental Figure 3. RBR1 ChIP.

Supplemental Figure 4. CDKA;1 Overexpression Partially Rescues *cdkb1;1 cdkb1;2* Stomata Defects.

Supplemental Table 1. Time Frame of Cortex-Endodermis Initial Daughter Division.

Supplemental Table 2. Stomata Density in *cdka;1* Mutants.

Supplemental Table 3. Oligonucleotides.

ACKNOWLEDGMENTS

We thank Tom Beeckman and Pierre Hilson (VIB) for the $Pro_{CYCD6;1}$:*GUS* reporter line, Frédéric Berger (National University of Singapore) for the Pro_{RBR1}:*RBR1-mRFP*–expressing plants, Renze Heidstra (University of Wageningen) for the *SCR* and *CO2* marker lines, Fred Sack (University of British Columbia) for the *TMM* promoter construct, and Lieven De Veylder, Vlaams Instituut voor Biotechnologie, for the E2FA antibody. We thank Marnik Vuylsteke, Vlaams Instituut voor Biotechnologie, for help with the statistical analysis and Jonathan Bramsiepe for assistance in producing *cdka;1* $Pro_{CDKA;1}$:$CDKA;1^{T14D;Y15E}$ *rbr1* plants. We also thank Annick Bleys for critical reading and helpful comments on the article. This work was supported by an EMBO Long-Term Fellowship (to M.K.N.), by Grant "Action Thématique et Incitative sur Programme" from the Centre

National de la Recherche Scientifique (to A.S.), by a European Union Interreg IV project (to A.S.), and by a European Research Council Starting Independent Researcher grant (to A.S.).

AUTHOR CONTRIBUTIONS

A.K.W., M.K.N., D.B., X.A.Z., H.H., N.D., N.G., and A.S. conceived and designed the experiments. A.K.W., M.K.N., D.B., X.A.Z., H.H., S.N., F.D.W., and N.D. performed the experiments. A.K.W., M.K.N., D.B., X.A.Z., H.H., S.N., F.D.W., N.D., N.G., and A.S. analyzed the data. A.K.W., M.K.N., N.G., and A.S. wrote the article.

Received August 28, 2012; revised September 22, 2012; accepted October 2, 2012; published October 26, 2012.

REFERENCES

Abrash, E.B., and Bergmann, D.C. (2009). Asymmetric cell divisions: A view from plant development. Dev. Cell **16:** 783–796.

Alassimone, J., Naseer, S., and Geldner, N. (2010). A developmental framework for endodermal differentiation and polarity. Proc. Natl. Acad. Sci. USA **107:** 5214–5219.

Andersen, S.U., Buechel, S., Zhao, Z., Ljung, K., Novák, O., Busch, W., Schuster, C., and Lohmann, J.U. (2008). Requirement of B2-type cyclin-dependent kinases for meristem integrity in *Arabidopsis thaliana*. Plant Cell **20:** 88–100.

Benfey, P.N., and Scheres, B. (2000). Root development. Curr. Biol. **10:** R813–R815.

Bergmann, D.C., and Sack, F.D. (2007). Stomatal development. Annu. Rev. Plant Biol. **58:** 163–181.

Berr, A., McCallum, E.J., Ménard, R., Meyer, D., Fuchs, J., Dong, A., and Shen, W.H. (2010). *Arabidopsis* SET DOMAIN GROUP2 is required for H3K4 trimethylation and is crucial for both sporophyte and gametophyte development. Plant Cell **22:** 3232–3248.

Borghi, L., Gutzat, R., Fütterer, J., Laizet, Y., Hennig, L., and Gruissem, W. (2010). *Arabidopsis* RETINOBLASTOMA-RELATED is required for stem cell maintenance, cell differentiation, and lateral organ production. Plant Cell **22:** 1792–1811.

Boudolf, V., Barrôco, R., Engler, Jde.A., Verkest, A., Beeckman, T., Naudts, M., Inzé, D., and De Veylder, L. (2004). B1-type cyclin-dependent kinases are essential for the formation of stomatal complexes in *Arabidopsis thaliana*. Plant Cell **16:** 945–955.

Bouyer, D., Roudier, F., Heese, M., Andersen, E.D., Gey, D., Nowack, M.K., Goodrich, J., Renou, J.P., Grini, P.E., Colot, V., and Schnittger, A. (2011). Polycomb repressive complex 2 controls the embryo-to-seedling phase transition. PLoS Genet. **7:** e1002014.

Busso, D., Delagoutte-Busso, B., and Moras, D. (2005). Construction of a set Gateway-based destination vectors for high-throughput cloning and expression screening in *Escherichia coli*. Anal. Biochem. **343:** 313–321.

De Smet, I., and Beeckman, T. (2011). Asymmetric cell division in land plants and algae: The driving force for differentiation. Nat. Rev. Mol. Cell Biol. **12:** 177–188.

Dissmeyer, N., Nowack, M.K., Pusch, S., Stals, H., Inzé, D., Grini, P.E., and Schnittger, A. (2007). T-loop phosphorylation of *Arabidopsis* CDKA;1 is required for its function and can be partially substituted by an aspartate residue. Plant Cell **19:** 972–985.

Dissmeyer, N., Weimer, A.K., Pusch, S., De Schutter, K., Alvim Kamei, C.L., Nowack, M.K., Novak, B., Duan, G.L., Zhu, Y.G., De Veylder, L., and Schnittger, A. (2009). Control of cell proliferation, organ growth, and DNA damage response operate independently of dephosphorylation of the *Arabidopsis* Cdk1 homolog CDKA;1. Plant Cell **21:** 3641–3654.

Dyson, N. (1998). The regulation of E2F by pRB-family proteins. Genes Dev. **12:** 2245–2262.

Ebel, C., Mariconti, L., and Gruissem, W. (2004). Plant retinoblastoma homologues control nuclear proliferation in the female gametophyte. Nature **429:** 776–780.

Ferrell, J.E. Jr. (2002). Self-perpetuating states in signal transduction: positive feedback, double-negative feedback and bistability. Curr. Opin. Cell Biol. **14:** 140–148.

Geisler, M.D., Nadeau, J.A., and Sack, F.D. (2000). Oriented asymmetric divisions that generate the stomatal spacing pattern in arabidopsis are disrupted by the too many mouths mutation. Plant Cell **12:** 2075–2086.

Gutzat, R., Borghi, L., and Gruissem, W. (2012). Emerging roles of RETINOBLASTOMA-RELATED proteins in evolution and plant development. Trends Plant Sci. **17:** 139–148.

Harashima, H., and Schnittger, A. (2010). The integration of cell division, growth and differentiation. Curr. Opin. Plant Biol. **13:** 66–74.

Harashima, H., and Schnittger, A. (2012). Robust reconstitution of active cell-cycle control complexes from co-expressed proteins in bacteria. Plant Methods **8:** 23.

Harashima, H., and Sekine, M. (2011). Measurement of plant cyclin-dependent kinase activity using immunoprecipitation-coupled and affinity purification-based kinase assays and the baculovirus expression system. Methods Mol. Biol. **779:** 65–78.

Heidstra, R., Welch, D., and Scheres, B. (2004). Mosaic analyses using marked activation and deletion clones dissect Arabidopsis SCARECROW action in asymmetric cell division. Genes Dev. **18:** 1964–1969.

Heyman, J., Van den Daele, H., De Wit, K., Boudolf, V., Berckmans, B., Verkest, A., Alvim Kamei, C.L., De Jaeger, G., Koncz, C., and De Veylder, L. (2011). *Arabidopsis* ULTRAVIOLET-B-INSENSITIVE4 maintains cell division activity by temporal inhibition of the anaphase-promoting complex/cyclosome. Plant Cell **23:** 4394–4410.

Ingouff, M., Jullien, P.E., and Berger, F. (2006). The female gametophyte and the endosperm control cell proliferation and differentiation of the seed coat in *Arabidopsis*. Plant Cell **18:** 3491–3501.

Knoblich, J.A. (2010). Asymmetric cell division: Recent developments and their implications for tumour biology. Nat. Rev. Mol. Cell Biol. **11:** 849–860.

Kono, A., Umeda-Hara, C., Adachi, S., Nagata, N., Konomi, M., Nakagawa, T., Uchimiya, H., and Umeda, M. (2007). The *Arabidopsis* D-type cyclin CYCD4 controls cell division in the stomatal lineage of the hypocotyl epidermis. Plant Cell **19:** 1265–1277.

MacAlister, C.A., Ohashi-Ito, K., and Bergmann, D.C. (2007). Transcription factor control of asymmetric cell divisions that establish the stomatal lineage. Nature **445:** 537–540.

Menges, M., de Jager, S.M., Gruissem, W., and Murray, J.A. (2005). Global analysis of the core cell cycle regulators of *Arabidopsis* identifies novel genes, reveals multiple and highly specific profiles of expression and provides a coherent model for plant cell cycle control. Plant J. **41:** 546–566.

Morgan, D.O. (1997). Cyclin-dependent kinases: Engines, clocks, and microprocessors. Annu. Rev. Cell Dev. Biol. **13:** 261–291.

Nadeau, J.A., and Sack, F.D. (2002). Control of stomatal distribution on the *Arabidopsis* leaf surface. Science **296:** 1697–1700.

Nowack, M.K., Grini, P.E., Jakoby, M.J., Lafos, M., Koncz, C., and Schnittger, A. (2006). A positive signal from the fertilization of the egg cell sets off endosperm proliferation in angiosperm embryogenesis. Nat. Genet. **38:** 63–67.

Nowack, M.K., Harashima, H., Dissmeyer, N., Zhao, X., Bouyer, D., Weimer, A.K., De Winter, F., Yang, F., and Schnittger, A. (2012).

Genetic framework of cyclin-dependent kinase function in Arabidopsis. Dev. Cell **22:** 1030–1040.

Nowack, M.K., Shirzadi, R., Dissmeyer, N., Dolf, A., Endl, E., Grini, P.E., and Schnittger, A. (2007). Bypassing genomic imprinting allows seed development. Nature **447:** 312–315.

Pines, J. (1995). Cyclins and cyclin-dependent kinases: A biochemical view. Biochem. J. **308:** 697–711.

Pusch, S., Harashima, H., and Schnittger, A. (2012). Identification of kinase substrates by bimolecular complementation assays. Plant J. **70:** 348–356.

Rymen, B., Coppens, F., Dhondt, S., Fiorani, F., and Beemster, G.T. (2010). Kinematic analysis of cell division and expansion. Methods Mol. Biol. **655:** 203–227.

Sherr, C.J., and Roberts, J.M. (1999). CDK inhibitors: Positive and negative regulators of G1-phase progression. Genes Dev. **13:** 1501–1512.

Sozzani, R., Cui, H., Moreno-Risueno, M.A., Busch, W., Van Norman, J.M., Vernoux, T., Brady, S.M., Dewitte, W., Murray, J.A., and Benfey, P.N. (2010). Spatiotemporal regulation of cell-cycle genes by SHORTROOT links patterning and growth. Nature **466:** 128–132.

Ten Hove, C.A., and Heidstra, R. (2008). Who begets whom? Plant cell fate determination by asymmetric cell division. Curr. Opin. Plant Biol. **11:** 34–41.

Tio, M., Udolph, G., Yang, X., and Chia, W. (2001). cdc2 links the Drosophila cell cycle and asymmetric division machineries. Nature **409:** 1063–1067.

Tyson, J.J., and Novak, B. (2008). Temporal organization of the cell cycle. Curr. Biol. **18:** R759–R768.

Ubeda-Tomás, S., Federici, F., Casimiro, I., Beemster, G.T., Bhalerao, R., Swarup, R., Doerner, P., Haseloff, J., and Bennett, M.J. (2009). Gibberellin signaling in the endodermis controls Arabidopsis root meristem size. Curr. Biol. **19:** 1194–1199.

van den Berg, C., Willemsen, V., Hendriks, G., Weisbeek, P., and Scheres, B. (1997). Short-range control of cell differentiation in the *Arabidopsis* root meristem. Nature **390:** 287–289.

Van Leene, J., Boruc, J., De Jaeger, G., Russinova, E., and De Veylder, L. (2011). A kaleidoscopic view of the *Arabidopsis* core cell cycle interactome. Trends Plant Sci. **16:** 141–150.

Weinberg, R.A. (1995). The retinoblastoma protein and cell cycle control. Cell **81:** 323–330.

Weinl, C., Marquardt, S., Kuijt, S.J., Nowack, M.K., Jakoby, M.J., Hülskamp, M., and Schnittger, A. (2005). Novel functions of plant cyclin-dependent kinase inhibitors, ICK1/KRP1, can act non-cell-autonomously and inhibit entry into mitosis. Plant Cell **17:** 1704–1722.

Xie, Z., Lee, E., Lucas, J.R., Morohashi, K., Li, D., Murray, J.A., Sack, F.D., and Grotewold, E. (2010). Regulation of cell proliferation in the stomatal lineage by the *Arabidopsis* MYB FOUR LIPS via direct targeting of core cell cycle genes. Plant Cell **22:** 2306–2321.

Zhao, X., Harashima, H., Dissmeyer, N., Pusch, S., Weimer, A.K., Bramsiepe, J., Bouyer, D., Rademacher, S., Nowack, M.K., Novak, B., Sprunck, S., and Schnittger, A. (2012). A general G1/S-phase cell-cycle control module in the flowering plant *Arabidopsis thaliana*. PLoS Genet. **8:** e1002847.

SUPPLEMENTAL FIGURES AND TABLES

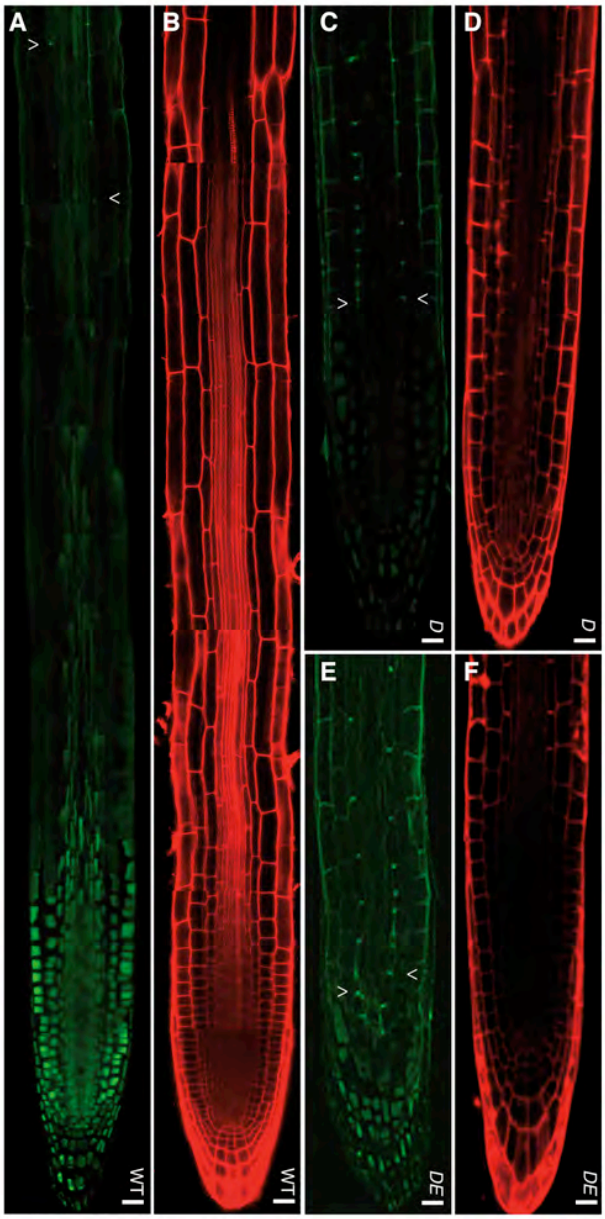

Supplemental Figure 1. Casparian strip formation is not affected in weak CDKA;1 alleles.

(**A)** Formation of the Casparian strip is the hallmark of endodermis differentiation in the wild type, as seen by autofluorescence (arrowheads). **(B**) After formation of the Casparian strip, propidium iodide (PI) cannot diffuse into the stele of the root. (**C-F)** Casparian strip formation is not affected in the weak loss-of-function *cdka;1* alleles *D* (**C** and **D**) and *DE* (**E** and **F**), as judged by autoflourescence and propidium iodide exclusion of the stele. All scale bars: 20 μm.

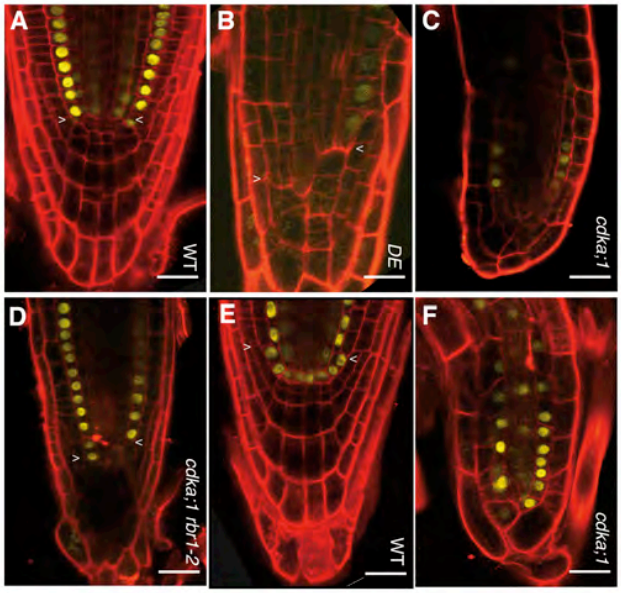

Supplemental Figure 2. Cortex and endodermis differentiation.

(**A**) Expression of the *ProCO2:H2B:YFP* construct labels the cortex of wild-type plants. (**B**) A weak but correctly positioned CO2 pattern is found in the weak loss-of-function *cdka;1* mutant *DE*. (**C**) CO2 activity is weak in the *cdka;1* null mutants and often appears to label a single file between the epidermis and the stele, i.e., fails to separate the endodermis and cortex cell files. (**D**) In the double mutant *cdka;1 rbr1-2*, strong activity of the CO2 promoter is restored and labels a clearly visible cortex layer. (**E**) *ProSCR:SCR:YFP* marks the initial, initial daughter and the endodermis layer in the wild type. (**F**) The subepidermal layer that is the cortex in wild-type plants occasionally shows SCR expression in homozygous *cdka;1* null mutants, indicating that the asymmetric division of an initial daughter into an endodermis and cortex file failed. All scale bars: 20 μm.

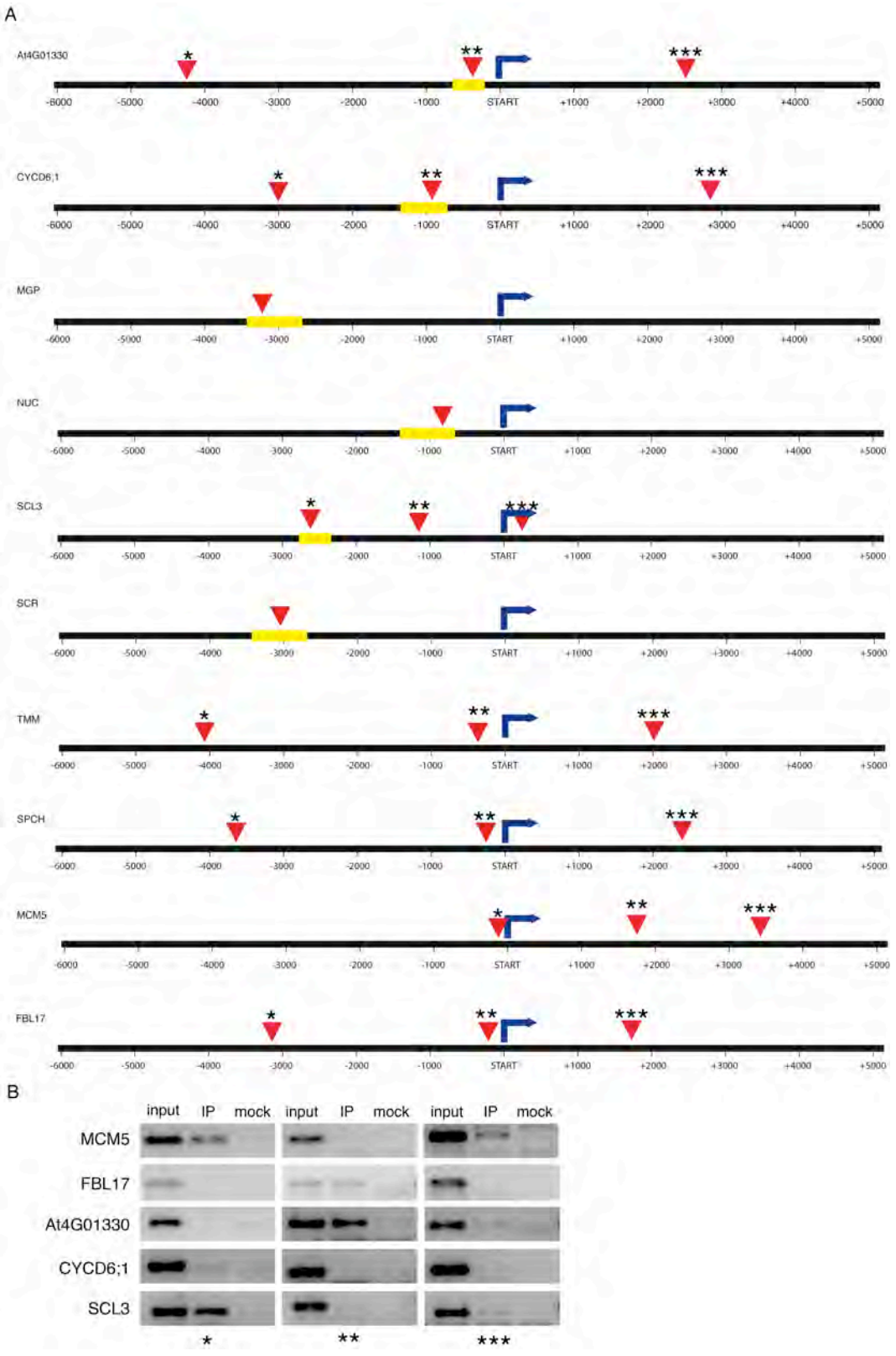
A
At4G01330
CYCD6;1
MGP
NUC
SCL3
SCR
TMM
SPCH
MCM5
FBL17
-6000
-5000
-4000
-3000
-2000
-1000
START
+1000
+2000
+3000
+4000
+5000
B
input
IP
mock
MCM5
FBL17
At4G01330
CYCD6;1
SCL3

Supplemental Figure 3. RBR ChIP.

(A) Upper panel, gene structure of genes tested by ChIP with an antibody against RFP in *ProRBR1:RBR1:RFP* plants. Red arrowheads indicate the primer binding sites for PCR (the three fragments are tested indicated with one to three asterisks) and (B) qPCR after ChIP. Yellow boxes mark the SHR binding region as identified by (Sozzani et al., 2010).

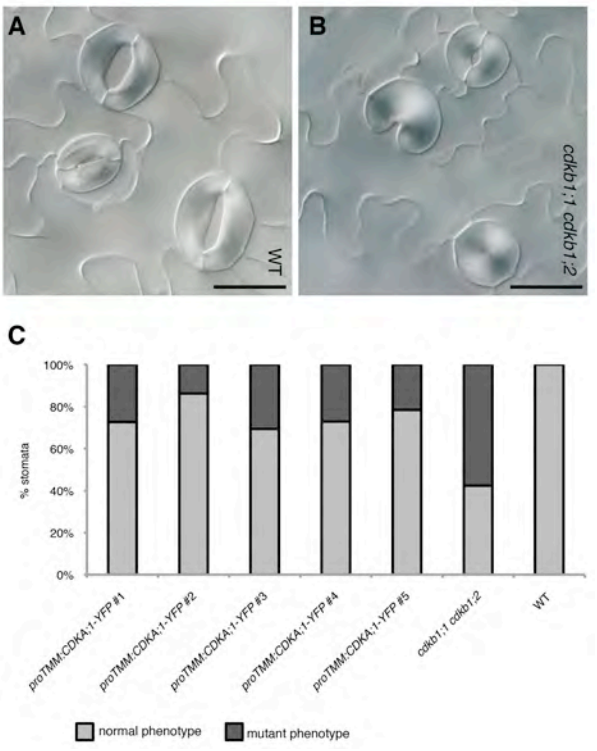

Supplemental Figure 4. *CDKA;1* expression partially rescues *cdkb1;1 cdkb1;2* stomata defects.

(**A**) Mature stomata on wild-type leaves are formed by two guard cells. (**B**) In the *cdkb;1;1 cdkb1;2* double mutant, arrested GMCs in the shape of one guard cell (middle), and circular arrested GMCs can be found besides regular stomata comprised of two guard cells (top). (**C**) Expression of *CDKA;1* under the control of the *TMM* promoter can partially rescue the mutant stomata phenotype in *cdkb1;1 cdkb1;2.* Scale bars: 25 µm.

Supplemental Tables

Supplemental Table 1: Time frame of cortex-endodermis initial daughter division

	division of cortex-endodermis initial daughter cell in %		
	immediately	delayed	N
WT	93	7	30
rbr1-2	71	29	92
DE	7	93	18
D	33	67	24
DE rbr1-2	18	82	28
cdkb1;1 cdkb1;2	83	17	36
cycd6;1	80	20	20
D cycd6;1	35	65	17
cdkb1;1 cdkb1;2 cycd6;1	74	26	43

Supplemental Table 2: Stomata density in *cdka;1* mutants

	number of stomata per mm^2	% of single GC	N
WT	130.4 ± 6.0	0	614
D	45.0 ± 4.5	0	106
DE	25.3 ± 9.6	4	124
cdka;1	0.0 ± 0.0	0	0*
cdka;1 rbr1-2	56.5 ± 31.2	0	266
cdka;1 ProCDKA;1:CDKB1;1	4.5 ± 1.3	0	21

* 25 leaves analyzed

Supplemental Table 3: Oligonucleotids

PRIMER SEQUENCES FOR GENOTYPING

T-DNA insertion	**primer**	**sequence 5' > 3'**
cdka;1-1	A01	GCGTGGACCGCTTGCTGCAACTCTCTCAGG
	A02	CCAGATTCTCCGTGGAATTGCG
rbr1-2	M206	CTTCCACAGCCCGGTCGTTTC
	J504	GCGTGGACCGCTTGCTGCAACTCTCTCAGG
cdkb1;1-1	A67	TGGTTCACGTAGTGGGCCATCGCCCTGATA
	A68	TGTCTTTGAGCAGCCATCTGTGTTG
cdkb1;2-1	A67	TGGTTCACGTAGTGGGCCATCGCCCTGATA
	A70	TTTTTGTACTCAGGGCCGGCTTTAC
cycd6;1	A220	AATTCGACGACCCATCTCTG
	A222	ATA TTG ACC ATC ATA CTC ATT GC

wild type	**primer**	**sequence 5' > 3'**
CDKA;1	A03	CAGATCTCTTCCTGGTTATTCACA
	A04	TGTACAAGCGAATAAAGACATTTGA
RBR1-2	M206	CTTCCACAGCCCGGTCGTTTC
	M207	GATTACCGCAGCATTCTAGTTGAACGC
CDKB1;1	A265	GCTTACCAATTGAGAACAACTGATTC
	A68	TGTCTTTGAGCAGCCATCTGTGTTG
CDKB1;2	A70	TTTTTGTACTCAGGGCCGGCTTTAC
	A71	GGTTCAAAACAAATTATCATCAACTAGG

CYCD6;1	A220	AATTCGACGACCCATCTCTG
	A221	CTGCAATCACCGATGGTTTA

PRIMER SEQUENCES FOR CLONING IN PROTEIN WORK

gene	**primer**	**sequence 5' > 3'**
CYCD6;1	dT-AP_M13	GTAAAACGACGGCCAGTTTTTTTTTTTTTT
	CYCD6;1_s1	ATGGAGTTTCATCTTGAACATCCTC
	M13-forward	GTAAAACGACGGCCAGT
	CYCD6;1_as2	TTAGTAACGACGAGTACTAGTTTTCCTCC
	attB1Ad-CYCD6;1_s	AAAAAGCAGGCTTCATGGAGTTTCATCTTGAACATCCTC
	attB2Ad-CYCD6;1_as	AGAAAGCTGGGTCTTAGTAACGACGAGTACTAGTTTTCCTCC
	attB1 adapter	GGGGACAAGTTTGTACAAAAAAGCAGGCT
	attB2 adapter	GGGGACCACTTTGTACAAGAAAGCTGGGT
D/DE in e.coli	ACYCDuetUP1	GGATCTCGACGCTCTCCCT
	ND35	CAGAGAGTAACAACCTCATGATCAAATGTCCTGACAGGGATAC
	ND34	GTATCCCTGTCAGGACATTTGATCATGAGGTTGTTACTCTCTG
	DuetDOWN1	GATTATGCGGCCGTGTACAA
	ND04	ATAAACCACACCCTCATCTCCTTCACCAAT
	ND03	ATTGGTGAAGGAGATGAGGGTGTGGTTTAT

PRIMER SEQUENCES FOR ChiP qPCR

gene	**primer**	**location of fragment**	**sequence 5' > 3'**
At4g01330	At4g01330_2F	upstream of START	CCCCAACACCGTTATCTCTC
	At4g01330_2R	upstream of START	GAGTGTGTGTGCTTGGGATG
CYCD6;1	CYCD6_2F	upstream of START	TGGACGAGATTCCAAAGTGA
	CYCD6_2R	upstream of START	GGCTGGGGAGATTAAATATGA
MGP	MGP_1F	upstream of START	CGGAAAAGGTAAGGTGGTTG
	MGP_1R	upstream of START	TCGGACTTGACCAATCCAAT
NUC	NUC_2F	upstream of START	GAGGAAAGGGCAACACAAAA
	NUC_2R	upstream of START	CAAATTCGAAGCGAGCTGTT
SCL3	SCL3_2F	upstream of START	CGTACCGGCTCTCTTCGATA
	SCL3_2R	upstream of START	GCATCGGTCATCGTCTCTCT
SCR	SCR_2F	upstream of START	AGTTGGTGCCCCATCTTAGT
	SCR_2R	upstream of START	TCATTATGTGAAATGAATGGGTTT
MCM5	MCM5_4F	upstream of START	TCCCGCCAAAACTCATAGTC
	MCM5_4R	upstream of START	TGACATCGTTGCTTCGTCTC
PCNA1	PCNA1_F	upstream of START	TCTTAAAACGATTGAGGCCG
	PCNA1_R	upstream of START	AATCGTTTGCGGCTATTTTG
RB32,5	LB32,5-F	upstream of START	CGAACACACGGATATGTTGC
	LB32,5-R	upstream of START	TGGTGATGTACTCGCTGTCAA
RB45	RB45-F	upstream of START	GCGGAACCAATTATAGATGAGG
	RB45-R	upstream of START	CGTCAACAGCTCCAAATCAC

SPCH	SPCHF1	upstream of START	ATCCTCCCCCAAATTTCATC
	SPCHR1	upstream of START	ATGAGGGACTCGCATTCATC

PRIMER SEQUENCES FOR ChIP-PCR

gene	**primer**	**location of fragment**	**sequence 5' > 3'**
At4g01330	AT4GUF1	upstream of START	GTTCGTGACTGCAACTAGAG
	AT4GUR1	upstream of START	ACATTGGAGCACTGAAAGAG
	AT4GDF2	downstream of START	TTCTCATCCTTTCGTAACTC
	AT4GDR2	downstream of START	ACATTCAGGAAGGTTAGGAC
CYCD6;1	CYCD6;1UF1	downstream of START	GAGACTTGGTCATGGTATGG
	CYCD6;1UR1	downstream of START	GGGAAATACATCAAACATGG
	CYCD6;1DF1	upstream of START	GGTCATCTTATAGCCACAAG
	CYCD6;1DR1	upstream of START	AGTGATTAGAATCGAGCAAC
SPCH	spchluf1	downstream of START	AGTAAACATGACGATGGCTG
	spchlur1	downstream of START	TACTCACTTTCTCTCCTTAG
	spchldf2	upstream of START	GCAAACACATATAGCGCATC
	spchldr2	upstream of START	AACAGGTGATAACGAACGCTC
MCM5	MCM5UF1	downstream of START	ACATCATCTGGTGTGGCCTC
	MCM5UR1	downstream of START	ACAGTGAGACAACTCGAAGC
	MCM5UF2	downstream of START	GATTTTGCAGTTGATGGGTC
	MCM5UR2	downstream of START	TTCTGTGCACTTTGTATACG
SCL3	SCL3DF1	upstream of START	GTTTGGACGTTTCCTTCTTC

	SCL3DR1	upstream of START	CATGGCATGAGGTGGATTTG
	SCL3DF2	downstream of START	CTCTCACCTCGCTTCTCCTG
	SCL3DR2	downstream of START	GAGTTGCGTTAAGAGCCTTG
TMM	TMMUF2	downstream of START	CGAGGACACATTTACTTGAG
	TMMUR2	downstream of START	CTCAGTAAAGCACAAGACAG
	TMMDF2	upstream of START	GGAAAAAGGTAACCTGACTC
	TMMDR2	upstream of START	GATTTTGGGTTTGTTGAGAG
	TMMF1	upstream of START	CAGTGCCCAGTTCAAAATAC
	TMMF2	upstream of START	AGATATTCCCTTCATTCGTC
FBL17	FBL17U1_1	upstream of START	TTCTGATTGCAGTTGGTGGA
	FBL17U1_2	upstream of START	CGGCATCAGAATCAATAGCA
	FBL17_1	upstream of START	GCTAGACCTCACGCTCTTTC
	FBL17_2	upstream of START	GAGATTTGTGAGATTGGGAG
	FBL17D4_1	downstream of START	TGCTCTCGCTAGTTCTTGGA
	FBL17D4_2	downstream of START	ACCTGAGGAAATGGCAGCTA

SUPPLEMENTAL FIGURES AND TABLES

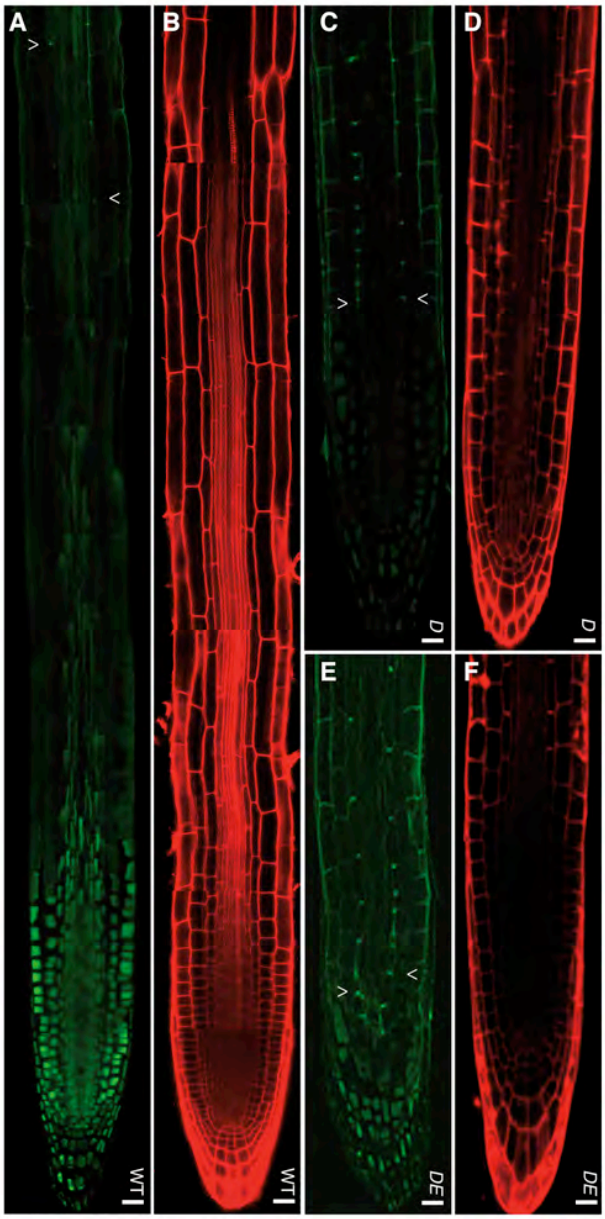

Supplemental Figure 1. Casparian strip formation is not affected in weak CDKA;1 alleles.

(**A)** Formation of the Casparian strip is the hallmark of endodermis differentiation in the wild type, as seen by autofluorescence (arrowheads). **(B**) After formation of the Casparian strip, propidium iodide (PI) cannot diffuse into the stele of the root. (**C-F)** Casparian strip formation is not affected in the weak loss-of-function *cdka;1* alleles *D* (**C** and **D**) and *DE* (**E** and **F**), as judged by autoflourescence and propidium iodide exclusion of the stele. All scale bars: 20 μm.

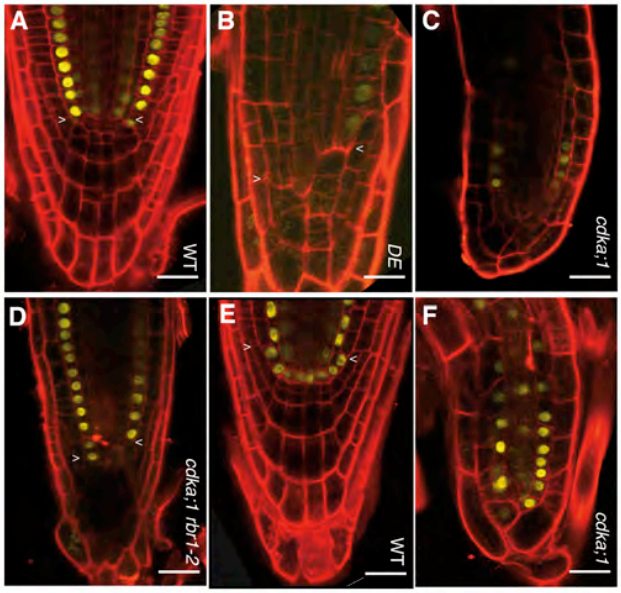

Supplemental Figure 2. Cortex and endodermis differentiation.

(**A**) Expression of the *ProCO2:H2B:YFP* construct labels the cortex of wild-type plants. (**B**) A weak but correctly positioned CO2 pattern is found in the weak loss-of-function *cdka;1* mutant *DE*. (**C**) CO2 activity is weak in the *cdka;1* null mutants and often appears to label a single file between the epidermis and the stele, i.e., fails to separate the endodermis and cortex cell files. (**D**) In the double mutant *cdka;1 rbr1-2*, strong activity of the CO2 promoter is restored and labels a clearly visible cortex layer. (**E**) *ProSCR:SCR:YFP* marks the initial, initial daughter and the endodermis layer in the wild type. (**F**) The subepidermal layer that is the cortex in wild-type plants occasionally shows SCR expression in homozygous *cdka;1* null mutants, indicating that the asymmetric division of an initial daughter into an endodermis and cortex file failed. All scale bars: 20 μm.

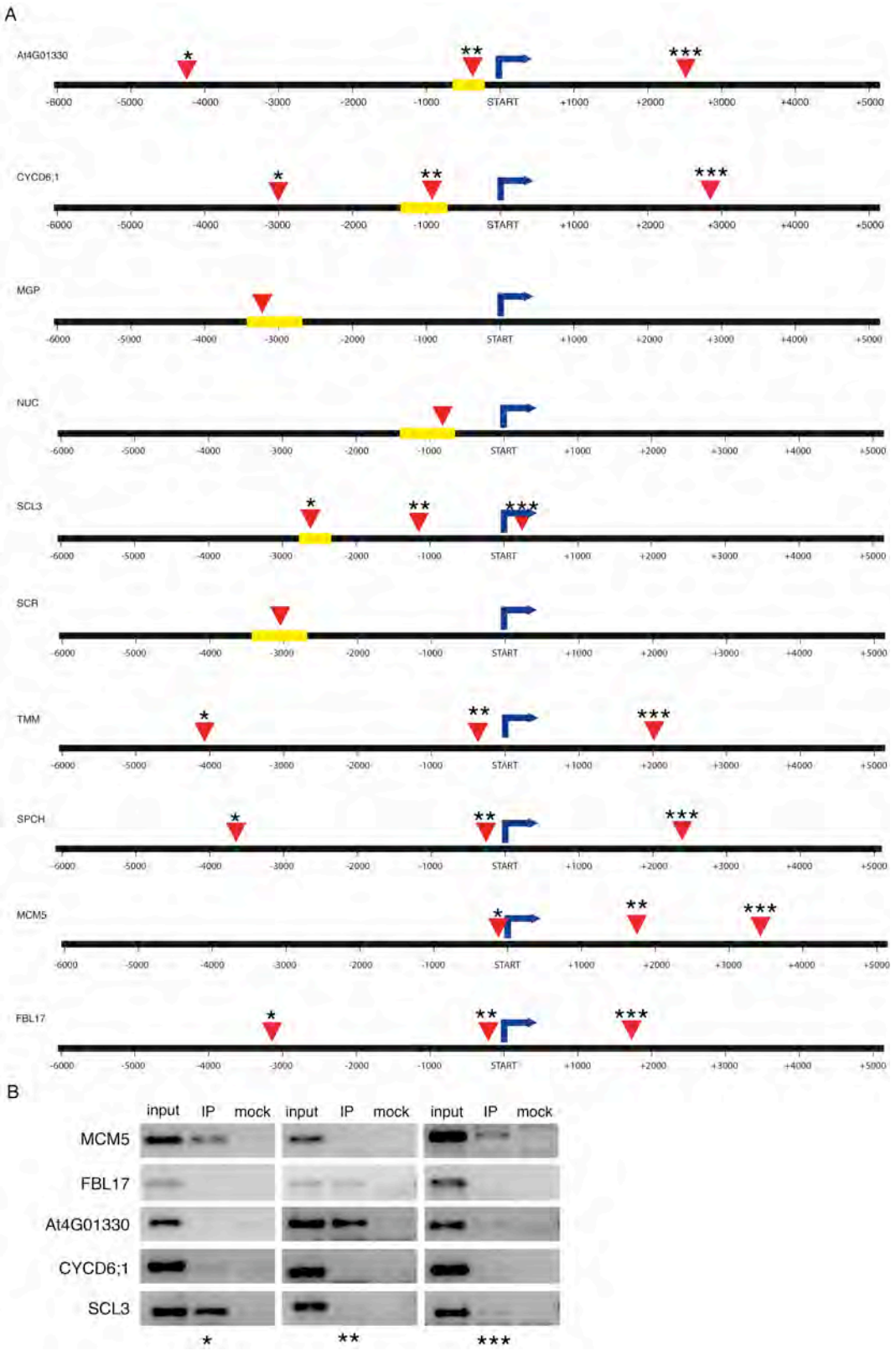
A
At4G01330
CYCD6;1
MGP
NUC
SCL3
SCR
TMM
SPCH
MCM5
FBL17
-6000
-5000
-4000
-3000
-2000
-1000
START
+1000
+2000
+3000
+4000
+5000
B
input
IP
mock
MCM5
FBL17
At4G01330
CYCD6;1
SCL3

Supplemental Figure 3. RBR ChIP.

(A) Upper panel, gene structure of genes tested by ChIP with an antibody against RFP in *ProRBR1:RBR1:RFP* plants. Red arrowheads indicate the primer binding sites for PCR (the three fragments are tested indicated with one to three asterisks) and (B) qPCR after ChIP. Yellow boxes mark the SHR binding region as identified by (Sozzani et al., 2010).

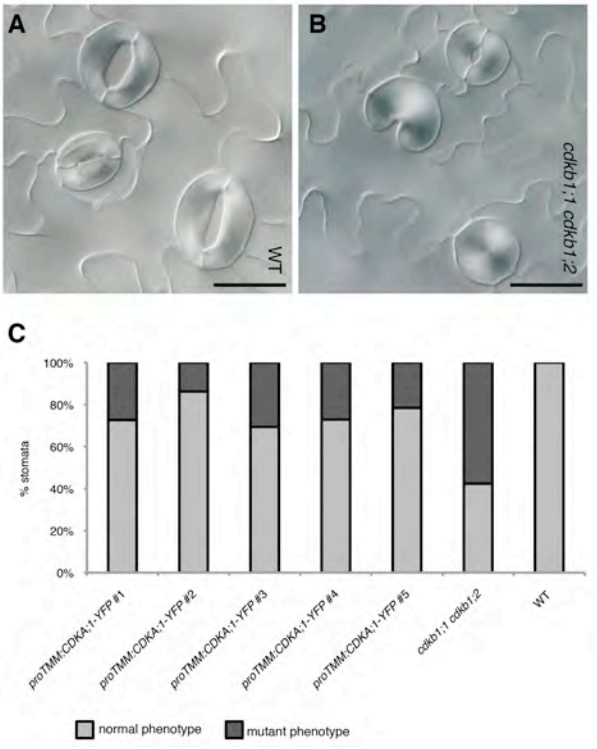

Supplemental Figure 4. *CDKA;1* expression partially rescues *cdkb1;1 cdkb1;2* stomata defects.

(**A**) Mature stomata on wild-type leaves are formed by two guard cells. (**B**) In the *cdkb;1;1 cdkb1;2* double mutant, arrested GMCs in the shape of one guard cell (middle), and circular arrested GMCs can be found besides regular stomata comprised of two guard cells (top). (**C**) Expression of *CDKA;1* under the control of the *TMM* promoter can partially rescue the mutant stomata phenotype in *cdkb1;1 cdkb1;2.* Scale bars: 25 µm.

Supplemental Tables

Supplemental Table 1: Time frame of cortex-endodermis initial daughter division

	division of cortex-endodermis initial daughter cell in %		
	immediately	delayed	N
WT	93	7	30
rbr1-2	71	29	92
DE	7	93	18
D	33	67	24
DE rbr1-2	18	82	28
cdkb1;1 cdkb1;2	83	17	36
cycd6;1	80	20	20
D cycd6;1	35	65	17
cdkb1;1 cdkb1;2 cycd6;1	74	26	43

Supplemental Table 2: Stomata density in *cdka;1* mutants

	number of stomata per mm^2	% of single GC	N
WT	130.4 ± 6.0	0	614
D	45.0 ± 4.5	0	106
DE	25.3 ± 9.6	4	124
cdka;1	0.0 ± 0.0	0	0*
cdka;1 rbr1-2	56.5 ± 31.2	0	266
cdka;1 ProCDKA;1:CDKB1;1	4.5 ± 1.3	0	21

* 25 leaves analyzed

Supplemental Table 3: Oligonucleotids

PRIMER SEQUENCES FOR GENOTYPING

T-DNA insertion	**primer**	**sequence 5' > 3'**
cdka;1-1	A01	GCGTGGACCGCTTGCTGCAACTCTCTCAGG
	A02	CCAGATTCTCCGTGGAATTGCG
rbr1-2	M206	CTTCCACAGCCCGGTCGTTTC
	J504	GCGTGGACCGCTTGCTGCAACTCTCTCAGG
cdkb1;1-1	A67	TGGTTCACGTAGTGGGCCATCGCCCTGATA
	A68	TGTCTTTGAGCAGCCATCTGTGTTG
cdkb1;2-1	A67	TGGTTCACGTAGTGGGCCATCGCCCTGATA
	A70	TTTTTGTACTCAGGGCCGGCTTTAC
cycd6;1	A220	AATTCGACGACCCATCTCTG
	A222	ATA TTG ACC ATC ATA CTC ATT GC

wild type	**primer**	**sequence 5' > 3'**
CDKA;1	A03	CAGATCTCTTCCTGGTTATTCACA
	A04	TGTACAAGCGAATAAAGACATTTGA
RBR1-2	M206	CTTCCACAGCCCGGTCGTTTC
	M207	GATTACCGCAGCATTCTAGTTGAACGC
CDKB1;1	A265	GCTTACCAATTGAGAACAACTGATTC
	A68	TGTCTTTGAGCAGCCATCTGTGTTG
CDKB1;2	A70	TTTTTGTACTCAGGGCCGGCTTTAC
	A71	GGTTCAAAACAAATTATCATCAACTAGG

CYCD6;1	A220	AATTCGACGACCCATCTCTG
	A221	CTGCAATCACCGATGGTTTA

PRIMER SEQUENCES FOR CLONING IN PROTEIN WORK

gene	**primer**	**sequence 5' > 3'**
CYCD6;1	dT-AP_M13	GTAAAACGACGGCCAGTTTTTTTTTTTTTT
	CYCD6;1_s1	ATGGAGTTTCATCTTGAACATCCTC
	M13-forward	GTAAAACGACGGCCAGT
	CYCD6;1_as2	TTAGTAACGACGAGTACTAGTTTTCCTCC
	attB1Ad-CYCD6;1_s	AAAAAGCAGGCTTCATGGAGTTTCATCTTGAACATCCTC
	attB2Ad-CYCD6;1_as	AGAAAGCTGGGTCTTAGTAACGACGAGTACTAGTTTTCCTCC
	attB1 adapter	GGGGACAAGTTTGTACAAAAAAGCAGGCT
	attB2 adapter	GGGGACCACTTTGTACAAGAAAGCTGGGT
D/DE in e.coli	ACYCDuetUP1	GGATCTCGACGCTCTCCCT
	ND35	CAGAGAGTAACAACCTCATGATCAAATGTCCTGACAGGGATAC
	ND34	GTATCCCTGTCAGGACATTTGATCATGAGGTTGTTACTCTCTG
	DuetDOWN1	GATTATGCGGCCGTGTACAA
	ND04	ATAAACCACACCCTCATCTCCTTCACCAAT
	ND03	ATTGGTGAAGGAGATGAGGGTGTGGTTTAT

PRIMER SEQUENCES FOR ChiP qPCR

gene	**primer**	**location of fragment**	**sequence 5' > 3'**
At4g01330	At4g01330_2F	upstream of START	CCCCAACACCGTTATCTCTC
	At4g01330_2R	upstream of START	GAGTGTGTGTGCTTGGGATG
CYCD6;1	CYCD6_2F	upstream of START	TGGACGAGATTCCAAAGTGA
	CYCD6_2R	upstream of START	GGCTGGGGAGATTAAATATGA
MGP	MGP_1F	upstream of START	CGGAAAAGGTAAGGTGGTTG
	MGP_1R	upstream of START	TCGGACTTGACCAATCCAAT
NUC	NUC_2F	upstream of START	GAGGAAAGGGCAACACAAAA
	NUC_2R	upstream of START	CAAATTCGAAGCGAGCTGTT
SCL3	SCL3_2F	upstream of START	CGTACCGGCTCTCTTCGATA
	SCL3_2R	upstream of START	GCATCGGTCATCGTCTCTCT
SCR	SCR_2F	upstream of START	AGTTGGTGCCCCATCTTAGT
	SCR_2R	upstream of START	TCATTATGTGAAATGAATGGGTTT
MCM5	MCM5_4F	upstream of START	TCCCGCCAAAACTCATAGTC
	MCM5_4R	upstream of START	TGACATCGTTGCTTCGTCTC
PCNA1	PCNA1_F	upstream of START	TCTTAAAACGATTGAGGCCG
	PCNA1_R	upstream of START	AATCGTTTGCGGCTATTTTG
RB32,5	LB32,5-F	upstream of START	CGAACACACGGATATGTTGC
	LB32,5-R	upstream of START	TGGTGATGTACTCGCTGTCAA
RB45	RB45-F	upstream of START	GCGGAACCAATTATAGATGAGG
	RB45-R	upstream of START	CGTCAACAGCTCCAAATCAC

SPCH	SPCHF1	upstream of START	ATCCTCCCCCAAATTTCATC
	SPCHR1	upstream of START	ATGAGGGACTCGCATTCATC

PRIMER SEQUENCES FOR ChIP-PCR

gene	**primer**	**location of fragment**	**sequence 5' > 3'**
At4g01330	AT4GUF1	upstream of START	GTTCGTGACTGCAACTAGAG
	AT4GUR1	upstream of START	ACATTGGAGCACTGAAAGAG
	AT4GDF2	downstream of START	TTCTCATCCTTTCGTAACTC
	AT4GDR2	downstream of START	ACATTCAGGAAGGTTAGGAC
CYCD6;1	CYCD6;1UF1	downstream of START	GAGACTTGGTCATGGTATGG
	CYCD6;1UR1	downstream of START	GGGAAATACATCAAACATGG
	CYCD6;1DF1	upstream of START	GGTCATCTTATAGCCACAAG
	CYCD6;1DR1	upstream of START	AGTGATTAGAATCGAGCAAC
SPCH	spchluf1	downstream of START	AGTAAACATGACGATGGCTG
	spchlur1	downstream of START	TACTCACTTTCTCTCCTTAG
	spchldf2	upstream of START	GCAAACACATATAGCGCATC
	spchldr2	upstream of START	AACAGGTGATAACGAACGCTC
MCM5	MCM5UF1	downstream of START	ACATCATCTGGTGTGGCCTC
	MCM5UR1	downstream of START	ACAGTGAGACAACTCGAAGC
	MCM5UF2	downstream of START	GATTTTGCAGTTGATGGGTC
	MCM5UR2	downstream of START	TTCTGTGCACTTTGTATACG
SCL3	SCL3DF1	upstream of START	GTTTGGACGTTTCCTTCTTC

	SCL3DR1	upstream of START	CATGGCATGAGGTGGATTTG
	SCL3DF2	downstream of START	CTCTCACCTCGCTTCTCCTG
	SCL3DR2	downstream of START	GAGTTGCGTTAAGAGCCTTG
TMM	TMMUF2	downstream of START	CGAGGACACATTTACTTGAG
	TMMUR2	downstream of START	CTCAGTAAAGCACAAGACAG
	TMMDF2	upstream of START	GGAAAAAGGTAACCTGACTC
	TMMDR2	upstream of START	GATTTTGGGTTTGTTGAGAG
	TMMF1	upstream of START	CAGTGCCCAGTTCAAAATAC
	TMMF2	upstream of START	AGATATTCCCTTCATTCGTC
FBL17	FBL17U1_1	upstream of START	TTCTGATTGCAGTTGGTGGA
	FBL17U1_2	upstream of START	CGGCATCAGAATCAATAGCA
	FBL17_1	upstream of START	GCTAGACCTCACGCTCTTTC
	FBL17_2	upstream of START	GAGATTTGTGAGATTGGGAG
	FBL17D4_1	downstream of START	TGCTCTCGCTAGTTCTTGGA
	FBL17D4_2	downstream of START	ACCTGAGGAAATGGCAGCTA

6 Chapter VI: Conclusive remarks and Perspectives

6.1 Casparian Strip: Localized lignified impregnation in the endodermis

During my thesis, I have provided strong evidence to support the claim that the CS is made of lignin rather than suberin. However, the general mechanisms of lignin polymerization and transport have remained largely unclear. In parallel to my work, a recent advancement in lignin research has been the discovery of ABCG29, a member of the ATP-binding cassette transporters subfamily. In this study, ABCG29 was characterized as a major transporter of p-coumaryl alcohol, one of the three monolignols involved in the lignin biosynthesis (Alejandro et al. 2012). It has been reported that the loss of *Arabidopsis* ABCG29 function, results in the reduced levels of all three lignin monomers, named p-hydroxyphenyl (H), guaiacyl (G), and syringyl (S) sub-units. Results obtained by expression of ABCG29 in yeast describe p-coumaryl alcohol as its main substrate. H-subunit of lignin monomer is derived from p-coumaryl alcohol, suggesting a role of ABCG transporters as exporters of monolignols to the apoplast. Regarding the expression and sub-cellular localization of this transporter, it was reported that it is expressed only in the endodermis and xylem vessels, lending further support to the idea that the Casparian Strip is made of lignin. It was shown that ABCG29 is localized in the plasma membrane of endodermal cells, but it did not localize at the plasma membrane domain (CSD) subjacent to the CS. This work nevertheless suggests the presence of lignin in the endodermis and it suggest that ABCG transporters might be the general pathway by which monolignol reach the site of lignin deposition in the apoplast.

More importantly, Yuree Lee in our group, recently reported that NADPH oxidases, (respiratory burst oxidase homologs; RBOHF), together with peroxidases are involved in the polymerization of lignin monomers at very localized region of the CSD (Lee et al. 2013). The rbohf T-DNA insertion allele found during a reverse genetic screen, was also found as *schengen4 (sgn4)* by our former PhD student Julien Alassimone by a forward genetic EMS-mutagenesis screen. *rbohf* mutants show a delay in the formation of functional CS. As mentioned in Chapter 1, the formation of lignin through the polymerization of monolignols depends on the enzymatic action of different classes of proteins like Peroxidases and/or Lacasses. Peroxidases require hydrogen peroxide

production for oxidation of monolignols, which has been assumed to be provided by NADPH oxidases. Strikingly, Lee and collaborators reported that the inhibition of peroxidases and NADPH oxidases activity also blocked the formation of a functional CS. Moreover, they reported that both peroxidases and NADPH oxidases were localized to the CSD formed by the CASPs. These results suggests role of Casparian Strip domain proteins (CASPs) in the assembly of the whole lignin polymerization machinery. During this process, reactive oxygen species (ROS) generated by the NADPH oxidases are channeled towards the cell wall peroxidases through the action of CASPs. These use the ROS for the polymerisation of monolignols. These findings suggest that the process of lignin polymerization in the primary cell wall of endodermis might be different from the mechanism of lignin polymerization in xylem vessels. In the latter, lignin deposition occurs in a pre-existing cellulosic secondary cell wall of the xylem vessel without necessarily requiring any specific localization machinery. Furthermore, the process of lignin impregnation of the CS keeps the endodermal cell alive, while lignification in xylem vessels is largely a post-mortem process (Pesquet et al. 2013).

Moreover, recently an additional actors of the lignin polymerization machinery, a dirigent domain containing protein ESB1 (Enhanced suberin 1) was identified (Hosmani et al. 2013/Chapter V.A). Interestingly, ESB1 localization exhibit the same pattern as reported before for the CASP1 (Roppolo et al. 2011). Moreover, the loss ESB1 function in *esb1* mutant causes the interrupted Casparian Strip formation (non-functional Propidium iodide diffusion barrier) and ectopic deposition of suberin. The same phenotypic defects were also reported for *casp1 casp3* double mutant. This study suggests an essential role of ESB1 in driving the correct localization of lignin in a primary cell wall of the endodermis. Dirigent proteins were firstly identified in the *Forsythia* species and reported to be involved in the stereoselective coupling of lignin monomers *in vitro* (Davin et al.1997). This study provides the first *in vivo* evidence for the involvement of dirigent protein in lignin polymerization.

Altogether, these subsequent discoveries strongly support and confirm my findings that the early CS, at least in *Arabidopsis*, are made of lignin. Secondly, they suggest how different actors play specific roles in the establishment of functional CS, where CASPs act as scaffold proteins that assembles the different actors (NADPH oxidases, peroxidases and ESB1) of the lignin polymerization machinery. These findings establish

the endodermis as an interesting new model system for the further dissection and manipulation of lignin in plants.

6.2 The endodermis: A system to study contributions of lignin and suberin to barrier formation

In the past few decades, the process of endodermis development and its function has been investigated in many plant species. My PhD thesis work describes that in *Arabidopsis* the developmental stages of endodermis is well defined and separated, where lignin depositions were followed by the suberin deposition in the form of lamellae over the entire endodermal cell. In addition, my work clearly demonstrates that a lignified CS is functionally sufficient to block extracellular diffusion barrier. However, is the strict separation of lignin and suberin deposition in *Arabidopsis* also occurs in other plant species? For example in young roots of maize the separation of CS and suberin lamellae formation were also reported in term of distance from the root apex in both exodermis and endodermis (Vaculík Marek et al. 2012).

In general, the endodermis is an extraordinary system to examine the formation of lignin and suberin formation. In the future, it will be important to precisely investigate the relative contribution of lignin and suberin to the apoplastic barrier formation specifically in young roots.

6.3 What is the role of Suberin in young roots?

All our efforts have demonstrated that, in young roots, early-lignified CS are sufficient to act as an apoplastic barrier. Later on, with the formation of a secondary stage of endodermis differentiation, suberin may also play a role in the establishment of a functional diffusion barrier. However, it is hard to define a precise role for suberin at present, since our transgenic plants completely devoid of suberin have no effect on the formation of an apoplastic barrier and grow without any evident, strong phenotype. Moreover, the delay in CS establishment in the *esb1* mutant and *casp1 casp3* double mutant could not be compensated by the deposition of an increased level of suberin. If suberin is inefficient to provide a diffusion barrier in young roots, what could be the role of suberin in young roots? Suberin lamellae are formed surrounding endodermal cells, but not between them. Therefore, it might not provide an apoplastic barrier. It would

rather provide a barrier for transport across the plasma membrane of individual suberized cells. It is thought that suberin lamellae formation may intrupt

In the root, water usually uses the low resistance pathways. However, this may change with the development of lignified CS and suberin lamellae. In the past few years, there has been considerable progress in order to characterize the role of the CS and suberin lamellae as barriers against radial water transport in different plant species. In addition, different models have been proposed in order to define the contribution of apoplastic and symplastic water transport. The formation of CS and suberin lamellae may largely interrupt the flow of water and in contrast enforce a coupled transcellular pathway. It is thought that the formation of suberin lamellae may interrupt the water flow through this pathway. However, tranascellular pathway is dominated by the presence of aquaporins/water channels, activity of these channels is reported to be responsible for providing “gating” under drought condition (Clarkson et al.2000). Moreover, water stress not only affects the whole root anatomy, but also alters the root barrier properties. For example, there is an increase in suberization during water stress condition. The work carried out by Steudle and Peterson has shown that during water stress, the formation of suberin lamellae could increase the resistance to water flow. In addition, they reported that injures in the endodermis did not have any effect on hydraulic conductivity. Moreover, it has been reported that CS do not contribute significantly to water transport, not only at primary developmental states but later in development as well (Steudle 2000; Steudle and Peterson 1998).

Recently, it has been shown that in *Arabidopsis* reduced amounts of suberin resulted in increased water permeability (Höfer R et al. 2008). However, in contrast enhanced suberin mutant (*esb1)* with enhanced levels of suberin, failed to reduce the water permeability, but exhibits increased tolerance to drought stress condition (Baxter et al. 2009). Moreover, studies regarding the natural variations of root hydraulic conductivity in different accessions of *Arabidopsis thaliana* reports no correlation between the distinct suberization pattering and hydraulic conductivity along whole the root (Sutka M et al. 2011).

Regarding these examples, we must bear in mind that CS could be effective only in blocking the apoplastic flow of water. On the other hand, suberin lamellae could only be

effective in blocking cell-to-cell water flow. At this point, we cannot neglect the presence of aquaporins that are reported to be responsible for passive transport of water through plasma membrane (Vandeleur etal.2009).

As it is mentioned before, transport of some ions was also markedly decreased with the deposition of suberin, suggesting that deposition of this substance over the entire endodermal cells make ion transport more difficult. The role of suberin deposition as an external apoplastic barrier, especially when it is deposited in the external tissue layers (like cork cells of root periderm and outer skin of potato tubers) has been well described previously. In 2008, work carried out by Olga Serra and collaborators demonstrated that in potato tubers, silencing of CYP86A33 (a member of the Cytochrome P450 of the CYP86A subfamily) gene, not only altered the chemical composition of suberin but also affects the lamellar structure and water barrier properties of periderm cell wall. On the contrary, in *Arabidopsis,* a loss of CYP86A1 activity, member of same subfamily reduced the total amount of suberin but this reduction has no effect on the functional barrier formation (Hofer et al. 2008; Naseer et al. 2012). These findings support the role of suberin in the establishment of an efficient barrier formation when it is deposited in the external tissues as shown in potato tubers, but does not clarify the question regarding its function when deposited in the endodermis.

One possible role of suberin deposition in internal root tissues might be to protect cells against pathogen attack. As mentioned in Chapter III, during the endodermal differentiation not all the primary stage endodermal cells undergo secondary differentiation meaning that some endodermal cells remain non-suberized. Formation of these cells raises several questions, such as, what is the role of these non- suberized passage cells? As these cells do not develop suberin lamellae, do these cells have control on the entry of fungi, bacteria or other toxic substances into the stele? Several earlier investigations reported that for example in myccorhizal host plant species that develop an exodermis (often also termed hypodermis; protective layer located below the epidermis that separates the cortex from the surrounding medium), exodermal passage cells (non-suberized cells) act as channels for hyphal entry into the cortex. Endodermis and vascular tissues, however, remain untouched (Majstriks et al.1970; Esnault et al. 1994). Recently, it has been reported that in *Arabidopsis,* the pathogenic bacteria *Ralstonia solanacearum* penetrates into the vasculature centripetally through

intercellular spaces by invading only xylem-pole associated pericycle cells (Digonnet et al. 2012). As described in Chapter III, non-suberised endodermal cells are also located on the xylem-poles, suggesting that these non-suberised cells might allow the penetration of bacterium from outside into the xylem-pole pericycle cells and finally into the xylem vessels. These observations suggest a protective role of suberin deposition in preventing manipulation of internal root tissues by the fungus or bacterium infection.

Marie Barberon in our lab is now trying to address the question of the role of suberin deposition specifically in young roots. Our major aim is to distinguish the role of lignin and suberin deposition in the endodermis during primary and secondary differentiation of endodermis and to precisely investigate the role of suberin in the young roots. As mentioned in chapter III, non-suberized passage cells exhibit a specific pattern in that they are always formed on the xylem-pole. Understanding the specific patterning of passage cells will also be useful understand the role of suberized cells in the endodermis.

We now have a set of different mutants that are unable to make a functional diffusion barrier formation due to interrupted/disorganized CS formation. Moreover, we have transgenic plants that only form CS, but no suberin lamellae (as shown in Chapter II). In addition, we also have mutants with an enhanced suberin formation. In the future, these mutants and transgenic lines will enable us to define the role of suberin as an apoplastic barrier against water and nutrient uptake in the young root. Especially, the comparison of mutant lines with no suberin or enhanced level of suberin will help to determine the contribution of suberin to the transport of water and nutrients in the young root.

6.3.1 Is lignification necessary for the apoplastic barrier properties of suberized layers?

We show that in young roots lignin and suberin deposition is precisely distinct in endodermis. Our analysis also indicates that suberin itself is not playing an important role to block Propidium iodide diffusion barrier at least when deposited in the young root. Moreover, my study strongly suggests that the suberin biosynthetic machinery is absent during the primary development of endodermis. However, one exception was the early expression of ASFT (Aliphatic Suberin Feruloyl Transferase). ASFT expressed as early as CASP1, i.e. it precedes CS formation. Considering this, I checked the effect of loss of ASFT function on functional CS formation in two different alleles of *asft*

mutants. Both CS formation and Propidium iodide diffusion barrier remained unaffected. According to the previously published data, ASFT was identified as *O*-acyltransferase involved could act as a linker between so-called polyaromatic (lignin-like) and polyaliphatic domain of suberin. However, what the role of ASFT in the formation of a lignified CS could be remains unclear. May be its early activity allow the integration of aliphatic chains into CS. In potato periderm, FHT (fatty alcohol hydroxycinnamoyl transferase) silencing affects the composition of soluble phenolics in periderm and was shown to be important for the functionality of the periderm as a barrier against water loss.

How much similarities exist between suberized periderm and endodermis? Could it be that lignin deposition in the primary cell wall is essential to seal the apoplastic barrier even in the suberized multilayered periderm – as it is in the endodermis? Recently, lignified CS like structure has been identified in mature phellem cells of *Pelargonium hortorum* roots (Mayer et al. 2011). These findings make us speculate that the apoplastic barrier properties of suberized layers might be always mediated by the deposition of lignin or lignin-like polymer in the primary cell walls.

In the future, all the molecular and histochemical tools that we developed will allow to solve diverse issues regarding the nature, formation, and role of CS in the establishment of a diffusion barrier. My tools will also be useful to dissect and manipulate CS formation in other plant species and to study its impact on plant growth and survival. Furthermore, identification of different actors involved in the localized deposition of lignin in the endodermis might provide new insights into the mechanism of lignin polymerization in other cell types.

7 Chapter VII: References

Agrios GN. 1997. Plant pathology. Academic Press, San Diego.

Alassimone J, Naseer S, Geldner N. 2010. A developmental framework for endodermal differentiation and polarity. Proc. Natl. Acad. Sci. USA, 107:5214–19.

Alassimone J, Roppolo D, Geldner N, JE Vermeer. 2011. The endodermis-development and differentiation of the plant's inner skin. Protoplasma, 249:433-43.

Carlsbecker A and Helariutta Y. 2005. Phloem and xylem specification: pieces of the puzzle emerge. Current Opinion in Plant Biology, 8:512–517.

Baxter I, Hosmani P, Rus A, Lahner B, Borevitz J, Muthukumar B, Mickelbart M, Schreiber, Franke R, Salt D. 2009. Root suberin forms an extracellular barrier that affects water relations and mineral nutrition in Arabidopsis. PLoS Genet, 5(5): 492.

Benfey P, Linstead J, Roberts K, Schiefelbein J, Hauser M, Aeschbacher R. 1993. Root development in *Arabidopsis*: four mutants with dramatically altered root morphogenesis. Development, 119:57–70.

Bernards MA, Razem FA. 2001. The poly(phenolic) domain of potato suberin: a non-lignin cell wall bio-polymer. Phytochemistry, 57:1115–22.

Bernards MA. 2002. Demystifying suberin. Can. J. Bot, 80:227–40.

Beisson F, Li Y. H, Bonaventure G, Pollard M, Ohlrogge J. B. 2007. The acyltransferase GPAT5 is required for the synthesis of suberin in seed coat and root of *Arabidopsis*. Plant Cell, 19: 351–368.

Bonnett HT Jr.1968. The root endodermis: fine structure and function. J Cell Biol, 37: 199-205.

Byrne JM et al.1975. Adventitious root development from the seedling hypocotyl of

Lycopersicon esculentum. American Journal of Botany, 731–737.

Digonnet C, Martinez Y, Denance N et al. 2012. Deciphering the route of *Ralstonia solanacearum* colonization in *Arabidopsis thaliana* roots during a compatible interaction: focus at the plant cell wall. Planta, 236:1419–1431.

Clarkson DT, Robards AW, and Sanderson J.1971. The tertiary endodermis in barley roots: Fine structure in relation to radial transport of ions and water. Planta, 96, 292–305.

Clarkson DT and Robards A. 1975. The endodermis, its structural development and physiological role. In: Torrey JG and Clarkson DT [ed.], The development and func-tion of roots, 415-436. Academic Press, London, NewYork, San Francisco.

Clarkson DT.1984. Calcium transport between tissues and its distribution in the plant. Plant Cell and Environment, 7:449-456.

Clarkson DT. et al.1987. Suberin Lamellae in the Hypodermis of Maize (*Zea-Mays*) Roots-Development and Factors Affecting the Permeability of Hypodermal Layers. Plant Cell and Environment, 10:83–93.

Davin LB, Wang HB, Crowell AL, Bedgar DL, Martin DM, Sarkanen S and Lewis NG. 1997. Stereoselective bimolecular phenoxy radical coupling by an auxiliary (dirigent) protein without an active center. Science, 275:362-366.

De Rufz de Lavison J. 1910. Du mode de pènètration de quelques sels dans la plante vivante. Rev. Gèn. Bot. 22:225-41.

Di Laurenzio L, Wysocka-Diller J, Malamy JE, Pysh L, Helariutta Y, Freshour G, Hahn MG, Feldmann KA, Benfey PN. 1996. The SCARECROW gene regulates an asymmetric cell division that is essential for generating the radial organization of the *Arabidopsis* root. Cell, 86:423-433.

Dolan L, Janmaat K, Willemsen V, Linstead P, Poethig S, et al. 1993. Cellular organisation of the Arabidopsis thaliana root. Development, 119:71-84.

Eilon Shani, Roy Weinstain, Yi Zhang, et al. 2013. From the Cover: Gibberellins accumulate in the elongating endodermal cells of *Arabidopsis* root. PNAS, 110: 4834-483.

Elisei F.1941. Richerche microfluoroscopiche sui punti de Caspary. Pavia Univ Inst Bot Atti, 13:1-64.

Enstone D, Peterson C, and Ma F. 2003. Root Endodermis and Exodermis: structure, function, and responses to the environment. Journal of Plant Growth Regulation, 21:335-351.

Esau K. 1977. Plant Anatomy of seed plants 2nd edition, Wiley, New York.

Esnault, AL, Mashuhara G et al. 1994. Involvement of exodermal passage cells in mycorrhiizal infection of some orchids. Mycological Research, 98: 672 - 676.

Espelie and Kolattukudy.1979. Composition of the aliphatic components of suberin of the endodermal fraction from the first internode of etiolated sorghum seedlings. Plant Physiology, 63: 433-435.

Franke R, Schreiber L. 2007. Suberin- a biopolyester forming apoplastic plant interfaces. Curr. Opin. Plant Biol, 10:252-259.

Geldner N. 2013. The endodermis. Annu Rev Plant Biol,64:531-58.

Gilroy S. and Jones D.L. 2000. Through form to function: root hair development and nutrient uptake. Trends in Plant Science, 5:56-60.

Helariutta Y, Fukaki H, Wysocka-Diller J, Nakajima K, Jung J, Sena G, Hauser MT, Benfey PN. 2000. The SHORT-ROOT gene controls radial patterning of the *Arabidopsis* root through radial signaling. Cell, 101:555-567.

Himanen K, Elodie Boucheron, Steffen Vanneste, Janice de Almeida Engler, Dirk Inzé, and Beeckman T. 2002. Auxin-mediated cell cycle activation during early Lateral root initiation. The Plant Cell, 14: 2339-2351.

Hőfer R, Briesen I, Beck M, Pinot F, Schreiber L, Franke R. 2008. The *Arabidopsis* Cytochrome P450 CYP86A1 encodes a fatty acid ω-hydroxylase involved in suberin monomer biosynthesis. J. Exp. Bot, 59:2347-60.

Hosmani P, Kamiya T, Danku J, Naseer S, Geldner N, Guerinot ML, Salt D. 2013. Dirigent domain-containing protein is part of the machinery required for formation of the lignin-based Casparian Strip in the root. PNAS, 110:14498-14503.

Hose E et al. 2001. The exodermis: a variable apoplastic barrier. Journal of Experimental Botany, 52:2245–2264.

Humphreys JM and Chapple C. 2002. Rewriting the lignin roadmap. Curr. Opin. Plant Biol, 5: 224-229.

Jalean J. Petricka, Cara M. Winter, Benfey PN. 2012. Control of *Arabidopsis* Root Development. Annual Review of Plant Biology, 63: 563-590.

Seago JL, Peterson CA, Enstone DE, Scholey CA. 1999. Development of the endodermis and hypodermis of *Typha glauca Godr* and *Typha angustifolia L*. roots. Canadian Journal of Botany, 77: 122-134.

Zhou J, Wang X, Lee JY, and Lee JY. 2013. Cell-to-Cell Movement of two Interacting AT-Hook Factors in *Arabidopsis* Root Vascular Tissue Patterning. The Plant Cell, 25: 187–201.

Joshi A, Knipfer T, Steudle E.2009. Effects of water storage in the stele on measurements of the hydraulics of young roots of corn and barley. New Phytol,3:631-43.

Kaisa Marjamaa, Eija M. Kukkola and Kurt V. Fagerstedt. 2009. The role of xylem class III peroxidases in lignification Journal of Experimental Botany, 60:367–376.

Karahara and Shibaoka H.1992. Isolation of Casparian Strips from Pea Roots. Plant Cell Physiol, 33:555-561.

Karahara et al. 2004. Development of the Casparian Strip in primary roots of maize under salt stress. Planta, 219:41-7.

Himanen K, Boucheron E, Vanneste S, Janice de Almeida Engler, Inzé D and Beeckman T.2002. Auxin-Mediated Cell Cycle Activation during Early Lateral Root Initiation. The Plant Cell, 10: 2339-2351.

Kolattukudy PE, Espelie KE. 1989. Chemistry, biochemistry and functions of suberin associated waxes. Natural Products of Woody Plants I. Springer-Verlag, New York, 235-287.

Lauchli A.1976. Apoplasmic transport in Tissues : Transport in plants II. Part B, Tissues and organs new series. M. G. pitman and U. luttge, eds., Encyclopedia of Plant Physiology.

Lee Y, Rubio MC, Alassimone J, Geldner N. 2013. A Mechanism for localized lignin deposition in the endodermis. Cell, 153:402-412.

Lersten N.1997. Occurrence of endodermis with a Casparian Strip in stem and leaf. The Botanical Review, 63: 265–272.

Levesque MP, Vernoux T, Busch W, Cui H, Wang JY, et al. 2006. Whole-genome analysis of the SHORT-ROOT developmental pathway in Arabidopsis. PLoS Biol. 4:e143.

Li Y, Beisson F, Koo AJ, Molina I, Pollard M, Ohlrogge J. 2007. Identification of acyltransferases required for cutin biosynthesis and production of cutin with suberin-like monomers. PNAS USA, 104: 18339-18344.

Lucas WJ.1995. Plasmodesmata: intercellular channels for macromolecular transport in plants. Current Opinion in Cell Biology, 7:673–680.

Lulai EC, Corsini DL. 1998. Differential deposition of suberin phenolic and aliphatic domains and their roles in resistance to infection during potato tuber (*Solanum tuberosum L.*) wound-healing. Physiol Mol Plant Pathol, 53: 209–222.

Ma F, Peterson CA. 2003. Recent insights into the development, structure and chemistry of the endodermis and exodermis. Can J Bot, 81: 405–421.

Martinka M, Dolan L, Pernas M, Abe J, Lux A. 2012. Endodermal cell-cell contact is required for the spatial control of Casparian band development in Arabidopsis thaliana. Ann Bot (Lond), 110(2):361–371.

Maule AJ. 2008. Plasmodesmata: structure, function and biogenesis. Current Opinion in Plant Biology, 11:680–686.

Meyer CJ, Peterson CA. 2013. Structure and function of three suberized cell layers: epidermis, exodermis, and endodermis. In Plant Roots: The Hidden Half, 4thed.

Meyer CJ, Peterson CA. 2011. Casparian bands occur in the periderm of *Pelargonium hortorum* stem and root. Ann. Bot, 107:591–98

Nakajima K, Sena G, Nawy T, Benfey PN, 2001. Intercellular movement of the putative transcription factor SHR in root patterning. Nature, 413:307–311.

Nagahashi G, Thomson W and Leonard R.1974. The Casparian Strip as a barrier to the movement of lanthanum in corn roots. Science, 183:670–671.

Ŏnnerud H, Zhang L, Gellerstedt G, Henriksson G. 2002. Polymerization of monolignols by redox shuttle-mediated enzymatic oxidation: a new model in lignin biosynthesis. I. Plant Cell, 14: 1953–62.

Pesquet E, Zhang B, Gorzsás A, Puhakainen T, Serk H, Escamez S, *et al.,* 2013. Non-cell-autonomous postmortem lignification of tracheary elements in *Zinnia elegans*. Plant Cell 25, 1314–1328.

Peterson CA. 1987. The Exodermal Casparian Band of Onion Roots Blocks the ApoplasticMovement of Sulphate Ions. Journal of Experimental Botany, 38:2068–2081.

Peterson CA, Murrman M. and Steudle E. 1993. Location of the Major Barriers to Water and Ion Movement in Young Roots of Zea-Mays L. Planta, 190:127–136.

Peterson CA, Enstone DE. 1996. Functions of passage cells in the endodermis and exodermis of roots. Physiologia Plantarum, 97, 592-598.

Robards AW. and Robb ME. 1972. Uptake and binding of uranyl ions by barley roots. Science, 178:980-982.

Robards AW et al.1973. The structure of barley roots in relation to the transport of ions into the stele. Protoplasma, 77: 291-311.

Robards AW and Robb ME. 1974. Entry of Ions and Molecules into roots Investigation Using Electron-Opaque Tracers. Planta, 120:1-12.

Robert G and Kolattukudy.1975.Evidence for Covalently Attached p-Coumaric Acid and Ferulic Acid in Cutin and Suberin.Plant Physiol, 56: 650-654.

Roppolo D, De Rybel B, Tendon VD, Pfister A, Alassimone J, Vermeer JE, Yamazaki M, Stierhof YD, Beeckman T, Geldner N. 2011. A novel protein family mediates Casparian Strip formation in the endodermis. Nature, 473:380-383.

Ros Barcelo A. 1997.Lignification in plant cell walls. International Review of Cytology, 176: 87±132.

Alejandro S, Lee Y, Tohge T, SudreSonia D et al. 2012. AtABCG29 is a Monolignol transporter involved in lignin biosynthesis. Current Biology, 22: 1207-1212.

Scheres, B et al.1995. Mutations affecting the radial organization of the *Arabidopsis* root display specific defects throughout the embryonic axis. Development, 121:53-62.

Schreiber L, Breiner H-W, Riederer M, Duggelin M, Guggenheim R. 1994. The Casparian Strip of *Clivia miniata Reg.* roots: isolation, fine structure and chemical nature. Bot Acta, 107: 353±361.

Schreiber L et al. 1999 .Review article. Apoplastic barriers in roots: chemical composition of endodermal and hypodermal cell walls,1267-1280.

Schönherr J, Ziegler H. 1980. Water permeability of betula periderm. Planta, 147:345-354.

Seago JL, Peterson CA, Enstone DE. and Scholey CA. 1999. Development of the endodermis and hypodermis of *Typha glauca Godr*. and *Typha angustifolia L.* roots. Can. J. Bot. 77: 122-134.

Serra O, Soler M, Hohn C, Sauveplane V, Pinot F, Franke R, Schreiber L, Prat S, Molinas M, Figueras M. 2009. CYP86A33-targeted gene silencing in potato tuber alters suberin composition, distorts suberin lamellae, and impairs the periderm's water barrier function. Plant Physiol, 149: 1050-1060.

Singh C. and Jacobson L.1977. Radial and Longitudinal Path of Ion Movement in Roots. Physiologia Plantarum, 41:59-64.

Sozzani R, Cui H, Moreno-Risueno MA, Busch W, Van Norman JM, Vernoux T, Brady SM, Dewitte W, Murray JA, Benfey PN.2010. Spatiotemporal regulation of cell-cycle genes by SHORTROOT links patterning and growth. Nature, 466:128-132.

Tanton TW and Crowdy SH., 1972. Water Pathways in Higher Plants. Journal of Experimental Botany, 23:600-618.

Tripplett JT.1984. The role of periderm in resistance of *Eucalyptus maginata* roots against *Phytophthora cinnamomi*. Eur J Pathol, 14:431-439.

Ubeda-TomAs S. et al. 2008. Root growth in *Arabidopsis* requires gibberellin/DELLA signalling in the endodermis. Nature Cell Biology,105:625–628.

Vaculík M, Landberg T, Greger M, Luxová M, Stoláriková M, Lux A.2012. Silicon modifies root anatomy, and uptake and subcellular distribution of cadmium in young maize plants. Annals of Botany, 2012;110. 433–443.

Van Fleet D. 1961. Histochemistry and function of the endodermis. The Botanical Review, 27:165-220.

White PJ. and Broadley MR. 2003. Calcium in plants. Annals of Botany, 92:487–511.

Wilson CA. and Peterson CA.1983.Chemical composition of the epidermal, hypodermal, endodermal and intervening cortical cell walls of various plant roots. Annals of Botany 51, 759–769.

Williamson VM. and Gleason CA. 2003. Plant–nematode interactions. Current Opinion in Plant Biology, 6:327-333.

Wisselingh Van. 1926. Mikrochemische Untersuchungen iiber die Zellwtinde der Fungi. Jahrb. wass. Botan. 31, 619-687.

Wout Boerjan, John Ralph, and Marie Baucher. 2003 Lignin Biosynthesis. Annu. Rev. Plant Biol, 54:519-46.

WuX, Lin J, Zhu J, Hu Y, Hartmann K, Schreiber L. 2003. Casparian Strips in needles of *Pinus bungeana*: isolation and chemical characterization. Physiol. Plant, 117:421-24

Ye Z-H, Kneusel RE, Matern U, Varner JE. 1994. An alternative methylation pathway in lignin biosynthesis in Zinnia.N Plant Cell, 6:1427-39.

Ye Z-H. and Varner JE. 1996. Induction of cysteine and serine proteases during xylogenesis in *Zinnia elegans*. Plant Mol. Biol. 30, 1233-1246.

Zimmermann HM, Hartmann K, Schreiber L, Steudle E.2000. Chemical composition of apoplastic transport barriers in relation to radial hydraulic conductivity of corn roots *(Zea mays L.)*. Planta, 210: 302–311.

Zeier J, Schreiber L. 1997. Chemical composition of hypodermal and endodermal cell walls and xylem vessels isolated from *Clivia miniata*: identification of the biopolymers lignin and suberin. Plant Physiol, 113: 1223±1231.

Zeier J, Schreiber L. 1998.Comparative investigation of primary and tertiary endodermal cell walls isolated from the roots of five monocotyledonous species: chemical composition in relation to fine structure. Planta, 206: 349±361.

Zeier J, Ruel K, Ryser U, Schreiber L. 1999. Chemical analysis and immunolocalisation of lignin and suberin in endodermal and hypodermal/ rhizodermal cell walls of developing maize (*Zea mays L.*) primary roots. Planta, 209:1-12.

8 Chapter VIII: Annex

8.1 VIII.A. Protocols and experimental procedures

8.1.1 Propidium Iodide (PI) Staining

Stock solution of Propidium iodide:

1mg/mL of propidium iodide (Invitrogen) in distilled water.

1. Grow seedlings in ½ MS-agar plates vertically for 5 days.

2. Incubate seedling in the dark for 10 min in 15 μM (10 μg/mL in distilled water) propidium iodide.

3. Rinse twice in distilled water.

Remarks:

• Use enough water when mounting the samples. Be careful not to let the samples dry out.

• Do not squeeze roots; use forceps with “soft” steel blades.

• Do not touch the root when holding the seedlings, hold them from the cotyledons.

• Avoid pressing the cover slip, otherwise the PI may penetrate the root and stain the xylem.

• Do not analyze seedlings that have been in PI for longer than 30 min.

Counting:

Excitation and Emission wavelengths: 488 nm, 500–550 nm

When counting, “Onset of elongation” was defined as the point where endodermal cells in a median optical section are clearly more than twice the width of the previous cell.

Adapted from: Alassimone J, Naseer S, Geldner N. 2010. A developmental framework for endodermal differentiation and polarity. Proc Natl Acad Sci USA, 107:5214–5219.

8.1.2 Fluorol Yellow Staining (Suberin Staining)

1. Incubate vertically grown (on ½ MS-agar plates) 5-days old seedlings are in a freshly prepared solution of Fluorol Yellow 088 (0.01%w/v, in lactic acid) at 70°C for 30 min.
2. Rinse them in water (three baths of 5 min each).
3. Counter-staining with aniline blue (0.5% w/v, in water) at room temperature for 30min in darkness.
4. Wash the samples in water for, at least, 30min (change the bath to fresh water every 10 minutes).
5. Mount on slides using glycerol 50% prior to microscope examination.

Remarks:

• Always use a freshly prepared solution of Fluorol Yellow.

• Use 12-wells microtiter plates for incubations.

• Avoid squeezing roots, use forceps with “soft” steel blades.

Microscopy and Quantitative Analysis:

Use a wide-field microscope with a standard GFP filter to observe Fluorol Yellow.

Remarks:

• After staining, keep samples in the dark.

• Do not use samples 3 hours after preparation, as the fluorescent signal may leak into the xylem.

• Do not keep the seedling under fluorescence for longer than 20 minutes, as FY is easily bleached.

• Samples should be stained and observed under the microscope in the same day.

Counting:

Wash seedlings several times in water in order to eliminate the counter-staining (Aniline blue). Otherwise, it is impossible to count as counterstaining turns the root dark blue and cells are no longer visible. It is not easy to count cells even after thorough washing. Nevertheless, it is possible to know the borders of cells knowing approximately the average length of endodermal cells. Errors are unavoidable, but with training one can get reproducible results with a reasonable error.

In order to count the endodermal cells, it is easier to go to the point where the Fluorol Yellow signal appears under GFP conditions and switch to bright field or DIC optics to count the number of cells from this point towards the root tip until the first cell of the elongation zone.

Remarks:

When counting, "Onset of elongation" was defined as the point where endodermal cells in a median optical section are clearly more than twice the width of the previous cell. The Fluorol Yellow signal initially shows a "patchy" appearance, which at one point turns into a continuous signal, where all endodermal cells are stained. It is better to count both areas, the patchy signal and the onset of a continuous signal.

Adapted and modified from: Lux A, Morita S, Abe J, Ito K. 2005.An improved method for clearing and staining free-hand sections and whole-mount samples. Ann Bot (Lond), 96:989–996.

8.1.3 Observation of autofluorescence after clearing of whole roots

In order to visualize Casparian Strip, clear the roots as follows:

1. Incubate vertically grown (onn ½ MS-agar plates), 5-days old seedlings in 0.24 N HCl (prepare in 20% methanol), at 57°C for 15 minutes.

2. Replace this solution with 7% NaOH in 60% ethanol and incubate the samples at room temperature for 15 minutes.

3. Hydrates the roots in subsequent baths of 5 minutes in 40%, 20% and 10% ethanol.

4. Infiltrate the roots in 5% ethanol and 25% glycerol for 15 minutes.

5. Mount samples in 50% glycerol for analysis under the microscope.

Microscopy:

Use a wide-field microscope with a standard GFP filter or a confocal microscope with excitation and emission frequencies for GFP (488 nm, 500–600 nm).

Remarks:

• Use 12-wells microtiter plates for incubations.

• Avoid squeezing roots, use forceps with “soft” blades.

Adapted and modified from: Malamy JE, Benfey PN. 1997. Organization and cell differentiation in lateral roots of *Arabidopsis thaliana*. Development, 124:33–44.

8.1.4 Fuchsine Staining (Lignin staining)

1. Cleared the vertically grown (on ½ MS-agar), 5-days old seedlings with an acidified methanol solution (10ml of methanol, 2ml of 37% HCL, 38ml of water) at 57°C for 15 minutes.

2. Replace acidified methanol solutionwith an alkaline solution of 7% NAOH in 60% ethanol and incubate the samples at room temperature for 15 minutes.

3. Rehydrate the samples in subsequent baths of 40%, 20% and 10% ethanol, of 5 minutes each.

4. Stain the samples in 0.01% basic fuchsin solution in 70% ethanol for 5 minutes at room temperature.

5. Unstain them in 70% ethanol and rehydrate in 10% ethanol. Each bath should be of 5 minutes.

6. Incubate for 30 minutes in 50% glycerol.

7. Mount with 50% glycerol for microscopic analysis.

Microscopy:

Use a wide-field microscope with standard GFP filter or a confocal microscope with excitation and emission frequencies for GFP (488 nm, 500–600 nm).

Adapted from: AP Mähonen, M Bonke, L Kauppinen, M Riikonen, P N Benfey, Y Helariutta. 2001. A novel two-component hybrid molecule regulates vascular morphogenesis of the *Arabidopsis* roots. Genes and Development, 14(23):2938-43.

8.1.5 Phloroglucinol Staining (Lignin Staining)

In order to visualize the Casparian Strip use vertically grown (on ½ MS-agar) 5-days old seedlings.

A saturated solution of Phloroglucinol is prepared as follows:

1. Dissolve 25mg of Phloroglucinol in 25ml of ethanol and 25ml of concentrated HCL (38%).
2. Filtered the solution to remove non-dissolved crystals.
3. For microscopic analysis place the solution on the glass slide containing the seedlings and observe under a stereomicroscope with bright field/DIC optics.

Remarks:

- The stain is light sensitive; therefore, keep the stained sample and solution in the dark.
- Always use freshly prepared solution.

Adapted from: Jensen WA. 1962. Botanical Histochemistry-principles and practice. University of California Berkeley.

8.1.6 Lignin extraction and quantification

1. Incubate the 5-days old seedlings (grown vertically on ½ MS-agar plates) with 10µM Piperonylic acid (PA) solution (prepare stock solution of PA in ethanol) for 24 hours. Incubate control samples in ethanol for 24 hours.

2. Rinse the samples with water.

3. Collect 200mg of roots (in 3 replicates of 200mg each) and grind in 1ml of ethanol.

4. Spin at 1000g for 15 minutes and dry pellets overnight at 60°C.

5. Weighed the dried pellet and resuspend in 500µL of 2N HCL and 50µL Tioglycolic acid (Fluka).

6. Incubate the resuspended mixture in boiling water for 4 hours.

7. Let it cool down and spin at 1000g for 15 minutes.

8. Wash the samples with 500µL of water, and resuspend the pellet in 500µL of 0.5N NaOH.Shake gently for 18 hours at room temperature.

9. Eliminate the insoluble residues by centrifugation (15 minutes at 1000g).

10. Collect the supernatant and precipitate lignin thioglycolate with 100µL of concentrated HCl (38%) for at least 4 hours at 4°C.

11. Spin at 1000g for 15 minutes and resuspend the obtained pellet in 1mL of NaOH.

12. Quantify the absorbance at 280 nm. Use a blank of NaOH as a control.

Calculate he total amount of lignin as µg of lignin/mg fresh weight from a linear calibration curve (0 to 50 µg) using lignin alkali (Sigma-Aldrich) as a standard.

Remarks:

- After drying fresh material (step 4), the dry samples must be weighed as to the final quantity is expressed as µg of lignin/mg of fresh weight
- Use a chemical hood and mask to handle thioglycolic acid.
- Step 8 should be done under a chemical hood as it generated a strong and unpleasant scent.

Adapted and modified from: Bruce RJ, West CA 1989. Elicitation of lignin biosynthesis and isoperoxidase activity by pectic fragments in suspension cultures of castor bean. Plant Physiol 91:889–897.

8.1.7 Protocol for the collection of material for direct chemical analysis (thioacidolysis) of Casparian Strips by using the *ahp6-1* mutant

Stock solution:

10mM of benzyl-adenine (Cytokinin) in DMSO

Concentration used:

10nM

Procedure:

1. *ahp6-1* mutants seeds were directly germinated on ½ MS-agar plates containing 10nM of benzyl-adenine vertically for 5 days.
2. Wild type (Col-0) seedlings were grown on ½ MS-agar plates containing 10nM of DMSO vertically for 5 days. They were used as a control.
3. In our plant growth conditions, benzyl-adenine treatment strongly delayed xylem differentiation up to approximately 5mm (distance from root tip) but did not affect the formation of Casparian Strips.

Determine the delay of xylem differentiation for material collection:

- In order to precisely collect the part of the root that only contained Casparian Strips, it is important to first determine the zone of xylem formation inhibition under a wide-field microscope.
- Place 8-10 seedlings on a glass slide with a drop of water.
- It is important to try to put them straight and in a uniform manner.
- Observe under microscope and mark the zone on the slide until the xylem formation is inhibited and cut precisely at that position.

Remarks:

- If all the seedlings are of the same length and the zone of xylem inhibition is the same among 50-80 seedlings the material can be collected by cutting them at less than 5mm (around 3.5-4mm) from the root tip directly on ½ MS-agar plates or under binocular microscope.
- Bear in mind that at around 2.5mm (distance from elongation zone) suberin lamellae start to be appear.
- Collected material was used for thioacidolysis.

8.1.8 Lignin Inhibition and complementation Assays

8.1.8.1 Lignin Inhibitor assay with Piperonylic acid (PA)

Stock Solution:

10mM of PA in ethanol

Concentration used:

10µM

Procedure:

1. 5-days-old seedlings were incubated in 10µM PA in ½ MS liquid for 24 h in dark.
2. Seedlings were washed with ½MS before histochemical analysis.

8.1.8.2 Complementation assay using monolignol (Lignin monomers):

Stock Solutions:

10mM of coniferyl alcohol in ethanol

10mM of sinapyl alcohol in ethanol

Concentration used:

20µm of each

Procedure:

1. 5-days-old seedlings were incubated in ½ MS liquid containing 10µM of PA and 20µm of each coniferyl and sinapyl alcohol for 24 h in dark.

2. Seedlings were washed with ½MS before histochemical analysis.

8.1.9 Gus-staining

Used solutions:

Fixative:

Ethanol/acetic acid in a 3:1 ratio.

Chloral hydrate solution:

Chloral hydrate/water/glycerol in 8:2:1 ratio.

Gus-staining buffer solution:

Sodium phosphate buffer pH 7.2	50mM
Triton X-100	0.1 % (v/v)
Ferrocyanide (Fe2+CN)	2mM
Ferricyanide (Fe3+CN)	2mM
EDTA	10mM
X-Gluc	1mg/mL

Staining Protocol:

Incubate roots in X-Gluc/GUS staining solution at 37°C for 5-24 hours in darkness. Transfer stained roots to the fixative solution for 10 minutes or until unstained samples become transparent. After fixation, rehydrate samples in 75% ethanol. Mount on choral hydrate solution for microscopic analysis.

8.2 VIII.B. Tables

8.2.1 Table 1. List of Passage cell specific, suberized cell-specific and endodermal cell specific fluorescent marker lines

Stock No.	Passage cell Marker lines	Bacterial resistance	Plant resistance
Psn011	pPHO1:NLS-3XVenus	Kanamycin	Basta
pSN022	pIRT3:NLS-3XVenus	Kanamycin	Basta
pSN023	pYSL2:NLS-3XVenus	Kanamycin	Basta
pSN024	pSKOR:NLS-3XVenus	Kanamycin	Basta
pSN012	pPHO1 :NLS-3XTagRFP	Kanamycin	Basta
pSN026	pIRT3:NLS-3XTagRFP	Kanamycin	Basta
pSN027	pYSL2:NLS-3XTagRFP	Kanamycin	Basta
pSN028	pSKOR:NLS-3XTagRFP	Kanamycin	Basta
pSN038	pIRT3:NLS-GFP-GUS	Kanamycin	Kanamycin
pSN039	pYSL2:NLS-GFP-GUS	Kanamycin	Kanamycin
pSN040	pPHO1:NLS-GFP-GUS	Kanamycin	Kanamycin
p SN041	pSKOR:NLS-GFP-GUS	Kanamycin	Kanamycin
pSN057	pIRT3:3XmCHERRY-SYP122	Kanamycin	Hygromycin
pSN058	pPHO1:3XmCHERRY-SYP122	Kanamycin	Hygromycin
pSN059	pSKOR:3XmCHERRY-SYP122	Kanamycin	Hygromycin
pSN060	pYSL2: 3XmCHERRY-SYP122	Kanamycin	Hygromycin
	Suberized cells Marker lines		
pSN025	pGAPT5:NLS-3XTagRFP	Kanamycin	Hygromycin
pYL253	pGPAT5:NLS-GFP-GUS	Kanamycin	Kanamycin
pSN056	pGPAT5:CIT-SYP122	Kanamycin	Basta
	Endodermal cells Marker lines		
pSN029	pCASP1:NLS-3XTagRFP	Kanamycin	Hygromycin

8.2.2 Table 2. List of different mutants and transgenic lines used for crossings.

Mutants/Transgenic lines	Description
esb1(Enhanced suberin)	Enhanced suberin/lack passage cells (Baxter *et al.,* 2009)
ahp6-1 (Arabidopsis histidine protein)	Loss of protoxylem identity (Mähönen AP *et al.,* 2006)
axr3-1 (Auxin- resistant)	No xylem formation
wol(Woodenleg)	No protoxylem formation (Ben Scheres *et al.,* 1995)
pCASP1::CDEF1(pSN007)	Lack of suberin lamellae formation (Naseer *et al.,* 2012)

8.2.3 Table 3. List of transgenic lines generated for the cell-specific gene expression profiling.

Stock No.	Transgenic lines	Bacterial resistance	Plant resistance
	Two component system		
pSN042	pCASP1:: 3xMyc-BirA	Spectinomycin	Kanamycin
pSN043	peLTP:: 3xMyc-BirA	Spectinomycin	Kanamycin
pSN044	pCASP1::BLRP-FLAG-RPL18	Spectinomycin	Basta
pSN045	pIRT3::BLRP-FLAG-RPL18	Spectinomycin	Basta
pSN046	pPHO1::BLRP-FLAG-RPL18	Spectinomycin	Basta
pSN047	pGPAT5::BLRP-FLAG-RPL18	Spectinomycin	Basta
pSN048	pYSL2::BLRP-FLAG-RPL18	Spectinomycin	Basta
pSN055	pSKOR::BLRP-FLAG-RPL18	Spectinomycin	Basta
	INTACT	Spectinomycin	Basta
pSN049	pCASP1::NTF	Spectinomycin	Basta
pSN050	pGPAT5::NTF	Spectinomycin	Basta
pSN051	pYSL2::NTF	Spectinomycin	Basta
pSN052	pSKOR::NTF	Spectinomycin	Basta
pSN053	pIRT3::NTF	Spectinomycin	Basta
pSN054	pPHO1::NTF	Spectinomycin	Basta

8.2.4 Table 4. List of Passage cell-specific fluorescent marker lines crossed with different set of mutants, suberized cell and endodermal cell specific fluorescent marker lines.

Transgenic lines	Background
pPHO1 :NLS-3XVenus	*esb1*
	axr3-1 and *axr3-3*
	ahp6-1
	wol
	pCASP1::CDEF1
pIRT3:NLS-3XVenus	*esb1*
	axr3-1 and *axr3-3*
	ahp6-1
	wol
pYSL2:NLS-3XVenus	*esb1*
	axr3-1 and *axr3-3*
	ahp6-1
	wol
Double marker lines	
Passage cell specific markers crossed with suberized cell specific markers	
pPHO1 ::NLS-3XVenus pGPAT5::NLS3XTagRfp	
pYSL2::NLS-3XVenus pGPAT5::NLS3XTagRfp	
pIRT3::NLS-3XVenus pGPAT5::NLS3XTagRfp	
pSKOR:NLS-3XVenus pGPAT5::NLS3XTagRfp	
Passage cell specific markers crossed with endodermis specific markers	
pPHO1::NLS-3XVenus pCASP1::NLS3XTagRfp	
pYSL2::NLS-3XVenus pCASP1::NLS3XTagRfp	

pIRT3::NLS-3XVenus pCASP1::NLS3XTagRfp
pSKOR::NLS-3XVenus pCASP1::NLS3XTagRfp
Suberized cell specific marker crossed with endodermis specific marker
pGPAT5::NLS3XTagRfp pCASP1::Citrin-SYP122
Passage cell specific marker crossed with passage cell specific marker
pPHO1 : NLS3XTagRfp pYSL2:NLS-3XVenus

9 Acknowledgement

I would like to thank my thesis committee Prof. Alexandre Reymond, Prof. Yves Poirier and Prof. Malcolm J Bennett for their support and helpful discussions.

I would like to express my deep gratitude to my Ph. D supervisor Prof. Niko Geldner, for his guidance, enthusiastic encouragement, appreciation, and useful critiques throughout my Ph. D research work. I would also like to thank our former Postdoc Daniele Roppolo for his valuable and constructive suggestions. I wish to thank various people for their contribution to this project; Rochus Franke Benni for his help, guidance and performing suberin monomer analysis, Catherine Lapierre who made it possible to do lignin monomer analysis with few mg of plant material, Yuree Lee for her participation in resulting publication and Christiane Nawrath for her useful suggestions during my research work. I wish to acknowledge Joop Vermeer for his support during writing of this manuscript and Alexandre Pfister for writing French version of the thesis summary. I would like to offer my special thanks to Enrique Neumann for his efforts, to correct my endless grammar and spelling mistakes.

I would also like to thank to our former technical Assistant Valérie Dénervaud-Tendon for her kind assistance and support to make lab running smoothly. I am particularly grateful all the former lab members Julien Alassimone, Mari-Carmen Rubio, Misako Yamazaki, Julien Spielmann and Esther M. N. Dohmann and the present lab members Yuree Lee, Verónica G. Doblas and Lothar Kalmbach for their support, guidance and for providing excellent atmosphere to work. Special thanks to Deborah Mühlemann for her help to compile the manuscript.

I would like to thank all the colleagues from DBMV for providing nice atmosphere for the successful completion of my thesis work.

I wish to thank all my family members for their support and encouragement throughout my studies. I would also like to thank my husband Dr. Kashif RIAZ who has always been with me through good and bad times to cheer me up. Finally, I would like to offer special thanks to my daughter Hamra who always stood by me with cute smile.